Understanding Viscoelastic Behavior of Asphalt Binders Through Molecular Structure Investigation

by

Akshay Gundla

A Dissertation Presented in Partial Fulfillment
of the Requirements for the Degree
Doctor of Philosophy

Graduate Supervisory Committee:

B. Shane Underwood, Co-Chair
Kamil Kaloush, Co-Chair
Michael Mamlouk
Narayanan Neithalath

ARIZONA STATE UNIVERSITY

August 2018

ABSTRACT

Asphalt binder is a complex viscoelastic hydrocarbon, whose performance depends upon interaction between its physical and chemical properties, both of which are equally important to the successful understanding of the material. Researchers have proposed various models linking linear viscoelastic (LVE) and microstructural parameters. However, none of these parameters provide insight into the relationship in the non- linear viscoelastic NLVE domain. The main goals of this dissertation are two fold. The first goal is to utilize the technique of Laser Desorption Mass Spectroscopy (LDMS) to relate the molecular structure of asphalt binders to its viscoelastic properties. The second goal of the study is to utilize different NLVE characterization tools and analysis procedures to get a clear understanding of the NLVE behavior of the asphalt binders. The goals of the study are divided into four objectives; 1) Performing the LDMS test on asphalt binder to develop at the molecular weight distributions for different asphalts, 2) Characterizing LVE properties of Arizona asphalt binders, 3) Development of relationship between molecular structure and linear viscoelasticity, 4) Understanding NLVE behavior of asphalt binders through three different characterization methods and analysis techniques.

In this research effort, a promising physico-chemical relationship is developed between number average molecular weight and width of relaxation spectrum by utilizing the data from LVE characterization and the molecular weight distribution from LDMS. The relationship states that as the molecular weight of asphalt binders increase, they require more time to relax the developed stresses. Also, NLVE characterization was carried out at intermediate and high temperatures using three different tests, time sweep fatigue test,

repeated stress/strain sweep test and Multiple Stress Creep and Recovery (MSCR) test. For the intermediate temperature fatigue tests, damage characterization was conducted by applying the S-VECD model and it was found that aged binders possess greater fatigue resistance than unaged binders. Using the high temperature LAOS tests, distortion was observed in the stress-strain relationships and the data was analyzed using a Fourier transform based tool called MITlaos, which deconvolves stress strain data into harmonic constituents and aids in identification of non-linearity by detecting higher order harmonics. Using the peak intensities observed at higher harmonic orders, non-linearity was quantified through a parameter termed as "Q", which in future applications can be used to relate to asphalt chemical parameters. Finally, the last NLVE characterization carried out was the MSCR test, where the focus was on the scrutiny of the J_{nrdiff} parameter. It was found that J_{nrdiff} is not a capable parameter to represent the stress-sensitivity of asphalt binders. The developed alternative parameter $J_{nrslope}$ does a better job of not only being a representative parameter of stress sensitivity but also for temperature sensitivity.

This dissertation is dedicated to all my teachers and professors who have contributed immensely in shaping my career and helped me achieve my goals. Special dedication to my first teachers, my parents, Revathi and Yoganand Gundla, for their guidance, support, and love without which none of this would be possible.

ACKNOWLEDGMENTS

First and foremost, I would like to express my sincere gratitude to Dr. Shane Underwood for providing me the opportunity to work with him. I am grateful to him for his mentorship, guidance and valuable inputs over the past six years. Dr. Underwood has shown me the importance of attending to details while performing experiments and analyzing the test data. His emphasis on minute details and consistency has helped me become an able researcher. His encouragement and support throughout the course of my masters and Ph.D. has been a major driving force. I greatly admire Dr. Underwood's willingness to travel that extra mile to help students with their work. His level of dedication towards research is something I aspire to achieve one day.

I would like to thank Dr. Kamil Kaloush for his unconditional support throughout the course of my stay at ASU. My interactions with Dr. Kaloush not only enriched me as a researcher but also as a person in general.

I would like to thank Dr. Michael Mamlouk for teaching me the important aspects of pavement engineering throughout my graduate studies.

I would like to thank Dr. Narayanan Neithalath for teaching me important fundamental mechanisms in material behavior through his course on "Properties of Concrete", which I thoroughly enjoyed.

My heartfelt gratitude to all my committee members for agreeing to serve on my Ph.D. supervisory committee. Their opinions and contributions are gratefully appreciated.

A big thank you to our laboratory managers, Mr. Jeff Long and Mr. Peter Goguen for providing all the required logistical and technical support I needed to complete my experiments. Their time and help has been invaluable.

I would like to explicitly thank Mr. Robert McGennis from Holly Frontier, Mr. Mohammad Rahman from Delek and Mr. Sam Huddleston from Andeavor for supplying binders for the ADOT-SPR 742 project which were used in my dissertation work also.

I would to like to specially thank Padmini Gudipudi, for she has been a great mentor to me always and especially during the initial years of my study. Also, collaborating with her on the NCHRP 9-54 project has been very rewarding.

I'd like to thank all my present, and past colleagues in the Advanced Pavement Laboratory, Padmini Gudipudi, Jose Medina, Ramadan Salim, Waleed Zeiada, Jeff Stempihar, Hossein Noorvand, Satish Kannan Nagarajan, Madhur Soam, Gurpreet Rai, Guru Sai Kumar Karnati, Babu Kanappan, Tarun Reddy, and Ryan Stevens for their support and assistance throughout my studies.

I'd like to explicitly thank Jose Medina, Ramadan Salim, Srivatsav Kandala, Sravani Vadlamani, Venu Garikapati, Akash Dakhane, Aditya Inbasekaran, Kishore Sekhar, Sateesh Madavarapu, and Sneha Narra for their friendship and delightful company.

My heartfelt gratitude to all my family members in India for their love, support and continuous encouragement.

Finally, I would like to thank the Arizona Department of Transportation (ADOT) and the National Cooperative Highway Research Program (NCHRP) for supporting my Ph.D. study.

TABLE OF CONTENTS

Page

CHAPTER Page

CHAPTER Page

LIST OF FIGURES

Figure Page

Figure Page

Figure Page

Figure Page

Figure Page

Figure Page

LIST OF TABLES

Table Page

Chapter 1 Introduction

1.1 Background

Asphalt binder or bitumen is a viscous hydrocarbon often obtained as the byproduct of the fractional distillation process of crude oil. Asphalt binder can be classified as a complex hydrocarbon based on its chemistry (American Chemical Society 1999). It contains saturated and unsaturated aliphatic and aromatic compounds with up to 150 carbon atoms. The elemental composition of asphalt depends primarily on the source of the crude. Typically, it contains about 80% by weight of carbon, around 10% hydrogen, up to 6% sulfur, small amounts of oxygen and nitrogen, and trace amounts of metals such as iron, nickel, and vanadium. (American Chemical Society 1999, Petersen 1984). Since the elemental composition of asphalt is so heavily weighted towards one element, carbon, approaching the chemistry of asphalt at the elemental scale is often not sufficient to understand its properties. Instead, the molecular structures formed by the carbon and hydrogen are more often studied. In this case the molecules are separated into four chemical families based on their size and solubility, namely saturates, aromatics, resins and asphaltenes. They are usually referred to as SARA fractions. The percentage of these SARA components dictate the molecular structure of asphalt and its associated parameters such as molecular weight distribution, molecular weights, and also the mechanical properties of asphalt (Branthaver et al. 1993). The molecular weight distribution of a material describes a relationship between number of moles of particular species and the molar mass of that species in that material. Whereas, molecular weight is a central tendency parameter of this distribution. In an effort to better engineer the material, past researchers

have related the microstructure of asphalt to its linear viscoelastic (LVE) properties (Petersen et al. 1993, Christensen and Anderson 1993, Leseur et al. 1996). However, the stresses or strains experienced by the pavement far exceed the linear viscoelastic region. Therefore, a good understanding of the non-linear viscoelastic (NLVE) behavior of asphalt followed by a relationship between NLVE parameters and asphalt microstructural parameters may be a more useful relationship to relate pavement behaviors to asphalt composition.

1.2 Research Objective

This study has two main objectives. The first objective of this study is to gain insight into the molecular structure of asphalt by studying their molecular weight distributions, obtained from the mass spectroscopy technique of Laser Desorption Mass Spectroscopy (LDMS) and then relate these molecular structure attributes to asphalt's linear viscoelastic (LVE) properties. This work supplements and expands the current knowledge and on the relationship between the two fundamental characteristics of asphalt, its molecular structure and LVE properties. Another parallel objective of the study is to have a clear understanding of the NLVE behavior of asphalt through its various characterization techniques and analysis methodologies. The specific objectives of the study are as listed below:

1. Performing the LDMS test on asphalt binder to develop at the molecular weight distributions for different asphalts. This objective includes three subtasks.
    a. Development of a sample preparation method for the LDMS test.
    b. Understanding the LDMS test equipment and performing the test.
    c. Filtering of the raw data obtained from the test, to develop MWD.

2. Characterizing LVE properties of Arizona asphalt binders. This objective includes three subtasks.
    a. Performing temperature-frequency sweep experiments on asphalt binders and using time-temperature superposition principle to develop mastercurves
    b. Using the data from the temperature-frequency sweep experiments, to calculate various LVE parameters.
    c. Characterization of both discrete and continuous relaxation spectra.
3. Development of relationship between molecular structure and linear viscoelasticity. This objective involves two subtasks.
    a. In-depth investigation as why the molecular structure and linear viscoelastic parameters should be related.
    b. Development of the relationship between the molecular structure attribute from LDMS test and LVE parameters.
4. Understanding NLVE behavior of asphalt binders through characterization methods and analysis techniques. These include:
    a. Performing time sweep tests and development of damage characteristic curves.
    b. Performing large amplitude oscillatory shear (LAOS) tests on asphalt binders at high temperatures and their subsequent analysis using MITlaos. These tests include time sweep tests and repeated strain/stress sweep tests (RSS) at large strain amplitude.

c. Analyzing the results from the multiple stress creep and recovery (MSCR) test with in-depth scrutiny of the Jnr difference parameter, its physical significance.

5. Summarize the insight gained from the LVE and NLVE studies and propose a research approach that can enhance the knowledge provided by this study and possibly investigate the relationship between molecular structure and NLVE.

The experimental plan adopted to achieve the above-mentioned study objectives is presented in Figure 1-1.

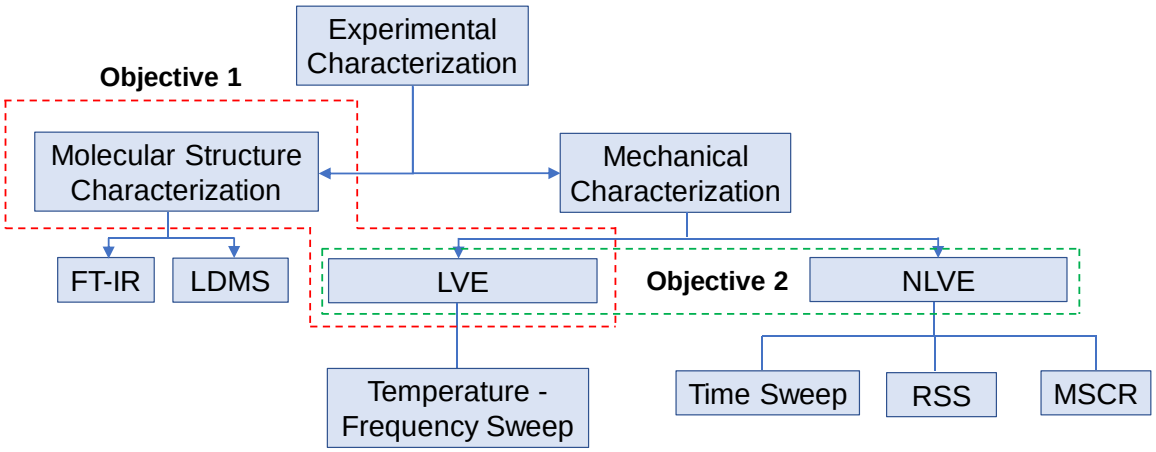

Figure 1-1: Experimental Layout of the Research Study.

1.3 Dissertation Outline

This dissertation is segmented into eight chapters. The first seven chapters introduce the research, present the tasks performed towards achieving the research study objectives, and discuss the findings. The eighth chapter details the concluding remarks from the overall

research plan and recommendations for future research. A brief summary of each chapter is provided below.

Chapter 1: *Introduction* - This chapter provides an overall introduction and background of this study, the needs for this research as well as detailed research objectives.

Chapter 2: *Literature Review* - This chapter reviews the literature regarding the chemical composition of asphalt, its molecular and micro structure attributes, and the work performed relating microstructure to LVE. Presented in this chapter is a brief introduction of LDMS, its applications in the field of asphalt science. Also, the studies regarding the various LVE models, relaxation spectra of asphalt and its importance are presented. The last piece of literature provided in this chapter is regarding the existing knowledge regarding the NLVE behavior of asphalt, the characterization, and analysis tools that are available.

Chapter 3: *Materials and Experimental Methods* - In this chapter, the study materials and the experimental techniques that will be used in the study are described in detail. Information pertaining to the types of asphalt, modification, suppliers, the crude sources are provided. The sample preparation techniques employed in LDMS, and FTIR are discussed. Details pertaining to the LDMS test, FT-IR test, temperature-frequency test and NLVE tests are discussed.

Chapter 4: *Comprehensive Discussion of Relationship b/w LVE and MWD* - This chapter is segmented into three parts. In the first part, the molecular weight distributions obtained from the LDMS technique and subsequent molecular structure parameters are discussed. In the second part, the result from the LVE characterization, calculation of LVE

parameters, and development of relaxation spectra are discussed. The third part involves developing of the relationship between the molecular weight distribution and LVE parameters with a comprehensive discussion around the fundamental basis for existence of such a relationship.

Chapter 5: *NLVE Studies I - Time Sweep Test* - This chapter provides details regarding the NLVE characterization performed on the study binders using the time sweep test. The details regarding results from the time sweep experiment, as well as the subsequent analysis involving the damage characteristic curves are provided.

Chapter 6: *NLVE Studies III – Non-Linearity Assessment based on High Temp. LAOS* - In this chapter the results from the high temperature large amplitude oscillatory shear tests, RSS test and time sweep tests are discussed. Also, discussed is the analysis of the data from these tests using MITlaos program, which is based on Fourier transform analysis and is used to deconvolve stress-strain history into their harmonic constituents and identify nonlinearity. In order to identify non-linearity in asphalt binders, stress-strain data is input into the MITlaos program, which expresses this data in harmonic form. The principal harmonic is associated with LVE behavior of the material and any higher order harmonics if present, indicate presence of non-linearity. The discussion in the chapter surrounds around detection of non-linearity, distortion of the stress-strain curves and quantification of non-linearity.

Chapter 7: *NLVE Studies II – Jnr Difference Study* - In this chapter, the results from the MSCR test for the Arizona binders are provided. However, the primary focus of this

chapter is to scrutinize the effectiveness of the J_{nr} difference parameter, its limitations, its physical significance and also evaluate alternatives that can possibly replace J_{nr} difference.

Chapter 8: *Summary, Conclusions and Future Work* - Provides a summary of conclusions drawn from the research conducted and the scope of future work. This especially entails to how the present insight gained from the LVE and NLVE studies in this research may be in future used to develop a characteristic relationship between molecular structure and NLVE.

Chapter 2 Literature Review

2.1 Asphalt Chemical Composition

Asphalt, a complex hydrocarbon is predominantly comprised of three elements, carbon, hydrogen, and sulfur an trace amounts of oxygen, nitrogen, vanadium and nickel (Petersen 1984). The percentage of these components vary based on crude type but typically asphalt contains about 80% by weight of carbon, around 10% hydrogen, and up to 6% sulfur. While the asphalt elemental composition is good to know, it does not provide much information about the fundamental characteristics of its chemistry. For this reason, asphalt is separated into four chemical families saturates, aromatics, resins and asphaltenes using fractionation techniques such as size exclusion chromatography (SEC). The saturates and aromatics together form the oil portion of the asphalt binder. The saturates fraction is a colorless liquid whereas the aromatics is a colored oil. Based on the values reported by Corbett for different crudes, the oils comprise of about 40-60% of the asphalt by weight. Wherein, 8-12% is saturates and the resins are 30-48%. The next fraction of asphalt is resins, or polar aromatics, which is a dark colored crystalline semisolid. The resins comprise of 30-40% by weight of asphalt. The last component of asphalt is asphaltenes, which is a solid black powdery material and it comprises of about 8-20% of asphalt by weight. Corbett in his work evaluated the viscosities of asphalts from three different crudes and found that asphalts with highest percentage of asphaltenes possessed highest viscosity and the asphalt

with the lowest percentage of asphaltenes possessed the lowest viscosity amongst the three asphalts.

Asphalt fractionation was performed first by Boussingault in as early as 1836, where asphalt was separated into two fractions, a distillable fraction, petrolene, and a solid fraction, asphaltenes (Boussingault 1836). Richardson re-defined asphalt as a combination of asphaltenes and maltene (Richardson 1905). Richardson defined asphaltene as the insoluble part of asphalt in naphtha and maltenes as the soluble part. Separation of asphalt into only two fractions proved unsatisfactory due to the numerous components of maltene phase. A refined solvent extraction procedure by Hoiberg et al. was developed in 1939 and they separated maltenes into resins and oils (Rostler 1965). The process was replaced by a chromatography technique proposed by Corbett (Corbett 1969), who fractionated maltenes into saturates, aromatics, and resins. The modern-day asphalt fractionation is carried out by size exclusion chromatography. Thus, the SARA fractions are more often referred to as Corbett fractions as well.

2.2 Asphalt Microstructure

Early studies have looked into asphalt as a two-phase system and its molecular structure has been described as a colloidal or a micellar structure. The origins of this theory can be traced to Nellensteyn who theorized that the asphaltenes are close in resemblance to free carbon and form a colloidal suspension with the maltene phase (Nellensteyn 1924). Pfeiffer further developed the colloidal model and explained the rheological properties of the asphalt based on a sol-gel structure (Pfeiffer and Saal 1940). Sol asphalts were thought to occur when asphaltene micelles were fully dispersed and non-interacting, whereas gel

asphalts were described as asphalts with fully interconnected asphaltene micelles. Pfeiffer and Saal theorized that sol asphalts would exhibit Newtonian behavior whereas gel asphalts would be non-Newtonian. This non-Newtonian behavior was attributed by Saal and Labout as delayed elasticity with some non-linearity in the viscoelastic properties (Saal and Labout 1940). The sol asphalts are known to occur when the asphaltenes are fully dispersed and non-interacting and the gel asphalts which possess non-Newtonian behavior are thought of having a structure with interconnected asphaltenes micelles. Researchers had disagreements over such theory mainly because the gel structure would result in a plateau of modulus vs temperature and frequency, which is never observed in asphalts (Leseur et al. 2011). However, the interpretation was in line with the theory that softer asphalts differ from harder asphalts originating from the same crude, by containing a higher asphaltene content and lower aromatic content with no change in resin and saturate contents (Read and Whiteoak 2003).

During the initial SHRP work in the early 1990's, researchers theorized that asphalt existed as a simple homogenous fluid structured as a dispersed polar fluid (DPF) (Petersen et al. 1994). The authors proposed the model as an alternative to the traditional colloidal or micellar model. The most important difference between the two models is that the DPF considers asphalt as a single-phase system as against the two-phase system presumed by the colloidal models. According to the DPF model, the mechanical properties of asphalt cement are dependent not upon the relative abundance of dispersed and continuous phases, but upon the magnitude and dispersion in molecular weights as well as intermolecular forces.

More recent studies utilized small angle X-Ray scattering (SAXS) and small angle neutrons scattering (SANS) confirm that asphaltenes do form micelles in asphalt cements (Leseur et al. 2011). Viscoelastic studies by Leseur et al. also suggested that asphaltenes micelles do exist inside bitumen and they experience Brownian motion at high enough temperature (Leseur et al. 1996). These evidences make it difficult to deny the colloidal nature of asphalt.

The use of advanced microscopic techniques such as Atomic Force Microscopy (AFM) and Scanning Electron Microscopy (SEM) made it possible to gain visual insight into the structure of asphalt (Loeber et al. 1996). Loeber et al. observed that incase of gel asphalts there were typical alternate dark and light lines aligned symmetrically with each strip being 100-200 nm thick. When the same asphalt was observed under the SEM, a network structure made of interconnected round aggregated particles were found floating in a matrix. The authors believed these aggregated particles were the asphaltene particles of diameter around 100 nm and the matrix was oil i.e. the maltene and resin components. This led to what is called by Loeber at al. “bee like structure” of asphalt.

2.3 Molecular Weight Distribution

Complex organic composites such as asphalt and polymers are made of up combinations of molecules of varying weight and complexity. The relative contribution of each of these molecules to the overall composite composition is captured by measuring and quantifying the individual or cumulative distribution of weights in these composites. These molecular weight distributions represent a fundamental compositional characteristic of these materials and ultimately govern many of the fundamental and chemical properties of these

materials. While the molecular weight distribution of polymers is well established, there has been relatively less interest to examine the molecular distribution of asphalt. The dispersed polar fluid (DPF) model theorized that the mechanical properties of asphalt depend on the dispersion in molecular weights. This dispersion or rather distribution of molecular weights has been studied using chromatographic and mass spectroscopic techniques.

The first known mass spectroscopic analysis conducted on asphalt was by Clerc and O'Neal in 1961 (Clerc and O'Neal 1961). The authors sought to get insight into the composition of the West Texas straight run asphalt. A high vacuum analyzer system was used for the spectroscopic analysis. The mass spectrum was recorded using a recording oscillography. The mass range detected ranged from about 24 to 1900 daltons. Six prominent peaks in the range of 91 to 302 daltons were detected and approximate chemical structures for the detected peaks were shown. The authors attributed these peaks to the aromatics or heterocyclics present in asphalt.

More recent techniques such as size exclusion chromatography (SEC), gas permeation chromatography (GPC), plasma desorption mass spectroscopy (PDMS) have been used for the measurement of molecular weight distribution of asphalts (Domin et al. 1999, Branthaver et al. 1993). While the above techniques provide the molecular weight distribution of asphalt, vapor pressure osmometry (VPO) used by Strategic Highway Research Program (SHRP) projects of the early 1990's provides the number average molecular weight (Branthaver et al. 1993). While all of these techniques are still in practice, issues with the use of VPO were mentioned in the SHRP-A-368 study. The authors

mentioned that the method of VPO which uses pyridine solvent forms molecular associations with polar asphalts there giving a higher number for molecular weights.

2.3.1 MALDI and it's Applications in Asphalt Science

In 1985, German scientists Karas et al. devised a technique for laser desorption mass spectroscopy of organic molecules (Karas et al. 1985). The authors illustrated their theory using an example of enhanced ion yield of non-absorbing molecules in an absorbing matrix. This was the first published work where the idea of matrix assisted laser desorption mass spectroscopy was presented and was later termed as Matrix Assisted Laser Desorption and Ionization (MALDI). The method is based on the principle of proton transfer is shown in Figure 2-1. Consider a sample (A) is mixed with a matrix (M) which has great ionizing potential. This mixture is prepared and dried on the MALDI plate. Laser flash ionizes the matrix molecules and subsequently the sample molecules are ionized by proton transfer from the matrix. The equation showing the proton transfer is also shown in Figure 2-1. After the sample molecules are ejected from the sample plate, they travel through a flight tube as shown in Figure 2-2. Depending upon the size of the ions, the taken to reach the detector varies. Smaller ions reach the detector before the larger ions and the time for the ions to reach the detector is measured. The governing equation for the MALDI experiment is presented in Equation (1).

$$\frac{m}{z} = \frac{2t^2 K}{L^2} \tag{1}$$

Where,

t = Drift time;

L= Drift length;

m = Mass;

K = Kinetic energy of ion

z = Number of charges on ion

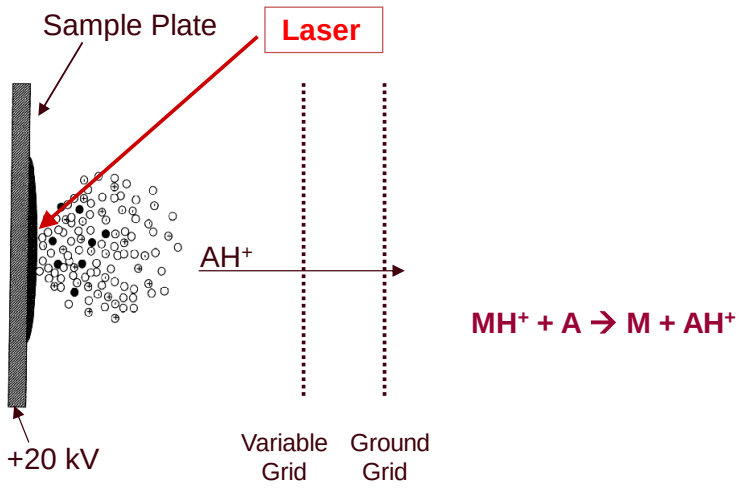

Figure 2-1. Schematic of the Ionization Process in MALDI Experiment (University of California, San Francisco 2003).

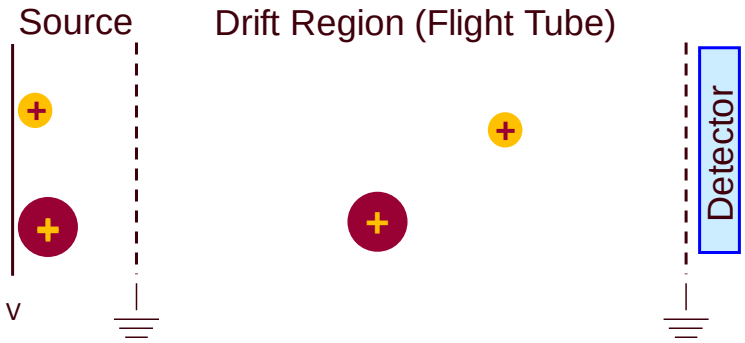

Figure 2-2. The Drift Region in the MALDI Experiment (University of California, San Francisco 2003).

The method of MALDI gained popularity in the field of bio-chemistry and soon found its way into asphalt science, wherein the researchers used it as is and also without

the use of matrix and termed it as Laser Desorption Mass Spectroscopy (LDMS). Presented below are few studies which have used MALDI / LDMS in the field of asphalt science.

In mid-1990's Lazaro et al. used LDMS to study the molecular masses of coal tar (Lazaro et al. 1997). The authors studied the effect of various instrument related parameters such as ion extraction voltage, laser power level on the mass spectra obtained by LDMS. The authors did not use any matrix as they found that the sample was highly absorptive. The authors found that the lower laser powers were more suitable in providing structural information of lower molecular masses where as to obtain structural information of high molecular masses higher laser power was required.

The technique was further applied to asphalts by Fonnesbeck in 1997 (Fonnesbeck 1997). Fonnesbeck in her study to elucidate the structural features of asphalt has applied the technique of MALDI along with other methods such as vapor pressure osmometry (VPO) and NMR. The author performed MALDI on asphalt as well as laser desorption mass spectroscopy (LDMS) technique without use of matrix. The author found that the mass resolution obtained using the LDMS technique was superior to that using MALDI. The author believed this was because asphalt itself appears to serve as its own (liquid matrix).

A similar study was conducted by Domin et al. to study the bitumen molecular weight distributions (Domin et al. 1999). The authors used Athabasca bitumen and then fractionated it using size exclusion chromatography (SEC) and the molecular distributions of the five fractions and the original sample were determined using VPO, LDMS, and MALDI. Other mass spectroscopy techniques such as plasma desorption mass

spectroscopy (PDMS) were also employed. The discussion presented here is only with regard to the results obtained from the MALDI technique. The samples were prepared both in presence as well as absence of matrix. The author found similar spectra with and without the use of matrix and the samples showed a continuous mass distribution out to very high mass of at least 15000 daltons. The author also found that the spectra obtained using LDMS and MALDI matched closely with that obtained using VPO and consistent as well as reliable. The authors however mentioned that one potential problem with LDMS or MALDI is that the technique favors the observation of lower mass components at the expense of high ones.

2.4 Understanding Linear Viscoelastic Behavior of Asphalt Binders

Asphalt is a thermorheologically simple material which means the concept of time-temperature superposition can be applied to to develop mastercurves that can describe the behavior of asphalt over a range of temperatures and loading frequencies. There have been a number of well-known semi-empirical algebraic functions that have been developed to model these curves.

2.4.1 Jongepier and Kuilman (1969)

Jongepier and Kuilman suggested that the relaxation spectra for asphalt binders can be best assumed as a log-normal distribution and derived rheological models based on this assumption. The equations for relaxation spectra, storage modulus, and loss modulus as proposed by Jongepier and Kuilman are shown in Equations (2), (3), and (4).

$$H(\tau) = \frac{G_g}{\beta\sqrt{\pi}} \exp - \left\{ \frac{\ln \tau / \tau_m}{\beta} \right\}^2 \quad (2)$$

$$G'(x) = \frac{G_g}{\beta\sqrt{\pi}} \exp - \left\{ \frac{\beta(x-0.5)}{2} \right\}^2 x \int_0^\infty \exp - \left(\frac{u}{\beta} \right)^2 \frac{\cosh(x+0.5)u}{\cosh u} du \quad (3)$$

$$G''(x) = \frac{G_g}{\beta\sqrt{\pi}} \exp - \left\{ \frac{\beta(x-0.5)}{2} \right\}^2 x \int_0^\infty \exp - \left(\frac{u}{\beta} \right)^2 \frac{\cosh(x-0.5)u}{\cosh u} du \quad (4)$$

where:

$H(\tau)$ = the relaxation spectrum distribution;

β = the scale parameter for the log normal distribution

= 1.414 σ (standard deviation);

G_g = the glassy modulus, Pa;

τ = relaxation time, s;

τ_m = the exponential of the mean of the natural logarithms of the relaxation times.

ω_r = reduced frequency, rad/s;

u = ln $\omega_r\tau$; and

x = $(2/\beta^2)$ ln ω_r

During the SHRP studies (SHRP-A-369) researchers have found the assumption of log-normal distribution to be false, as asphalt relaxation spectra can only be approximated as log-normal at very large relaxation times and the assumption does not hold true at shorter relaxation times. One of the main shortcomings of Jongepier and Kuilman's model apart from the log-normal relaxation spectra assumption was the mathematical complexity of its formulation.

2.4.2 Dickson and Witt (1974)

In 1974, Dickinson and Witt developed a model in which the master curve of a complex modulus is mathematically treated as a hyperbola. The equation proposed by the authors for describing the complex modulus as a function of frequency is given by Equation (5)

$$\log\left|G_r^*(\omega)\right| = 0.5\left\{\log\omega_r - \left[(\log\omega_r)^2 + (2\beta)^2\right]^{0.5}\right\} \quad (5)$$

Where:

$|G_r^*(\omega)|$ = the relative complex modulus at frequency, ω

= $|G^*(\omega)| / G_g$,

ω_r = $\omega\eta_0 a(T)/G_g$,

η_0 = the Newtonian viscosity,

$a(T)$ = the shift factor at temperature T relative to the selected reference temperature,

β = a "shear susceptibility" parameter, which is defined as the distance on a log-log scale between the glassy modulus and the modulus at ω_r

In general, the model was simpler than the model proposed by Jongepier and Kuilman. Also, Dickinson and Witt found that the relaxation spectra were not log-normal but somewhat skewed and asymmetrical.

2.4.3 Christensen and Anderson (1992)

The other model of relevance, is the Christensen – Anderson (CA) model developed by authors during SHRP studies of early 1990's (Christensen and Anderson 1992). The authors developed a model that was reasonably accurate and mathematically simple to allow direct engineering calculations and if required perform iterations easily. The model

presented by the authors to describe complex shear modulus is shown in Equation (6). The temperature shift factor is modeled using the William-Landel-Ferry (WLF) equation as shown in Equation (7).

$$G^* = G_g \left[1 + \left[\frac{\omega}{\omega_c} \right]^{\frac{\log 2}{R}} \right]^{\frac{-R}{\log 2}} \tag{6}$$

$$\log a(T) = \frac{-19(T - T_d)}{(92 + T - T_d)} \tag{7}$$

where:

G^* = complex dynamic modulus, Pa

G_g = glassy modulus, typically 1 GPa

ω = test frequency, rad/s

ω_c = crossover frequency, rad/s

R = rheological index

a(T) = shift factor at temperature T (T in °C)

T_d = the defining temperature, °C

The glassy modulus, G_g, represents the limiting complex modulus for a given asphalt binder usually obtained at low temperatures and high frequencies. Crossover frequency is the frequency at which storage and loss modulus values "crossover" i.e. are equal. The phase angle at such condition is 45°. The rheological index fundamentally represents the width of the relaxation spectrum and mathematically is equal to the logarithmic ratio of glassy modulus to modulus at crossover frequency. The defining temperature, T_d, is a

parameter characteristic of the temperature dependency of asphalt. As the defining temperature increases, the change in shift factor which respect to temperature increases, thus showing greater temperature dependency. The rheological index, *R*, is indicative of the width of the relaxation spectrum. Mathematically is equal to the logarithmic ratio of glassy modulus and modulus at crossover frequency.

One of the main concerns with the CA model was its assumption of glassy modulus (G_g) as 1 GPa. When Stastna et al. (1997) investigated this issue, greater prediction accuracy especially at high stiffness was obtained when the G_g is treated as a free parameter than as a constant. Another attribute of the CA model which makes it less beneficial is that it only works well for the $|G^*|$ values where the phase angle lies between 10° and 70°. That is, the model doesn't perform well at higher temperatures, long loading times (lower frequency), or the combination of these two conditions.

2.5 Studies Relating Molecular Structure to Linear Viscoelasticity

Christensen and Anderson in early 1990's presented the chemical-physical property relationships for asphalt cements in cognizance with the dispersed polar fluid model as discussed earlier (Christensen and Anderson 1992). The work carried out by the authors was under the auspices of the strategic highway research program (SHRP) where in chemical and physical properties of asphalt were evaluated and performance related specifications were developed for asphalt binders. In their work the authors present a mathematical model for describing the linear viscoelastic behavior of asphalt binders and subsequently develop a series of empirical chemical-physical property relationships. These relationships relate the chemical compositions of these binders to the viscoelastic model

parameters. It should be remembered that these relationships were developed assuming a dispersed polar fluid model for asphalt microstructure, which assumes asphalt to be a single phase system. The linear viscoelastic parameters which were used for deriving these relationships included the defining temperature or the reference temperature (T_d) in the temperature shift factor function or the Willian-Landel-Ferry (WLF) equation. The defining temperature was related to the asphaltene content and the number average molecular weight of the asphalt as obtained from VPO in toluene at 60°C. The crossover frequency at T_d was related linearly to the asphaltene content. The rheological index, R, which is numerically equal to the log of the ratio of glassy modulus and the complex modulus at the cross over frequency was related to the contents of saturates, polar aromatics and napthene aromatics. The final relationship derived by the authors is the one which relates the steady state viscosity at T_d to the asphaltene and the polar aromatics content in the binder.

The authors argue that the relationships which are semi-empirical in nature cannot be used for engineering design purposes but are certainly useful for a semi-quantitative evaluation of the effect of chemical compositional parameters on the mechanical behavior of asphalts. The authors provide an example of using these relationships to estimate the modulus values and thereby predict the performance of a given asphalt. The authors believe the relationships can be used to estimate limiting stiffness temperature, which represented the temperature for a given stiffness achieved at a selected loading time. This limiting stiffness temperature is then shown to represent the predicted cracking temperature for a given asphalt binder.

Another structural model which relates the structural features of asphalt binders to its linear viscoelastic parameters was developed by Leseur et al. in 1996 (Leseur et al. 1996). The authors first reviewed the existing models on asphalt viscoelasticity. The authors stated that the existing models used time-temperature superposition principle (TTSP) to develop mastercurves for G′ and G″ and subsequently derive relationships based on parameters used to derive these mastercurves, an example of which is the model presented by Christensen and Anderson discussed above. The authors use phase angle mastercurves to show that TTSP holds good only at low temperatures but fails at higher temperatures especially in asphalt which have high asphaltene contents and which contain high crystallized fractions. The authors then developed their own model which is based on assuming colloidal structure for bitumen. The colloidal structure assumes that asphalt is a colloidal dispersion of temperature dependent solid phase in a liquid matrix. Two separate models were developed, one for high temperature and another for low temperatures. The model developed was bimodal in nature which combined a Roscoe-Brinkman viscosity law to Havriliak – Negami equation at high temperatures and at low temperatures to the Anderson model at low temperatures. The input parameters required to deduce the viscoelastic response of an asphalt binders included, the glass transition temperature, WLF coefficients, asphaltene content, maltene zero shear viscosity, reduced solvation parameters, corresponding activation energies and the asphaltene core radius.

2.6 Understanding Non-Linear Viscoelastic Behavior of Asphalt Binders

The nonlinear viscoelastic behavior of asphalt binder has been a topic of interest in the recent years and has been studied extensively. However, one of the first researchers to

provide insight into non-linear behavior of asphalt was Trouton in 1906, who observed non-Newtonian behaviors in asphalt like substances (Trouton 1906). Although the non-Newtonian behavior showed by the author was of linear viscoelastic, Leseur pointed out that non-linear effects could also be observed especially when studying bitumens with constant stress or strain experiments (Leseur 2009). Non-linearity was precisely described first by Saal and Koens, who found that bitumen had a plastic behavior (Saal and Koens 1933).

Material scientists have studied non-linear phenomenon since 1960's for different viscoelastic materials and proposed methods for analysis, which included Fourier transform and stress waveform analysis (Komatsu et al. 1973, Dodge and Krieger 1971, and Tee and Dealy 1975). The importance of non-linearity consideration can be explained from the composition standpoint. Asphalt binder may constitute about 10-15% by volume of a typical asphalt concrete mixture, which is sufficiently large to cause notable and important impacts on the mechanical properties (Underwood and Kim 2015).

The current specifications for asphalt binder are based on rheological experiments performed in the linear viscoelastic range (LVE) range of the material. In the field of polymer science, such tests are referred to as small amplitude oscillatory shear (SAOS) tests (Kyu et al. 2011). However, studies have also been carried out to examine material properties beyond LVE limits. The strain levels employed in these tests are beyond the LVE limits and the tests are termed as large amplitude oscillatory sweep (LAOS) tests.

Masad et al. studied the influence of non-linear viscoelasticity (NLVE) on asphalt binders using temperature frequency tests and stress sweep tests at 10, 20, 30, and 40°C

and 10, 5, 1, and 0.1 Hz (Masad et al. 2008). The authors identified non-linearity in asphalt binders for the conditions tested, but no distinction of the cause of these nonlinearities was proposed. Motamed et al. evaluated NLVE in polymer modified asphalts at 28°C and 40°C (Motamed et al. 2012). The authors suggested that NLVE arises due to free volume change and three-dimensional stress state interaction. The strain decomposition principle by Schapery (Schapery 1999) is adopted in many such studies wherein the NLVE mechanism is separately modelled and the resulting strains are summed together to yield the total material response.

Underwood and Kim (Underwood and Kim 2015) theorized that the existing methods used to assess NLVE may not explicitly account for NLVE in the strain decomposition and the impact is only considered through the influences it may have on the non-linear functions describing behaviours of fracture, continuum damage, permanent deformation, etc. In the same paper, Underwood and Kim proposed an experimental methodology to isolate the NLVE impacts in a cyclic sinusoidal loading test. The test employed by the authors for characterizing non-linearity in asphalt binders and mastics is the repeated stress sweep (RSS) test. The test is a simple stress sweep experiment in which the sample is loaded at a fixed frequency and temperature but with incrementally increasing stress levels. Similar experiment can be performed by incrementally increasing the strain levels. The experiment and the steps involved have been explained in great detail by Underwood and Kim.

There are two other test methods which have gained prominence recently, they are the MSCR (Multiple Stress Creep and Recovery) test (D'Angelo 2007, AASHTO T350)

and Linear Amplitude Sweep (LAS) test (Hintz and Bahia 2013). The reason both these tests can be used to study non-linearity is because the range of strains in which the test is conducted far exceeds the LVE range of asphalt binders. While the main motivation behind the development of MSCR test is to identify a parameter that is a better indicator of rutting, LAS test was developed as a test that can evaluate the fatigue characteristics of asphalt binder fairly quickly.

The MSCR test was developed based on the creep and recovery work conducted on asphalt binders and mixtures. During SHRP, the Repeated Simple Shear Test ay Constant Height (RSST-CH) was developed by researchers at UC Berkeley. The test was developed to characterize the rutting performance of asphalt mixtures and was conducted using repeated cycles of 0.1 second shear followed by a rest period of 0.6 seconds. This concept was adopted in binders during the NCHRP 9-10, where the researchers used a repeated creep and recovery test to characterize the expected rutting performance of modified asphalt binders (Bahia et al. 2001). The NCHRP 9-10 project recommended a test to be performed on a DSR with a stress in the range of 30 Pa to 300 Pa for 100 cycles, with one second of loading time followed by nine seconds of unloading time. D'Angelo showed that a single stress level did not completely account from the stress dependency of the modified binders and thereby proposed that multiple stress levels need to be used. This gave rise to the MSCR test.

The MSCR test consists of performing 20 creep and recovery cycles on asphalt binder sample on a DSR at high performance grade temperatures. Of the 20 cycles, 10 cycles are performed at 0.1 kPa and remaining 10 cycles at 3.2 kPa. All cycles have a

loading period of 1 second, followed by recovery of 9 seconds. The parameter of interest from the test are the non-recoverable creep compliance, J_{nr}, at each stress level. relates the strain response of the sample to the applied stress. A material that deforms by a large amount under a prescribed load has a high Jnr, while one that deforms very little has a low J_{nr}. For specification, low J_{nr} asphalts would be used for high value applications (interstates, US routes, etc.), higher J_{nr} asphalts would be used for less critical and lower traffic volume applications, and very high J_{nr} asphalts would be avoided altogether. The parameter and he test in general is being currently used by many states in the US, to grade their asphalt binders as per the new grading criteria listed in AASHTO M332.

The binder fatigue parameter, $|G^*|\sin\delta$ introduced during the SHRP work is based on small strain rheology and does not consider damage resistance. Required was a performance based assessment of binder fatigue resistance. For which Linear Amplitude Sweep Test was proposed. The test was proposed as a surrogate to the time sweep test, which is a conventional fatigue test with repeated cyclic loading at constant strain amplitudes. One of the drawbacks of the time sweep test, which prevents it from being considered for specification, is the uncertainty in test duration. The linear amplitude sweep (LAS) test is a strain controlled cyclic torsion test conducted on a dynamic shear rheometer at a fixed frequency, loading cycles and incrementally increasing strain levels (Hintz and Bahia 2013). The test is run at 10 Hz, with 1% strain increments from 0% to 30%) and a total of 3000 cycles are applied, this means the test is essentially completed in five minutes. The uncertainty in duration with the time sweep test was overcome with the LAS test, which has fixed loading cycles. The damage characterization conducted in the LAS test is

similar to the time sweep test with considers simplified viscoelastic continuum damage (S-VECD) formulation. However, one of the main drawbacks of the LAS test is that it cannot separate damage from non-linear viscoelasticity. This can be done using the repeated stress sweep test, which was used for the NLVE characterization in this dissertation.

Chapter 3 Materials and Experimental Methods

In this chapter, the experimental techniques and the study materials used in the study are discussed. An overview of all the asphalt binders, conditioning techniques, and sample preparation methods are provided. As outlined in chapter 1, the experiments to be performed are divided into two main categories, molecular structure characterization and mechanical characterization. The main molecular structure characterization technique employed was performing the LDMS on all study asphalts. Apart from the LDMS experimentation, Fourier-Transform Infrared Spectroscopy (FT-IR) was also performed on all study binders. Detailed discussion about the two methods and their subsequent analysis is also provided. With regard to the mechanical characterization techniques, the experimental procedure along with the subsequent data analysis for temperature-frequency sweep, time sweep test, MSCR test and RSS test are explained.

3.1 Study Materials: Asphalt Binder Set 1

For this study two sets of asphalt binders have been used. Set 1 consisted of fifteen different asphalt binders have been sourced from the three asphalt suppliers in Arizona (Alon Asphalt Company, Holly Frontier, and Western Refining). Ten of the fifteen binders are non-polymer modified (referred to as the Group 1 Asphalts) and five are polymer modified (referred to as the Group 2 Asphalts). For set 1 asphalts, the crude sources of the asphalts have been provided by two suppliers, X and Y. All asphalt binders from supplier X are based out of crude from Canadian Bow River. The non-polymer modified binders of supplier Y are based on Western Canadian Select (WCS) crude, where as its polymer modified binders are a blend of WCS and West Texas Intermediate (WTI). All fifteen

binders with their designations are presented in Table 1 A detailed discussion regarding the basis of selection of asphalts is presented in sections below.

Table 1: Set 1 Asphalt Binder Grades Used in the Current Study and their Notations.

Group	Supplier	Notation	Grade	Group	Supplier	Notation	Grade
1	X	X1	PG 70-10	2	X	X3	PG 64H-22
		X2	PG 76-16			X4	PG 64V-22
	Y	Y1	PG 64-22			X5	PG 76-22TR+
		Y2	PG 70-22		Y	Y5	PG 70H-16
		Y3	PG 70-16			Y6	PG 70V-16
		Y4	PG 76-16				
	Z	Z1	PG 64-22				
		Z2	PG 70-22				
		Z3	PG 70-10				
		Z4	PG 76-16				

3.1.1 Group 1 Asphalts

This group consists of the non-polymer modified asphalts. The basis of the selection of these asphalts is current usage in the state of Arizona. The most prevalent grades specified in ADOT projects were identified and are shown in Figure 3-1. The three most prevalent grades in Arizona (PG 64-22, PG 70-10, and PG 76-16) constitute approximately 89% of the asphalt (by lane mileage). Of these, PG 76-16 is the singularly most used asphalt grade. Based on this usage, PG 76-16 has been sampled from each of the three suppliers and PG 70-10 and PG 64-22 are sampled from two of the three suppliers. Other relevant grades in the state included PG 70-22 and PG 70-16, which have also been sampled based on the supplier's current usage.

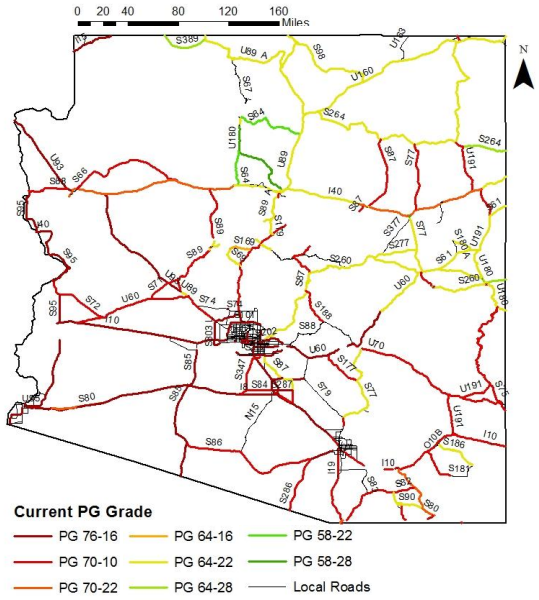

Figure 3-1. Distribution of Current Asphalt Binder Grades across Arizona.

3.1.2 Group 2 Asphalts

This group consists of the polymer modified asphalts. Currently, the use of polymer modified asphalt binders is not prevalent in the state of Arizona, with PG 76-22TR+ being the only such material specified. As shown in Table 1, five different polymer modified asphalts have been used in the study. These include, first, the PG 76-22TR+ binder that is currently specified in the state and then four other polymer modified asphalts, PG 64(H,V)-22 and PG 70(H,V)-16, that meet the AASHTO M332 specification and that could likely be supplied in Arizona under a similar specification.

While the polymer used in PG 64(H,V)-22 and PG 70(H,V)-16 is SBS, the type of SBS and its dosage is proprietary to the supplier. However, since PG 76-22 TR+ is a specification binder, details regarding its composition are available. The binder has 8-10% of digested crumb rubber, along with 3% of SBS.

3.1.3 Oxidation Conditions for Set 1 Asphalt Binders

For set 1 asphalts, all materials were subjected to short term aging using Rolling Thin Film Oven (RTFO) and subsequently long-term aging using Pressurized Aging Vessel (PAV) at 110°C. The short-term aging in RTFO was conducted in accordance with AASHTO T 240, where in the samples are aged for a period of 85 minutes at a temperature of 163°C and air flow rate of 4 l/min. After short term aging, the asphalt binder samples were aged in a pressurized aging vessel (PAV) to simulate long term aging. The samples were aged for 20 hours at 110°C, and 2.1 MPa pressure.

3.2 Study Materials: Asphalt Binders Set 2

Set 2 asphalt binders consisted of three asphalt binders, two of which were non-polymer modified and one polymer modified. While for majority of the study set 1 was used, set 2 were used in this study as part of the time sweep tests performed in chapter 5. These asphalt binders were sourced as part of the NCHRP 09-54 project (Kim et al.). The sources of the binders, the notations and the PG grades are presented in Table 2. There are two non-polymer modified asphalts in this study, which are B1 and B2 and the lone polymer modified binder is a SBS modified PG 70-28 binder, sourced from FHWA, used at their accelerated loading facility.

Table 2. Set 2 Asphalt Binder Grades Used in the Current Study and their Notations.

Source/Supplier	Notation	Grade
Asphalt Research Consortium	B1	PG 58-28
NC-Wilmington	B2	PG 64-22
FHWA-ALF	B3	PG 70-28

3.2.1 Oxidation Conditions for Set 2 Asphalt Binders

The oxidation conditions for these set of binders are different from that used for set 1 asphalts. The reason for this difference is that these binders were specifically aged at the temperatures given in Table 3 to serve the purposes of the NCHRP 09-54 project. For the project, it was desired to age asphalt binders in a RTFO as per AASHTO T 240 followed by in a PAV at temperatures that would simulate 7, 15, and 22 years of service. While the methodology used in the calculation of these temperatures doesn't pertain to the scope of the study, detailed description of the same is provided by Gundla et al. (2017). The PG grades of the aged asphalt binders are presented in Table 4.

Table 3. PAV Aging Temperatures Used for Set 2 Asphalt Binders

PG Grade	**Notation**	**T_{PAV} (°C)**		
		Simulated Years in Service		
		7	15	22
PG 58-28	B1	89	97	104
PG 64-22	B2	91	101	107
PG 70-28	B3	90	98	103

Table 4. Summary of the Conventional and Continuous PG Grades Characterized for the Aged Binders

Binder Type	**Aging Level (years)**	**Conventional PG Grade**	**Continuous PG Grade**
B1	7	76	71
	15	76	73
	22	82	77
B2	7	82	79
	15	82	82
	22	88	86
B3	7	88	83
	15	88	85
	22	88	87

3.3 Experimental Methods: Chemical Characterization

In this section, the experimental methods, pertaining to the chemical characterization of asphalt binders used in this study are discussed.

3.3.1 Laser Desorption Mass Spectroscopy (LDMS)

While most of the theoretical details regarding the basics of the experiment have been provided in the previous chapter, in this chapter sample preparation techniques along with techniques to obtained distribution spectra with good S/N ratio are discussed. Shown in Figure 3-2 is the Applied BioSystems LDMS instrument used in the current study.

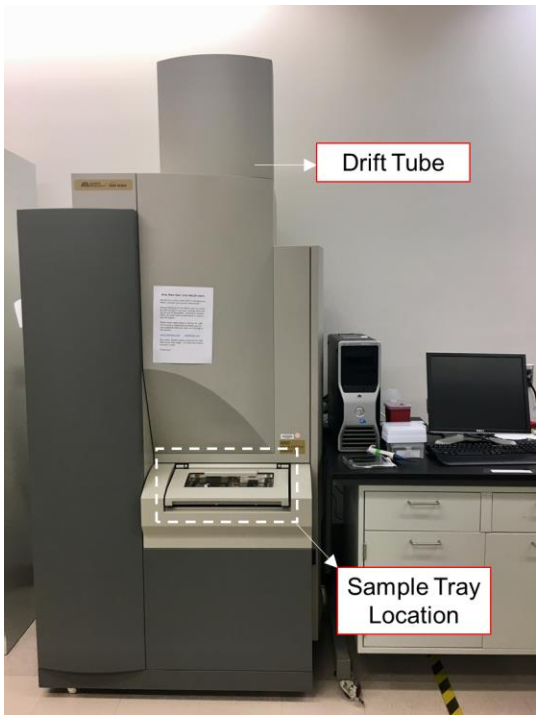

Figure 3-2: Applied BioSystems MDS SCIEX LDMS Instrument at Arizona State University.

3.3.1.1 Sample Preparation

For preparing the samples for LDMS testing, different trials were performed to identify the most suitable method to prepare the samples. These trials included testing at different

dilution ratios and using different matrices to evaluate the method that provided the best spectra among all. The attributes that were evaluated among different methods were the general shape of the spectra, the signal quality and noise. Most of the trials were performed using only one asphalt binder, which is B2 binder, PG 64-22. In some cases, binder B1, PG 58-28, was also used. The different matrices and dilution ratios evaluated and it was decided that a dilution level of 125 mg/ml will be used for preparation samples for LDMS and no matrix will be used. Detailed description of the analysis conducted to arrive at this conclusion is presented in Appendix A.

For preparation of sample using 125 mg/ml dilution ratio, first, 0.625 g of asphalt was weighed out in a small beaker. To this, 5 ml of toluene was added. The beaker containing the solute and the solvent was manually agitated to speed up the dilution. The samples were agitated for about 10 minutes or until complete dissolution was seen. Note, that polymer modified asphalts took slightly longer time to dissolve. Once the solution was prepared it was transferred in a small glass vial. Care was taken so that the solution doesn't come into contact with plastic cap on top of the glass vials. Subsequently, from the vial, using a micro pipette, 0.5µl of this solution was placed on the LDMS sample target.

A total of three targets were spotted for each binder condition i.e. original, RTFO, and PAV. The main reason for using three targets was to utilize the feature of spectral accumulation to improve the S/N ratio of the spectra. The instrument was an Applied Biosystems MALDI-TOF analyzer. The laser employed was a N_2 laser and was operated at an intensity of 5300 (no units) for optimal signal quality. Each target was bombarded with the laser at 5 different locations within the target, with each bombardment constituting

375 laser shots. After the first bombardment, spectral quality was checked to maintain the S/N ratio greater than 1000. The manufacturer's software feature was used to automatically combine the five spectra to arrive at one singular spectra for that target. Spectral accumulation in simplistic terms is a technique of data overlapping. Once the spectra for the first target was gathered, spectral accumulation was continued onto the second and then the third target. This way, for each condition, using the technique of spectral accumulation, 15 spectra can be accumulated to form one singular spectra for that condition.

This procedure was performed on asphalt binder in the tank storage condition, the short-term oven oxidized condition (using the rolling-thin film oven), and long-term oven oxidized condition (using the pressure aging vessel). Care was taken to complete testing of all three conditions as quickly as possible to minimize the evaporation of volatiles. The entire procedure, from placing the solution on the targets to accumulation of the spectra was completed in 15 minutes.

3.3.1.2 Data Filtering and Obtaining Molecular Weight Distribution

The molecular weight distribution is essential a plot between the masses encompassed by the asphalt binder to the spectral intensity at those mass ranges. The spectral intensity at a particular mass can be thought of as a surrogate to the number of moles of a molecule at that mass. The spectral height basically denotes the abundance of these molecules. The spectra obtained from the above mentioned experimental process is a raw spectra, which was subsequently filtered using the Savitzky-Golay filtering technique. An example of raw molecular weight distribution for X3, PG 64H-22 at its original condition is shown in Figure 3-3. The spectral intensity was normalized for ease of comparison. The data filtering

technique adopted in the study identifies peak at each mass, and fits the distribution to a first order polynomial function.

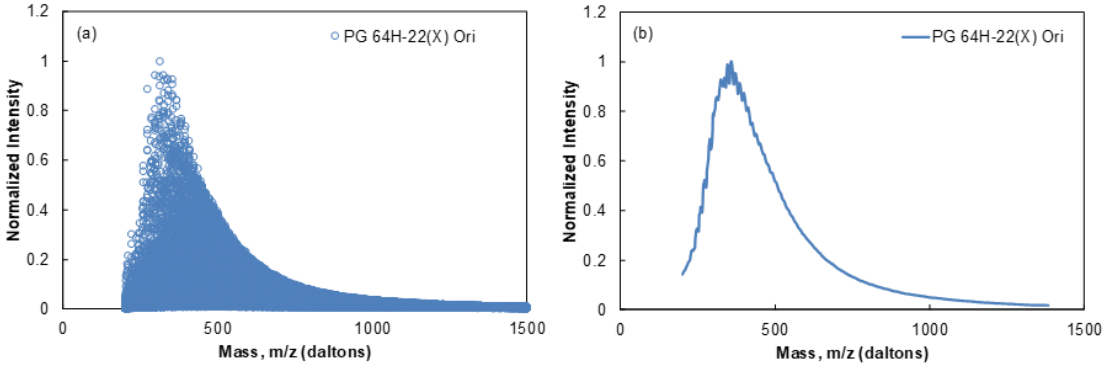

Figure 3-3. Molecular Weight Distribution of Binder X3 in (a) Raw form; and (b) Filtered form.

3.3.2 Fourier Transform Infrared Spectroscopy

In the current study, the changes to the chemical properties due to oxidation are measured using the Attenuated Total Reflectance Fourier Transform Infrared Spectroscopy (ATR-FT-IR) method. The test measures the infrared spectrum of energy absorption of the aged and unaged binder at multiple wavelengths. The spectra resulting from the ATR-FT-IR method contains peaks at wavenumbers that correspond to different types of bonds within the asphalt cement. Oxidation results in an increase in the number of double bonds between hydrocarbons and oxygen, which can be detected with the ATF-FT-IR test. The two specific functional groups examined in this study are the carbonyl and sulfoxide groups. Studies have linked the increase in absorbances at these groups to oxidation of asphalt. The metrics adopted are the area under the carbonyl and sulfoxide peaks (Jemison et al. 1992, Petersen and Glaser 2011), referred to as CA and CA+S respectively. The effect of

oxidation is quantified by examining the changes in these quantities with RTFO and PAV aging.

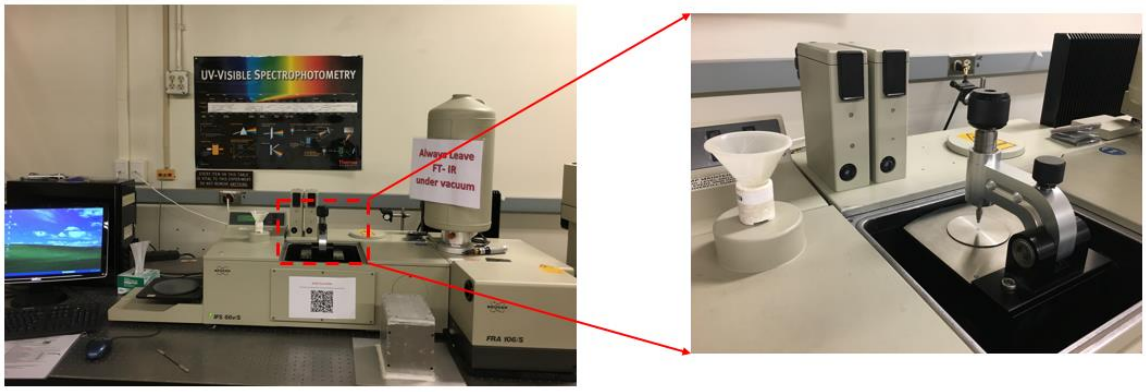

Figure 3-4. Fourier Transform Infrared Spectroscopy Instrument at Arizona State University.

The spectra were obtained in the mid-IR range using a KBr beam splitter. The sample preparation consisted of first scooping a small amount asphalt binder at room temperature onto a aluminum petri dish. The dish subjected to gentle heat of about 135°C on a hot plate for about 30 seconds, to bring the asphalt into liquid consistency. This asphalt was then placed on the diamond using a silicone spatula. After which the test was conducted.

A typical FT-IR spectrum for asphalt binder is shown in Figure 3-5. The figure also points out the dominant peaks in the spectrum, along with the bonds that those peaks represent. The two peaks that are of interest are the sulfoxide and the carbonyl peaks. Asphalt oxidation studies (Jemison et al. 1992, Petersen and Glaser 2011) have shown that the level of oxidation can be linked directly to the area under the sulfoxide and carbonyl peaks. A graphical representation of how the area is calculated is presented in Figure 3-6. A program was specifically developed for the purpose of calculation of carbonyl and

sulfoxide areas. A step by step procedure which conveys the implementation process of the program is presented Appendix B.

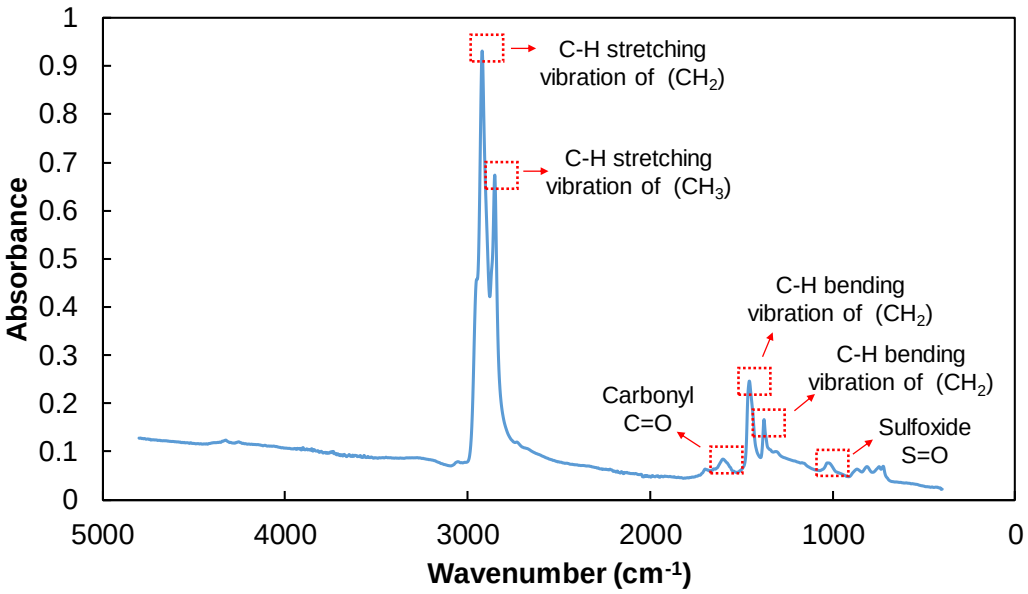

Figure 3-5. Typical FT-IR Spectrum of Asphalt Binder with Dominant Peaks and the Bonds they Represent.

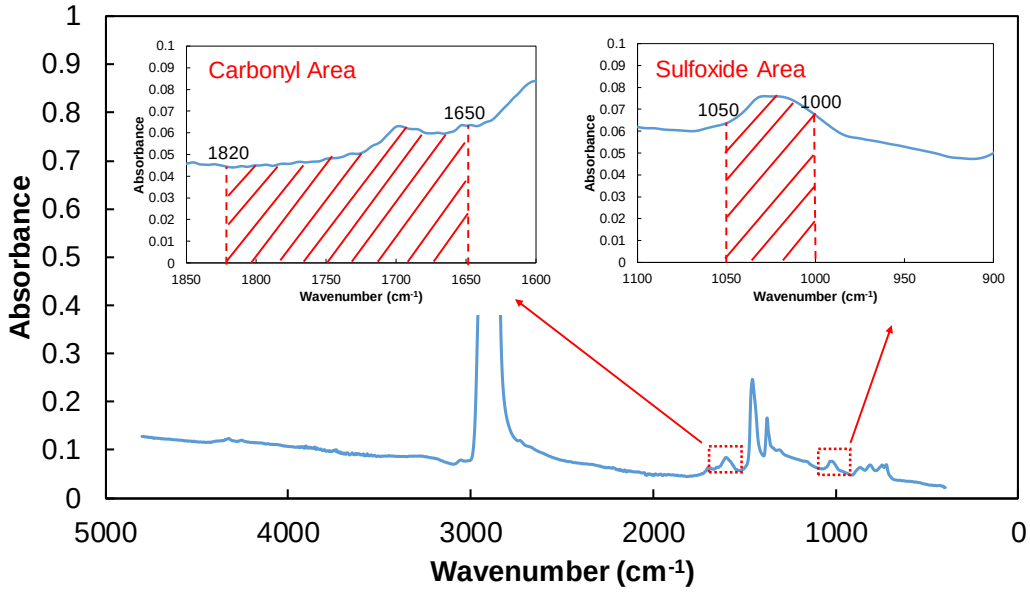

Figure 3-6. Graphical Representation of Carbonyl and Sulfoxide Area Calculation.

3.4 Experimental Methods: Rheological Characterization

3.4.1 Linear Viscoelastic Characterization

Temperature and frequency sweeps were conducted at 10, 20, 30, 40 and 54°C and at a frequency range of 30 - 0.1 Hz (30, 14, 6.5, 3, 1.4, 0.65, 0.3, 0.14, 0.1 Hz). The tests were performed on a Anton-Paar MCR 302 dynamic shear rheometer as shown in Figure 3-7. Prior to all testing a strain sweep experiment was conducted and the tests were performed at strain levels below the linear viscoelastic limit, but above the resolution limits of the equipment (100 – 400 με). Tests were conducted from low temperature to high temperature and from high frequency to low frequency. The modulus and phase angle values used in subsequent calculations were taken directly from the test equipment's internal calculation; however, the quality of the torque and encoder signals were monitored continuously throughout the testing to ensure that the calculated results were representative of the test.

After experimental characterization of the dynamic modulus, a form of the Christensen-Anderson-Marasteanu (CAM) model in Equation (8) was used to develop the master curves. The William-Landel-Ferry (WLF) equation shown in Equation (9) was used model the t-T shift factor.

$$\left|G^*\right| = \frac{10^g}{\left(1+\left(\frac{\omega_c}{\omega_R}\right)^k\right)^{\frac{m_e}{k}}} \tag{8}$$

$$\log a_T = \frac{C_1(T-T_R)}{C_2+T-T_R} \tag{9}$$

where; $|G^*|$ is the dynamic shear modulus (Pa), 10^g is the binder glassy modulus (Pa) (determined through optimization), ω_c is the crossover frequency (rad/s) (a fitting coefficient), m_e and k are fitting coefficients, T is the test temperature (°C), T_R is the reference temperature (°C), and C_1 and C_2 are the time-temperature shift factor function fitting coefficients.

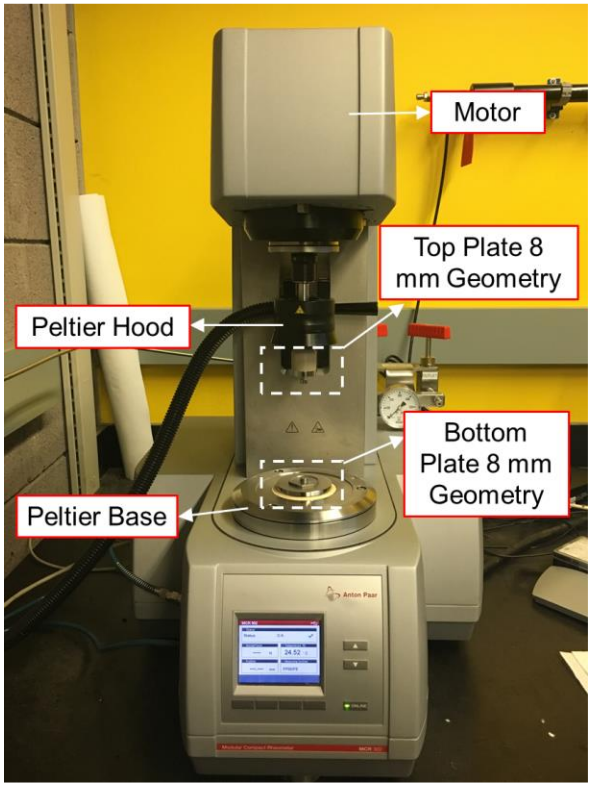

Figure 3-7. Anton Paar MCR 302 Dynamic Shear Rheometer at Arizona State University.

3.4.2 Non-Linear Viscoelastic Characterization

3.4.2.1 Time Sweep Tests

Controlled strain fatigue tests were performed to assess the fatigue properties of the binders and to characterize the continuum damage model. The samples were subjected to a continuous constant shear strain sinusoidal loading. The tests were performed on TA

Instruments AR 2000 EX dynamic shear rheometer shown in Figure 3-8. The time sweep tests were conducted two serve two purposes in this dissertation. First, they were used to study the non-linear behavior of asphalts at intermediate temperature. For this purpose, the tests were conducted at 13°C, a frequency of 10 Hz, and four different zero to peak strain magnitudes of 2.5%, 5%, 6%, and 7.5%. For any asphalt only two of the above-mentioned strain levels were used. The asphalt binders under set 2 were used for this assessment. Secondly, the time sweep test in this dissertation is used in studying the non-linear viscoelastic behavior under large amplitude oscillatory shear (LAOS) at high temperatures. The tests were performed at 40°C and 64°C. The zero to peak strain level used for this study ranged from 10% to 60%. These tests were conducted on selected set 2 asphalts, at original and PAV aged condition. For tests at both intermediate and high temperatures, the raw data was acquired using an independent program setup on LabVIEW. The acquired data is used for data analysis. The signal obtained by the LabVIEW program is corrected for inertia and bearing friction during the data analysis process. The values of calibrated inertia and bearing friction can be obtained from the calibration tab of the Trios test file. Trios is operational software for the TA Instruments AR 2000 EX dynamic shear rheometer. The modulus values used in the analysis were calculated by the internal algorithm in Trios.

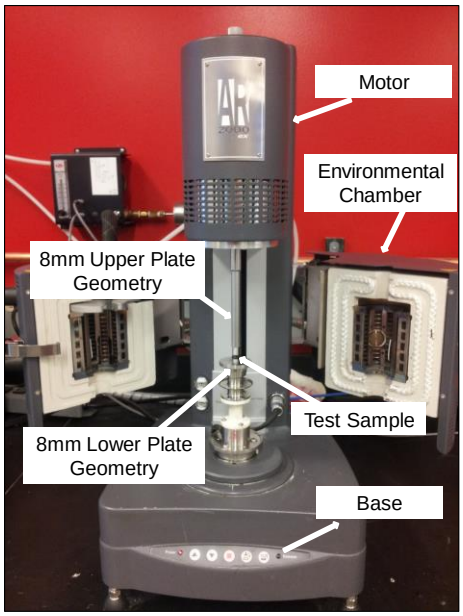

Figure 3-8: TA Instruments AR 2000 EX Dynamic Shear Rheometer at Arizona State University.

3.4.2.2 Multiple Stress Creep and Recovery Test

The Multiple Stress Creep and Recovery (MSCR) test is standardized by both the American Association of State Highway and Transportation Officials (AASHTO) and the American Society of Test Methods (ASTM): AASHTO T 350 and ASTM D7405 respectively. The essential elements in both standards are the same: a sample of asphalt 25 mm in diameter and 1 mm thick is situated between two parallel plates mounted to a DSR; the sample is conditioned to a fixed and specified temperature; the sample is loaded repeatedly with a series of square shaped stress-rest pulses (1 second loading and 9 seconds rest) at 0.1 kPa and 3.2 kPa; and quantities relating the stress input to the strain response are calculated. A typical strain response from the 10, 3.2 kPa loading cycles are shown in Figure 3-9.

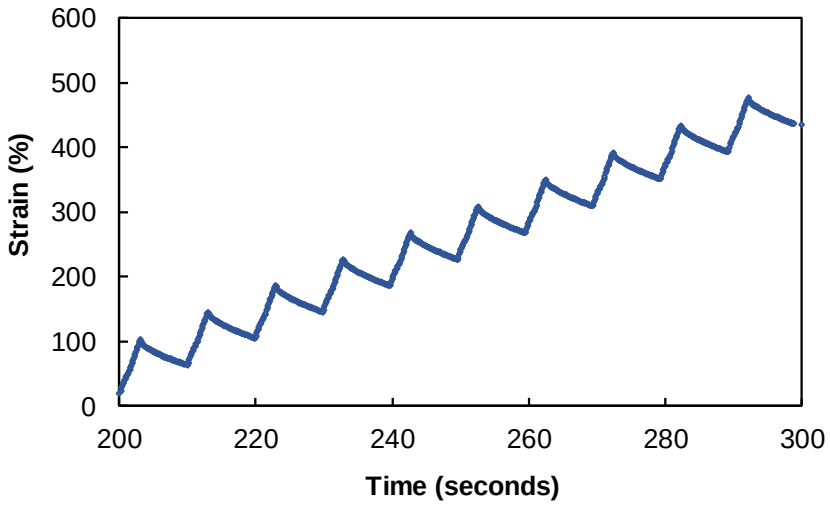

Figure 3-9. Typical MSCR Strain Response During 3.2 kPa Stress Cycles.

The four parameters extracted from this test are the non-recoverable compliance at both 3.2 kPa and 0.1 kPa stress levels, $J_{nr3.2}$ and $J_{nr0.1}$ respectively, the percentage of difference between these two quantities (J_{nrdiff}), and the percent of strain recovery during the 3.2 kPa loading, $R_{3.2}$. Details of the calculations are presented in AASHTO T350. The tests are conducted on the set 1 asphalt binders at their AASHTO M320 high temperature grade and at ±6°C, except for the PG 76-XX asphalts, which are tested at 76, 70, and 64°C.

In this study, the MSCR test is part of the experimental plan implemented to gain insight into the NLVE behaviors of Arizona asphalt binders. More specifically, the objective of performing the MSCR test in this study is to scrutinize the effectiveness of the J_{nrdiff} parameter, its limitations, its physical significance and also evaluate alternatives that can possibly replace J_{nrdiff}.

3.4.2.3 Repeated Strain/Stress Sweep Test

Repeated stress sweep (RSS) tests are used in the present study to assess the strain level non-linearity of binders. An alternative way of determining the same would be to perform a temperature frequency sweep test at high strain levels, but this test will smear the effect of damage in to the responses, hence it is not used. The loading history can consist of multiple groups, with each group consisting of a finite number of blocks that have incremental stress levels. These stress levels are constant within a group, but increase from one group to another. The schematic of the loading history is shown in Figure 3-10.

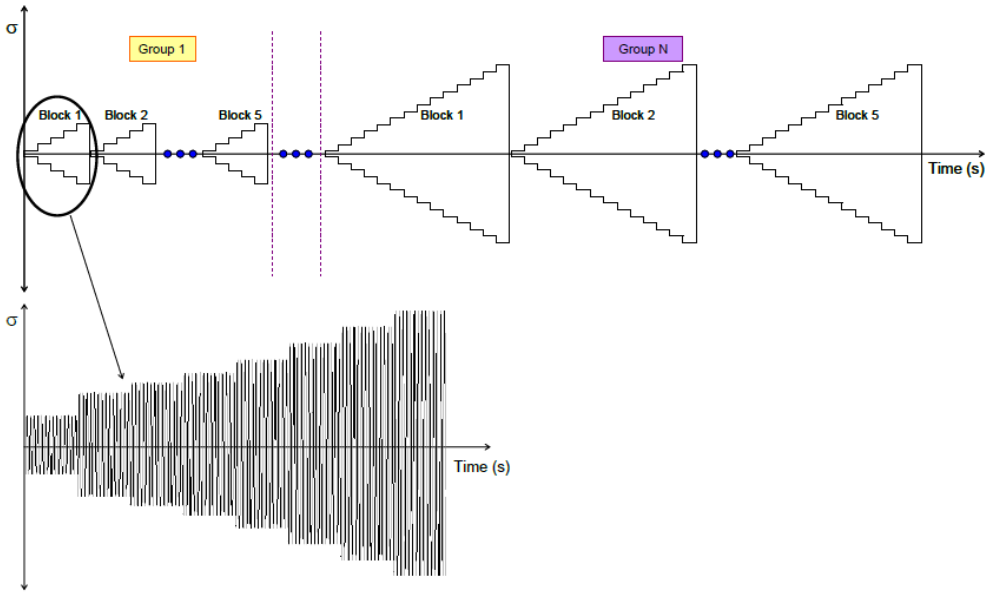

Figure 3-10. Schematic of Repeated Stress Sweep Test Loading History.

In the present study, two loading groups are proposed. Loading group 1 consists of two blocks and loading group 2 consists of five blocks. Figure 3-11 presents an example of the modulus response patterns for the loading groups taken from a previous study. This test

was performed on an asphalt mastic sample at 13°C. The different series shown in the figure correspond to a particular loading group (*G*) and block (*B*). |*G**| is the primary property of interest in the RSS test and is denoted as $|G^*|_{RSS}$. This parameter in turn is affected by other mechanisms in addition to nonlinear viscoelasticity, and thus, additional steps must be taken to isolate only the nonlinear viscoelastic effects. The term $|G^*|_{NL}$ is used in the present study to reflect only the nonlinear viscoelastic component of the $|G^*|_{RSS}$. Equation (10) is used to distinguish $|G^*|_{NL}$ from $|G^*|_{RSS}$. This step, along with important observations from Figure 3-11, is explained in the following paragraphs.

$$\left|G^*\right|_{NL} = \frac{\left|G^*\right|_{RSS}}{F} \tag{10}$$

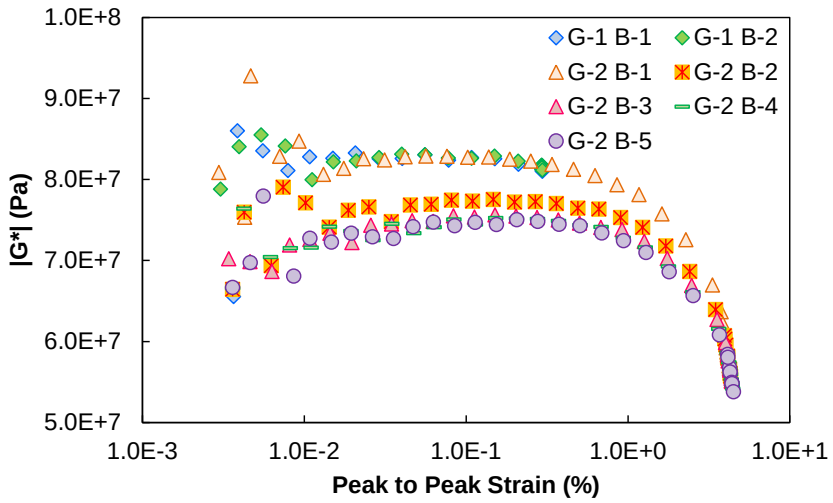

Figure 3-11. Typical Modulus Responses of RSS Loading Group.

The important observations that can be made from Figure 3-11 are as follows.

- For both loading groups, the modulus value decreases with an increase in strain level.

- No permanent change in the material is seen during group 1 loading, as the material response is the same for G-1 B-1 and G-1 B-2.
- For group two, some permanent change in the material can be seen, but this change is not fully permanent, as the modulus values at the beginning of blocks 2 through 5 are higher than the modulus value at the end of the preceding block. For example, the modulus value at the beginning of block G-2 B-4 is higher than the modulus value at the end of G-2 B-3.
- The reduction in modulus value is not fully recoverable because the modulus value at the smallest strain levels decreases from block to block. For example, compare the modulus value at the beginning of block G-2 B-2 to that at the beginning of block G-2 B-3.
- After approximately three block repetitions, the balance between modulus recovery and permanent modulus change becomes stable. For example, compare the vertical distance between G-2 B-1 and G-2 B-3 to the vertical distance between G-2 B-3, G-2 B-4, and G-2 B-5.

Underwood and Kim (2014) postulated that the reduction in modulus value can be attributed partly to the nonlinear viscoelastic response of the material, whereas the pattern of apparent partial recovery can be attributed to microstructural damage. This damage will cause a proportional change in the modulus such that $|G^*|_{NL}$ and $|G^*|_{RSS}$, the modulus values obtained from the RSS test, are related to each other, as shown in Equation (10) The proportionality constant F is expected to evolve slowly and its value will change only from

one block to another. However, within a block, its value for different strains is assumed to be the same as long as the $|G^*|_{RSS}$ data collapse into a single function for subsequent blocks.

To understand the role of this *F* variable, the G1 loading results shown in Figure 3-11 should be examined. The group test results (G-1 B-1 and G-1 B-2) are unaffected by the damage. Thus, F would be equal to one. Group one tests are insufficient to characterize $|G^*|_{NL}$ as they extend only up to small strain levels of about 0.3 percent. However, group two loadings go to higher strain levels and the vertical separation of the modulus responses between the blocks suggests that F is not equal to one for all loading blocks. The overlap of G-2 B-3, G-2 B-4, and G-2 B-5 provides an opportunity to separate nonlinearity from damage. Underwood and Kim (2014) hypothesized that this type of overlap indicates that a minimum amount of damage occurs during G-2 B-3 loading, and the authors assumed that the damage is now constant for all strain levels in blocks four and five. The value of F for G-2 B-5 was determined by calculating the ratio of |G*|RSS for this block between 0.01 percent and 0.1 percent from G-1 B-1 between 0.01 percent and 0.1 percent. Upon calculating F, Equation (10) was used to calculate $|G^*|_{NL}$. The results from the RSS tests for all the materials are denoted as a ratio of the value of $|G^*|_{NL}$ at block G-2 B-5 to the average value of $|G^*|_{RSS}$ for G-1 B-1 between 0.01 percent and 0.1 percent where the material is still in the linear viscoelastic region.

In the current study, along with the time sweep test, this test is used to study the non-linear viscoelastic behaviors of asphalt binders under LAOS at high temperatures. The temperatures used for this test are similar to that used for the time sweep test, i.e. 40°C and 64°C.

3.5 Summary

In this chapter the asphalt binders used in the study along with their conditioning methodologies are described. The various experiments that will be performed as part of the study and also the test conditions are provided. Also, a brief description of the testing methodologies is given in this chapter.

Chapter 4 Relationship between Linear Viscoelasticity and Molecular Structure

The main goal of this chapter is to convey the relationship between the linear viscoelastic properties of the study binders and their corresponding molecular structure. The chapter is segmented into three main parts. In the first part, the linear viscoelastic properties of the study asphalts deduced from the temperature-frequency test are discussed. In the second part, the molecular weight distributions of the study asphalts determined using the LDMS technique, other associated molecular structure parameters are presented. Also presented in this part are the results from the FT-IR analysis on the study asphalts. Finally, a detailed discussion on the relationship between the LVE properties and the molecular structure properties is presented.

4.1 Linear Viscoelastic Characterization

4.1.1 Results from Temperature-Frequency Test

LVE characterization of the asphalt binders in this study is performed using temperature-frequency sweep experiments. The specific details of the test were provided in Chapter 3. The outputs from the temperature – frequency tests are the dynamic shear modulus ($|G^*|$) and the phase angle (δ) obtained at each of the five temperature and nine frequencies tested. The Christensen-Anderson-Marasteanu (CAM) model shown in Equation (8) is used to develop the $|G^*|$ mastercurves and the William-Landel-Ferry (WLF) equation shown in Equation (9) is used to model the time-temperature shift. The mastercurves are developed at a reference temperature of 15°C and for for all 15 study binders at three aging levels, i.e. original, RTFO, and PAV. For the sake of brevity, mastercurves of only two asphalts one non-polymer modified (PG 64-22(Z)) and one polymer modified asphalt (PG 64V-

22(X)) are shown in Figure 4-1 and Figure 4-2 respectively. The mastercurves of the remaining asphalts are shown in Appendix C. In both binders, it can be seen that the modulus increases with aging level. However, what is worth noticing is the vertical spacing between aged and original conditions between the two asphalts. It can be clearly observed that vertical spacing between original and aged conditions is greater in non-polymer modified asphalt, PG 64-22(Z) than polymer modified asphalt, PG 64V-22(X). The same is reflected in Figure 4-2. These visual observations, though not particularly important for the current study, can be quantified using the aging ratio parameter, which is the ratio of aged dynamic shear modulus to complex shear modulus at original or unaged condition for a given temperature and frequency (Gundla et al. 2017).

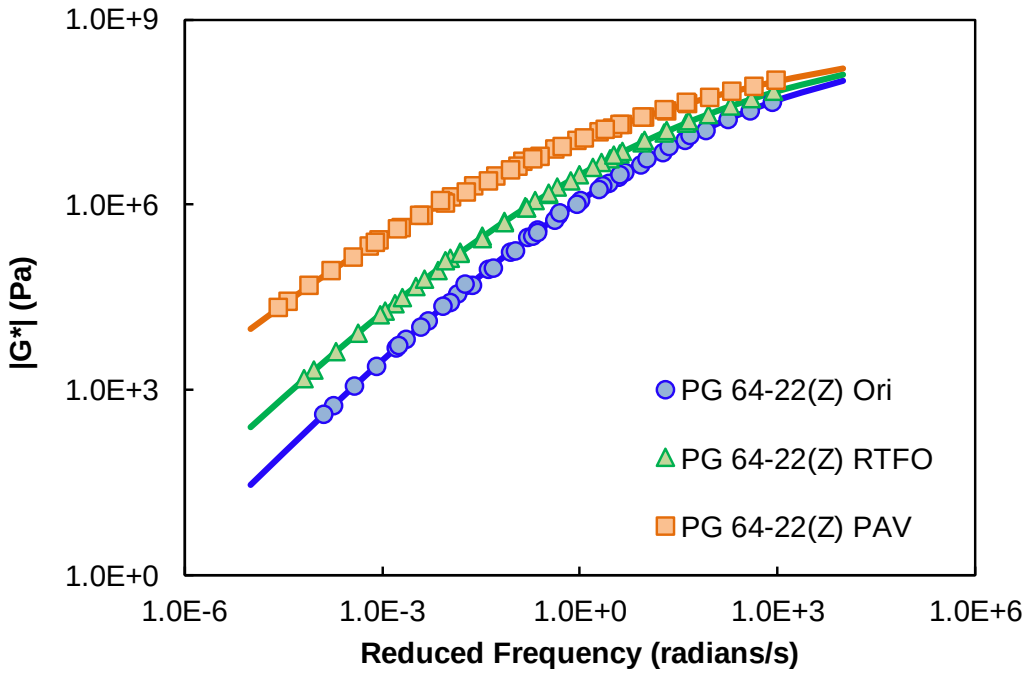

Figure 4-1: Dynamic Modulus Mastercurves for PG 64-22(Z) at Original, RTFO, and PAV Aged Conditions.

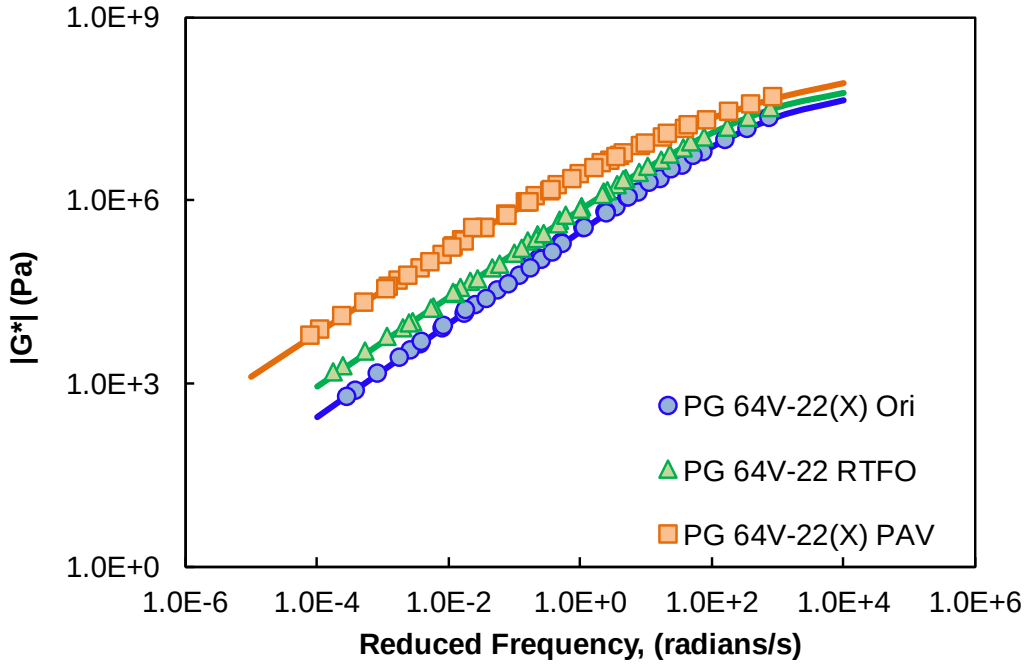

Figure 4-2: Dynamic Modulus Mastercurves for PG 64V-22(X) at Original, RTFO, and PAV Aged Conditions.

4.1.2 Calculating LVE Parameters

After the modulus mastercurves are constructed, three parameters are calculated using the CAM model fit parameters. They are; crossover modulus $|G^*_c|$, glassy modulus $|G^*_g|$, and rheological index (R). The term "crossover modulus" essentially refers to the value of the complex shear modulus at the condition where storage modulus (G') and loss modulus (G'') crossover, i.e. are equal. This condition occurs when the phase angle is 45°. The glassy modulus refers to the dynamic modulus at extremely low temperatures, high frequencies or short loading times where the asphalt encounters "glass" like behaviors. In SHRP studies which used the Christensen – Anderson (CA) model, this value is fixed at 1 GPa. In this study the glass modulus, which is also a parameter of the CAM model, is set as a free variable in the optimization process. The final parameter that is calculated is the rheological

index (*R*). *R* is the shape parameter in the CA model and is mathematically equal to the logarithmic ratio of glassy modulus and cross over modulus as shown in Equation (11). According to Christensen and Anderson (1992), the rheological index is directly proportional to the width of the relaxation spectra. The concept of relaxation spectra and the means to characterize it will be discussed in detail in the next section. The values of these three LVE parameters at original, RTFO, and PAV aged conditions are summarized in Table 5.

$$R = \log\left(\frac{|G_g^*|}{|G_c^*|}\right) \tag{11}$$

The main observation that can be made from Table 3 is that the *R* value increases with aging, indicating that the relaxation spectra broadens for asphalts with higher stiffness.

Table 5: R value, Crossover Modulus and Glassy Modulus Values for the Study Binders at Original, RTFO, and PAV Conditions

Code	Binder	Original			RTFO			PAV		
		G*$_c$	**G*$_g$**	**R**	**G*$_c$**	**G*$_g$**	**R**	**G*$_c$**	**G*$_g$**	**R**
X1	PG 70-10 (X)	2.83E+07	3.79E+08	1.13	2.01E+07	5.69E+08	1.45	9.74E+06	6.99E+08	1.86
X2	PG 76-16 (X)	2.02E+07	6.24E+08	1.49	1.27E+07	6.33E+08	1.70	3.01E+06	1.02E+09	2.53
X3	PG 64H-22 (X)	2.52E+07	5.89E+07	0.37	1.62E+07	9.05E+07	0.75	4.94E+06	2.44E+08	1.69
X4	PG 64V-22 (X)	2.56E+07	6.30E+07	0.39	1.67E+07	8.29E+07	0.70	4.86E+06	2.41E+08	1.70
X5	PG 76-22 TR (X)	2.45E+07	7.51E+07	0.49	1.96E+07	1.33E+08	0.83	9.30E+06	3.22E+08	1.54
Y1	PG 64-22 (Y)	2.68E+07	5.85E+08	1.34	6.98E+06	6.31E+08	1.96	3.70E+06	1.06E+09	2.46
Y2	PG 70-22 (Y)	2.14E+07	6.79E+08	1.50	1.78E+07	8.98E+08	1.70	8.15E+05	2.37E+09	3.46
Y3	PG 70-16 (Y)	1.97E+07	1.02E+09	1.71	8.58E+06	1.18E+09	2.14	1.21E+06	1.44E+09	3.07
Y4	PG 76-16 (Y)	2.24E+07	5.16E+08	1.36	1.67E+07	5.84E+08	1.54	5.14E+06	1.04E+09	2.31
Y5	PG 70H-16 (Y)	2.01E+07	6.68E+07	0.52	1.25E+07	8.36E+07	0.82	1.03E+06	2.52E+08	2.39
Y6	PG 70V-16 (Y)	1.05E+05	5.40E+07	2.71	1.10E+06	7.51E+07	1.83	6.94E+05	2.26E+08	2.51
Z1	PG 64-22 (Z)	1.77E+07	4.78E+08	1.43	1.17E+07	6.30E+08	1.73	3.75E+06	9.49E+08	2.40
Z2	PG 70-22 (Z)	1.73E+07	6.94E+08	1.60	8.15E+06	6.40E+08	1.89	1.19E+06	1.35E+09	3.05
Z3	PG 70-10 (Z)	1.10E+07	3.57E+08	1.51	6.98E+06	6.31E+08	1.96	1.92E+06	9.76E+08	2.71
Z4	PG 76-16 (Z)	1.82E+07	6.71E+08	1.57	1.05E+07	7.61E+08	1.86	1.46E+06	1.44E+09	3.00

4.1.3 Relaxation Spectra and its Characterization

As mentioned earlier in this Chapter, the studies by (Christensen and Anderson 1992), and (Leseur et al. 1996) provided the necessary motivation to probe if there exists a relationship between the molecular weight distribution parameters obtained from LDMS and the LVE characteristics of asphalt. One such fundamental LVE characteristic of interest is the relaxation spectra. The theoretical interest in calculating relaxation spectra is based on the supposition that it provides insights to dynamics of molecular structure (molecular weight distribution, branching, network formation) (Malkin 2006). The writing below provides a brief introduction to relaxation, and it what it means.

When loaded, materials deform and experience an increase in energy. Upon removal of the load, molecular rearrangement takes place with the macromolecules comprising the material shifting towards equilibrium to minimize the total energy of the system (Kontogiorgos 2010). These molecular rearrangements are termed as “relaxation”. The time taken for these rearrangements to occur depends upon the type of material, elastic, viscous or viscoelastic. In the case of the viscoelastic materials when stress is applied, some energy is stored in the material during deformation and is used for return to equilibrium state whereas as some energy is dissipated as heat. The time taken for the material to relax (reach equilibrium) is called the relaxation time. The distribution of these relaxation times is the relaxation spectra. As will be discussed in the following paragraphs, relaxation spectra is a plot between a modulus density function and the relaxation time. A broader relaxation spectra implies a material will require more time to relax the stress, and a narrower spectra suggests that a material will relax any induced stresses faster.

4.1.3.1 Modeling Discrete Relaxation Spectra

Relaxation spectra can be modeled using the generalized Maxwell model with "N" elements as shown in Figure 4-3. G_∞ is the spring constant, G_m and η_m are the stiffness of the spring and the viscosity of the dashpot respectively of the individual Maxwell elements. Based on these parameters, the relaxation time can be calculated as shown in Equation (12).

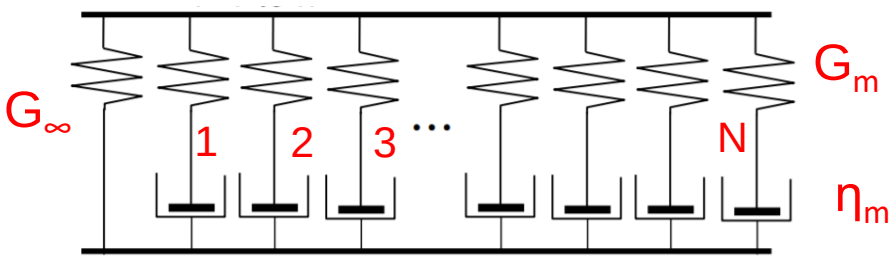

Figure 4-3: Generalized Maxwell Model

$$\text{Relaxation Time } (\rho_m) = \frac{\eta_m}{G_m} \tag{12}$$

Solving the constitutive relationships from the generalized Maxwell model, the stress relaxation modulus can be mathematically defined as shown in Equation (13) becomes,

$$G(t) = G_\infty + \sum_{m=1}^{N} G_m e^{-t/\rho_m} \tag{13}$$

However, for viscoelastic liquids like asphalt binders G_∞ tends to zero and thus, Equation (13) becomes,

$$G(t) = \sum_{m=1}^{N} G_m e^{-t/\rho_m} \tag{14}$$

The equation for relaxation modulus from Ferry's work (Ferry 1980) is shown in Equation (15). Ferry defined relaxation spectra as a spectral plot of the modulus density function (H) plotted against time (ρ) in logarithmic space. If we compare equations (13) and (15), they are both are essentially the same equations. Thus, the relaxation spectra is essentially a plot between the Prony series parameters, G_m and ρ_m in logarithmic space.

$$G(t) = G_e + \int_{-\infty}^{\infty} He^{-t/\tau} d\ln\tau \tag{15}$$

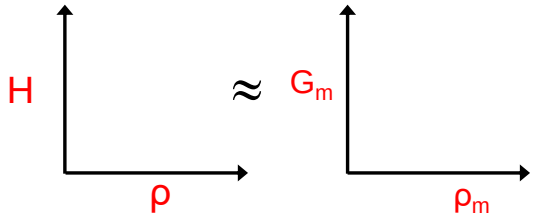

Figure 4-4: Parameters Involved in the Development of Relaxation Spectra

The calculation of the Prony series coefficients is carried out using the method of collocation (Schapery 1999). The main source of data for performing the collocation operation and subsequently calculating the relaxation spectra is the storage/loss modulus of the respective binder, obtained from the temperature-frequency sweep tests. In this study the storage modulus was selected as the basis for performing the collocation. This choice was based on the data reported by Dickinson and Witt (1976) wherein minimal difference was observed in relaxation spectra calculated using storage modulus and loss modulus. However, it will be shown in the subsequent sections, that differences do exist in relaxation spectra calculated from storage modulus in comparison to the spectra developed from loss modulus.

The storage modulus data that was used for Prony calculations was seen to fit well to the CAM model. The example of the fit for PG 76-16(Y) asphalt at its original condition is shown in Figure 4-5.

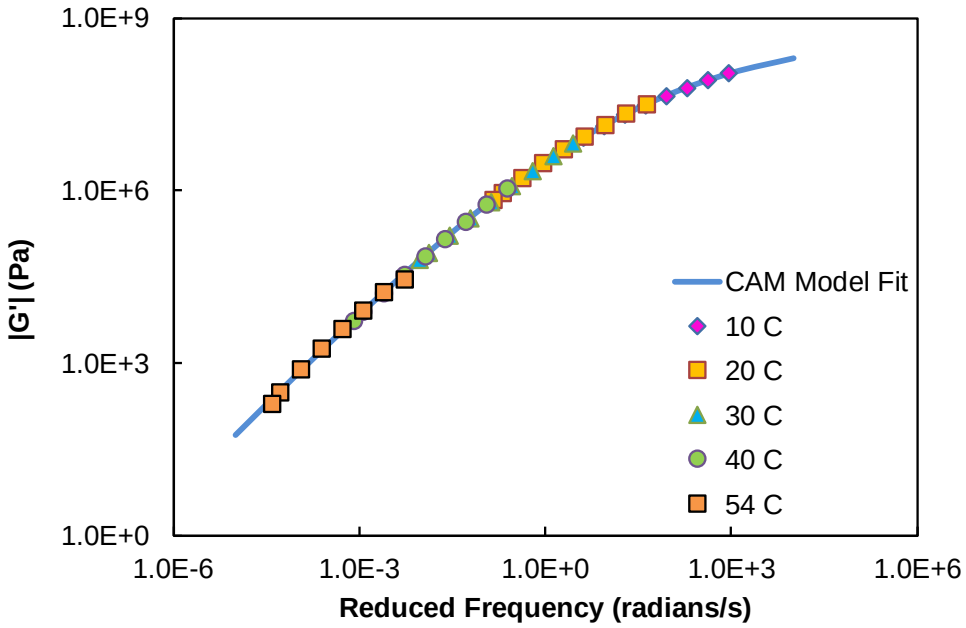

Figure 4-5: Storage Modulus Mastercurve for PG 76-16(Y) at Original Condition Fit to CAM Model.

The model fit function is now used to determine storage modulus values for a range of reduced frequency values, spanning several decades. Subsequently, the Prony parameters G_m, and ρ_m are calculated using the process of collocation. The process is explained below using Equations (16) through (22).

From the generalized Maxwell model for viscoelastic liquids, the relaxation modulus is expressed using,

$$G(t) = \sum_{m=1}^{N} G_m e^{-t/\rho_m} \tag{16}$$

In Prony terms, the storage modulus of asphalt binder can be written as,

$$G'(\omega) = \sum_{m=1}^{N} G_m \frac{\omega^2 \rho_m^2}{1+\omega^2 \rho_m^2} \tag{17}$$

In order to calculate ρ_m's, and G_m's we need to optimize Equation (17) using matrix analysis.

$$\begin{aligned} G'(\omega_1) &= \frac{G_1 \omega_1^{\,2} \rho_1^2}{1+\omega_1^{\,2} \rho_1^2} + \frac{G_2 \omega_1^{\,2} \rho_2^2}{1+\omega_1^{\,2} \rho_2^2} + \ldots \\ G'(\omega_2) &= \frac{G_1 \omega_2^{\,2} \rho_1^2}{1+\omega_2^{\,2} \rho_1^2} + \frac{G_2 \omega_2^{\,2} \rho_2^2}{1+\omega_2^{\,2} \rho_2^2} + \ldots \end{aligned} \tag{18}$$

$$\{G'\} = \{G'(\omega_1), G'(\omega_2), \ldots\} \tag{19}$$

$$\{G_m\} = \{G_1, G_2, G_3, \ldots\} \tag{20}$$

$$[A] = \begin{bmatrix} \frac{\omega_1^{\,2} \rho_1^2}{1+\omega_1^{\,2} \rho_1^2} & \frac{\omega_1^{\,2} \rho_2^2}{1+\omega_1^{\,2} \rho_2^2} & \frac{\omega_1^{\,2} \rho_3^2}{1+\omega_1^{\,2} \rho_3^2} \ldots \\ \frac{\omega_2^{\,2} \rho_1^2}{1+\omega_2^{\,2} \rho_1^2} & \frac{\omega_2^{\,2} \rho_2^2}{1+\omega_2^{\,2} \rho_2^2} & \frac{\omega_2^{\,2} \rho_3^2}{1+\omega_2^{\,2} \rho_3^2} \ldots \\ : & & \\ : & & \\ \frac{\omega_N^{\,2} \rho_1^2}{1+\omega_N^{\,2} \rho_1^2} & \ldots\ldots\ldots\ldots\ldots\ldots\ldots & \frac{\omega_N^{\,2} \rho_M^2}{1+\omega_N^{\,2} \rho_M^2} \end{bmatrix} \tag{21}$$

Combining Equations (21), (22), and (23) we get,

$$[A]\{G_m\} = \{G'\} \tag{22}$$

Equation (22) was solved for Prony parameters, ρ_m, and G_m using matrix operation tools in Microsoft Excel.

Through the process of collocation, the validity of the Prony series coefficients can be checked by comparing the storage modulus calculated with the Prony series parameters with the experimental storage modulus data which was fit to the CAM model. This process for PG 76-16(Y) at the original condition is shown in Figure 4-6. Once the Prony coefficients are verified, the relaxation spectra is computed, by plotting G_m against ρ_m as shown in Figure 4-7. Two series are shown in this figure, in the first series the spectra is based on extrapolated storage modulus data spanning 30 decades and the second series, the spectra is calculated based on storage modulus data that was actually measured.

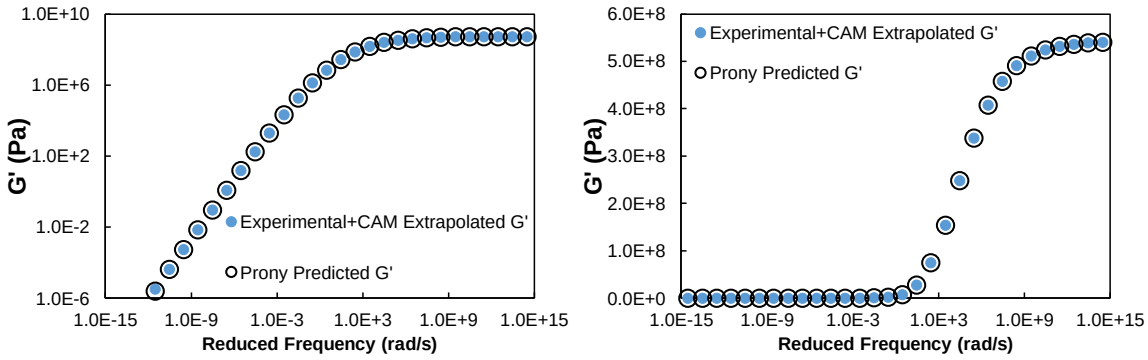

Figure 4-6: Verification of Prony Coefficients by Comparing Experimental and Prony Predicted Storage Modulus Values for PG 76-16(Y) Original in (a) Logarithmic; and (b) Semi-Logarithmic Space.

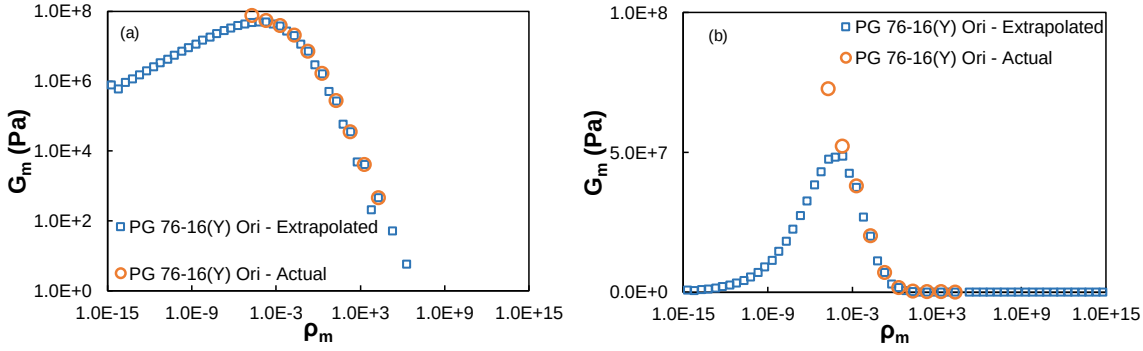

Figure 4-7: Relaxation Spectra for PG 76-16(Y) Original Showing Extrapolated as well and Actual Data in (a) Logarithmic; and (b) Semi-Logarithmic Space.

It was of interest to compare the relaxation spectra across aging levels. One such comparison for the PG 76-16(Y) binder is shown in Figure 4-8. It can be seen from the figure that the relaxation spectrum widens with aging. This is in line with SHRP-A-367 literature which shows that higher modulus asphalts possess higher *R* values and subsequently a wider relaxation spectrum. The same is seen for the study asphalts as well, as aged asphalts in Table 5 have a higher *R* value and are seen to possess wider relaxation spectra. This means that the time required for stress relaxation increases with increase in oxidation.

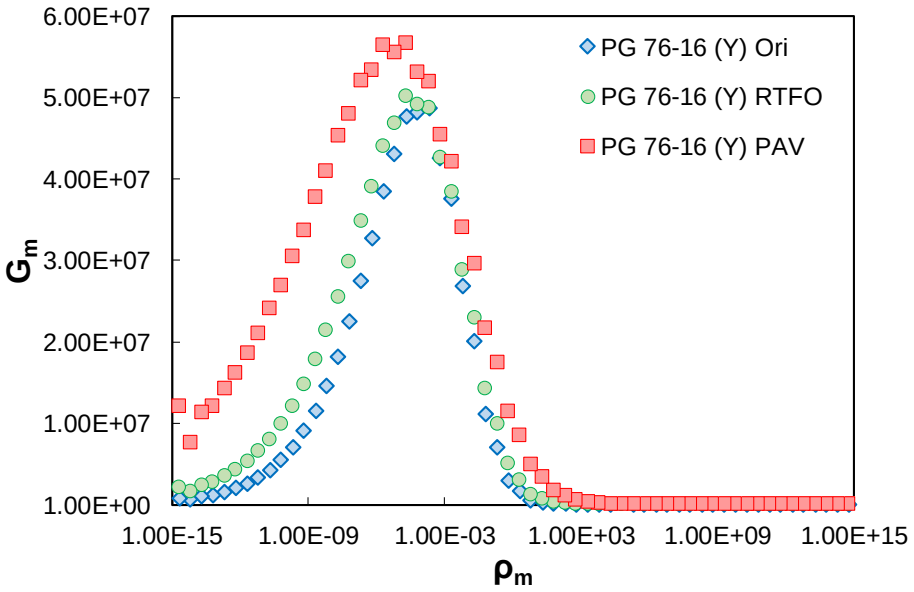

Figure 4-8: Relaxation Spectra for PG 76-16(Y) Asphalt at All Three Aging Conditions.

Another issue that was mentioned earlier in the section was that of difference in relaxation spectras obtained from storage modulus and loss modulus data. One such scenario with PG 76-16(Y) at original condition is shown in Figure 4-9. Though the spectra obtained based on storage modulus was good, the spectra calculated based on loss modulus was

unexpected and distorted. However, Prony predicted values of *G″* obtained from collocation matched the experimental data well. So, the values couldn't be rejected. This calculation of relaxation spectra using loss modulus will be re-verified. Recently published work by Liu et al. (Liu et al. 2018), have proposed a technique for determination of continuous relaxation spectrum that gives a singular spectrum for both G′ and G″.

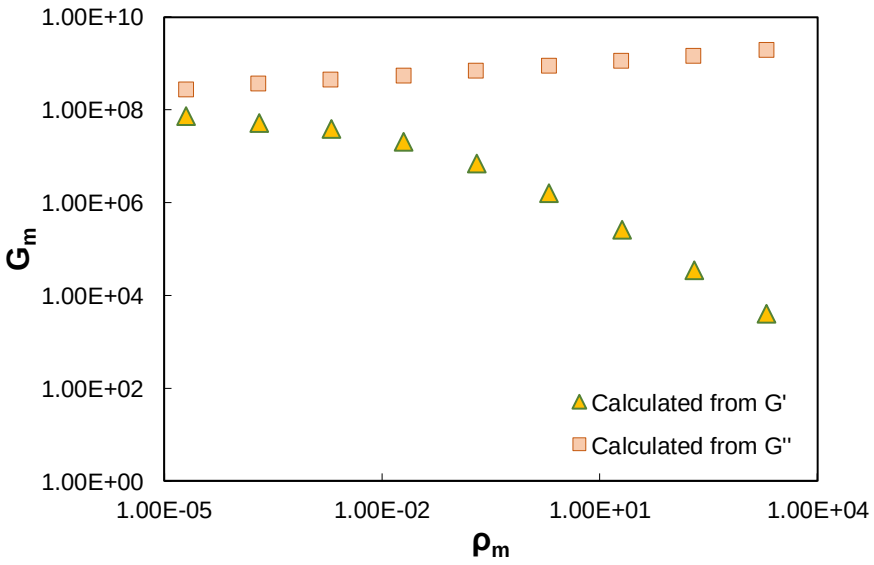

Figure 4-9: Relaxation Spectra for PG 76-16(Y) Original Calculated from G′ and G″.

4.1.3.2 Modeling Continuous Relaxation Spectra

The model proposed by Liu et al. (2018) for development of continuous relaxation spectra is used in this research. A brief description of the model is presented in this chapter. The unique characteristic of the model developed by Liu et al., is that the relaxation spectrum is defined with a relatively few number of coefficients and in a way that allows one to minimize the errors with respect to both loss and storage modulus. The authors derived the expressions for modulus of asphalt concrete and it is adapted in this research for shear modulus of asphalt binders, recognizing the fact that binders do not have a lower

asymptote. The parameters are determined by minimizing the fitting errors of the storage and the loss moduli functions, shown in equations (23) and (24).

$$\log G'(f) = \frac{\alpha}{\left\{1+\lambda \exp\left[\beta+\gamma \log\left(f\alpha_T\right)\right]\right\}^{1/\lambda}} \tag{23}$$

$$\begin{aligned}\log G''(f) = {} & \log\left(-\frac{\pi}{2}\alpha\gamma\right)+\left[\beta+\gamma \log\left(f\alpha_T\right)\right]\log e \\ & -\left(1+\frac{1}{\lambda}\right)\log\left\{1+\lambda \exp\left[\beta+\gamma \log\left(f\alpha_T\right)\right]\right\} \\ & +\frac{\alpha}{\left\{1+\lambda \exp\left[\beta+\gamma \log\left(f\alpha_T\right)\right]\right\}^{1/\lambda}}\end{aligned} \tag{24}$$

$$\log a_T = \frac{-C_1(T-T_r)}{C_2+T-T_r} \tag{25}$$

where:

f = loading frequency, Hz;

λ = shape parameter;

β and γ = model parameters;

α_T = time-temperature shift factor from the WLF equation;

T = test temperature, °C;

T_r = reference temperature, °C;

C_1 = fitting parameter, dimensionless; and

C_2 = fitting parameter, °C.

Liu et al. use these expressions along with Fourier Transformation to define the continuous spectra, equation (26).

$$H(\tau) = \pm \frac{2}{\pi} \mathrm{Im}\left\{ G'\left[\tau^{-1} \exp\left(\pm \frac{\pi}{2} i \right) \right] \right\} \tag{26}$$

where:

τ = relaxation time.

After substituting equation (23) into equation (26), and using mathematical transformations such as Euler's formula Liu et al. arrive at the expression shown in equation (27). The model form of relaxation spectrum shown in equation (27) is in terms of the same model parameters used to describe the master curve functions of G′ and G″

$$H(\tau) = -\frac{2}{\pi} \exp\left(F^{1/2\lambda} \cos\frac{G}{\lambda} \right) \sin\left(F^{1/2\lambda} \sin\frac{G}{\lambda} \right) \tag{27}$$

where:

$$\begin{aligned} F &= X^2(\tau) + Y^2(\tau); \text{ and} \\ G &= \arctan\frac{Y(\tau)}{X(\tau)} \end{aligned} \tag{28}$$

$$X(\tau) = \frac{B^{\lambda}\left[1 + \lambda \exp(E) \cos\frac{\pi D}{2} \right]}{1 + \lambda^2 \exp(2E) + 2\lambda \exp(E) \cos\frac{\pi D}{2}} \tag{29}$$

$$Y(\tau) = \frac{B^{\lambda} \lambda \exp(E) \sin\frac{\pi D}{2}}{1 + \lambda^2 \exp(2E) + 2\lambda \exp(E) \cos\frac{\pi D}{2}} \tag{30}$$

$$
\begin{aligned}
B &= \alpha \ln 10; \\
C &= \beta - \gamma \log(2\pi); \\
D &= \frac{\gamma}{\ln 10}; \\
E &= C + D \ln \frac{\alpha_T}{\tau}.
\end{aligned}
\tag{31}
$$

In this study, these relationships were used to deduce the continuous relaxations spectra of the study asphalt binders. Presented in Figure 4-10 are the storage and loss modulus mastercurves developed using the Liu et al. model for one of the study binders PG 76-16(Y) at all three aging conditions. The solid line represents the model and the filled in circles represent the experimental data points. Overall, the fit was reasonable with PAV aged binder having the best fit among all conditions. It was also seen that the model even after multiple iterations doesn't fit the loss modulus data well at high temperatures, especially at original and RTFO conditions. Presented in Figure 4-11 are the continuous relaxation spectra for the PG 76-16(Y) at all three aging conditions. The advantages of the continuous relaxation spectra presented in Figure 4-11, over the discrete relaxation spectra presented in Figure 4-8 are twofold: (i) the waviness of the spectra is eliminated, and (ii) allows for complete interpretation of the linear viscoelastic information as both storage and loss modulus are used in the construction of the spectra.

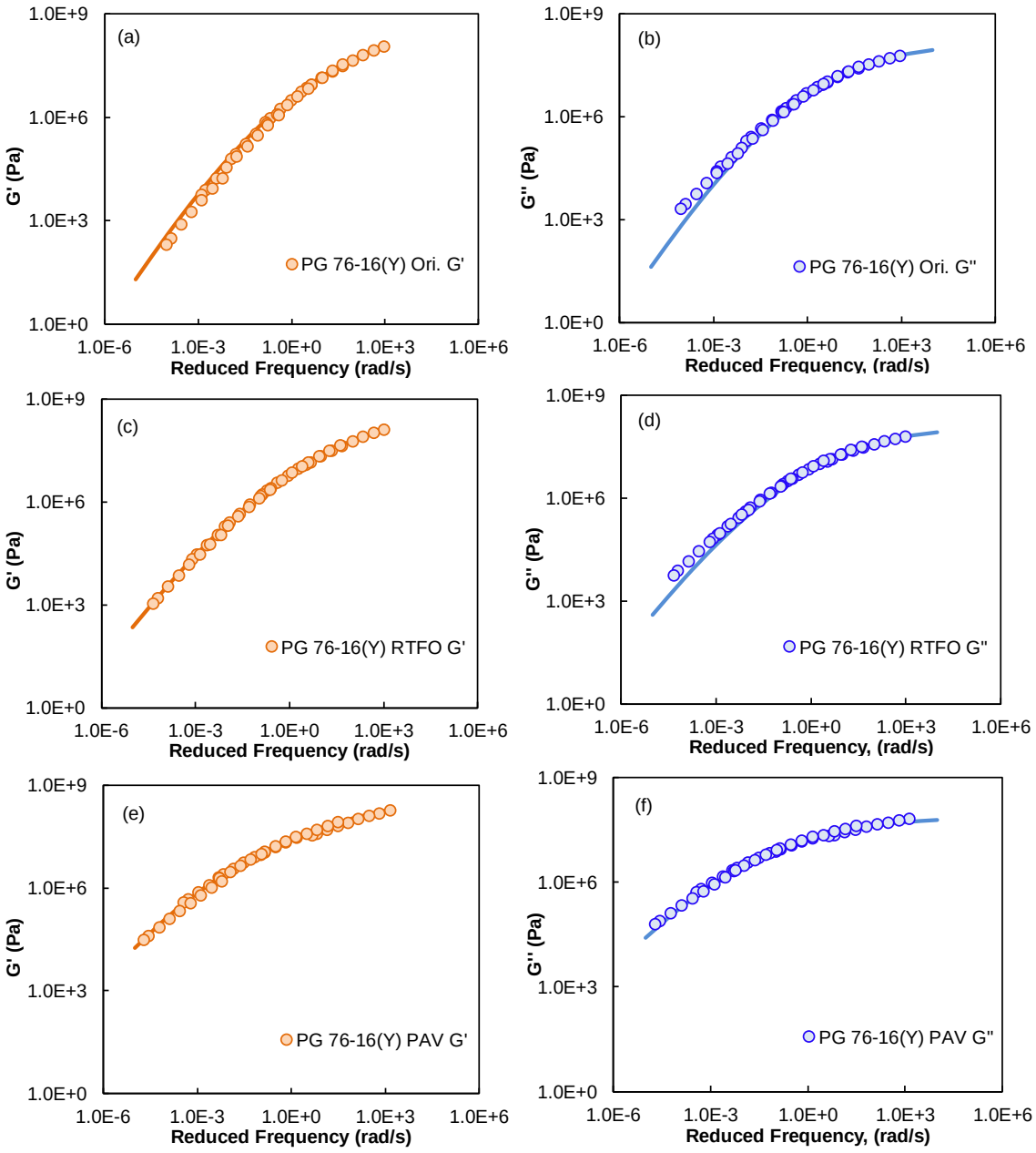

Figure 4-10: Storage and Loss Modulus Mastercurve for PG 76-16(Y) at Original, RTFO, and PAV Condition Based on Liu et al. Model.

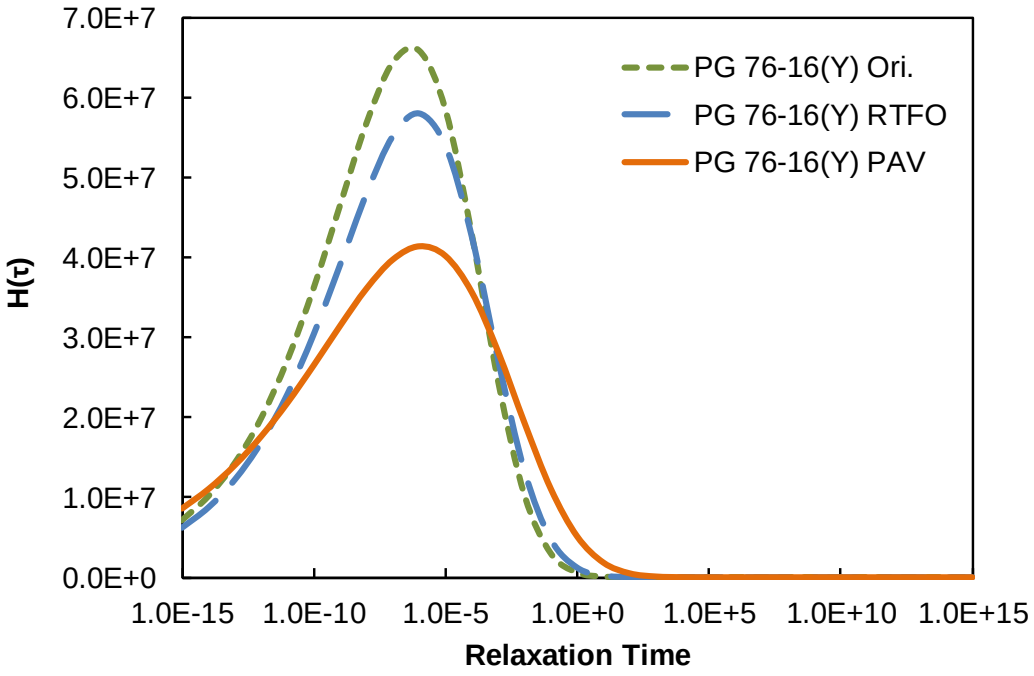

Figure 4-11: Continuous Relaxation Spectrum for PG 76-16(Y) at Original, RTFO, and PAV Condition Based on Liu et al. Model.

4.2 Molecular Structure Characterization

As mentioned in Chapter 3, laser desorption mass spectroscopy was used to study the molecular weight distribution of asphalt binders. In the same chapter, the details regarding the experimental process are discussed, which include sample preparation, performing the experiment, data processing employed and subsequent analyses. In this chapter, the molecular weight distributions, molecular weights for all study asphalts at different aging conditions are presented. Also presented are the results from the FT-IR spectroscopy.

4.2.1 Molecular Weight Distribution of Study Asphalts

The data filtering technique explained in chapter 3 was used to develop the refined MWD from the raw data. However, three of non-polymer modified asphalts, X1, Y1, and Y2 were not considered because of greater noise in obtained distribution even after filtering. The

molecular weight distributions for the remaining seven non-polymer modified asphalt binders are shown in Figure 4-12 and Figure 4-13. The distributions for the polymer modified asphalts are shown in Figure 4-14. These distributions were then analyzed to answer two main questions, (i) can non-polymer modified asphalts be distinguished from polymer modified asphalts, and (ii) Do molecular weight distributions of asphalt change with aging, if they do change, can any consistent trends be established.

Regarding the first question, based on observations from Figure 4-12 - Figure 4-14, it can be seen that no visual distinction exists between the non-polymer modified and the polymer modified asphalts. One of the main reasons for this is the fact that the polymer cannot be captured in the range shown in Figure 4-12 - Figure 4-14. Common polymers, used in asphalt like SBS, SBR etc. have molecular weights which are in excess of 100,000 daltons. So, the distribution being observed for the polymer modified binders is most likely of the base binder used to prepare those binders. Although, the mass range could have been stretched to 100,00 daltons to see if polymers can be detected, this would result in loss of resolution of the spectra that is captured in the 200-2000 dalton range. Regarding the second question, for the majority of the non-polymer modified asphalts (five out of seven) a consistent reduction in width of the distribution was seen with aging. For the remaining two asphalts, PG 76-16(Z) at all three conditions had very similar molecular weight distributions and PG 70-16(Y) at PAV had a broader distribution than original condition. Similar observations were seen in the polymer modified asphalts. The PAV aged binders of two of the five asphalts, PG 64V-22 and PG 70H-16, have distributions narrower than their original asphalts. The binders PG 70V-16(Y) and PG 76-22TR(X) have very similar

molecular weight distributions at all three aging levels. The binder PG 64H-22(X) was the only binder among the polymer modified binders where in the distribution at the aged condition was broader than at the original condition.

There are other visible features of the distribution that are worth noticing. It can be seen that the distributions for almost all of the asphalts are skewed towards the right with the peak at around 450 daltons. This shows that the majority of the asphalt molecules lie in the range of 200-700 daltons. Another striking observation that was made was with MWD obtained from asphalt binders provided by supplier Z as shown in Figure 4-13. It can be seen in all four asphalts from this supplier, across all aging levels there is a small shoulder that shows up in the spectra at around 500 daltons. This is particularly interesting because it occurs in only the asphalts provided by supplier Z, and more interestingly in all of its asphalts. While the reason for the shoulder is not exactly known, it can either be a characteristic of the crude that the supplier is using or it can be any chemical that supplier consistently uses in all its asphalts. It is not uncommon for a supplier to use two different crudes and mix them to meet the grade. Also, asphalt suppliers use chemical additives such as polyphosphoric acid (PPA), which increases the viscosity of asphalt, and helps asphalt suppliers meet the required grade. This is more so prevalent in states like Arizona, where binders with high temperature grade of PG 70, and 76 are commonplace. So, it could be PPA also. The linear form of polyphosphoric acid has the formula of $H_{n+2}P_nO_{3n+1}$, with "n" referring to the number of orthophosphoric acid molecules. If "n" equals 6, the formula for PPA becomes $H_8P_6O_{19}$, which has a molecular weight of 498 g/mol. This value is in close proximity of where peak was observed in case of the binders from supplier "Z". This

observation brings out an important utility of MWD obtained from LDMS technique, that the technique can also be utilized for material forensic evaluations similar to the technique of FT-IR.

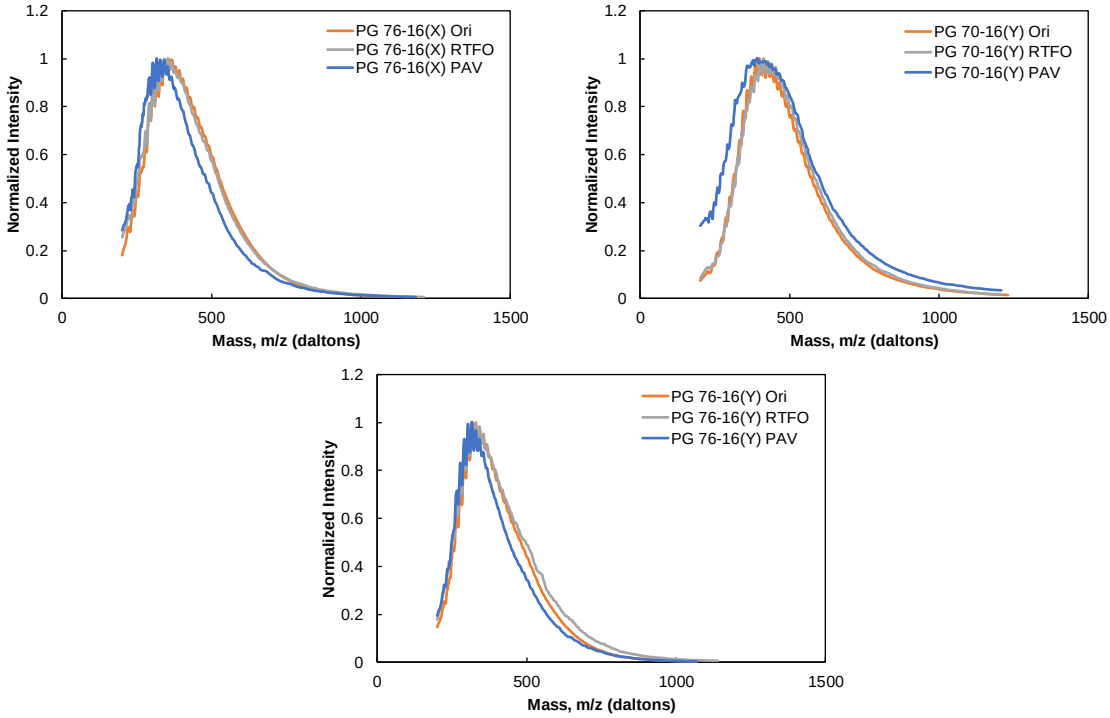

Figure 4-12: Molecular Weight Distribution for Non-Polymer Modified Asphalts from Suppliers X and Y.

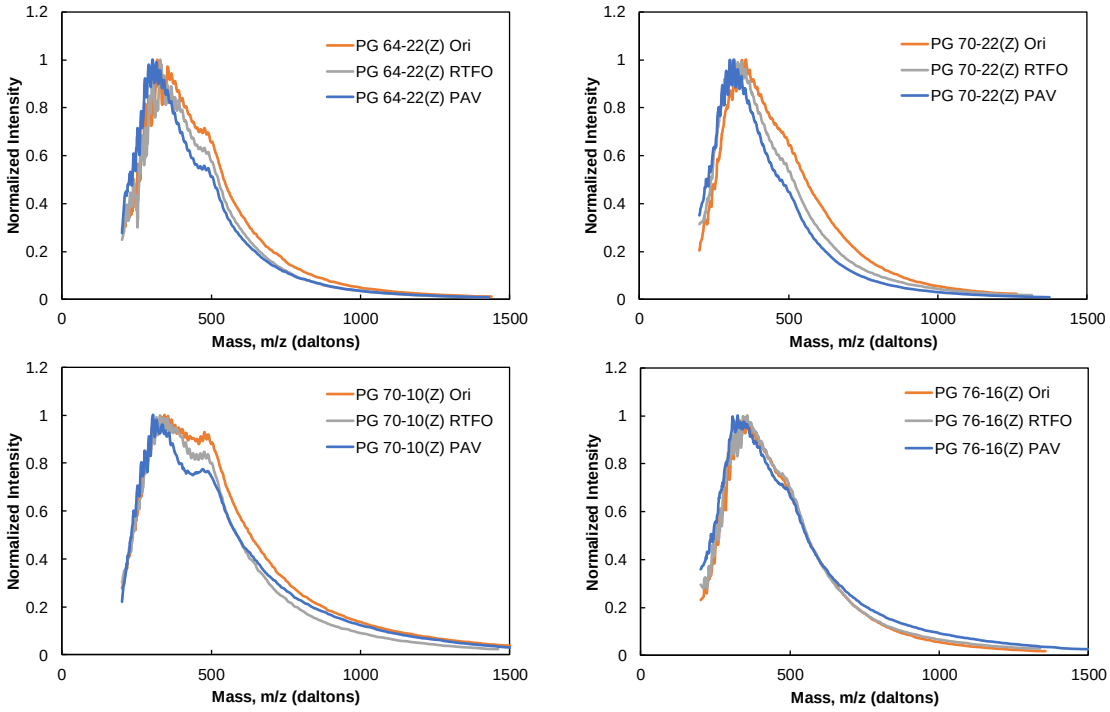

Figure 4-13: Molecular Weight Distribution for Non-Polymer Modified Asphalts from Supplier Z.

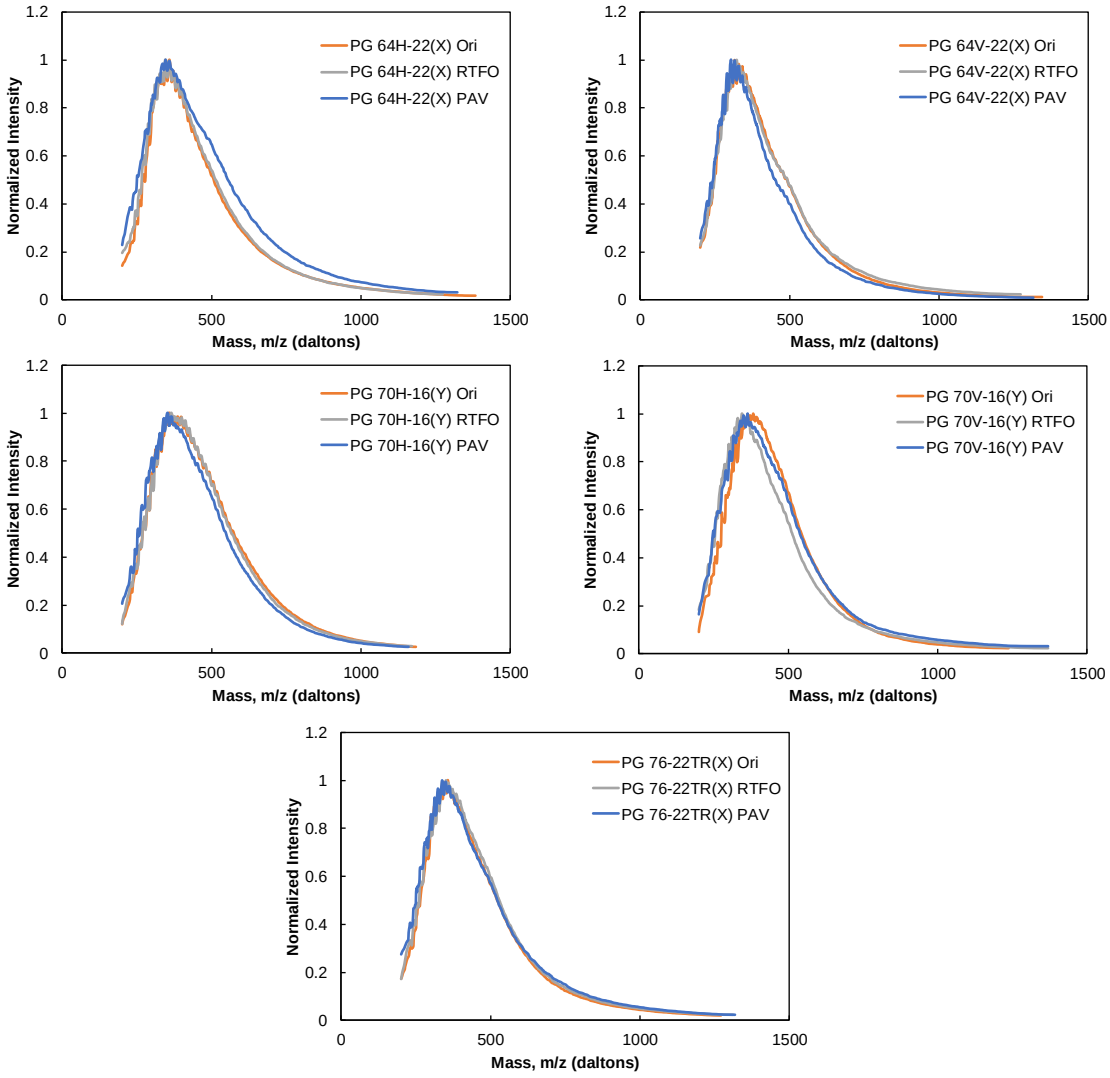

Figure 4-14: Molecular Weight Distribution for Polymer Modified Asphalts Used in the Study.

4.2.2 Calculating Molecular Weights

Based on the obtained distribution, molecular structure parameters such as number average (M_n) and weight average molecular weights (M_w) were calculated. While the general guidelines for calculation of M_n and M_w have been well established, the specific approach provided by Cooper is used as a reference here (Cooper 1989). The averages presented in Equations (32) and (33), are defined in terms of their molecular mass M_i and the number

of moles n_i of that component molecule. In the current study, the spectral intensity obtained from the MALDI data is a surrogate for the number of moles of each molecular component.

$$M_n = \frac{\sum n_i M_i}{\sum n_i} \tag{32}$$

$$M_w = \frac{\sum n_i M_i^2}{\sum n_i M_i} \tag{33}$$

The weight average molecular weight is particular sensitive to the presence of higher molecular weight molecules whereas the number average molecular weight is sensitive to the presence of lower molecular weight molecules. Using this information, it might be possible to make inferences about the overall distribution which encompasses lower as well as higher molecular weight molecules. For this purpose, the International Union of Pure and Applied Chemistry (IUPAC) coined the term dispersity (D_m) as the ratio of weight average molecular weight to the number average molecular weight and suggest that it is indicative of the broadness or the width of the molecular weight distribution. The parameter was calculated to see if the observed difference in the MWD in the asphalts between original and aged conditions, can be quantified. The weight and number average molecular weights, and dispersity values for the study asphalts at original and PAV aged conditions are tabulated in Table 6 below. The polymer modified asphalts are shown in yellow, whereas the non-polymer asphalts are shown in green.

The difference in molecular weights of asphalt with aging was seen to be minimal. In general, there was a reduction in molecular weight with oxidation, which follows from the narrower molecular weight distribution seen in PAV aged asphalt binders. Regarding

the dispersity values there exists minimal difference between the D_m values at original and PAV conditions, in order of 0.00-0.06. The width of the distribution can thus be numerically quantified using D_m, however the visual difference in molecular weight distribution between original and aged asphalts, does not translate to a likely significant quantitative measure.

Table 6: Summary of Number and Weight Average Molecular Weights, and Dispersity's of Study Asphalts.

Notation	Binder	Original			PAV			$\delta D_m = D_{mPAV} - D_{mOri}$
		M_n	M_w	D_m	M_n	M_w	D_m	
X2	PG 76-16 (X)	432.4	469.6	1.086	391.0	421.2	1.077	0.009
X3	PG 64H-22 (X)	459.4	503.3	1.096	454.5	512.0	1.126	-0.031
X4	PG 64V-22 (X)	422.0	464.5	1.101	393.9	429.0	1.089	0.012
X5	PG 76-22 TR (X)	446.1	484.4	1.086	435.0	474.8	1.091	-0.006
Y3	PG 70-16 (Y)	483.2	516.4	1.069	471.3	527.1	1.118	-0.050
Y4	PG 76-16 (Y)	408.6	442.6	1.083	378.9	406.6	1.073	0.010
Y5	PG 70H-16 (Y)	476.2	516.8	1.085	450.5	487.7	1.083	0.003
Y6	PG 70V-16 (Y)	463.4	498.2	1.075	455.6	492.2	1.080	-0.005
Z1	PG 64-22 (Z)	407.2	451.6	1.109	403.6	447.5	1.109	0.000
Z2	PG 70-22 (Z)	459.5	506.5	1.102	412.9	457.6	1.108	-0.006
Z3	PG 70-10 (Z)	452.1	501.1	1.108	417.8	487.6	1.167	-0.059
Z4	PG 76-16 (Z)	447.2	494.2	1.105	428.1	480.6	1.123	-0.018

4.2.3 Potential of LDMS for Forensic Assessment

In order to verify if the "hump" seen in asphalt binders procured from supplier Z was due to presence of PPA, an investigative study was carried out. In this study a non-polymer modified asphalt PG 70-16(Y) was doped with 1%, 5%, and 10% PPA and mixed using a high shear mixer at a temperature of 177°C. LDMS test was performed on these doped binders, to detect any abnormality in the distribution or similarities to that observed in supplier Z binders. The molecular weight distributions from the three doped binders are presented in Figure 4-15 along with the original PG 70-16(Y) which has no PPA.

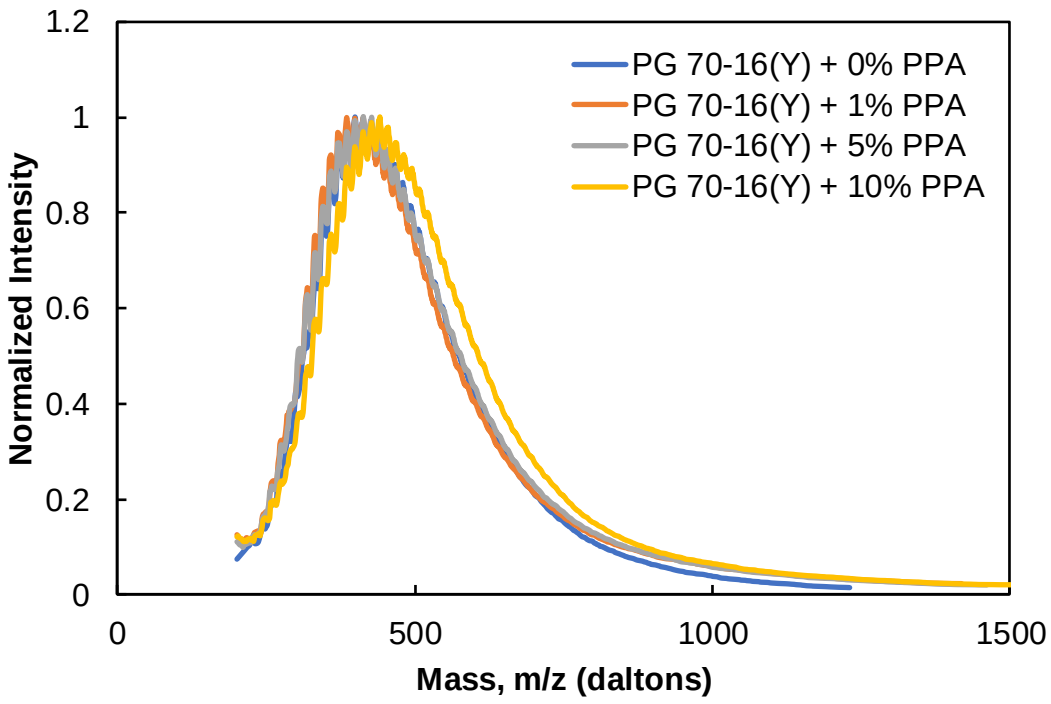

Figure 4-15: Molecular Weight Distribution of PG 700-16(Y) Binders Doped with Poly Phosphoric Acid (PPA).

It can be seen Figure 4-15 that firstly, there is no hump around 500 daltons, thereby negating the notion that the hump seen in binders from supplier Z might be due to PPA. Secondly, there also no other distinguishable peak/ abnormality in the distribution that would suggest that there is PPA in the binder. It has to be noted that the 5%, and 10% PPA is above and beyond what a state DOT might allow in its asphalts. Typically, the DOT's restrict the dosage to 0.5-1%. Another observation that can be made is that there is absolutely no change in distribution at 0%, 1%, and 5% dosage levels and it changes marginally at 10% dosage level, which is highly unlikely to be ever used. Based, on these observations it can be concluded that LDMS cannot confirm the presence of PPA in asphalt

and usage of PPA doesn't alter the molecular weight distribution of asphalt binders as calculated through LDMS.

Second forensic study that was conducted was with regard to utilizing LDMS as a tool to assess blending of asphalt binders. For this purpose, two asphalt binders, PG 70-16(Y) and PG 76-16(Y) which have very different molecular weight distributions were blended in a 1:1 weight ratio. The blending was conducted in a high shear mixer at 160°C for 45 minutes. The resultant blend was used for LDMS testing. The molecular weight distribution of the blended asphalt binder along with the two binders used for blending are shown in Figure 4-16. Also presented in the figure is a simple weighted average of the distributions of the two binders.

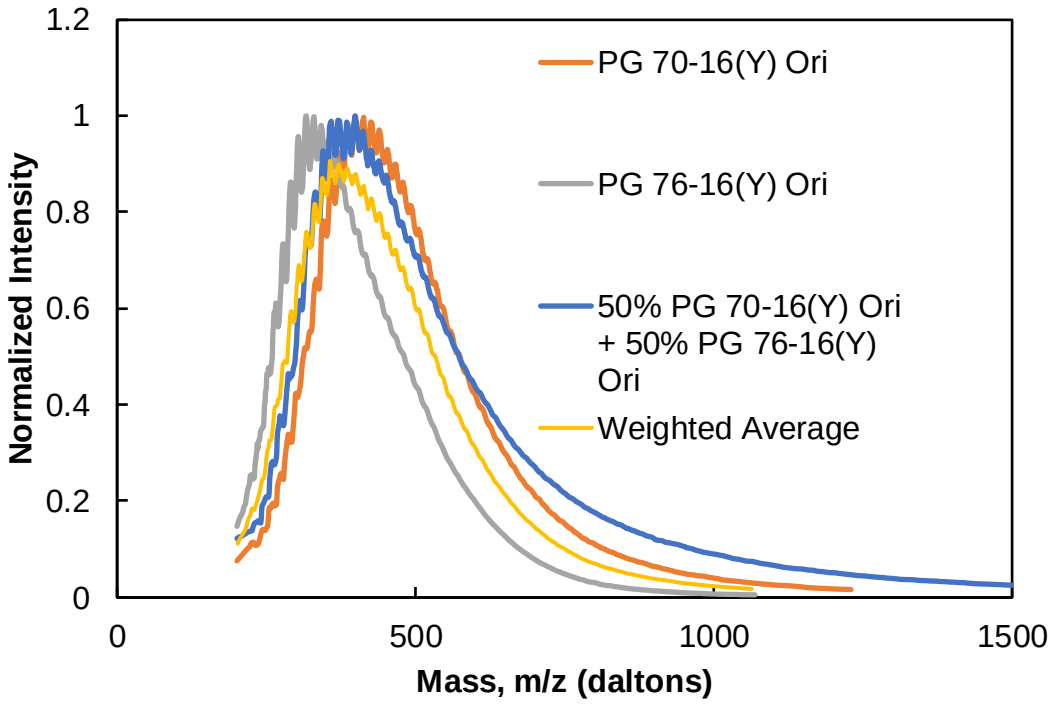

Figure 4-16: Molecular Weight Distribution of 1:1 Blend of PG 70-16(Y) and PG 76-16(Y) Asphalt Binders.

It can be observed from the figure that the blend MWD is in between the two binders until about 600 daltons after which it deviates as the number of higher molecular weight components are higher in the blended asphalt binder. More importantly it can be seen that distribution of the blended asphalt is dissimilar from the weighted average distribution calculated from the two asphalts. This shows that the resultant MWD of the blended asphalt is due to formation of products in the blended asphalt whose evolution cannot be described by a simple weighted average equation and that the resultant reactions and the product formation is more complicated. LDMS is therefore an efficient tool that can be used to capture the effects of binder blending as reflected through the molecular weight distribution of the blended asphalt.

4.2.4 Fourier Transform Infrared Spectroscopic Measurements

While the changes to the asphalt binders can be gauged using physical property measurements of $|G^*|$, as shown in Figure 4-1, in the current study, they were also gauged based on the chemical formation of oxidation products, assessed using the Attenuated Total Reflectance Fourier Transform Infrared Spectroscopy (ATR- FT-IR). The details regarding the test have been explained in detail in Chapter 3. Figure 4-17 shows the FT-IR spectra for the study binder PG 70-10(Z). Oxidation results in an increase in the number of double bonds between hydrocarbons and oxygen, which can be detected with the ATF-FT-IR test. The two specific functional groups examined in this study are the carbonyl and sulfoxide groups. The area of the spectra encompassed by these functional groups has shown to have direct correlation to the level of oxidation in the asphalt binders (Jemison et al. 1992,

Petersen and Glaser 2011). This can be seen in Figure 4-18 wherein the carbonyl and the sulfoxide regions for different aging levels of PG 70-10(Z) are shown.

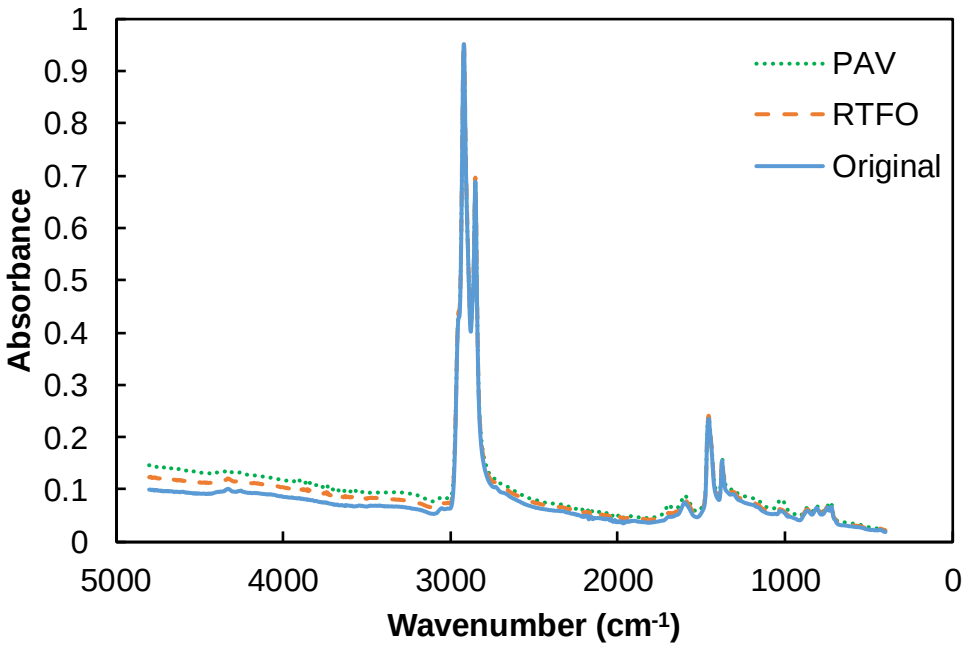

Figure 4-17: FT-IR Spectra for Original, RTFO, and PAV Aged Conditions for PG 70-10(Z).

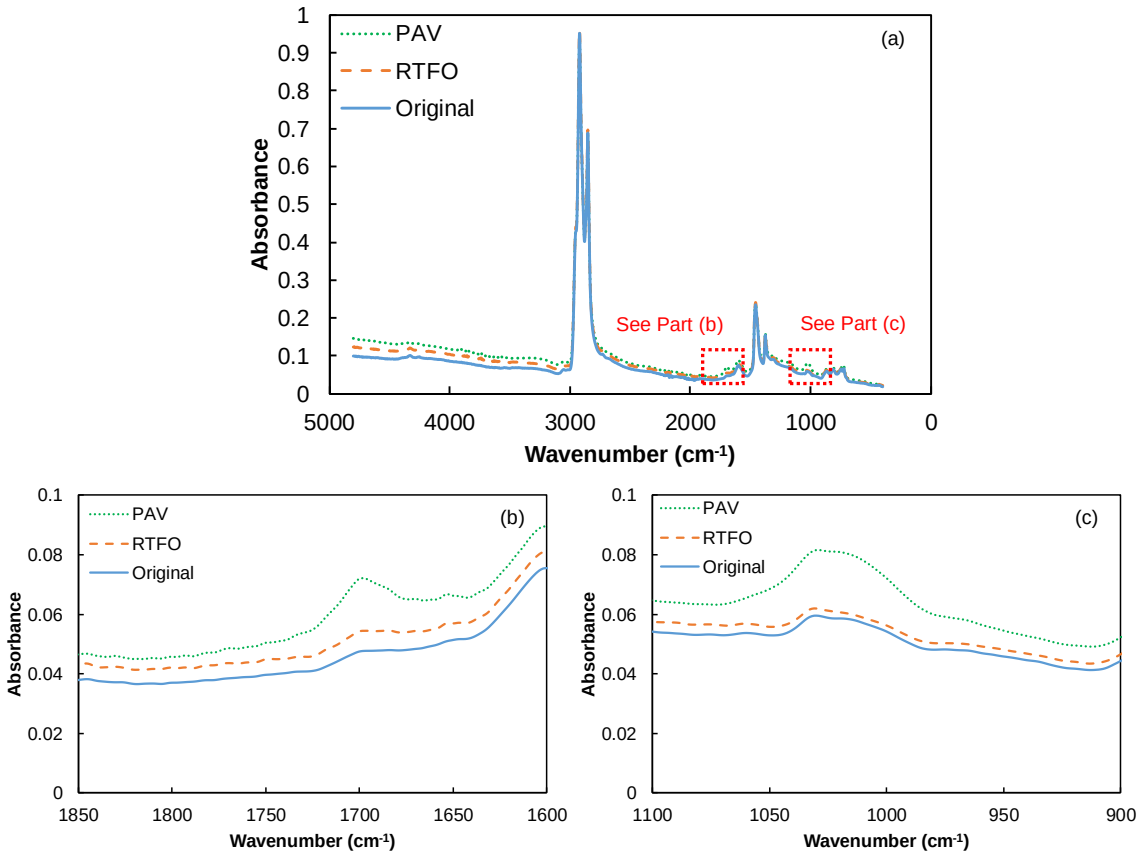

Figure 4-18: FT-IR Spectra for PG 70-10(Z) at Original, RTFO, and PAV Aging Levels; (a) Overall Spectra, (b) Carbonyl Region and (c) Sulfoxide Region.

The main objective of the FT-IR testing was to obtain chemical signature of the asphalts and to confirm the changes in $|G^*|$ as a result of oxidation. The carbonyl and the sulfoxide areas were calculated using the program as described in Appendix B. The sum of carbonyl and sulfoxide areas (CA+SA) for all the study asphalts are shown in Figure 4-19. It can be seen from the figure that the CA+SA increases with increase in aging level. The higher CA+SA of the polymer modified asphalts X3, X4, and X5 can be attributed to increased sulfoxide presence in these asphalts. Polymer modified asphalts when blended as infused with sulfur, which purportedly acts as a crosslinking agent. Thus, higher overall CA+SA. Although, CA+SA provides information regarding the chemical signatures of these

asphalts. What is more important is the relative increase in CA+SA with aging. The ratio of CA+SA after aging to the original condition, as shown in Equation (34) was used as the parameter to calculate this increase. This parameter was termed as $AR_{FT\text{-}IR}$. The values of $AR_{FT\text{-}IR}$ for all study asphalts are summarized in Figure 4-20. It can be seen from the figure that *AR* increase with aging level. It also seen that X3, X4, and X5 which are polymer modified asphalts have the least aging ratio among the study asphalts. This supports the observations from the rheological testing wherein polymer modified asphalts were seen to have a lower aging ratio. The rheology based *AR* values are presented in Appendix D.

$$AR_{FT-IR} = \frac{(Carbonyl\ Area + Sulfoxide\ Area)_{Aged}}{(Carbonyl\ Area + Sulfoxide\ Area)_{Original}} \tag{34}$$

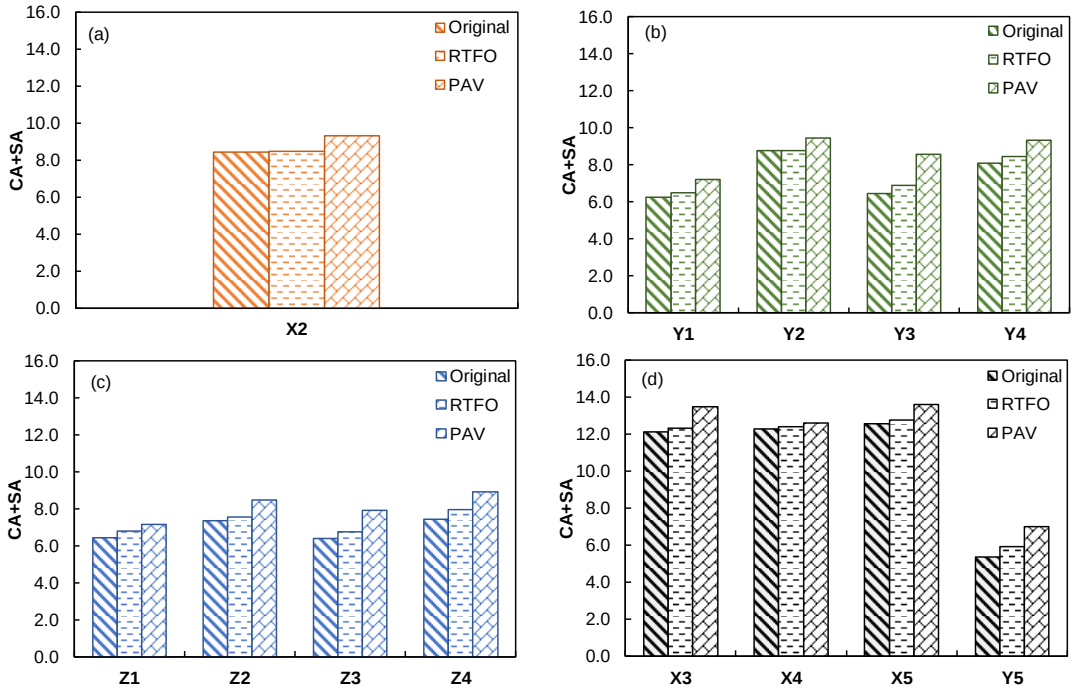

Figure 4-19: The Sum of Carbonyl and Sulfoxide Areas at Original, RTFO and PAV Aged Condition for Unmodified Binders from Supplier; (a) X, (b) Y, (c) Z, and (d) Modified Binders from Suppliers X and Y.

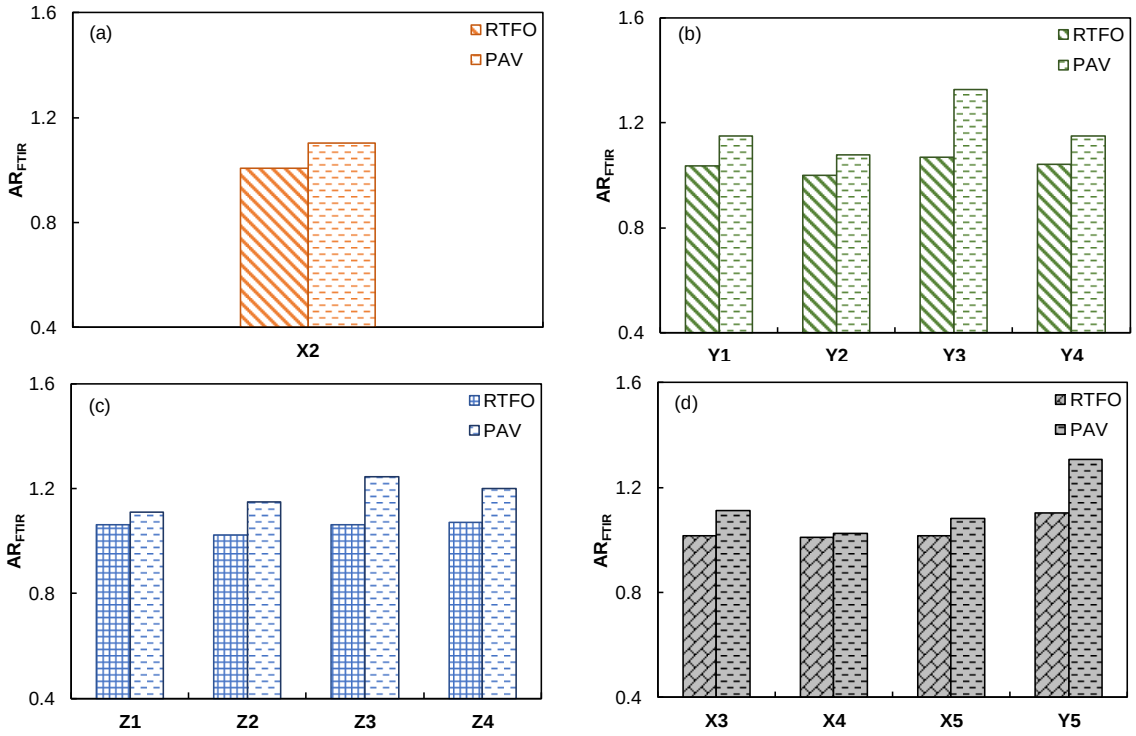

Figure 4-20: FT-IR based Aging Ratios for the Unmodified Asphalt Binders from Supplier, (a) X, (b) Y, (c) Z, and (d) Modified Binders from Suppliers X and Y.

4.3 Relating Molecular Structure and Linear Viscoelastic Properties of Asphalt

One of the main objectives of the current research was to relate asphalt linear viscoelastic parameters, more specifically relaxation spectra to asphalt microstructural parameters obtained from molecular weight distribution based assessment. In this process, it is important to understand why there should be a relationship between the physical and chemical attributes of asphalt binder in the first place. Effort is made here to explain the existence of relationship using examples from polymer literature, where the relationships are deduced from fundamental principles.

4.3.1 Physico-Chemical Relationship Basis: Lessons from Polymer Literature

In this section, the qualitative studies illustrated by Ferry (1960), are presented. The author while presenting the molecular origins to observed linear viscoelastic behavior argues that phenomenological theory of linear viscoelasticity though of great value for developing interrelationships between experimental measurements, provides little to no insight into the molecular origins of the linear viscoelastic behavior. Ferry associates the viscoelastic phenomenon in polymers to the adaptability of movement of flexible macromolecules and goes on to provide examples of correlations of different molecular motions to the shapes of the viscoelastic functions. The viscoelastic functions used in this case are the relaxation and retardation spectrum. The author mentions that the region where the relaxation spectra is relatively flat and retardation spectra goes through a maximum (around decade "-5") involves configurational re-arrangements of groups of molecules coupled tightly by entanglement, as shown by the author in Figure 4-21 and Figure 4-22.

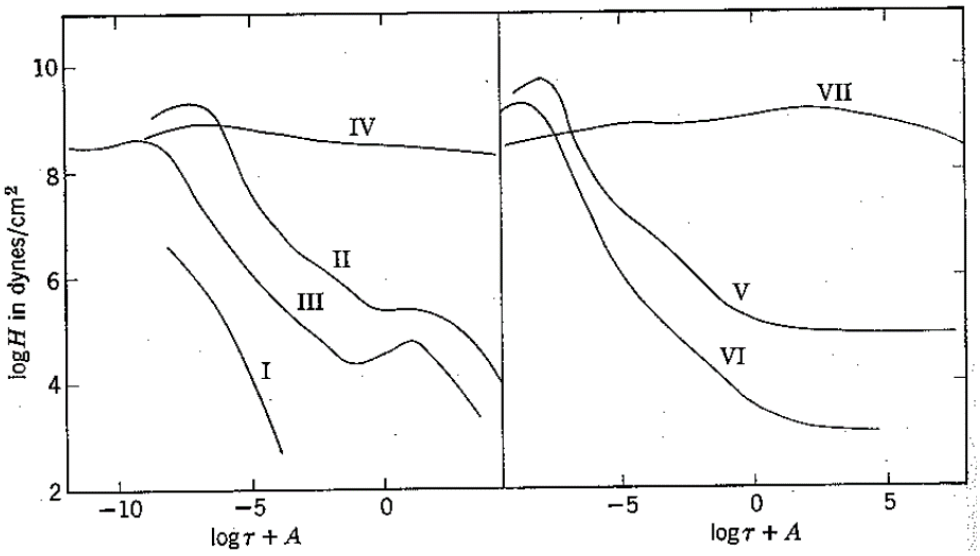

Figure 4-21: Relaxation Spectra for Seven Different Polymer Systems. (Ferry 1960)

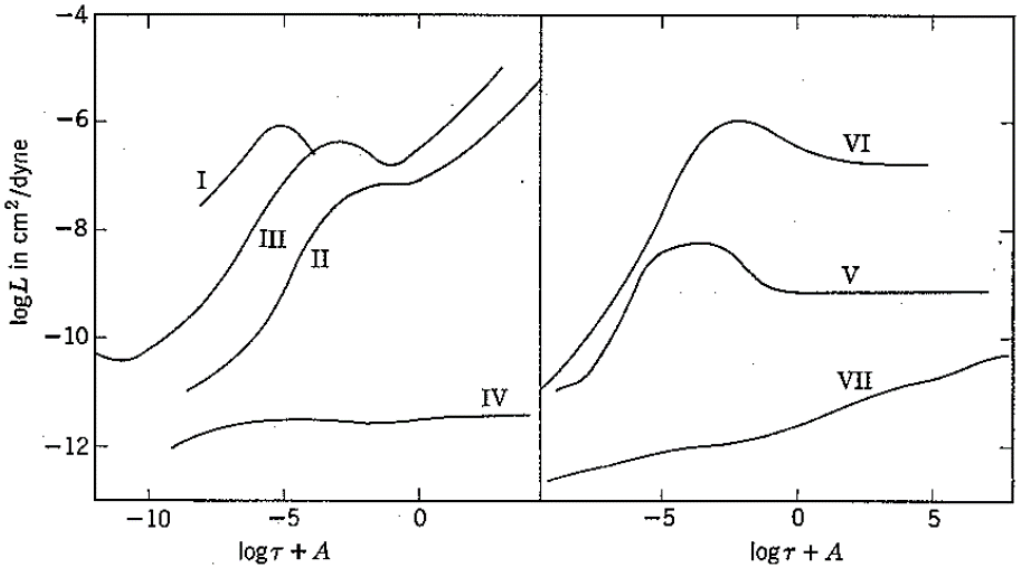

Figure 4-22: Retardation Spectra for Seven Different Polymer Systems. (Ferry 1960)

In order to provide more quantitative guidance to interpret the effects of chemical structure on viscoelastic functions, the author describes a theory based on the Brownian motion of isolated flexible polymer chains. An isolated polymer molecule diluted in a solvent is subject to random motions due to continuous re-arrangement of configuration. The driving force for these motions is the thermal energy and opposing force is the internal viscosity of the solvent. If the arrangement is disturbed by application of an external shear stress, small enough to be in the linear viscoelastic domain, then the Brownian motion goes on unperturbed. The author pursues this discussion in terms of viscoelastic functions of storage, J' and loss compliance, J''. As presented earlier in this chapter, the application of stress results in energy storage and the release of stress results in energy dissipation. Similarly, in this case, the amount of energy to stored and to be dissipated (contributions of polymer to J' and J'') depend on to what extent the random Brownian motions are correlated to the varying external forces. The author states that the displacement in phase

with the applied force, corresponds to energy storage and the velocity in phase with the applied force corresponds to energy dissipation.

Based on qualitative observations, Ferry says that at high frequencies there will be no time for change in molecular configuration, and the response to stress will be limited to bending and stretching of chemical bonds. Thus, such deformations correspond to high elastic stiffness and the compliance J' is small. However, at lower frequencies, the regions around the polymeric chain not too far detached from each other have enough time to change their respective positions within a period. It is then theorized that there will be components of displacement and velocity in phase with the changing stress and thereby substantial contributions to both J' and J''. At very low frequencies, J'' increases without limit, and J' reaches a limiting value. According to the author, this limiting value of J' at low frequencies is proportional to molecular weight and is orders of magnitude higher than the limiting value at high frequencies. The example of such behavior for low molecular weight polymer is provided by the author and is shown as Curve I in Figure 4-23 and Figure 4-24.

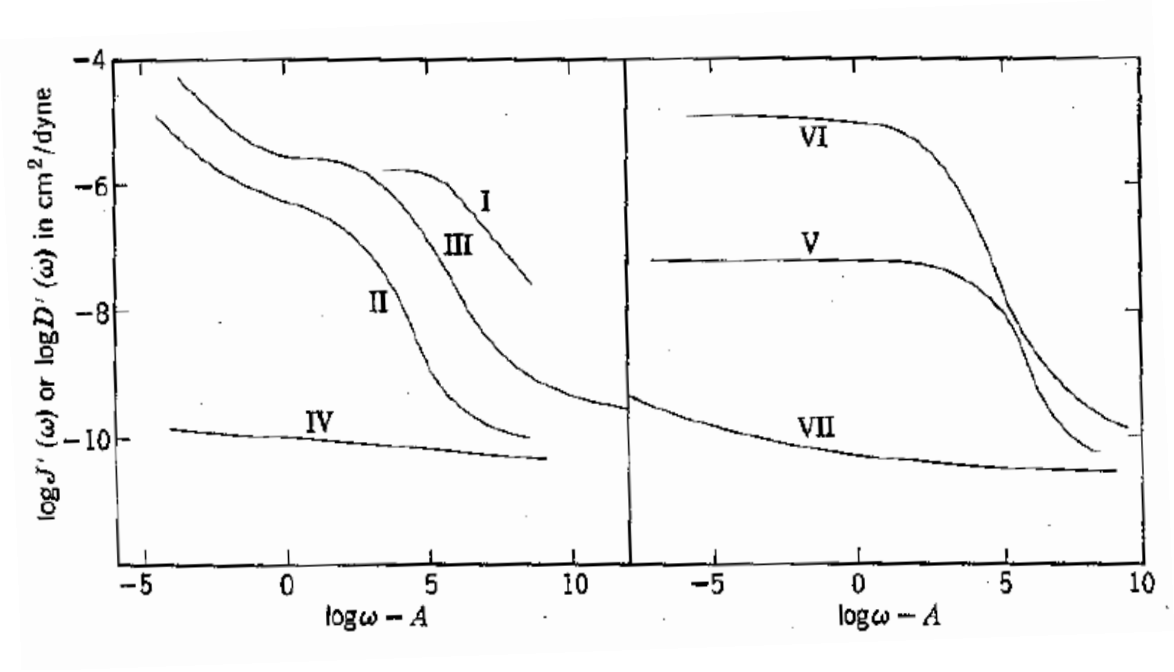

Figure 4-23: Storage Compliance for Seven Polymer Systems (Ferry 1960).

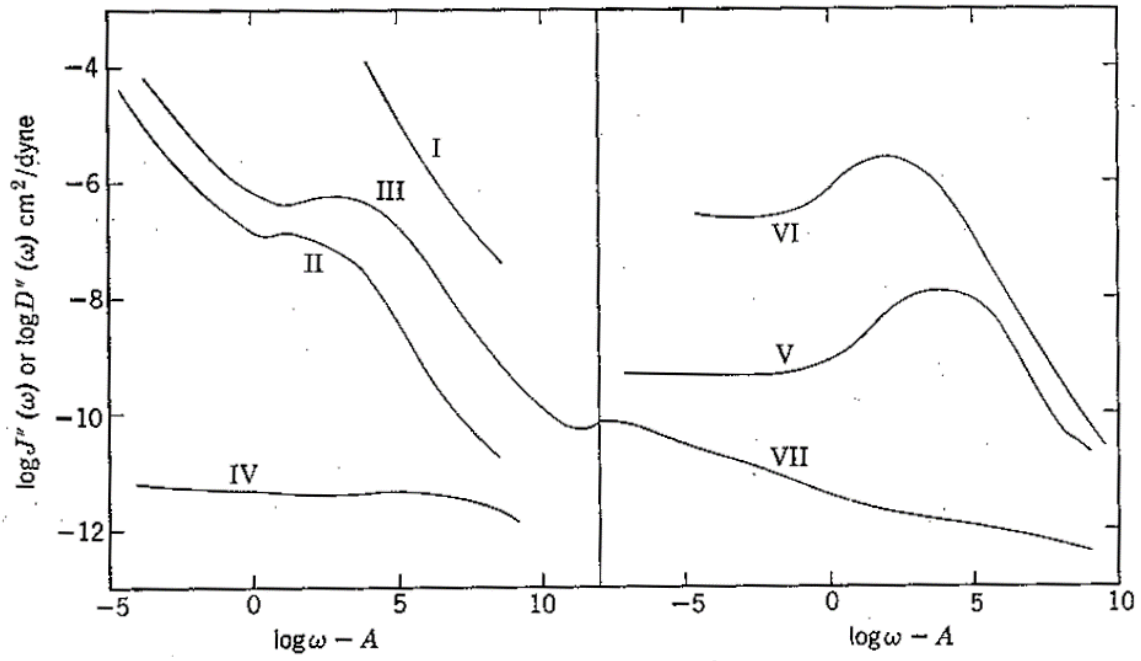

Figure 4-24: Loss Compliance for Seven Polymer Systems (Ferry 1960).

The theories presented above discuss the dependence of the physical property measurements on the molecular configuration of the polymers. Though, the molecular structure of asphalt and the molecular origin of linear viscoelastic behavior would be completely different to that observed in polymers, the above examples do provide a good basis for why physical – chemical property relationships exist.

4.3.2 Relating Molecular Weight and Relaxation Spectra

One such physical – chemical property relationship developed as part of this study was to relate the relaxation spectra to molecular weight obtained from molecular weight distribution obtained from LDMS assessment. In this process, correlations were developed by plotting *R* value against number average molecular weight (M_n). Initially all binders irrespective of polymer modified or not were plotted together on the same plot as shown in Figure 4-25 at original and PAV aged conditions. However, a closer look at the relationship shows that there exists a clear separation between the non-polymer modified asphalts and the polymer modified asphalts, as highlighted in the figure. The possible reason for this separation is as below. The *R* value, which is obtained from rheological testing of the asphalt binders is sensitive to the presence of polymer in these asphalts. However, the M_n value calculated for the polymer modified asphalts is not sensitive to the presence of polymer in the acquired mass range. This is not a one-one comparison and a possible reason for delineating from the actual trend. It has to be also recalled that when rheological index was developed as part of the SHRP work, the work was performed only on non-polymer modified asphalts. Taking these considerations into account, correlations were redeveloped after excluding the polymer modified asphalts. The results are presented in Figure 4-26.

There is a significant improvement in correlation at both original and PAV aged conditions. There existence of strong correlation between the two parameters indicates that the width of its relaxation spectrum increases with increase in molecular weight of the asphalts. The significance of which is that, higher molecular weight asphalts require more time to relax the induced stresses than low molecular weight asphalts.

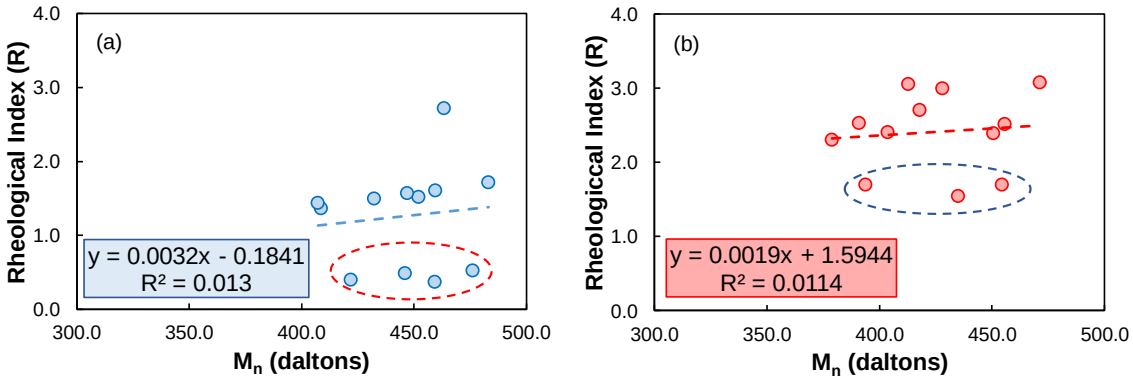

Figure 4-25: Relationship between Rheological Index (*R*) and Number Average Molecular Weight (M_n) for All Study Binders at (a) Original; and (b) PAV Conditions.

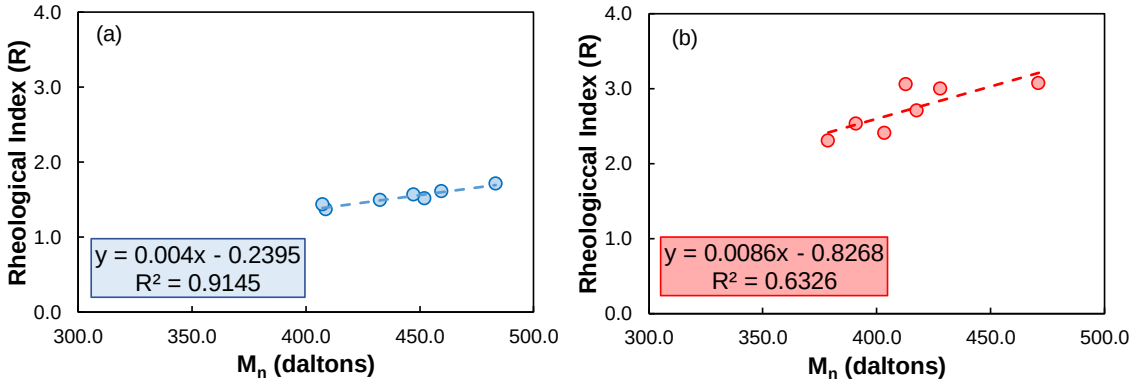

Figure 4-26: Relationship between Rheological Index (*R*) and Number Average Molecular Weight (M_n) for Non-Polymer Modified Asphalt Binders at (a) Original; and (b) PAV Conditions.

4.3.2.1 Developing Shape Parameters for MWD and their Relationship to *R* Value

The relationships developed in the section above relate relaxation properties of asphalt to one of the central tendency parameters of the MWD, M_n. However, there is no insight gained as to how the shape of the MWD may affect the LVE properties or in this case the *R* value. It can be observed from the MWD for the study asphalt binders that the distributions are skewed to the right. Effort was made to identify distributions which can be right skewed. One such distribution which was chosen is gamma distribution, which is a two-parameter continuous probability distribution. The molecular weight distributions of non-polymer modified asphalts presented in Figure 4-12 and Figure 4-13 were fit to gamma distribution function in excel using least squared error regression. It was seen that the gamma distribution function fits well to the MWD of the asphalts. The only exception would be that if a distribution function is used, capturing deviations from the norm, such as the hump observed around 500 daltons in binders from supplier Z, is not possible. The fit distributions for binder PG 76-16(X) is presented in Figure 4-27 and for the remaining binders they are presented in Appendix E. Based on the distribution, the shape parameters of the distribution can be calculated, these are skewness and kurtosis. Skewness is the measure of asymmetry of the distribution and kurtosis is the measure of tailedness of the distribution. The gamma distribution parameters, α and β, skewness and kurtosis values calculated from the fit distribution for the non-polymer modified asphalts is presented in Table 7.

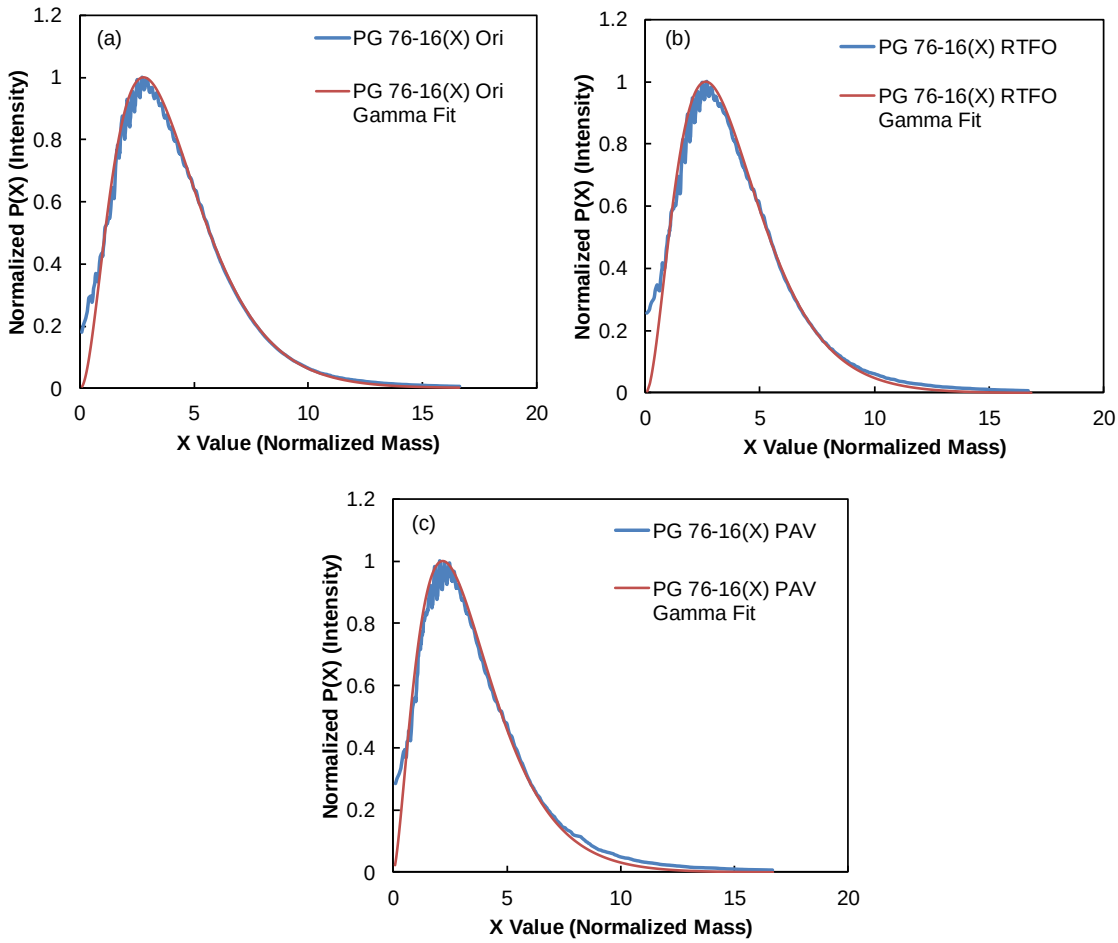

Figure 4-27: Molecular Weight Distribution of Asphalt Binder PG 76-16(X) at (a) Original; (b) RTFO; and (c) PAV Conditions Fit to Gamma Distribution.

Table 7: Descriptors of Gamma Distribution Fit and the Shape Parameters.

Binder	Condition	α	β	Skewness	Kurtosis
PG 70-16(Y)	Ori	4.75	0.96	0.92	1.26
	RTFO	3.24	1.19	1.11	1.85
	PAV	3.10	1.32	1.14	1.94
PG 76-16(Y)	Ori	2.57	1.37	1.25	2.34
	RTFO	2.02	2.20	1.41	2.98
	PAV	2.48	1.69	1.27	2.42
PG 76-16(X)	Ori	2.65	1.47	1.23	2.26
	RTFO	4.79	0.99	0.91	1.25
	PAV	2.92	1.28	1.17	2.05

PG 64-22(Z)	Ori	3.06	1.28	1.14	1.96
	RTFO	2.81	1.16	1.19	2.13
	PAV	2.11	1.93	1.38	2.84
PG 70-10(Z)	Ori	2.94	1.27	1.17	2.04
	RTFO	2.52	1.59	1.26	2.39
	PAV	2.78	1.78	1.20	2.16
PG 70-22(Z)	Ori	3.09	1.11	1.14	1.94
	RTFO	2.68	1.30	1.22	2.24
	PAV	2.16	1.40	1.36	2.78
PG 76-16(Z)	Ori	1.95	2.03	1.43	3.08
	RTFO	2.19	1.38	1.35	2.74
	PAV	2.17	1.65	1.36	2.77

In order to relate the shape of the MWD to the relaxation properties of the asphalt binder, skewness and kurtosis were plotted against the rheological index. The relationships are presented in Figure 4-28 through Figure 4-30 for original, RTFO aged and PAV aged asphalt binders. It can be seen that each of these figures, has two part figures. The part (a) includes PG 70-16(Y) in the relationship and part (b) excludes PG 70-16(Y) from the relationship. The data point corresponding to PG 70-16(Y) seems to be an outlier, in both skewness and kurtosis relationship for all three aging conditions. When PG 70-16(Y) is included in the relationship, the correlation between the R value and the shape parameters is very poor. However, when the binder is excluded the correlation improves with maximum R^2 of around 0.45 seen in RTFO aged asphalt binders. The trend suggests that as the asymmetry in the molecular weight distribution increases, the width of the relaxation spectrum increases. Thereby, asphalt binders with greater asymmetry in their molecular weight distribution will require more time to relax the induced stresses. Same trend was seen with kurtosis too. Therefore, an asphalt binder which has a greater tail in its molecular weight distribution will require more time to relax the induced stresses.

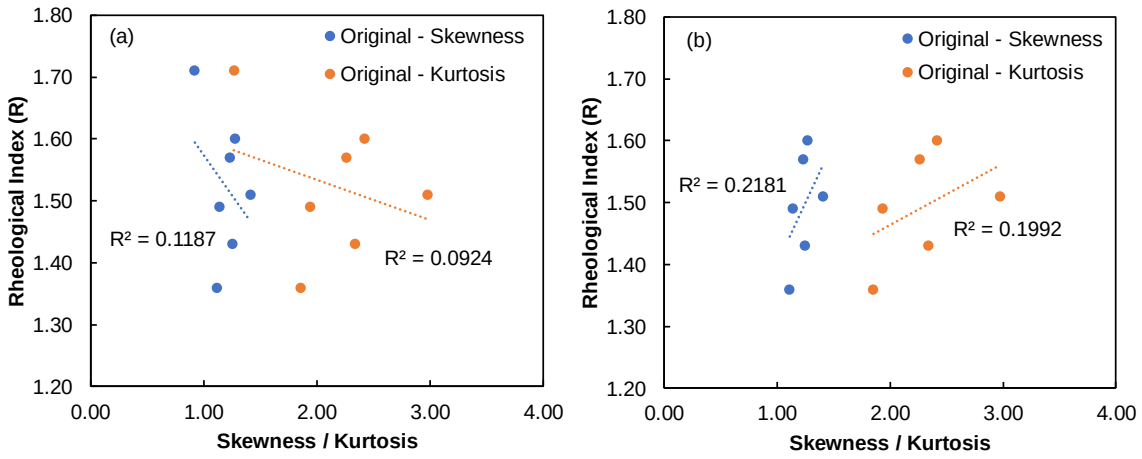

Figure 4-28: Relationship between Rheological Index and Skewness, Kurtosis for Original Asphalts (a) Including PG 70-16(Y); and (b) Excluding PG 70-16(Y).

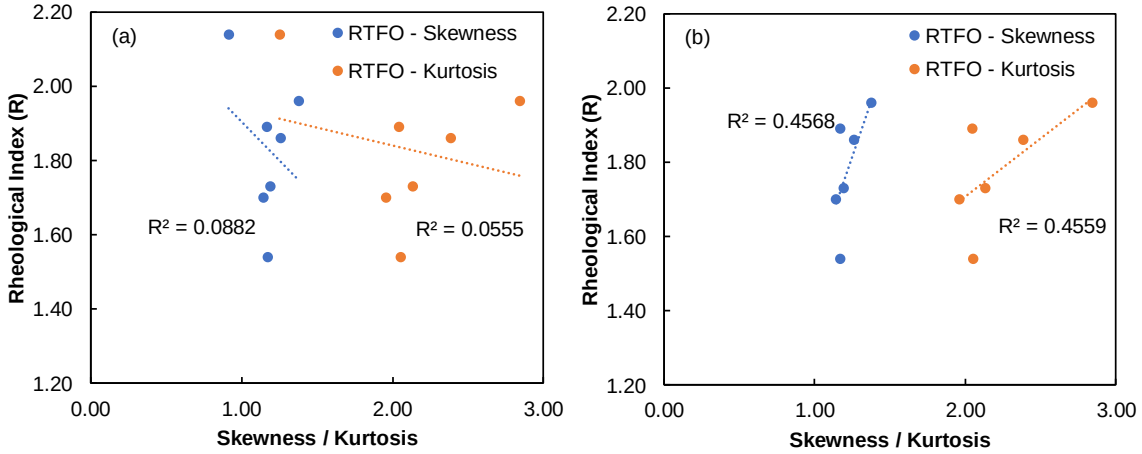

Figure 4-29: Relationship between Rheological Index and Skewness, Kurtosis for RTFO Aged Asphalts: (a) Including PG 70-16(Y); and (b) Excluding PG 70-16(Y).

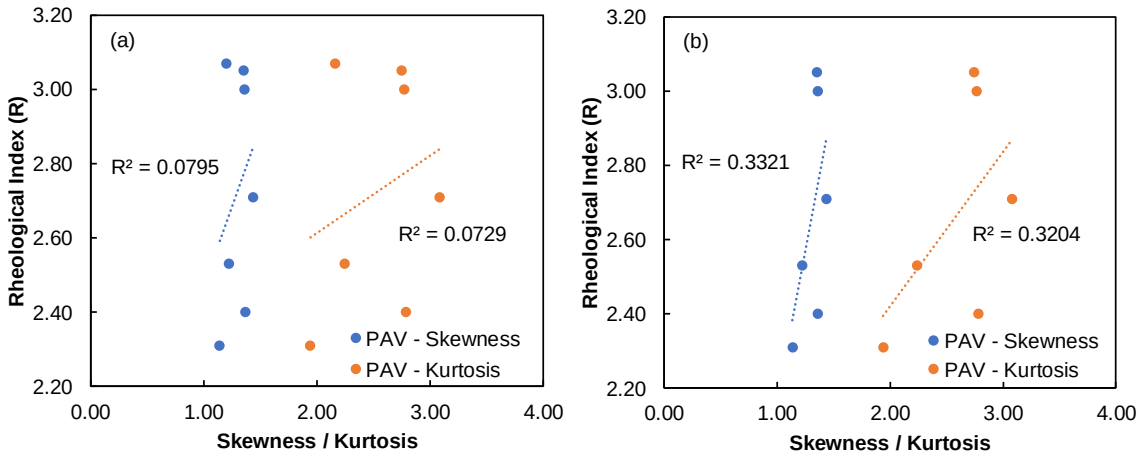

Figure 4-30: Relationship between Rheological Index and Skewness, Kurtosis for PAV Aged Asphalts: (a) Including PG 70-16(Y); and (b) Excluding PG 70-16(Y).

In order to justify the observations seen in Figure 4-28 through Figure 4-30, literature from polymer sciences was explored to learn more about the observed behavior. The literature relating to asymmetry of molecular weight distribution to stress relaxation properties is very limited. One such study by Nadgorny et al. (2017) looked at the shape of the molecular weight distribution as a manipulation strategy to control processing parameters. The authors looked at two polystyrene compounds, high polystyrene (PS_{High}) and low polystyrene (PS_{Low}). The distribution of high polystyrene is right skewed, and low polystyrene is left skewed as calculated through GPC. It is to be noted here that right skewed here means greater fraction of large molecular fraction in comparison of left skewed. This is in contrast to the definition of right skewed in LDMS data, where in comparison to left skewed, right skewed means a distribution has greater low molecular weight fractions. This is because the MWD plotted in GPC, has retention time increasing from left to right on the X axis, wherein low retention time corresponds to high molecular weight and vice-versa. The authors performed temperature-frequency sweep experiments

on the two materials and found that PS_{high} was seen to have greater storage modulus than PS_{low}. The authors attributed these differences to the different chain length compositions of the polymers. According to the authors, since PS_{high} contains larger fraction of high molecular weight fractions than PS_{low} therefore its response to induced oscillatory deformation at shorter time scales is more limited. This, the authors say is associated to strong elastic response, represented by high storage modulus values. Thereby, it can be concluded that due to a higher elastic response stress relaxation in PS_{high} will be faster than in PS_{low}. This observation is inline with the findings from the current study where binders with greater asymmetry in LDMS (more relative right skew) containing greater low fraction molecular weights were seen to require more time to relax the induced stresses. This study by authors Nadgorny et al., justifies the trends developed in the current study relating MWD shape parameters to LVE parameters.

In this chapter, the viscoelastic characteristics of asphalt binders, along with their molecular structure characteristics are presented. The viscoelastic characteristics presented include, the dynamic modulus, the discrete and the continuous relaxation spectra of the study asphalts. The molecular characterization included development of the molecular weight distribution from the raw data acquired through the LDMS experiment, subsequent calculation of molecular weights. Also, data from FT-IR spectroscopy tests on study binders are presented. Finally, the basis for exploration of physical-chemical property relationships is explained through examples from polymer literature along with the relationship developed in the current study, wherein the *R* value was related to the number

average molecular weight of asphalt binders. Also shown is the relationship between molecular weight distribution shape parameters and *R* value.

Chapter 5 NLVE Studies I - Non-Linearity Assessment Based on Intermediate Temperature Time Sweep Tests

In the previous chapter, the results and discussions from the linear viscoelastic characterization tests were discussed. In the next few chapters, the results and discussions from the non-linear viscoelastic tests will be discussed. The discussions have been segmented into three chapters, depending upon the tests and the strain level at which the tests are performed. The present chapter, deals with the time sweep fatigue tests performed on asphalt binders at intermediate temperature and for peak to peak strain level in the range of 5% to 15%. The tests and analyses performed in this chapter, are part of the NCHRP 09-54 project. Thereby, the study materials used in this chapter differ from remainder of the study and belong to Set 2 asphalt binders as mentioned in Chapter 3. The chapter has been segmented into three parts, first the study materials used in the tests are discussed, followed by the experimental results from the temperature-frequency sweep tests, time sweep tests, and RSS tests. Subsequently, the analyses performed with regard to development of the damage characteristic curves are discussed. The main goal of this chapter is to demonstrate the utility of time sweep test in characterization of NLVE.

5.1 Study Materials

The materials used in this study were part of the NCHRP 09-54 project and differ from the materials used in the remainder of the study. Though a detailed description of the materials has been provided in chapter 3, a brief introduction is presented here. The binders used in this chapter form the set 2, of the asphalt binders used in this dissertation. Three binders, B1, B2, and B3 with PG grades of PG 58-28, PG 64-28, and PG 70-28 respectively are

used. While B1 and B2 are non-polymer modified binders, B3 binder is a SBS based polymer modified binder. The binders have been aged at different temperatures in a PAV, corresponding to 7, 15, and 22 years of service. The time sweep fatigue tests were performed on the both the unaged as well as the aged asphalt binders.

5.2 Experimental Results

5.2.1 Temperature – Frequency Sweep Tests

While the focus of this chapter is the time sweep test, it is to be noted that in order to characterize the continuum damage model and to develop the damage characteristic curve, dynamic modulus data is required. The temperature and the frequency conditions at which the dynamic modulus tests were performed are similar to those presented in the previous chapter. The dynamic modulus mastercurves for the three binders at multiple aging levels are presented in Figure 5-1 through Figure 5-3. The general trend from all mastercurves is clear that the modulus increases with aging level.

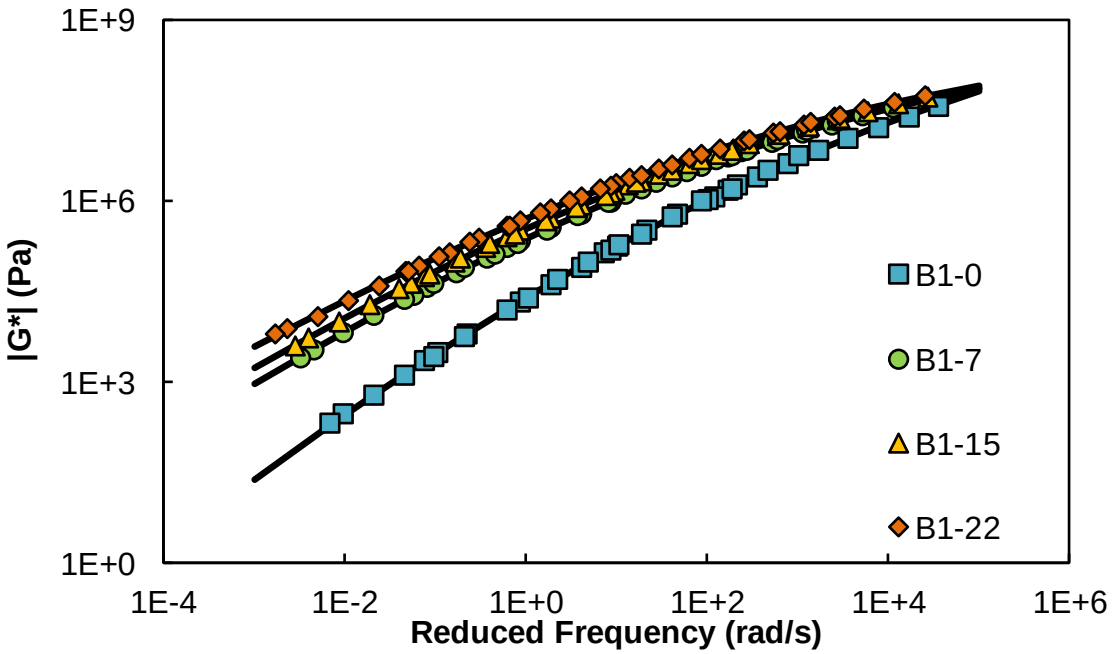

Figure 5-1: Dynamic Modulus Mastercurves for Binder B1, PG 58-28, at different aging levels.

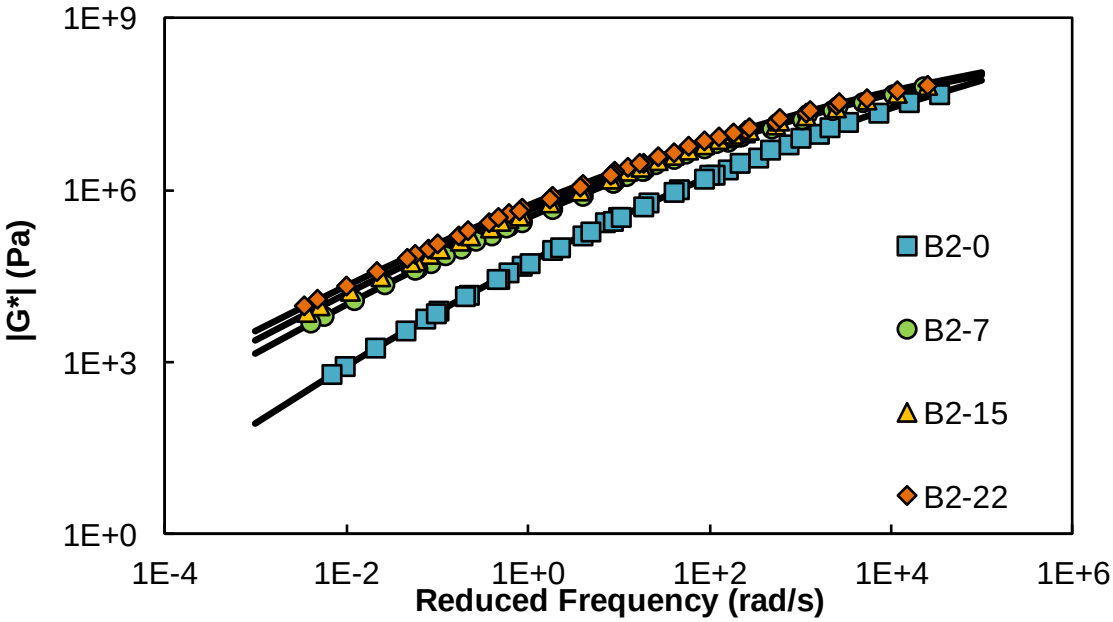

Figure 5-2: Dynamic Modulus Mastercurves for Binder B2, PG 64-22, at different aging levels.

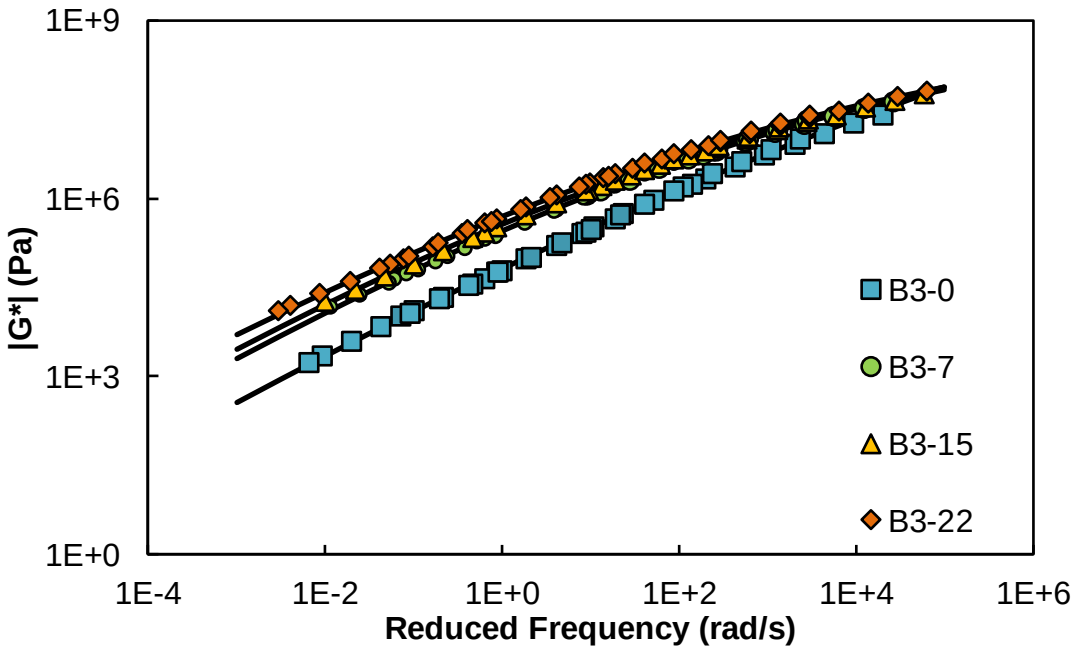

Figure 5-3: Dynamic Modulus Mastercurves for Binder B3, PG 70-28(SBS), at different aging levels.

5.2.2 Time Sweep Fatigue Tests

Strain controlled time sweep experiments were performed on the study materials to assess the fatigue properties and to characterize the continuum damage model. It should be noted that the tests were carried out at single temperature, 13°C and at two different strain levels which varied from binder to binder. The peak to peak strain levels used for each binder are summarized in Table 8. The temperature of 13°C was selected after a consideration for the edge flow phenomenon. The phenomenon, which is more likely to occur in softer materials, was evaluated using the unaged B1 binder since it has the lowest modulus among the materials in the test matrix. Thereby, the temperature sufficed for other binders also.

Table 8: Peak to Peak Strain Levels Used to Perform Time Sweep Tests at 13°C.

Sample	Strain Levels
B1-0	5%, 10%
B1-7	10%, 15%
B1-15	
B1-22	
B2-0	5%, 10%
B2-7	
B2-15	
B2-22	10%
B3-0	12%, 15%
B3-7	
B3-15	
B3-22	

The fatigue failure criteria adopted for the present study is that where a drop in the phase angle is observed during the experiment. The corresponding cycle number at the phase angle drop is the number of cycles to failure for the material at that strain level. A schematic of the phase angle drop is shown in Figure 5-4.

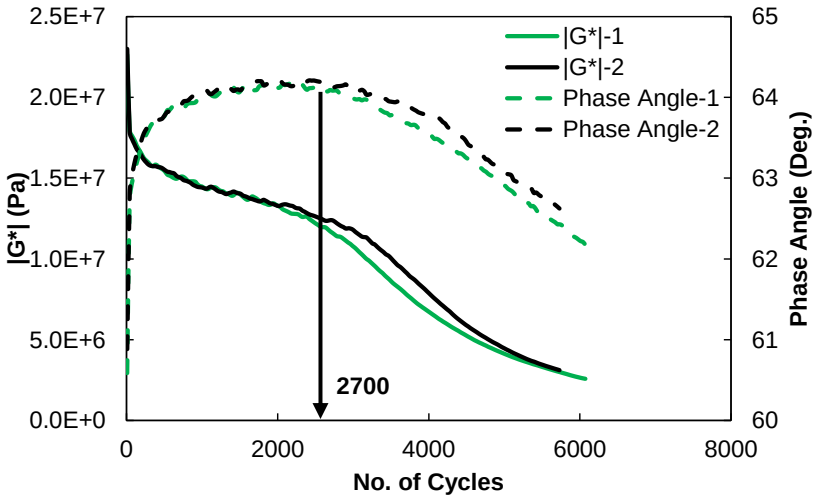

Figure 5-4: Schematic showing the phase angle drop and the number of cycles to failure determination.

The number of cycles to failure for the binders at different aging levels at their corresponding aging level is shown in Table 9 and graphically presented in Figure 5-5 through Figure 5-7.

Table 9: Number of Cycles to Failure for B1, B2, B3 Binders at Different Strain Levels.

Sample	5%	10%	12%	15%
B1-0	30250	4650	-	-
B1-7	-	28100	-	5950
B1-15	-	24250	-	7100
B1-22	-	31000	-	10800
B2-0	39500	6340	-	-
B2-7	33500	3150	-	-
B2-15	12200	2550	-	-
B2-22	-	3682	-	-
B3-0	-	-	24000	12350
B3-7	-	-	234250	122500
B3-15	-	-	189048	65508
B3-22	-	-	112500	63500

The general interpretation of the N_f varied from binder to binder. It was seen that among B1 binders the fatigue life increased with increase in aging level. Among B2 binders the general interpretation was that the fatigue life decreased with increase in aging level. However, interesting results are obtained for B3 binder. For both B3 binders, it is seen that the fatigue life increases from control to 7 years aging condition. However, with further increase in aging level i.e. at 15 and 22 years the fatigue life decreased. Clearly, it can be seen that polymer modification does have a positive effect on cycles to failure. The increase in N_f from 0 years to 7 years aging condition can be attributed to a theory developed by Jahangir et al. (2015). The theory states that aging reduces the modulus gradient or the mismatch within different phases in the binder microstructure. It is understood that crack initiation in asphalt binder may occur at the interface of such phases, with greater modulus

mismatch between the phases leading to early cracking or reduced fatigue resistance. Having a lower modulus mismatch, delays the occurrence of cracking, thus higher fatigue life. However, this explanation does not adequately explain why N_f at higher aging levels decreases for B3 binder.

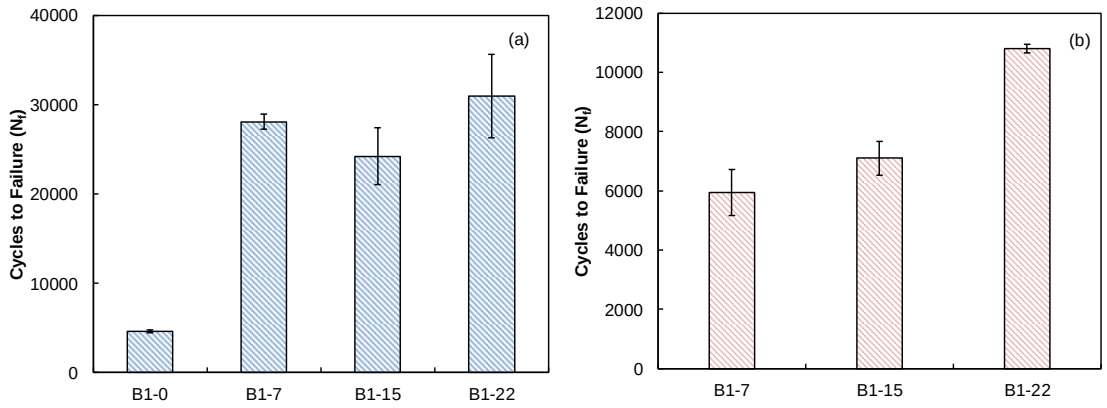

Figure 5-5: Variation of N_f at different aging levels for B1 binder at: (a) 10% and (b) 15% strain levels.

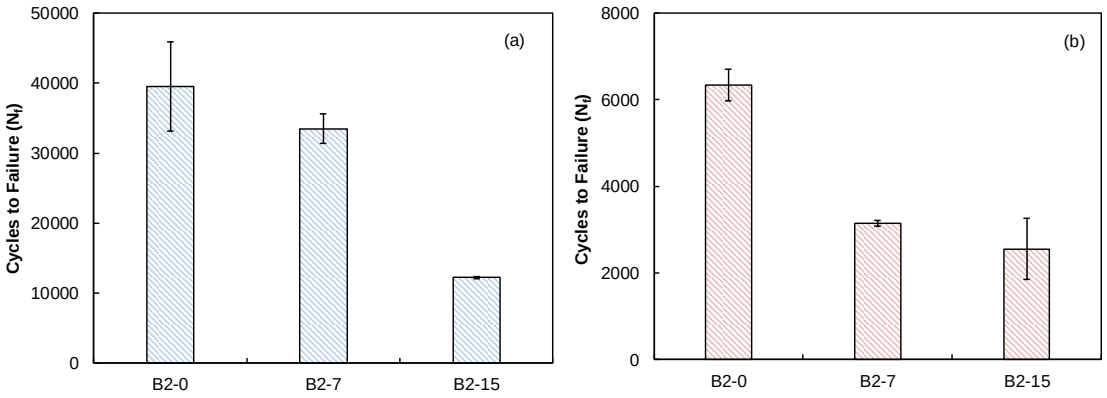

Figure 5-6: Variation of N_f at different aging levels for B2 binder at: (a) 5% and (b) 10% strain levels.

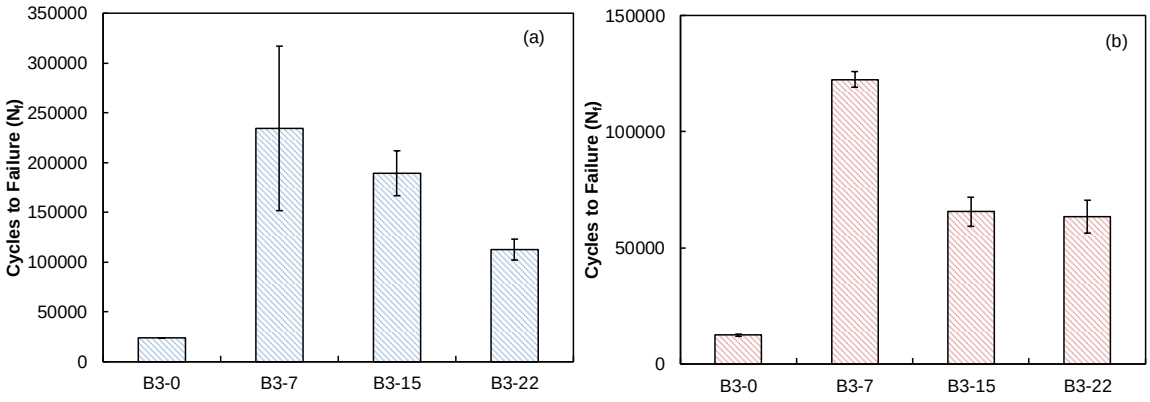

Figure 5-7: Variation of N_f at different aging levels for B3 binder at: (a) 12% and (b) 15% strain levels.

5.3 Damage Analysis

Underwood (2011) applied the S-VECD model to evaluate the fatigue performance of the asphalt binders at strain levels that were not tested and also to more systematically evaluate the cause of the unexpected binder and mastic fatigue performance with aging (Underwood 2011). The S-VECD model is based on the same S-VECD method that is applied to asphalt concrete mixtures, with exceptions to account for the greater nonlinear viscoelastic response of binders and the torsional loading that is applied to asphalt binders and mastics. In torsional loading, loading is referred to as either positive displacement (clockwise rotation) or negative displacement (counter-clockwise rotation). The damage that occurs in torsional loading is likely due to anti-plane shearing.

The S-VECD model formulation that was used to model asphalt binder and mastic behavior in this study is shown in Equation (35) through (42). The most important functional relationship in the model is the one between pseudo stiffness (*C*) and damage (*S*). The parameter *C* represents the loss in modulus value that occurs as the test progresses, *S* is the damage parameter that represents the amount of damage that occurs due to

cracking, and the functional relationship between the two variables represents the fundamental interaction between material integrity and damage. The importance of this function is that it has been shown to be independent of strain amplitude and frequency and, thus, when characterized can be used to predict behavior under many other conditions that were not used directly in the characterization.

$$C = \frac{\tau}{\gamma^R * DMR},\ for \xi \le \xi_p \tag{35}$$

$$C = C^* = \frac{\tau_{0,pp}}{\gamma^R * DMR},\ for \xi \ge \xi_p \tag{36}$$

$$\gamma^R = \gamma^R = \frac{h_1}{G_R}\int_0^{\xi} G(\xi' - \tau')\frac{dh_2\gamma}{d\tau'}d\tau',\ for \xi \le \xi_p \tag{37}$$

$$\left(\gamma^R_{0,pp}\right)_{cyclei} = \frac{1}{G_R} * \left((\gamma_{0,pp})_i * \left|G^*\right|_{NL}\right) for \xi > \xi_p \tag{38}$$

$$dS = (dS_{Transient})_{timestepj} = \left(-\frac{DMR}{2}(\gamma^R)_j^{\,2}\Delta C_j\right)^{\frac{\alpha}{1+\alpha}} * (\Delta\xi)_j^{1/\alpha},\ for \xi \le \xi_p \tag{39}$$

$$dS = (dS_{Cyclic})_{cyclei} = \left(-\frac{DMR}{2}(\gamma_{0,pp}{}^R)^2\Delta C_i\right)^{\frac{\alpha}{1+\alpha}} * (\Delta\xi_p * \mathrm{B}_1)_j^{1/1+\alpha},\ for \xi > \xi_p \tag{40}$$

$$B_1 = f_R\int_{\xi_i}^{\xi_f} (f(\xi))^{2\alpha} * d\xi \tag{41}$$

$$f(\xi) = -\frac{1}{2}\cos(\omega\xi) + \frac{(\tau_{peak})_i + (\tau_{valley})_i}{2\left[(\tau_{peak})_i - (\tau_{valley})_i\right]} \tag{42}$$

where;

C = pseudo stiffness in first half of first loading cycle,

C^* = pseudo stiffness during the remainder of the test,

DMR = $\frac{|G^*|_{fingerprint}}{|G^*|_{LVE}}$,

τ = torsional stress amplitude,

$\tau_{0,pp}$ = torsional stress amplitude (peak to peak),

γ^R = pseudo strain,

$\gamma^R_{0,pp}$ = pseudo strain (peak to peak),

$\gamma_{0,pp}$ = peak to peak strain,

h_1 , h_2 = non-linear functions,

$G(\xi')$ = strain dependent relaxation modulus,

ξ' = strain dependent reduced time variable,

G_R = reference shear modulus,

$|G^*|_{NL}$ = non-linear viscoelastic modulus,

ξ_p = reduced pulse time,

$dS_{Transient}$ = early portion of damage calculation,

dS_{Cyclic} = remaining portion of damage calculation,

α = factor that relates to viscoelastic time dependence,

B_1 = shape factor,

ω = angular frequency,

τ_{peak} = largest stress value within cycle *i*, and

τ_{valley} = smallest stress value within cycle *i*.

The inputs for this model were obtained from temperature-frequency sweep tests (linear viscoelastic properties), time sweep (strain-controlled fatigue) tests, and repeated stress sweep (RSS) tests (to obtain nonlinear viscoelastic properties). The torque and displacement inputs from the time sweep tests were obtained using a stand-alone data acquisition system created in LabVIEW that is able to acquire a data point approximately every 0.001 second. The Prony coefficients (relaxation modulus and creep compliance) to be used for the model were obtained from the temperature-frequency tests via collocation. Strain-level nonlinearity in the binder RSS tests was determined for the test materials at 13°C. Details regarding the RSS test is explained in chapter 3. An example of the typical response from the RSS test is shown in Figure 5-8 for binder B2-0.

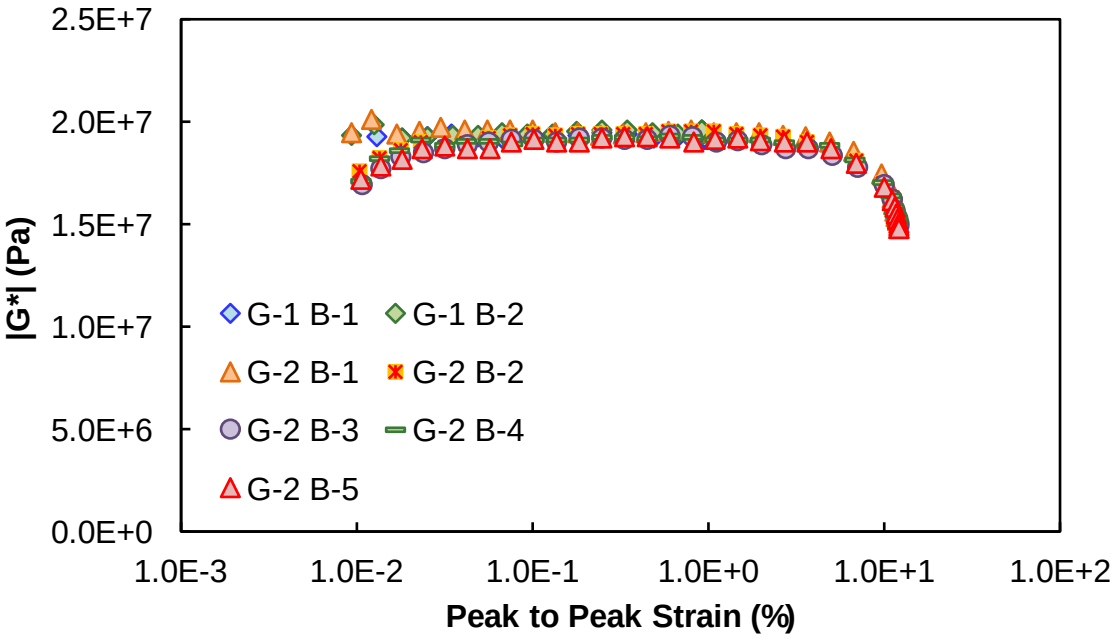

Figure 5-8: Response from RSS Test for Binder B2 at 0 years.

Once the nonlinear viscoelastic response is characterized, it can be used along with the measured time, stress, and strain values, and Equations (35) through (42) to characterize the damage characteristic curves for the different materials. These curves are shown in Figure 5-9 through Figure 5-11. The data in these figures represent the best fit function from the individual replicate data and are shown only up to the average damage at failure for each of these tests.

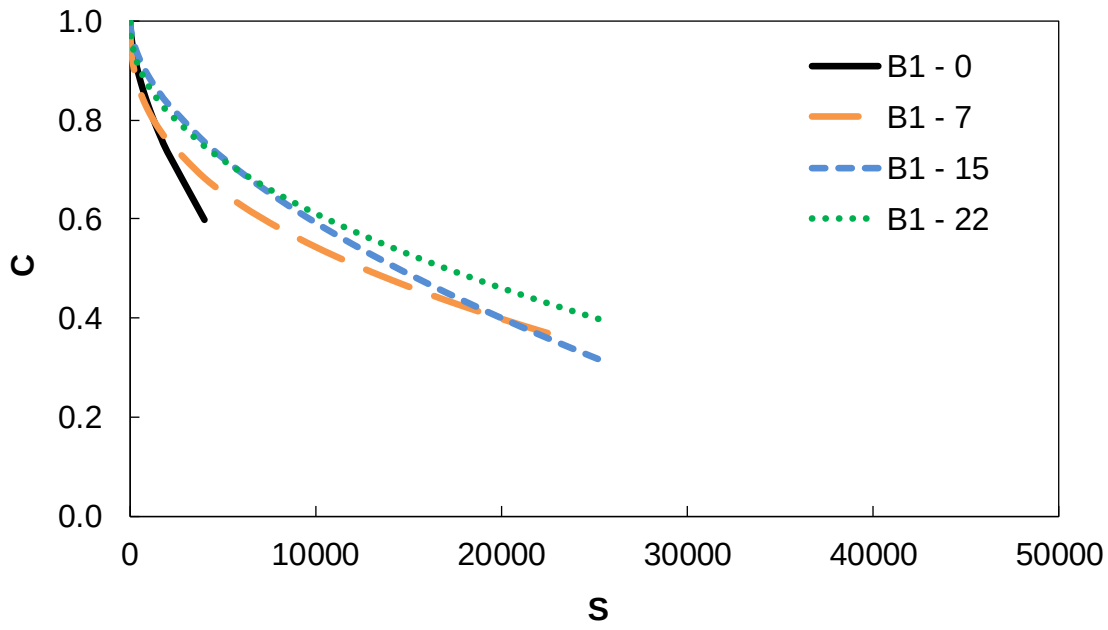

Figure 5-9: C vs. S curve for B1 binder at different aging levels.

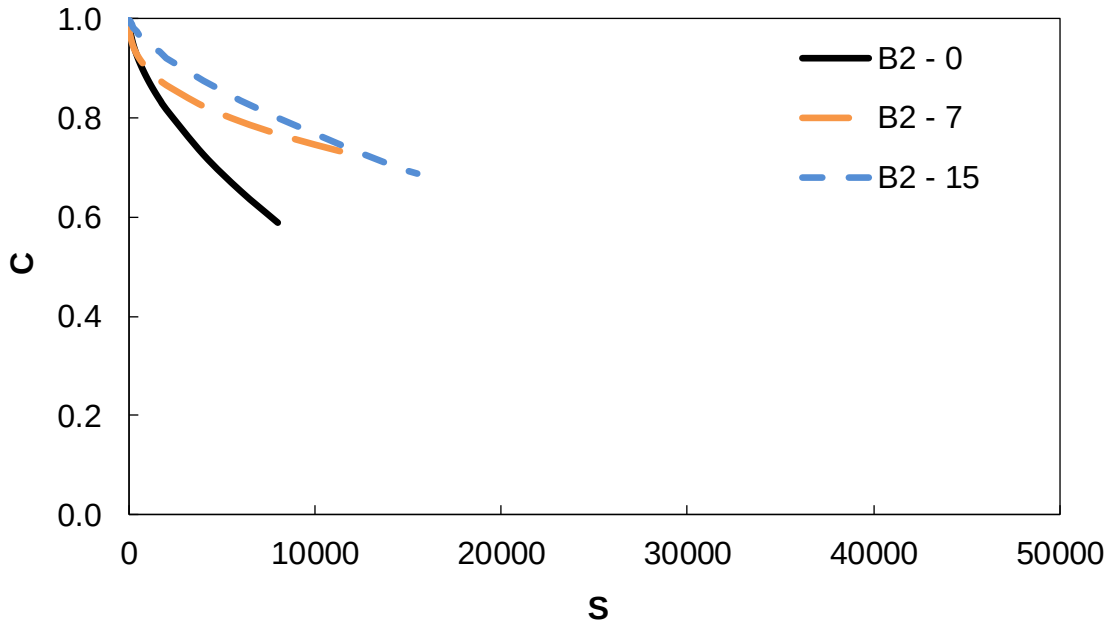

Figure 5-10: C vs. S curve for B2 binder at different aging levels.

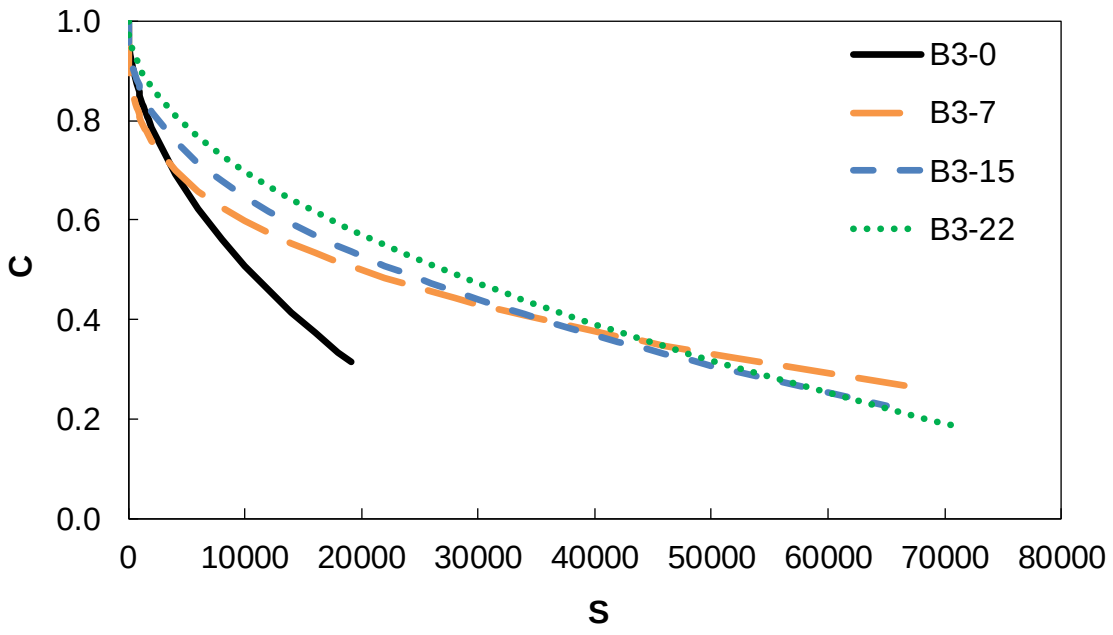

Figure 5-11: C vs. S curve for B3 binder at different aging levels.

The common observation that can be made for all binders B1, B2, and B3 is that the level of damage at failure increases with an increase in aging level. However, to draw conclusions about the fatigue behavior of these materials, it is important to consider the C value at failure for these materials. For the B1-based binders, shown in Figure 5-9, it is observed that the aged binders fail at a lower pseudo stiffness, C, than the unaged binders. This finding suggests that aged materials provide better resistance to fatigue damage than unaged materials, which is contrary to the common belief that fatigue resistance decreases with an increase in aging level. Also, among the aging levels, this figure shows that binder at an aging level of 15 years exhibits better resistance to fatigue than those at 7 years, as they fail at a lower C value. However, for binder B1 at 22 years, this failure occurs at a higher C value than for B1 at 7 years. The reason for this trend reversal could be related to

the natural variability of the tests, and thus, the differences would not be statistically significant. The general trend obtained from the C versus S approach adds support to the findings that are based on N_f value. These trends show that for the B1 binders, longer aging results in better resistance to fatigue.

For the B2-based binders shown in Figure 5-10, the unaged materials fail at a lower pseudo stiffness value than the aged materials. This finding is in direct contradiction to the observations made from the B1 binders. However, it is seen that within the aging levels, the binder corresponding to 15 years of aging have lower C values at failure than the materials that correspond to 7 years of aging.

Similar to the B1 binders, even aged binders in the B3 set of binders fail at a lower pseudo stiffness, C, than the unaged binders as shown in Figure 5-11. Among the aging levels, it is seen that binder at 22 years exhibits highest fatigue resistance, followed by the binders at 15 and 7 years respectively.

5.4 Summary

The goal of this chapter was to demonstrate the use of intermediate temperature fatigue tests for characterizing non-linear viscoelastic behavior of asphalt binders. This has been successfully accomplished by performing temperature-frequency tests, time sweep tests, and RSS tests on three asphalt binders at multiple aging levels. Subsequently, the results from the tests were used to characterize the continuum damage model and develop the damage characteristic curves.

Overall, the results from the intermediate temperature time sweep fatigue tests show that the fatigue performance across aging levels is a strong function of the type of binder being

used. Some proof for the trends observed, especially with regard to the increased fatigue resistance with aging for the B1 and B3 binders, is available in literature by Jahangir et al. (2015), which states having lower modulus mismatch among the phases in the asphalt microstructure delays the occurrence of cracking thus leading to a longer fatigue life.

Chapter 6 NLVE Studies II – Non-Linearity Assessment Based on High Temperature LAOS Tests

In the previous chapter, the LAOS tests were conducted using time sweep tests at intermediate temperature of 13°C. The strain amplitudes employed to run the time sweep tests ranged from 2.5%-7.5%. However, in this chapter the non-linear LAOS experimentation is carried out at high temperatures of 40°C and 64°C and at strain levels between 20% to 120%. In this chapter analysis of the non-linear viscoelastic response of asphalt binders using large amplitude oscillatory shear (LAOS) tests at high temperatures is discussed. The main motivation for high temperature LAOS stems from the idea that strain levels experienced by the binder at such high temperature will be similar to the strains experienced by the binder in an asphalt concrete pavement that is subject to rutting. For example, a 0.15 inch rut depth in a 1.5 inch layer of asphalt concrete = 10% strain in the asphalt concrete. The effective volume of asphalt in a typical mixture = 10%, which assuming simple blending means 100% strain in the binder. Also, literature provides some guidance in this regard. Kose et al. (2000) suggested that strain in asphalt binder may be about 15 times the strain in FAM. If FAM is assumed as a surrogate to asphalt concrete mixture, then the strain in binder would be about 150%. The LAOS experiments performed at these high temperatures have the capability of characterizing the material at these strain levels. Also, the stress-strain hysteresis developed using NLVE experiments at intermediate temperatures did not show any distortion, thus high temperature LAOS experiments are conducted to investigate the presence of distortion at these high strain levels.

As mentioned in Chapter 1, the program used for this LAOS analysis is called MITlaos, which is based on Fourier transform analysis and is used to deconvolve stress-strain history into their harmonic constituents and identify nonlinearity (Hyun et al. 2011). The idea for the use of MITlaos to detect non-linearities in asphalt binders was put forward by Farrar et al. (Farrar et al. 2014). And, in this study this idea is utilized and demonstrated using two LAOS tests, repeated strain sweep (RSS) test and time sweep test. The chapter is segmented into four parts, wherein first a brief mathematical description of LAOS is provided, next the steps involved in the analysis procedure employed using the MITlaos software is described. Next, the experimental reasoning for running the tests at high temperatures is described, and finally the results, analysis and the discussion from the high temperature LAOS tests on two study binders PG 70-16(Y), referred to as Y3 and PG 76-16(Y), referred to as Y4 are presented.

6.1 Mathematical Description of LAOS

In this section a brief mathematical description of LAOS is presented. If a sample is subjected to oscillatory shear, the strain and the rate of strain can be expressed as shown in equation (43).

$$\gamma(t) = \gamma_0 \sin \omega t, \quad \dot{\gamma}(t) = \omega \gamma_0 \cos \omega t \tag{43}$$

where:

γ_0 = strain amplitude

ω = angular frequency

t = time

The non-linear stress response to this strain input can be expressed as shown in equation (44).

$$\sigma(t) = \sum_{n=1,odd} \sigma_n \sin(n\omega t + \delta_n) \tag{44}$$

Where:

$\sigma_n(\omega, \gamma_0)$ = harmonic magnitude

$\delta_n(\omega, \gamma_0)$ = phase angle

The total non-linear viscoelastic stress shown in equation (44) is characterized by a stress amplitude and phase shift plus the odd higher harmonic contributions. The higher harmonic contributions are associated with high stress amplitude and phase shift.

If equation (44) is expressed in terms of a Fourier series, the expression is as shown in equation (45). Through this expansion a set of non-linear viscoelastic moduli can be expressed. It is known that the storage modulus, G′ and loss modulus, G″ are strictly defined only in the LVE domain. However, as per Hyun et al. (2011), the measurements of $G'(\gamma_0)$ and $G''(\gamma_0)$ at fixed frequency can also provide useful information in the NLVE domain also.

$$\sigma(t) = \gamma_0 \sum_{n,odd} \left[G_n^{'}(\omega, \gamma_0) \sin(n\omega t) + G_n^{''}(\omega, \gamma_0) \cos(n\omega t) \right] \tag{45}$$

Now if equation (44) is expressed in terms of a Taylor's series, the expression is as shown in equation (46).

$$\sigma(t) = \sum_{n,odd} \sum_{m,odd}^{n} \gamma_0^n \left[G_{nm}^{'}(\omega) \sin(m\omega t) + G_{nm}^{''}(\omega) \cos(m\omega t) \right] \tag{46}$$

The harmonic contributions can be calculated by equating the above two expressions. The first harmonic contribution is as shown in equation (47)

$$G_1^{'}(\omega,\gamma_0)=\left[G_{11}^{'}\gamma_0+G_{31}^{'}\gamma_0^3+...\right]$$
$$G_1^{''}(\omega,\gamma_0)=\left[G_{11}^{''}\gamma_0+G_{31}^{''}\gamma_0^3+...\right] \quad (47)$$

It can be seen from equation (47) that both $G_1'(\omega, \gamma_0)$ and $G_1''(\omega, \gamma_0)$ consist of odd polynomials of strain amplitude and non-linear coefficients of frequency (ω). Next, the Fourier transforms of the time signals for non-linear stress response should be calculated. A Fourier transform represents the inherent periodic contributions to a time dependent signal and shows the corresponding amplitudes and phases as a function of frequency. A Fourier transform for any time dependent signal, *S(t)* is defined according to equation (48).

$$S(\omega)=\int_{-\infty}^{\infty}S(t)e^{-i\omega t}dt \quad (48)$$

The remainder of this chapter presents the methodology adopted in this study to characterize this spectrum using MITlaos for the LAOS experiments performed in the study.

6.2 Non-Linear Viscoelastic Analysis Using MITlaos

The oscillatory waveforms of stress and strain data obtained from the time sweep test are used as inputs for the MITlaos program. According to Hyun et al. (2011), the first harmonic component in the deconvoluted Fourier transform relates to the principal frequency at which the test is performed. However, the presence of higher order harmonic components indicates the presence of non-linearity. These higher order harmonics will be used for non-

linearity quantification. The process to analyze LAOS data consists of three steps; data windowing, stress filtering, and finally nonlinearity detection and quantification. Each of these processes require specific steps, which are discussed below.

The non-linear viscoelastic characterization in this study was conducted using the repeated strain sweep test and the time sweep test. Both of which have been explained in detail in chapter 3. The first high temperature trials in the current study were conducted using original and PAV aged asphalt, however, due to edge fracture issues resulting from testing at the original condition, it was decided to run the tests at only PAV aged conditions. The issue is explained in detail in the third section of this chapter. The tests were performed at higher temperatures using the 25 mm plate on the dynamic shear rheometer (DSR). By performing the test at higher temperatures, it is easier to identify and quantify non-linear viscoelasticity. The detailed explanation of the motivation for performing the tests at high temperatures will be discussed in the next section.

In this section, the analysis is explained using the time sweep test performed on Y3 binder, PG 70-16, at PAV aged condition at 40°C, 1 Hz frequency, and at a peak-to-peak strain magnitude of 80%. Though the time sweep test is used here, the analysis itself is not test specific as the same analysis procedure can be applied to RSS test or any other test utilizing oscillatory shear loading. Figure 6-1 shows the data obtained from the test performed at 40°C and 80% peak to peak strain. The two main observations post-test completion are, (i) a clear modulus drop in shear modulus, which indicates presence of non-linearity, and (ii) drop in phase angle, indicating the failure of the test sample. For the

explanation of the analysis, a period during the test right after failure at around 350 seconds is used.

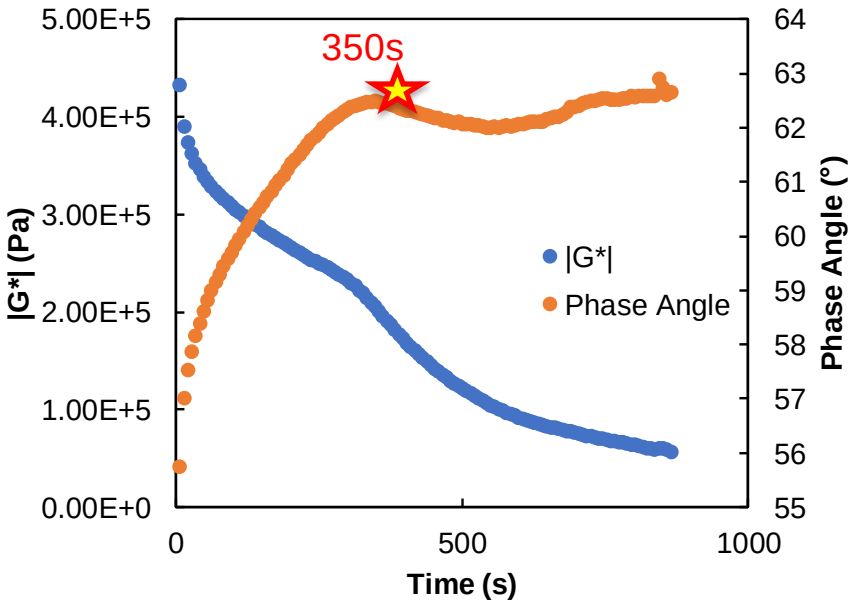

Figure 6-1: |G*| and Phase Angle Data from Time Sweep Test Performed on PG 70-16(Y) PAV Condition at 40°C and 1 Hz.

6.2.1 Data Windowing

The raw data obtained from the time sweep test consists of three attributes, time, torque, and displacement. These parameters are converted to stress and strain using an external program and were used as the input for the MITlaos analysis. It should be noted that, even the software, MITlaos, possesses the capability of converting torque and displacement to stress and strain respectively. A version of the time sweep test is depicted in Figure 6-2. One of the important aspects of data analysis is windowing the data. This refers to the selection of number test cycles for analysis. According to Kyu et al. (Kyu et al. 2011) it is very important to maintain high signal to noise ratio (S/N ratio) in the generated Fourier

transform. The authors mentioned that in order to achieve S/N ~ 10^5, about 5-50 cycles should be selected. However, the range of 5-12 cycles, works best for the analysis. In this analysis and for all the data presented in this study, eight cycles were selected, i.e. data from 346 seconds to 354 seconds. Detailed explanation on why eight cycles are chosen is presented in section 6.2.4.

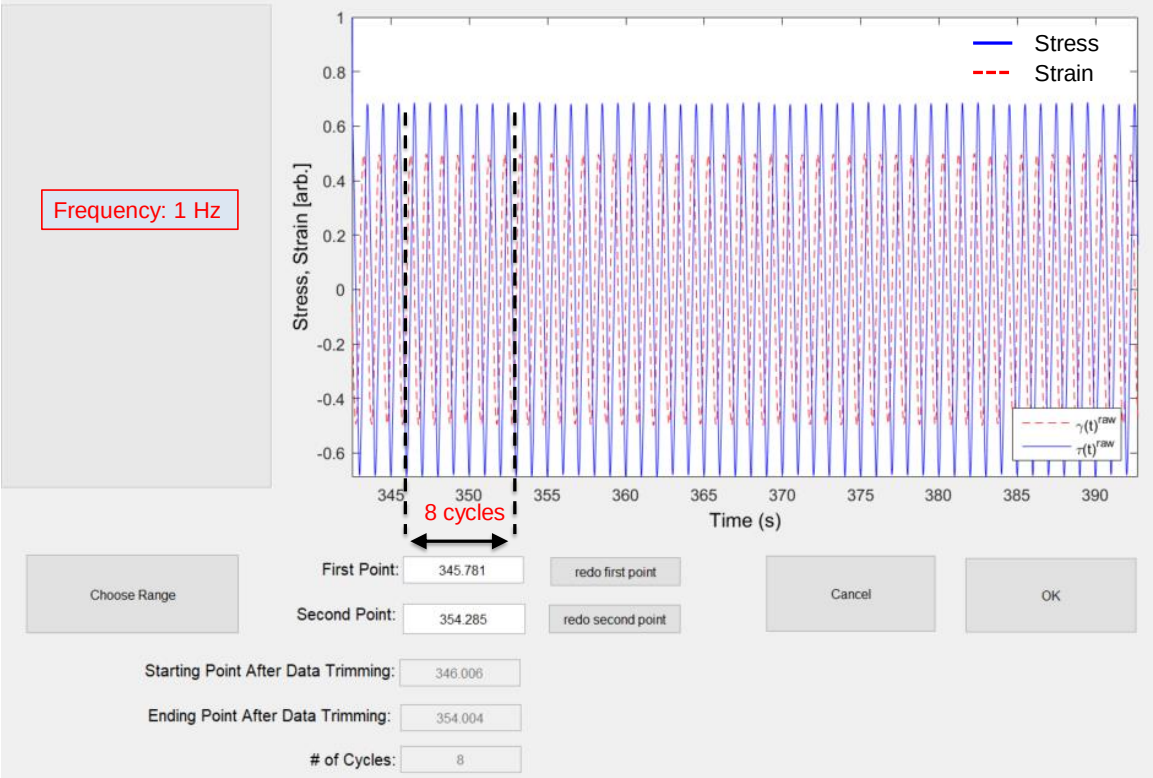

Figure 6-2: Data Windowing Option in MITlaos.

6.2.2 Stress Filtering

The process of stress filtering is where the stress signal is smoothed with the help of a Fourier transform. The raw stress signal is first decomposed into Fourier components. Subsequently the smoothed stress signal is then reconstructed using odd integer harmonics of the Fourier spectrum as according to Ewoldt et al. (Ewoldt et al. 2011) all other

harmonics are the consequence of noise, unsteady oscillations or systematic bias. This filtering technique helps in eliminating the noise and also aids in calculating non-viscoelastic parameters. Within the program, it is required to select the highest odd harmonic which is not affected by noise. For example, for the Fourier transform shown in Figure 6-3 the harmonic at n=7 is considered for stress filtering. The $n_{Nyquist}$ listed on top of the figure refers to the Nyquist harmonic order, which is equal to half of the sampling rate of a discrete signal processing system divided by loading frequency. In the current study, the sample rate chosen was 976 samples/sec, and in the example shown in Figure 6-3 the loading frequency was 1 Hz, threfore the Nyquist harmonic is 488. Though the value has no direct bearing on the current analysis, it should be noted that the MITlaos software will provide the values for peak intensities up to the Nyquist harmonic, i.e. n=488.

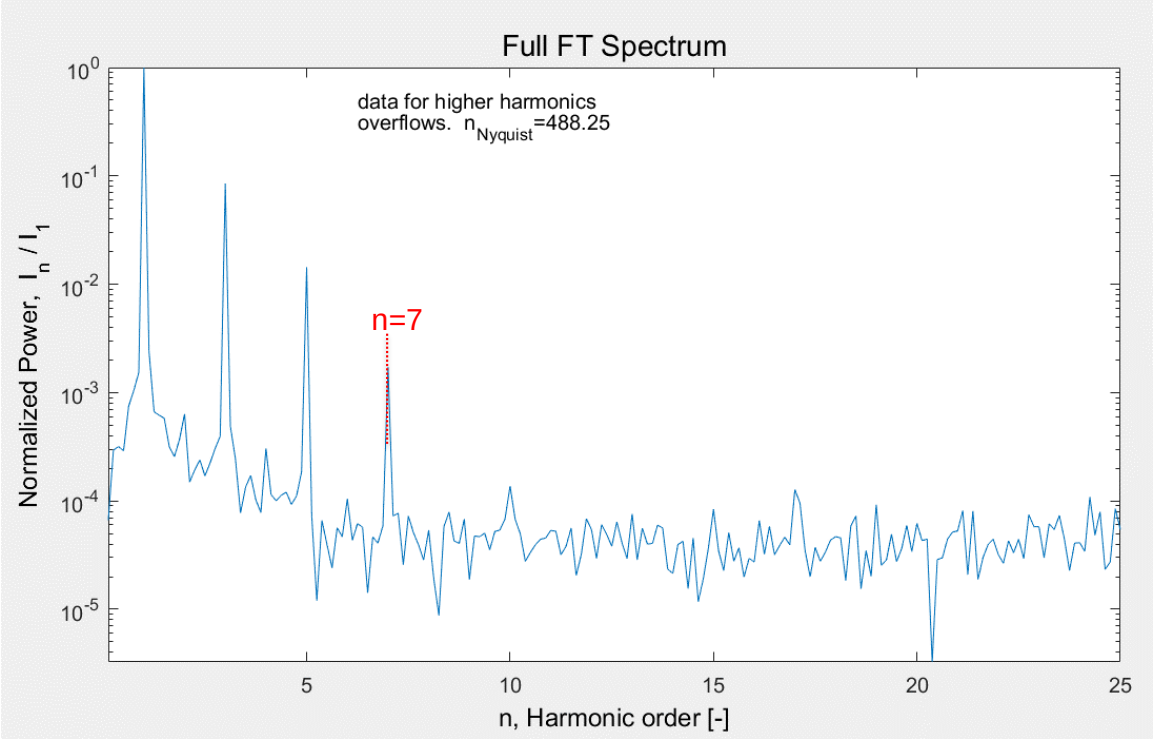

Figure 6-3: Stress Filtering Option in MITlaos.

6.2.3 Detection of Non-Linearity

After the process of filtering, the data is then analyzed. The output of interest is the Fourier transform spectrum which shows the normalized intensities over angular frequency. An example of the spectrum generated for the time sweep test at 350 seconds is shown in Figure 6-4. This figure is similar to the figure presented above, the data was exported and plotted in excel. It can be clearly seen from the spectrum that there exists a distinct peak at the first harmonic order (n=1) which corresponds to the test frequency which is 1 Hz (6.28 rad/s). This peak corresponds to linear viscoelasticity. However, we see there are other peaks at n >1 i.e ω > 6.28 rad/s. This shows the presence of non-linear viscoelasticity in the asphalt binder sample.

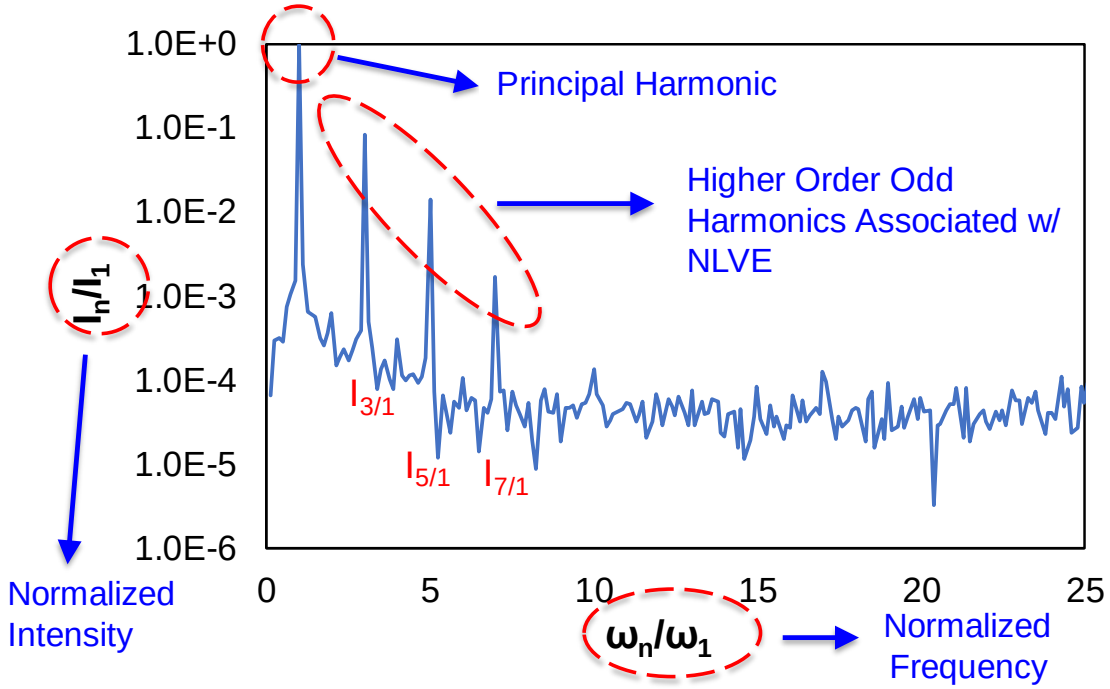

Figure 6-4: Components of a Fourier Transform Spectrum for PG 70-16(Y) PAV Aged Asphalt at 350 seconds During a Time Sweep Test.

Farrar et al. (Farrar et al. 2014) has shown that non- linearity in asphalt binders can also be detected from the plot of stress vs strain. He referred to the distortions in the stress strain curve as the indicator of non-linearity. Figure 6-5 shows the stress vs strain relationship, the stress and strain signature around 350 seconds, and it can be seen that there is clearly a distortion in the stress vs strain relationship, confirming the presence of non-linearity. Also, seen is the change in shape of the stress response, going from sinusoidal to triangular.

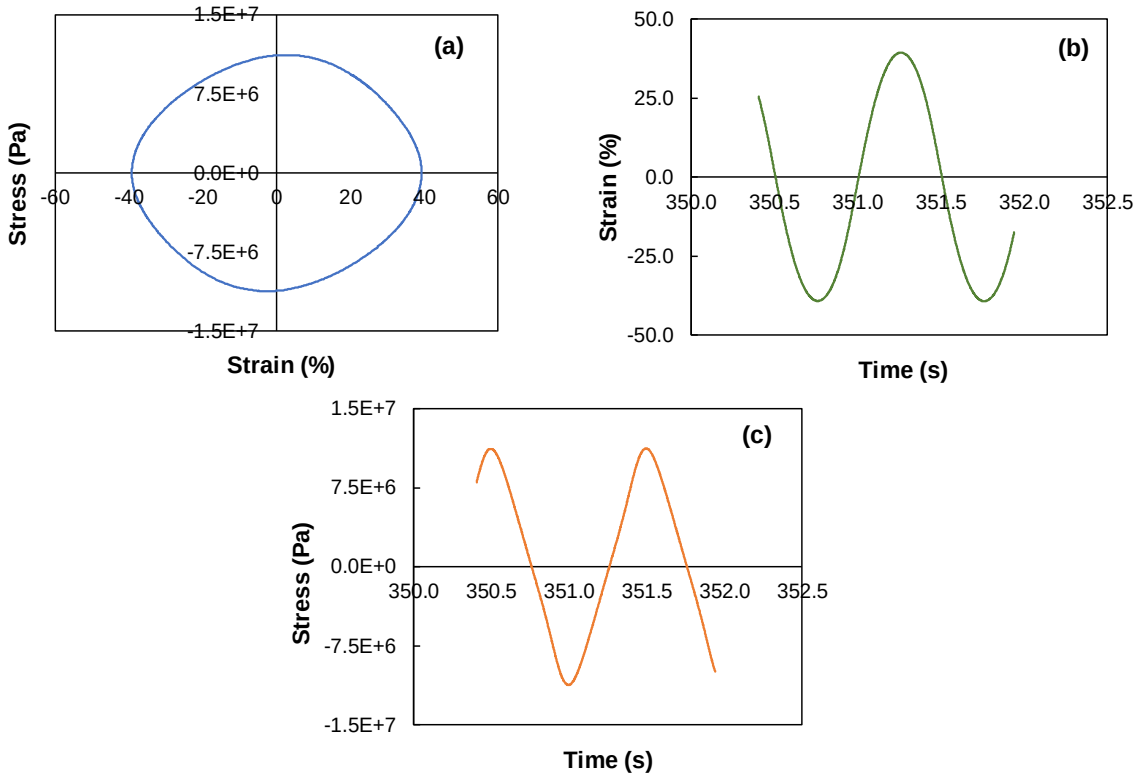

Figure 6-5: (a) The Stress vs Strain Relationship; (b) Strain Signature; and (c) Stress Signature for PG 70-16 PAV Aged Asphalt at 350 seconds During a Time Sweep Test

6.2.4 Pilot Study on Selection of Number of Cycles for MITlaos Analysis

The selection of eight cycles, was based on a pilot study comparing the influence of selecting 2 cycles all the way to 12 cycles. The parameters under consideration were the

normalized harmonic intensities. The harmonic intensities obtained from selecting 2 cycles to selecting 12 cycles were compared to see if the number of cycles has any bearing on them. The screenshot of the harmonic response from MITlaos for each selection of number of cycles is shown in Figure 6-6. The same data shown in Figure 6-2 is used for this purpose. It can be seen from the figure that, irrespective of the number of cycles chosen, three distinct higher order harmonics at n = 3, 5, and 7 are seen apart from the principal harmonic at n = 1. The magnitude of the normalized peak intensities are generated post the execution of the program. The values for $I_{3/1}$, $I_{5/1}$, and $I_{7/1}$ are tabulated in Table 10. It can be seen from Table 10 that the selection of number of cycles has no bearing on the normalized peak intensities at third and fifth harmonic. However, at the seventh harmonic, the peak intensity value seems to stabilize when the number of cycles is equal to eight. And further the intensity goes down when the number of cycles is increased to 12. The impact of this difference at the seventh harmonic cannot be ascertained but is likely to be minimal in the context of the current study as for the purposes of quantification of non-linearity, the parameter, Q, is dependent on the intensity of third harmonic. This value is very stable irrespective of the number cycles chosen. Considering these above observations, and with the interest to maintain consistency throughout the study, eight cycles were chosen for all the NLVE behaviors of the study binders analyzed using MITlaos.

Table 10: Normalized Peak Intensities at Third, Fifth and Seventh Harmonic for Varying Number of Cycles Selected for Analysis.

No. of Cycles	$I_{3/1}$	$I_{5/1}$	$I_{7/1}$
2	8.51E-02	1.44E-02	1.80E-03
4	8.48E-02	1.43E-02	1.67E-03
6	8.50E-02	1.43E-02	1.71E-03
8	8.51E-02	1.44E-02	1.72E-03

10	8.51E-02	1.44E-02	1.72E-03
12	8.50E-02	1.43E-02	1.61E-03

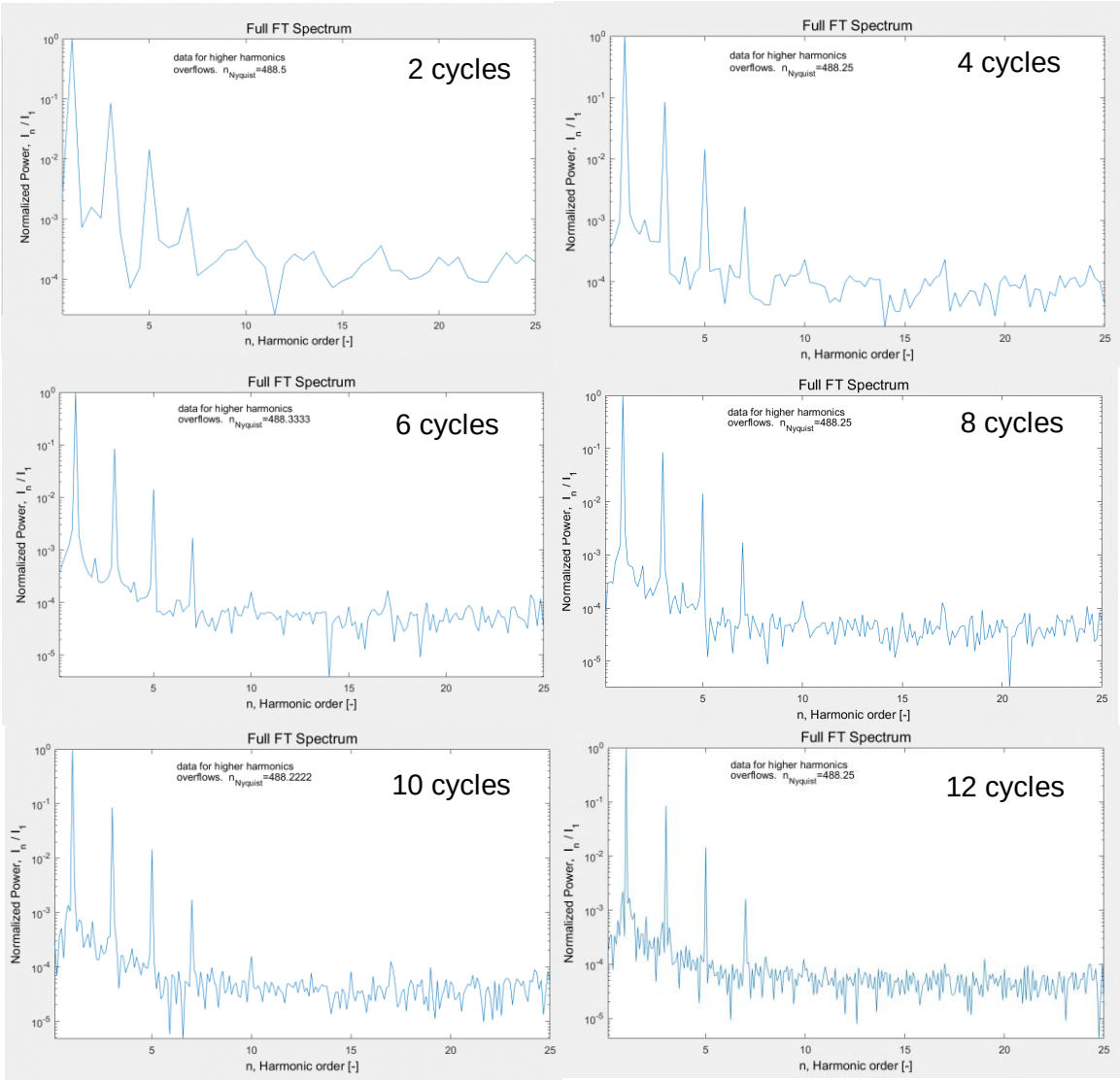

Figure 6-6: Harmonic Response for Varying Number of Cycles Selected for Analysis.

6.2.5 Non-linear Viscoelasticity Quantification Parameter, Q

Hyun et al. (Hyun et al. 2007) proposed a non-linearity quantification factor, *Q*, which depends upon the intensity of the normalized third order harmonic contributions obtained from FT spectrum and the strain level used in the analysis. The quantification factor, *Q* is

defined as shown in Equation (49). Where $I_{3/1}$ is the normalized third harmonic coefficient obtained from FT analysis and γ_o is the strain level of the selected data. While γ_o is known, it along with $I_{3/1}$ can be obtained from the output files generated post analysis.

$$Q = \frac{I_{3/1}}{\gamma_o^2} \tag{49}$$

For the data presented in Figure 6-5, the obtained Q value is 0.212, where the $I_{3/1}$ and γ_o values were 0.0851, and 0.4 respectively.

The writing above presents a detailed discussion of how non-linear viscoelasticity is analyzed in the current study using the MITlaos software. Same analysis procedure, and the quantification technique can be applied for any LAOS test, as long as the data selected for windowing is at the same strain level.

6.3 Experimental Reasoning for LAOS Tests at High Temperature

Before the current study was undertaken, a preliminary analysis (Gundla and Underwood 2016) was performed using repeated stress sweep tests conducted at intermediate temperatures at North Carolina State University (Underwood 2011). The main motivation of this preliminary study was to assess the feasibility of using the MITLaos software for non-linearity detection in asphalt binders and mastics.

The RSS tests were conducted at intermediate temperatures, which ranged from 10°C to 30°C. An experimental output of the RSS test on a PG 64-22 binder at 10°C as shown in Figure 6-7, has loading blocks, with step wise stress increments. This necessitated that the analysis was also segmented into various parts, in line with these increments. The

process is explained using Figure 6-8, which contains the data from RSS test conducted at the highest temperature used in the study i.e. 30°C. Figure 6-8 depicts a loading block with 10 stress increments (I-1 to I-10). The essential aspect of segmentation was to ensure that all of the segmented data belongs to only one stress increment. For example, in Figure 6-8, all the 9 cycles belong to 4^{th} stress increment (I-4) of the loading block. This ensures that the stress is constant throughout the segment. The segmentation of data was done within MITlaos using the window data option, in such a way that for each segment in a particular increment, approximately 5-12 cycles were selected for analysis. Once these cycles were analyzed, additional segments are created and the process is repeated until all cycles within a stress increment were analyzed. The process is further repeated for other stress increments until all the increments in a particular stress block are analyzed. For example, in Figure 6-8 the analysis for the block would be complete when all the 10 stress increments are segmented and analyzed.

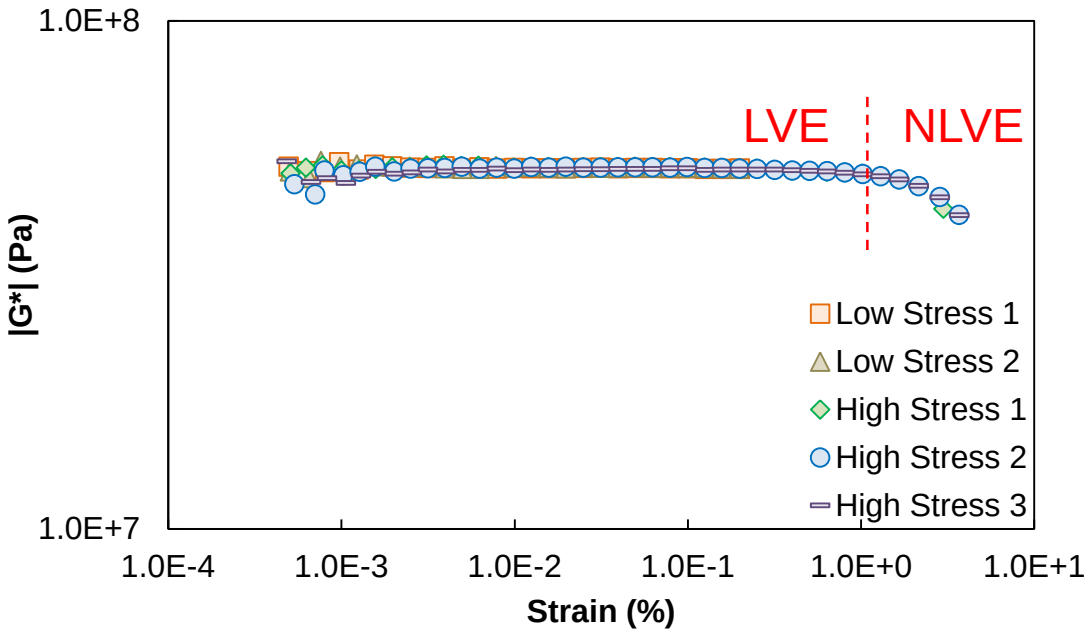

Figure 6-7: Experimental Output from Repeated Stress Sweep test at on PG 64-22 Binder at 10°C (Underwood 2011).

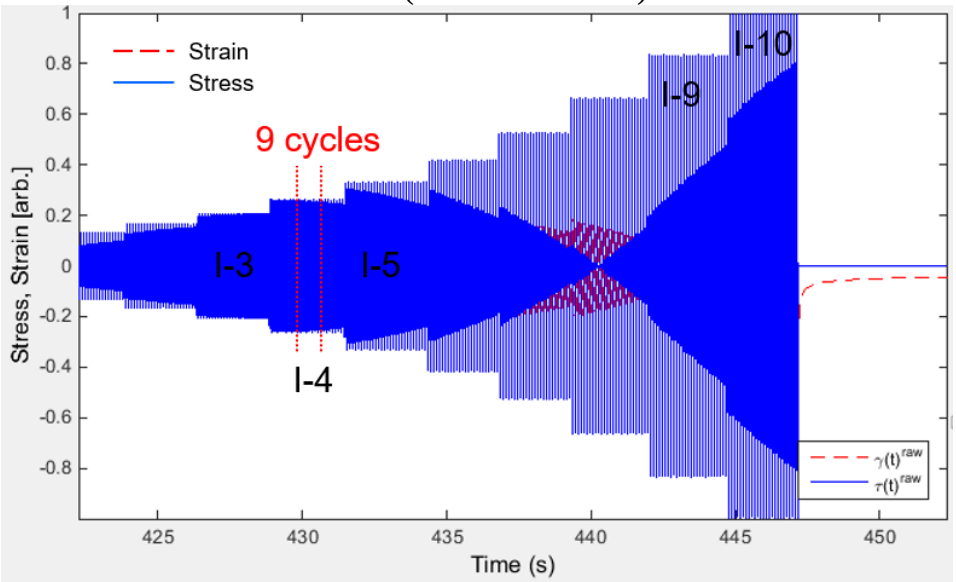

Figure 6-8: Data Windowing for RSS Test on PG 64-22 Binder at 30°C in Preliminary Study.

Stress filtering was conducted as mentioned in the earlier section, and is shown in Figure 6-9. The harmonic at n=3 was considered for stress filtering.

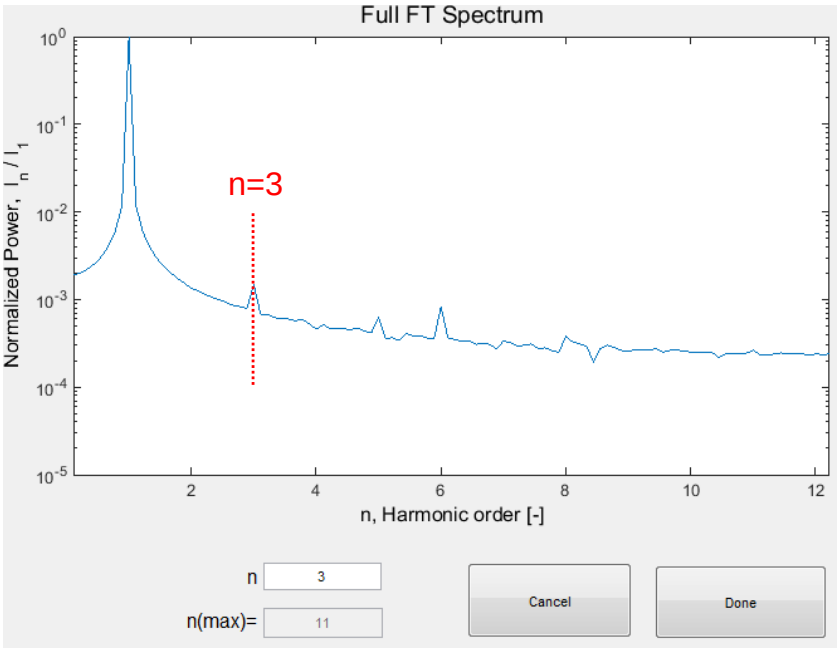

Figure 6-9: Stress Filtering in MITlaos for RSS Test on PG 64-22 Binder at 30°C in Preliminary Study.

After the process of filtering, the data was analyzed for detection of non-linearity. It can be clearly seen from the spectrum shown in that there exists a distinct peak at the first harmonic order (n=1) which corresponds to the test frequency which is 10 Hz (62.8 rad/s). This peak corresponds to linear viscoelasticity. However, we see there are other peaks at n>1 i.e $\omega > 62.8$ rad/s. It should be noted that these peaks are lower in intensity than that was shown in section 6.1. However, this shows the presence of non-linear viscoelasticity in the asphalt binder sample.

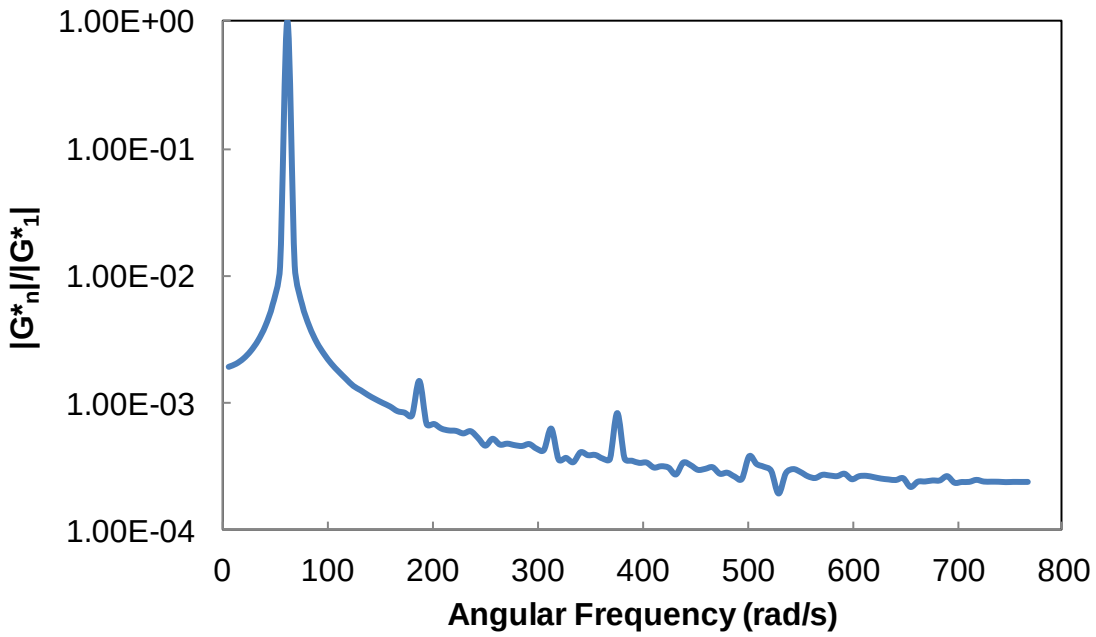

Figure 6-10: FT Spectrum Obtained for PG 64-22 Binder at 30°C from MITlaos Analysis Used in Preliminary Analysis.

In order to confirm the presence of non-linearity, stress vs strain relationships at different strain levels for PG 64-22 binder at 30°C were constructed as shown in Figure 6-11. The maximum strain level (zero to peak) achieved from the RSS test was 6% at 30°C. It can be seen that little to no distortion is observed even in presence of non-linearity. One possible cause for this is the strain level. Farrar et al. (Farrar et al. 2014) tested PG 76-22 binder at 28°C and saw distortions at a strain level in excess of 10% for a test run at 10 Hz. None of the tests analyzed in our study had strain levels in excess of 10%, which could be one possible reason why no distortion was detected in the stress strain curves. This was one of the main motivation was resorting to high temperature RSS tests, so that higher strains can be achieved.

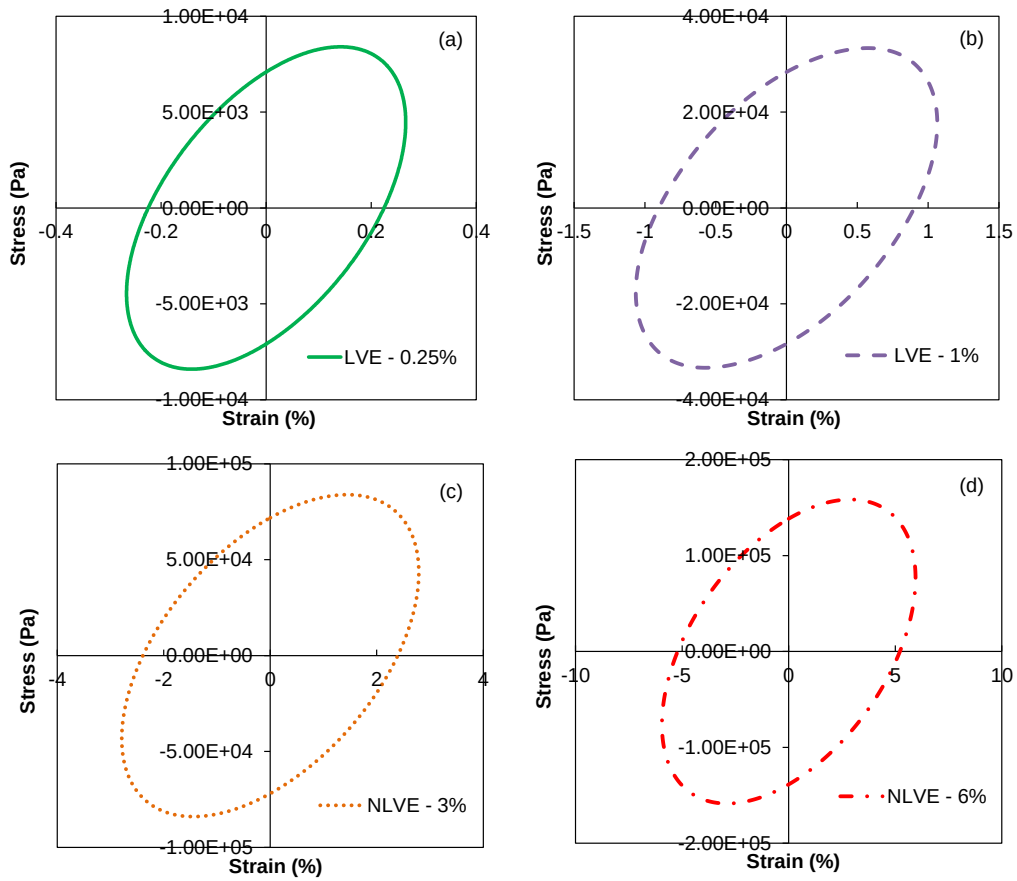

Figure 6-11: Stress Vs Strain Plots at 30°C for PG 64-22 in Linear Viscoelastic Region at (a) 0.25%; (b) 1% Strain Level and in Non-Linear Viscoelastic Region at (c) 3% And (d) 6% Strain Level.

6.4 LAOS Tests on Study Asphalt Binders

As mentioned earlier, two LAOS tests, repeated strain sweep test and time sweep tests were performed on study asphalt binders. Two asphalt binders were chosen for this purpose, they are Y3 and Y4. While, the objective of this chapter is to analyze the behavior of asphalt binders in LAOS conditions, it is the goal of the dissertation to understand the viscoelastic properties through molecular structure of the binders. For this purpose the binders, were chosen such that they had distinct molecular weights. Among the non-polymer modified

binders used in the study, at PAV condition, Y3 has the highest and Y4 had the lowest number average molecular weight.

6.4.1 Test Conditions

The RSS and time sweep tests were performed on PAV aged asphalt binders at two test conditions, 64°C and 10 Hz, and 40°C and 1 Hz. The reason for using PAV aged binders is that at the strain levels employed in the study and the conditions listed above, the original asphalts were subject to edge stability deficiency. The condition is visually explained using Figure 6-12. Figure 6-12(a) shows a typical bulge after the sample is trimmed and moved to its testing gap. In Figure 6-12(b) it can be seen that after the time sweep test at 50% strain level is completed, there is loss of material in the location where binder was originally present. This leads to erroneous interpretation of results and such condition should be avoided. The issue is due to the insufficient initial shear modulus of the binder for the conditions being tested. It can be seen through Figure 6-12(c) that when PAV aged sample is tested at 60% strain level, this condition is clearly avoided as post the test the bulge is still intact.

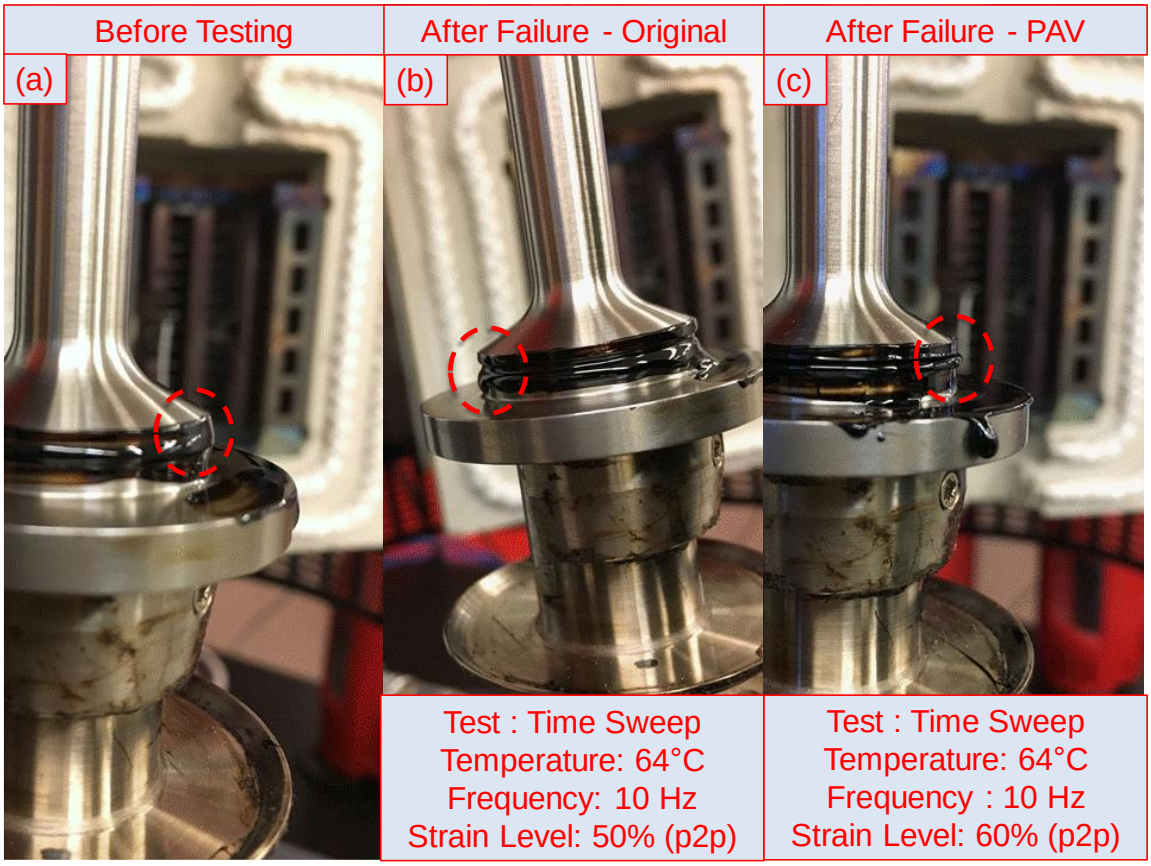

Figure 6-12: Demonstration of Edge Stability Issue Using PG 70-16(Y): (a) Showing Typical Bulge Using a 25 mm Plate; (b) Edge Stability Deficiency Using Original Asphalt Binder; and (c) Bulge Intact and No Edge Stability Deficiency in PAV Aged Asphalt Binder.

Regarding the temperature and frequency conditions, the choice of 64°C and 10 Hz was based on trials performed at ASU and the choice of 40°C and 1 Hz was based on the study by Diab and You (2017). The authors performed strain sweep tests on non-modified, crumb rubber modified and polymer modified binders at 30°C and 40°C and at frequencies of 5 Hz and 1 Hz. For their LAOS results the authors only report the results from 30°C and 1 Hz frequency. The authors saw distortion in stress-strain relationships at these conditions. The desire to perform the tests at higher temperatures, coupled with experience from previous RSS tests at 30°C and 10 Hz, played a role in selecting 40°C and 1 Hz, instead of

30°C. It should be noted that the tests at 40°C and 1 Hz were performed using an 8 mm plate and the tests at 64°C and 10 Hz were performed using a 25 mm plate.

6.4.2 Repeated Strain Sweep (RSS) Test Results

The results from RSS tests performed on PG 70-16(Y) and PG 76-16(Y) at PAV aged condition at 40°C, 1 Hz and 64°C, 10 Hz are presented in Figure 6-13. The success of this test, lies in two main observations post test completion (i) a clear modulus drop in shear modulus, which indicates presence of non-linearity, and (ii) there should not be progressive damage, especially after step G-2 B-2. Progressive damage can be clearly observed if there is a vertical separation between one step to another. The critical aspect of RSS test is that it can separate damage and non-linearity, and having progressive damage defeats this purpose. In Figure 6-13 it can be seen in parts (a) and (c) that there is a vertical separation after G-2B-1, which shows damage, however there is minimal vertical separation between one step to another after G-2B-2. In parts (b) and (d) there was no vertical separation in the first place. Thereby, all the tests qualify as satisfactory tests. The success of the test thereby depends on the range of strain values entered prior to the test. This is usually based on trial and error. Entering high strain values result in an unsuccessful test as shown in Figure 6-14 where progressive damage is seen even after G-2B-2. Also, while assessing progressive damage it is important that the modulus is plotted in arithmetic scale and not logarithmic scale, which will lead to obscuring of the separation thereby erroneous judgement.

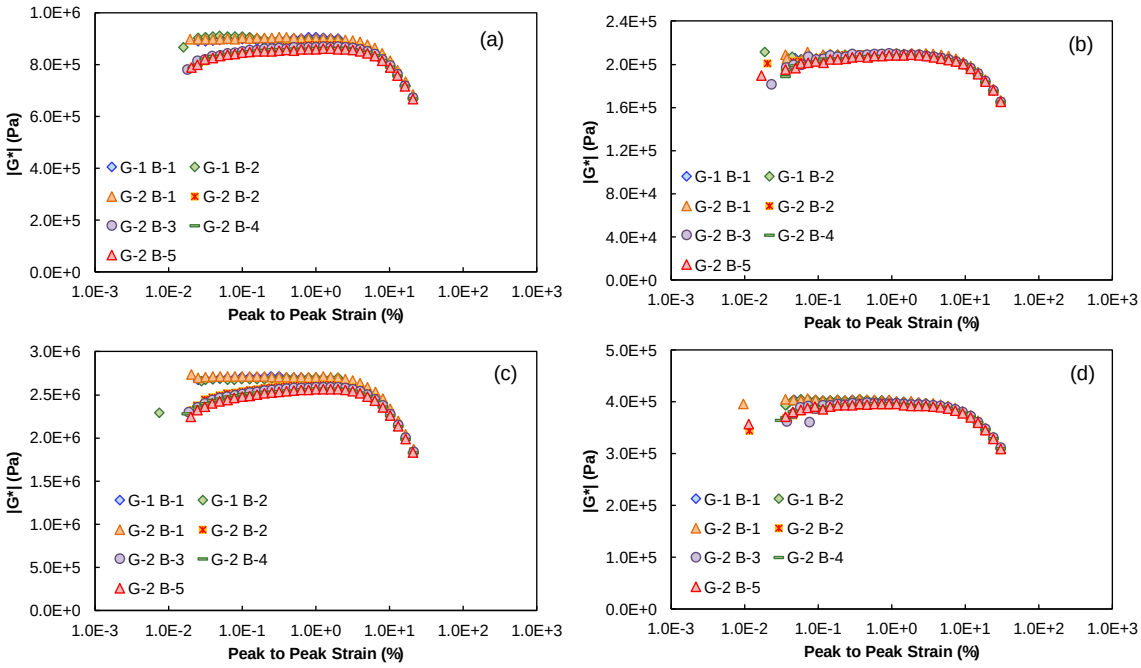

Figure 6-13: Results from RSS Tests at PAV Condition Performed on: (a) PG 70-16(Y) at 40°C, 1 Hz; (b) PG 70-16(Y) at 64°C, 10 Hz; (c) PG 76-16(Y) at 40°C, 1 Hz; and (d) PG 76-16(Y) at 64°C, 10 Hz.

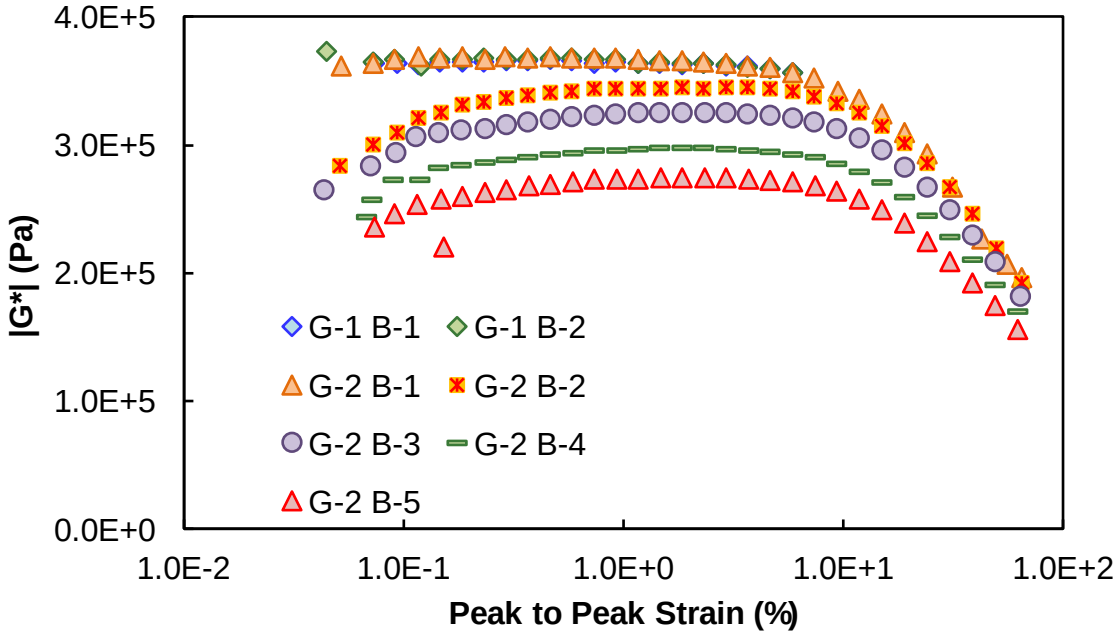

Figure 6-14: Unsuccessful Trial of RSS Test on PAV Aged Binder of PG 76-16(Z) at 64°C and 10 Hz.

6.4.3 Time Sweep Test Results

As discussed in Chapter 3, a time sweep test is a fatigue test performed at constant strain amplitude. The time sweep tests in this study were also performed at the same temperature and frequency conditions as the RSS test. For both binders, the tests were performed at at least three strain levels for each temperature, frequency condition as shown in Table 11.

Table 11: Peak to Peak Strain Levels for Time Sweep Test at Temperature Frequency Conditions Used in the Study.

Asphalt Binder at PAV Condition	Peak to Peak Strain Levels (%) for	
	40°C, 1 Hz	64°C, 10 Hz
PG 70-16(Y)	40, 80, 120	10, 30, 100
PG 76-16(Y)	40, 80, 120	10, 30, 100

In order to estimate the strain levels presented in Table 11, the results from the RSS test were taken as reference. The basic premise of running the tests at high temperatures and high strain levels was to obtain clear distinction of non-linearity and distortion in stress-strain relationship. Keeping the premise in mind and obtaining guidance form the RSS results, the strain levels were estimated. The location of these strain levels is presented along with the RSS data in Figure 6-15 to give a reference as to how far they are located from the LVE limit. Also indicated in the figure is the location of the LVE limit.

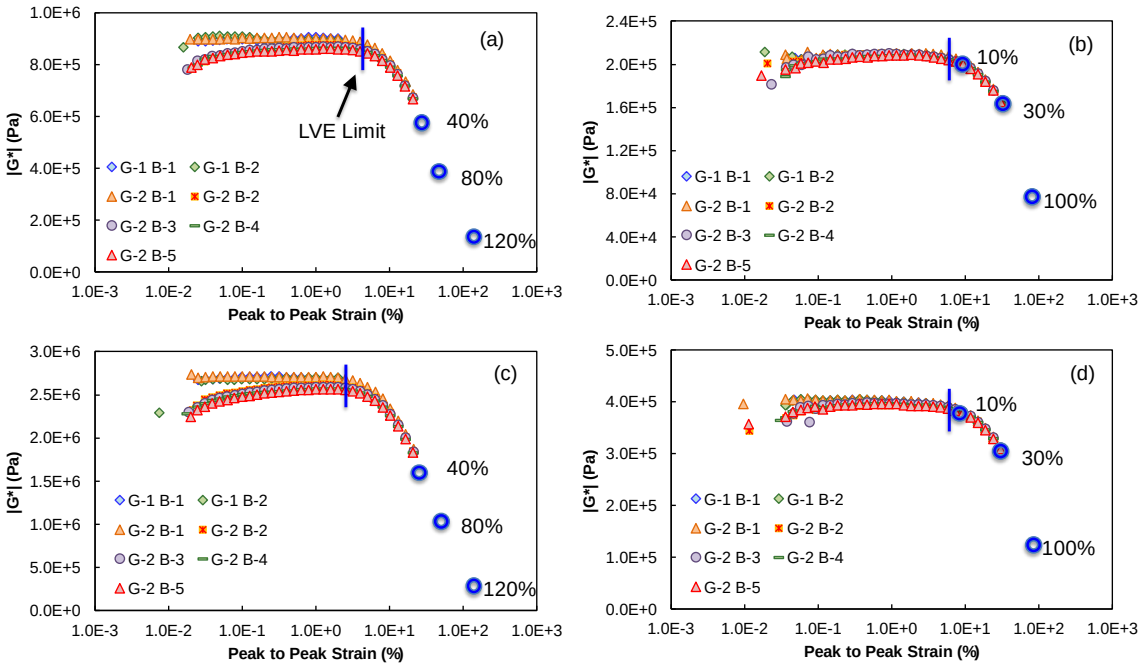

Figure 6-15: The Strain Levels Used in Time Sweep Test, Plotted Alongside RSS Test Results for: (a) PG 70-16(Y) at 40°C, 1 Hz; (b) PG 70-16(Y) at 64°C, 10 Hz; (c) PG 76-16(Y) at 40°C, 1 Hz; and (d) PG 76-16(Y) at 64°C, 10 Hz.

The results from the time sweep test include the simultaneous reduction in complex shear modulus and increase in phase angle with progression of time. The results for both binders at the strain levels mentioned in Table 11 are presented in Figure 6-16 through Figure 6-19. Non-uniform axes ranges are used for better depiction of failure. The sample is said to have failed, at the first observed instance of drop in phase angle. This location has been indicated in the respective figures using a blue colored “X” mark. Though not of primary importance to the study, it can be seen that there is a clear reduction in the cycles to failure (time x frequency) with increase in strain amplitude, i.e. from part (a) to part (b) to part (c).

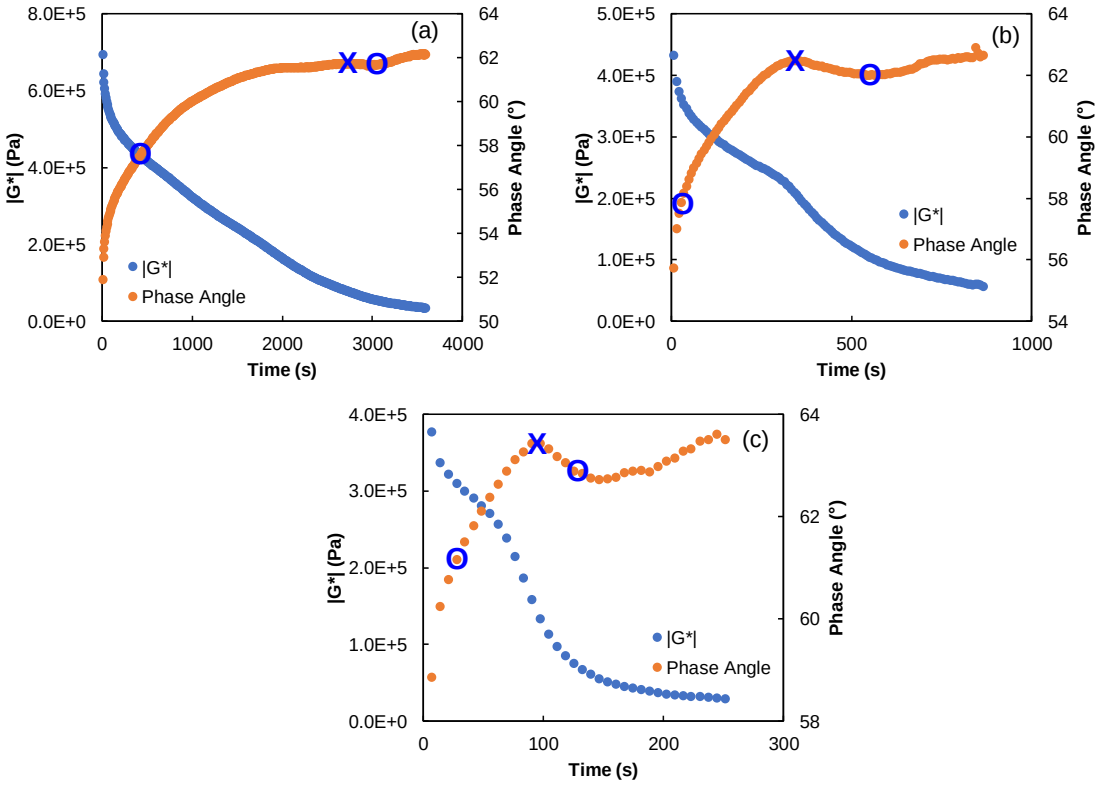

Figure 6-16: Results from Time Sweep Test on PAV aged PG 70-16(Y) Asphalt at 40°C and 1 Hz at strain level of: (a) 40%; (b) 80%; and (c) 120%.

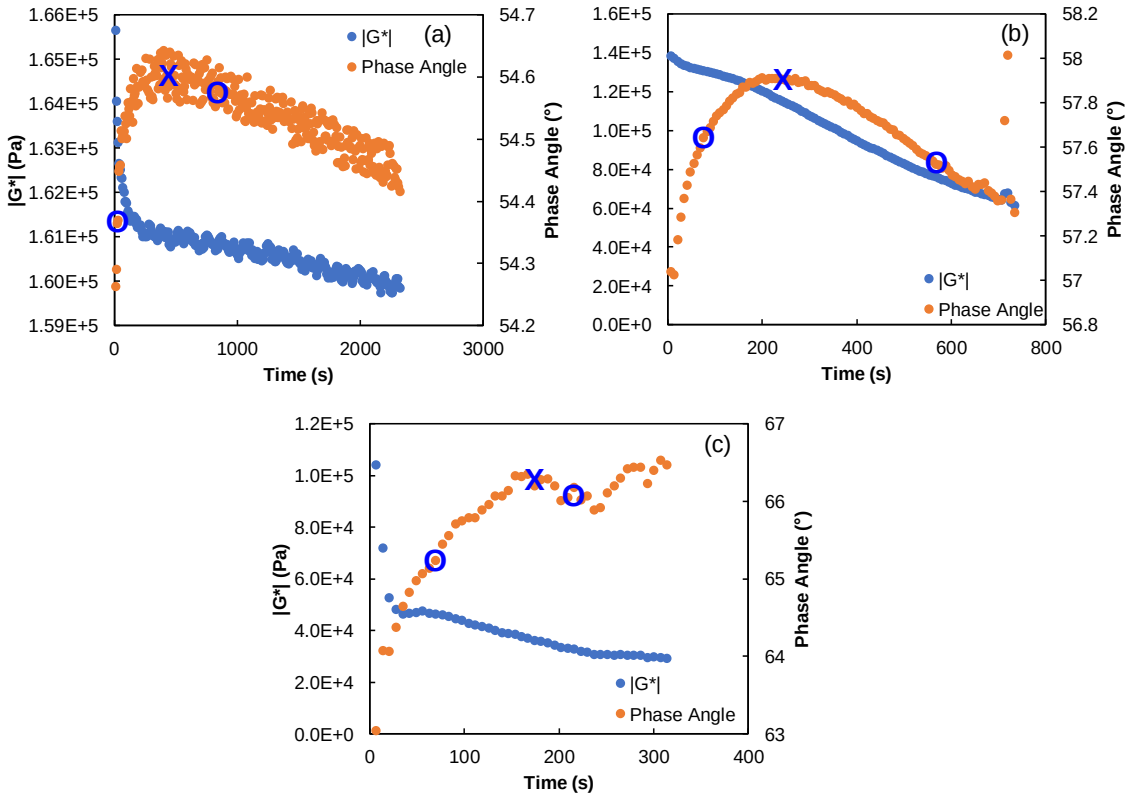

Figure 6-17: Results from Time Sweep Test on PAV aged PG 70-16(Y) Asphalt at 64°C and 10 Hz at strain level of: (a) 10%; (b) 30%; and (c) 100%.

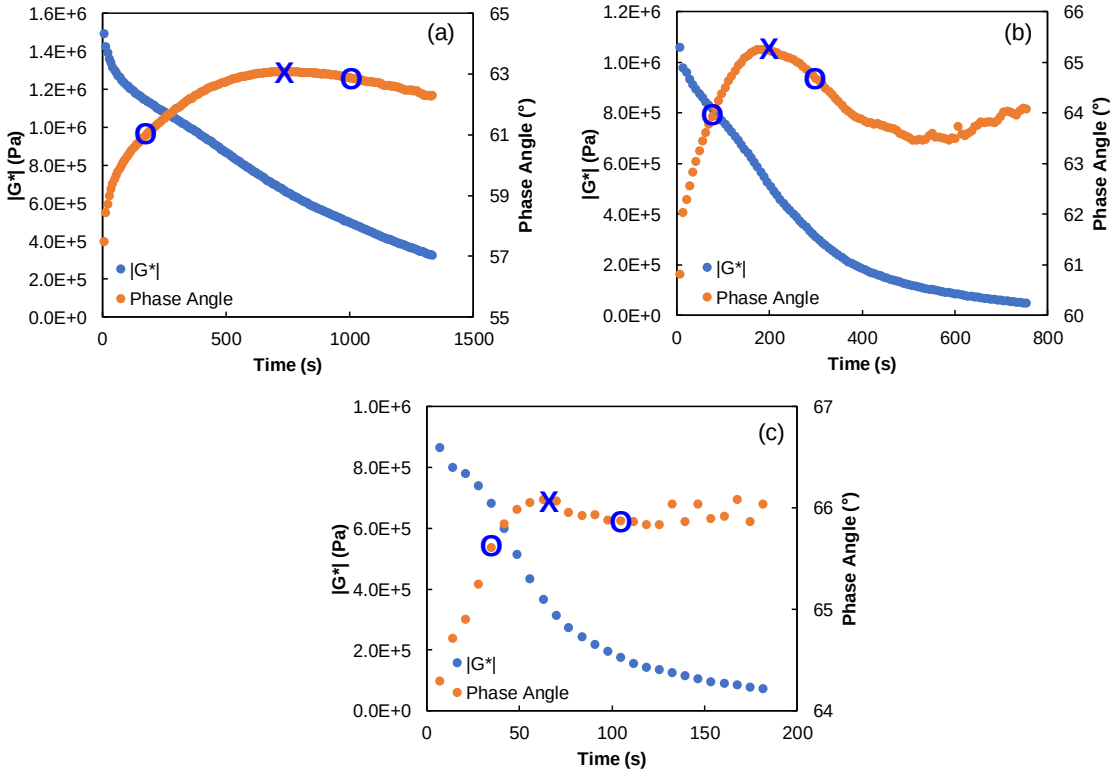

Figure 6-18: Results from Time Sweep Test on PAV aged PG 76-16(Y) Asphalt at 40°C and 1 Hz at strain level of: (a) 10%; (b) 30%; and (c) 100%.

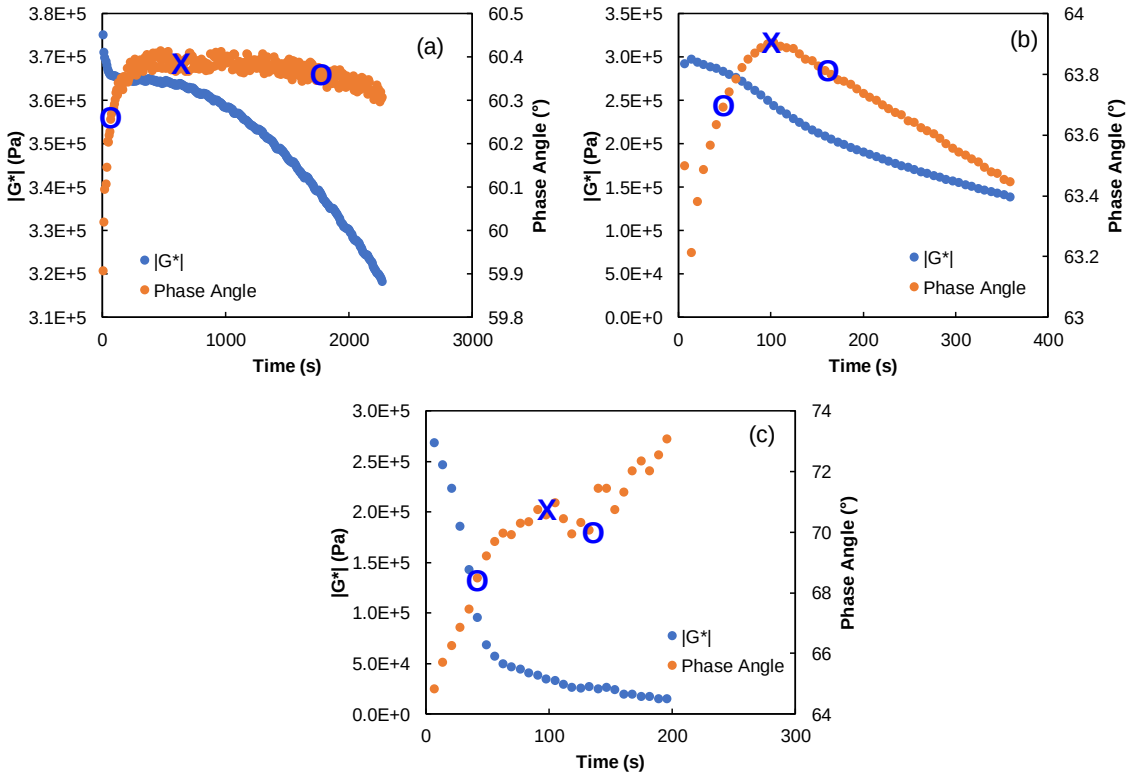

Figure 6-19: Results from Time Sweep Test on PAV aged PG 76-16(Y) Asphalt at 64°C and 10 Hz at strain level of: (a)10%; (b) 30%; and (c) 100%.

The next part of the analysis is focused on utilizing the stress-strain obtained from the LAOS tests of RSS and time sweep for detection and quantification of non-linearity using the analytical tool of MITlaos. Also, the stress-strain data is used for investigation of distortion in the stress-strain relationships in the non-linear region, which has been reported by Farrar (2014) and Diab and You (2017), and which was not seen in the LAOS tests performed at intermediate temperatures.

6.4.4 Investigation of Distortion in Stress-Strain Relationship

It should be recalled that the basic premise of running the LAOS experiments at high temperatures was so that high strain levels can be achieved which would then provide clear

distinction of non-linearity and possibly distortion in stress-strain behaviors. In order to investigate the stress-strain relationships, it was necessary to define the locations along the duration of the test that will be investigated. For the RSS test, two locations are defined. The stress-strain behavior will be investigated at the highest strain increment of step G2-B1 and G2-B5, which are first and the last repetitions of group 2. This is shown in Figure 6-20 and Figure 6-21 for 40°C, 1 Hz, and 64°C, 10 Hz respectively. From Figure 6-20 it can be seen that while the overall shape of the curve is intact, there are small ripple like distortions throughout the curve.

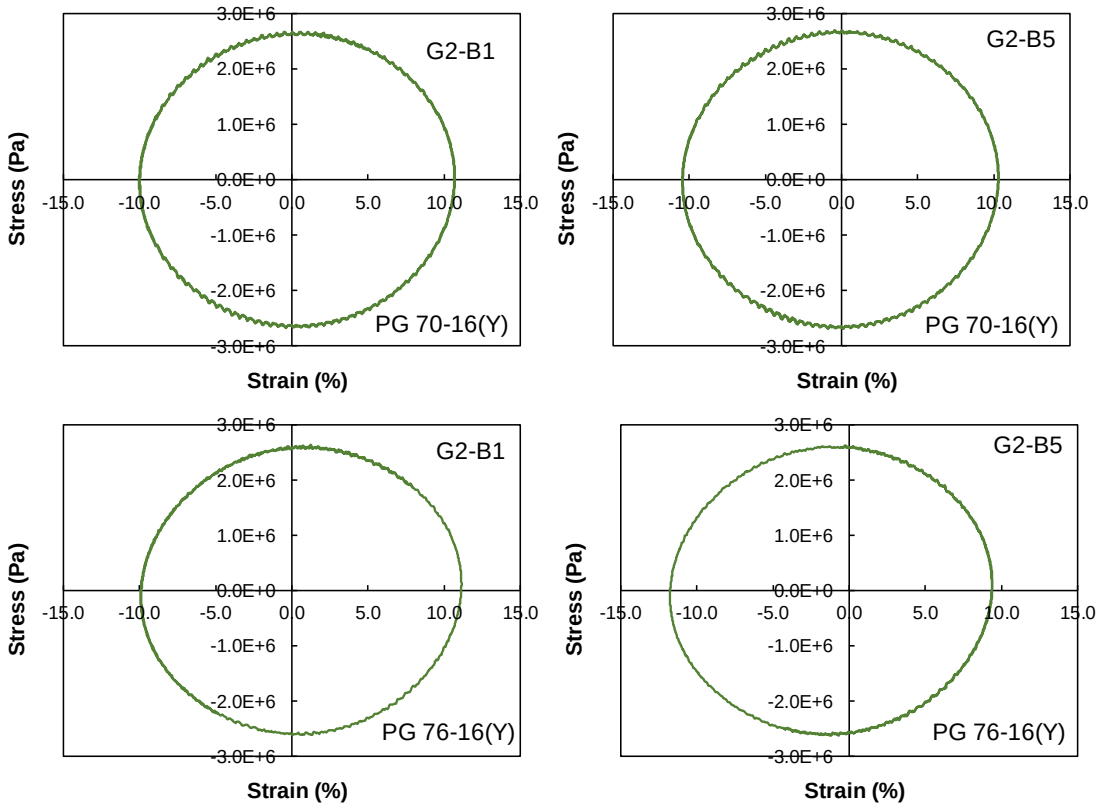

Figure 6-20: Stress-Strain Relationships for PAV Aged Binders PG 70-16(Y) and PG 76-16(Y) at the Highest Strain Increment of Step G2-B1 and G2-B5 for the Repeated Strain Sweep Test at 40°C, and 1 Hz Frequency.

In Figure 6-21, distortions can be seen in terms of a wavery ellipsoidal stress-strain relationship. While this is visible in all four part figures, it is more so evident in step G2-B5 of PG 70-16(Y) binder.

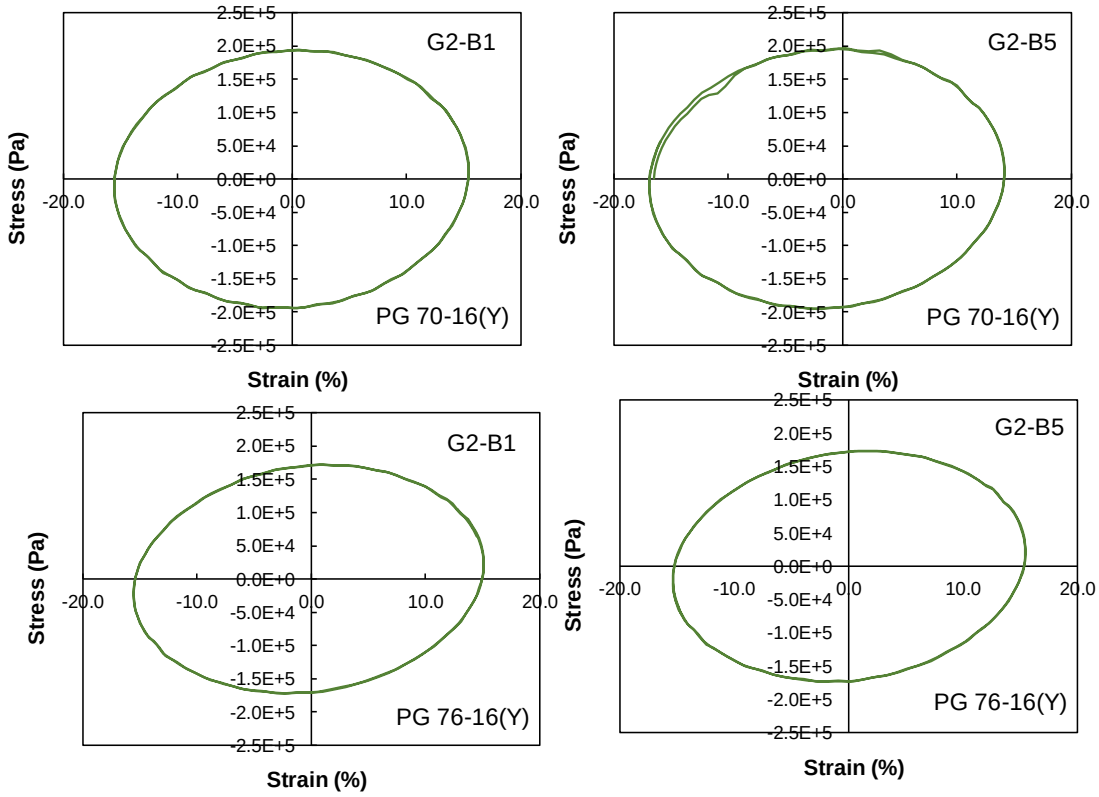

Figure 6-21: Stress-Strain Relationships for PAV Aged Binders PG 70-16(Y) and PG 76-16(Y) at the Highest Strain Increment of Step G2-B1 and G2-B5 for the Repeated Strain Sweep Test at 64°C, and 10 Hz Frequency.

For the time sweep test, the behavior is investigated at three locations. The first is before failure, i.e. before phase angle drop, the second is at failure, and the third is after failure. The location of the first and the third points are arbitrary and are shown in Figure 6-16 through Figure 6-19 using blue colored “O” symbol.

For the purpose conciseness only the stress-strain relationships at the highest strain level for both asphalts at 40°C, 1 Hz and 64°C, 10 Hz are shown in Figure 6-22 through

Figure 6-25. For the relationships presented in Figure 6-22 through Figure 6-25, the distortion was seen at all conditions except for PG 70-16(Y) at 64C, 10Hz. Even a peak to peak strain level of 100% was not sufficient to induce distortion in the stress-strain relationship. For other strain levels tested in the study, at 40C, 1 Hz distortion was seen for both binders at 80% strain level and little to no-distortion at 40%. No distortion was seen at 10% or 30% strain level at 64C, 10Hz for both PG 70-16(Y) and PG 76-16(Y). Also, for the conditions where distortion in stress-strain relationship was seen, the distortion was consistent at all three locations of investigation. At least visually no difference in severity was seen among the three locations. In the next section, this will be examined further by calculating the quantification coefficient, Q, and comparing the value across the three locations of investigation.

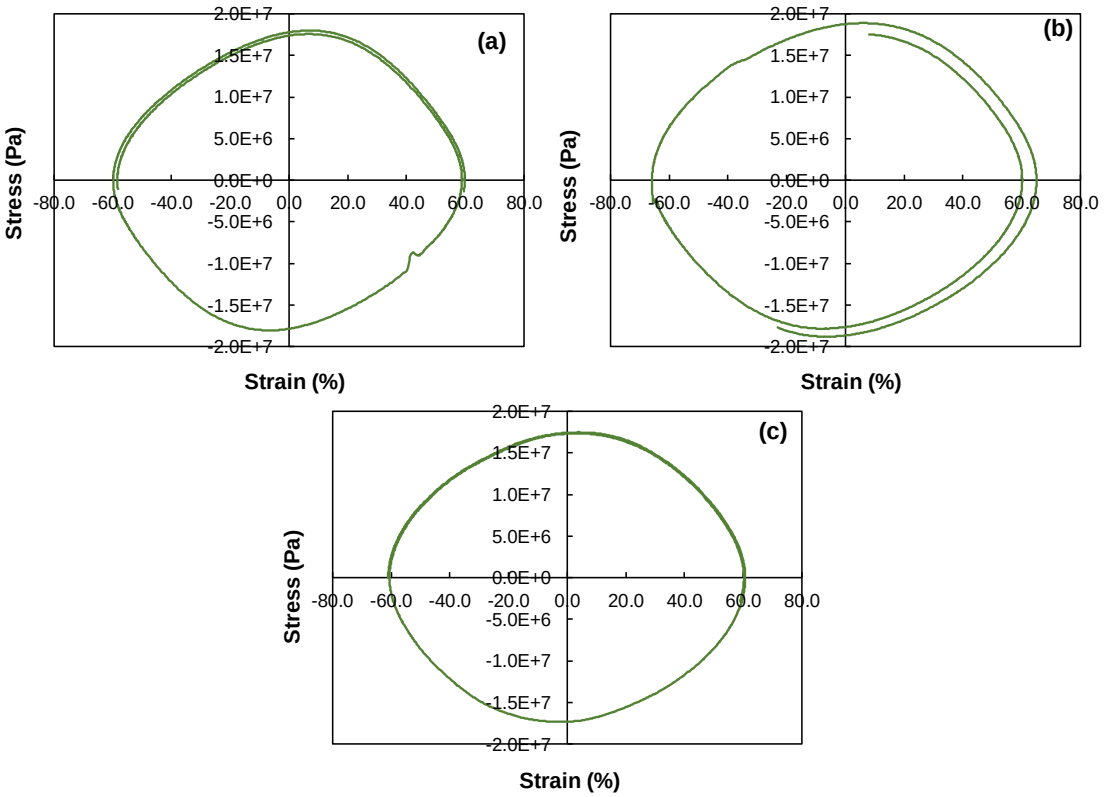

Figure 6-22: Stress-Strain Relationships for PAV Aged PG 70-16(Y) Binder at Three Locations: (a) Before Failure; (b) At Failure; and (c) After Failure for the Time Sweep Test at 40°C, 1 Hz and 120% Strain Level.

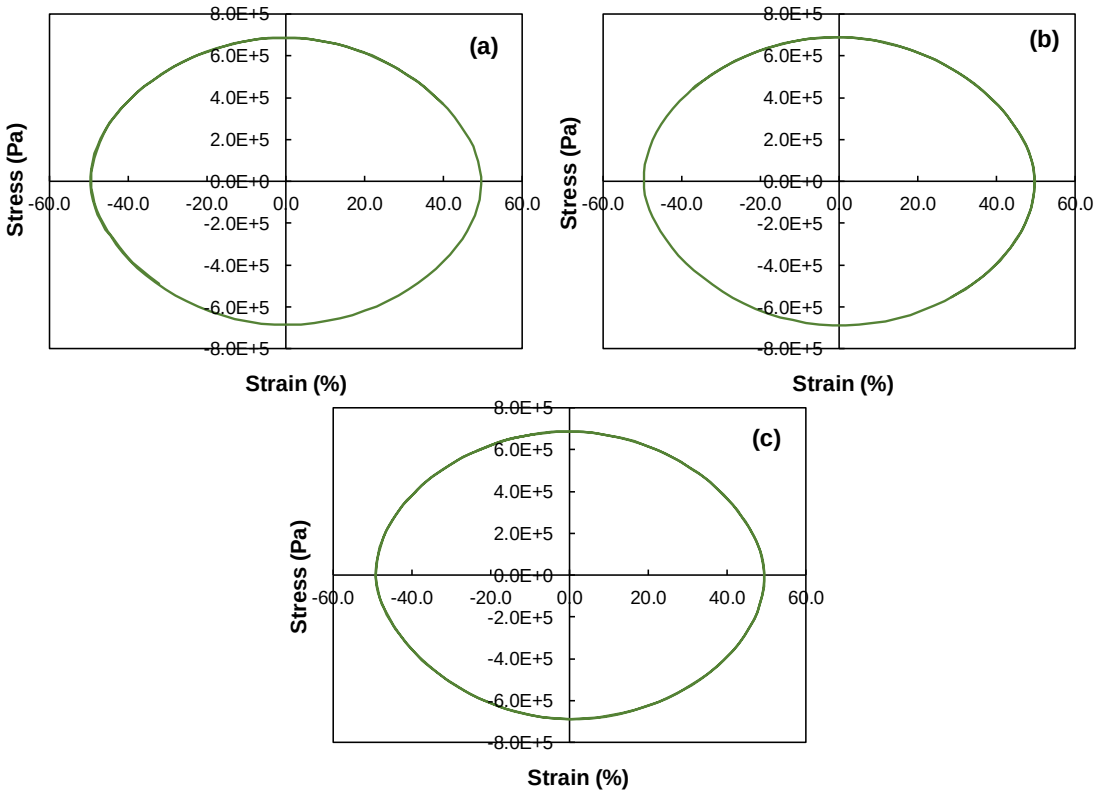

Figure 6-23: Stress-Strain Relationships for PAV Aged PG 70-16(Y) Binder at Three Locations: (a) Before Failure; (b) At Failure; and (c) After Failure for the Time Sweep Test at 64°C, 10 Hz and 100% Strain Level.

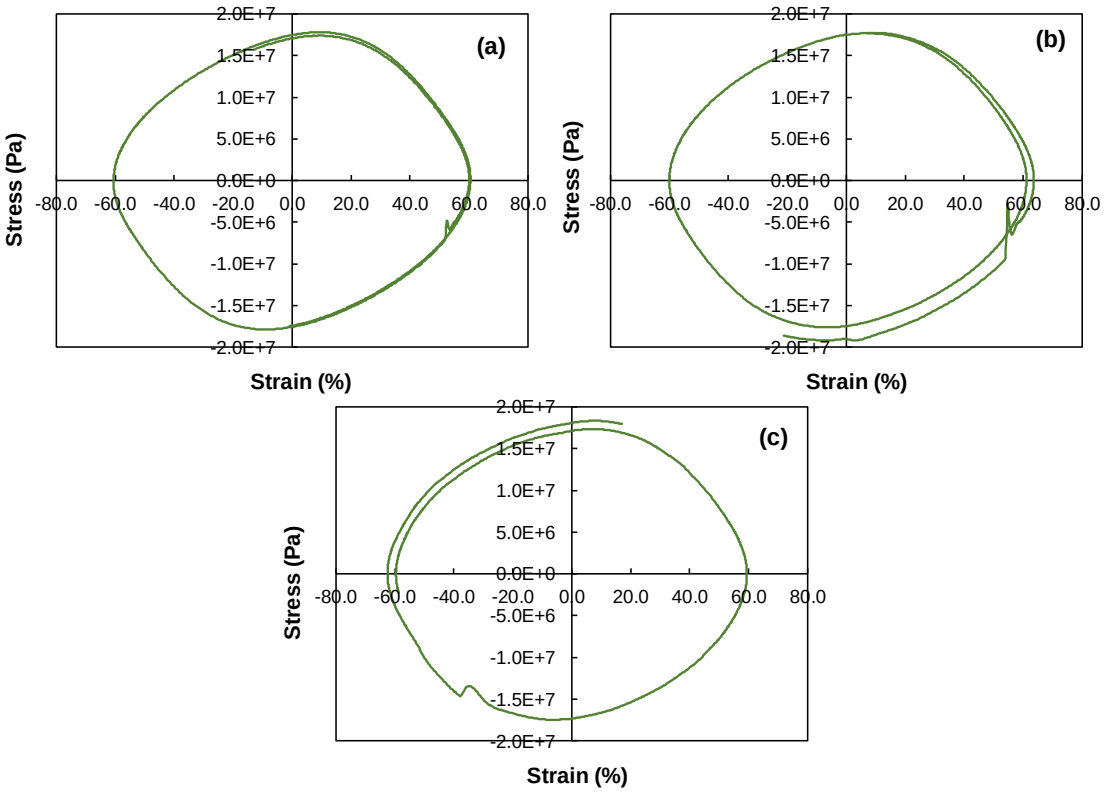

Figure 6-24: Stress-Strain Relationships for PAV Aged PG 76-16(Y) Binder at Three Locations: (a) Before Failure; (b) At Failure; and (c) After Failure for the Time Sweep Test at 40°C, 1 Hz and 120% Strain Level.

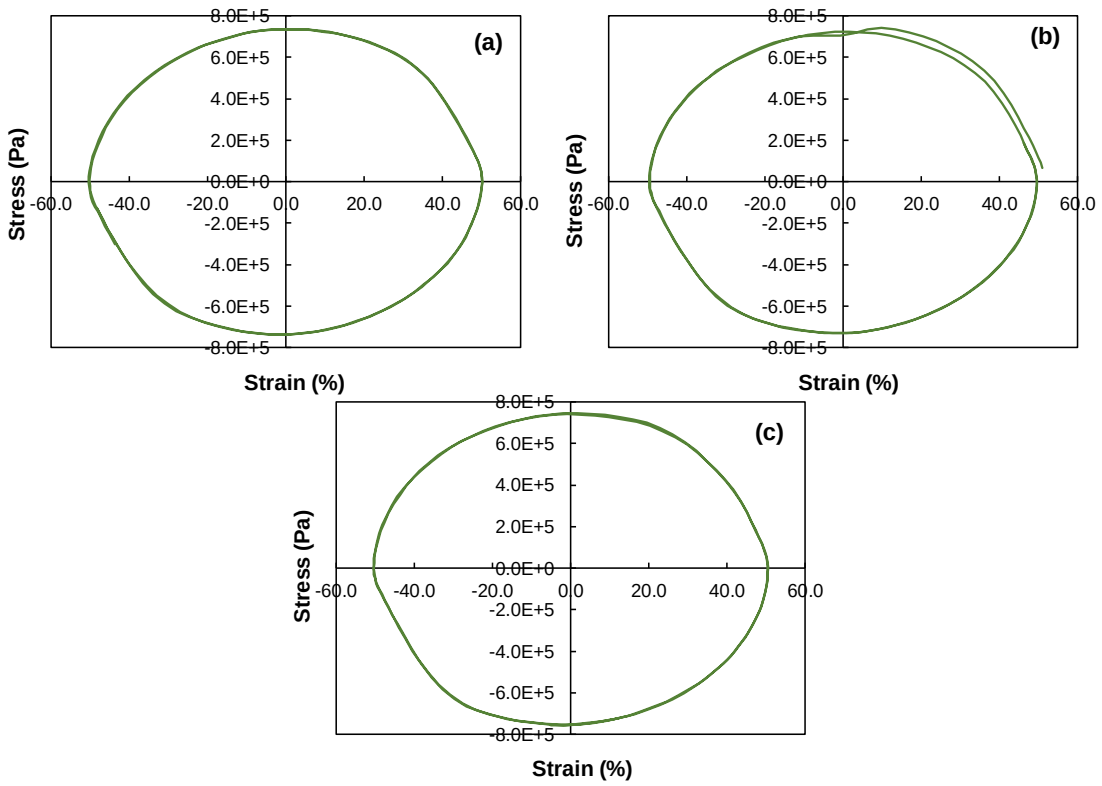

Figure 6-25: Stress-Strain Relationships for PAV Aged PG 76-16(Y) Binder at Three Locations: (a) Before Failure; (b) At Failure; and (c) After Failure for the Time Sweep Test at 64°C, 10 Hz and 100% Strain Level.

There are three main takeaways from the distortion investigation of time sweep tests and repeated strain sweep tests:

1. Presence of non-linear viscoelasticity does not necessarily imply distortion of the stress-strain relationship. This can be justified based on the observation from the stress-strain response of PG 70-16(Y) at 100% strain level. No distortion was seen even though the strain amplitude is in the NLVE domain.
2. The observation of distortion is clearly dependent on the magnitude of the strain employed to run the test. For example, consider PG 76-16(Y) at 64°C, 10Hz and 30% strain level. No distortion was observed at this strain level. However, when

the strain was increased to 100%, clear distortion was seen (Figure 6-25). This was however, not the case with PG 70-16(Y), which is the third takeaway.

3. The observation of distortion is binder dependent. Two binders, PG 70-16(Y) and PG 76-16(Y) were both sheared at 100% strain level at 64°C using 10Hz frequency to perform a time sweep test. While the former did not show any distortion, there was clear distortion in the latter case. This is a classic example of how two binders, with different chemical properties, can have different NLVE responses, which can be visually quantified. This visible NLVE response is distortion of stress-strain curve in this case. However, there will be situations when both binders under comparison exhibit distortion (40°C and 1 Hz time sweep cases) and thereby making it difficult to visually gauge which distortion is more severe. In such situations, what is required is a mathematical measure of distortion of stress-strain relationship or the NLVE behavior in general. The measure, the means of calculation, and the insight it provides is explored in the following section.

6.4.5 Quantification of Non-Linear Viscoelasticity of Study Materials

As mentioned earlier, the parameter used for the quantification of NLVE behavior is Q, whose mathematical definition is provided in Equation (49). It is important to know the basis for the quantitative coefficient. Hyun et al. (2011) mentions in his work that the Fourier intensities of the n^{th} harmonics grow with corresponding odd powers of the strain amplitude $(I_n \propto \gamma_o^n, n = 1,3,5...)$. Therefore, the normalized intensity of third harmonic is expected to scale quadratically with the strain amplitude $(I_{3/1} \equiv I_3 / I_1 \propto \gamma_o^3 / \gamma_o^1 = \gamma_o^2)$. According to the authors, the third harmonic is chosen because it is the first dominant

harmonic in the non-linear domain. This quadratic scaling was confirmed was Hyun et al. experimentally, wherein multiple polymers were tested at different frequencies and range of strain levels and it was found that the normalized intensity of third harmonic is related to strain amplitude, with a slope of 2. Thereby, the mathematical relationship presented in Equation (35) is derived.

The stress-strain data obtained from the LAOS tests on study asphalts was used in MITlaos to first detect the presence of higher order harmonics. Post the analysis, the program generates data files which contain the normalized peak intensities at different higher order harmonics. First, the analysis was carried out for the time sweep tests at the three locations described in the previous sections. For the purpose of conciseness, only the Fourier transform spectra at second location i.e. at failure is being shown for all time sweep tests. The spectra are plotted in Figure 6-26 through Figure 6-29. For the tests conducted at 40°C and 1 Hz frequency, harmonics up to seventh order can be detected without hindrance due to noise. For the tests conducted at 64C and 10 Hz, the spectra at 10% strain level produces no distinguishable higher order harmonics, whereas at least the third harmonic can be clearly distinguished in the 30% strain level case, and third and the fifth harmonics in the 100% strain level case.

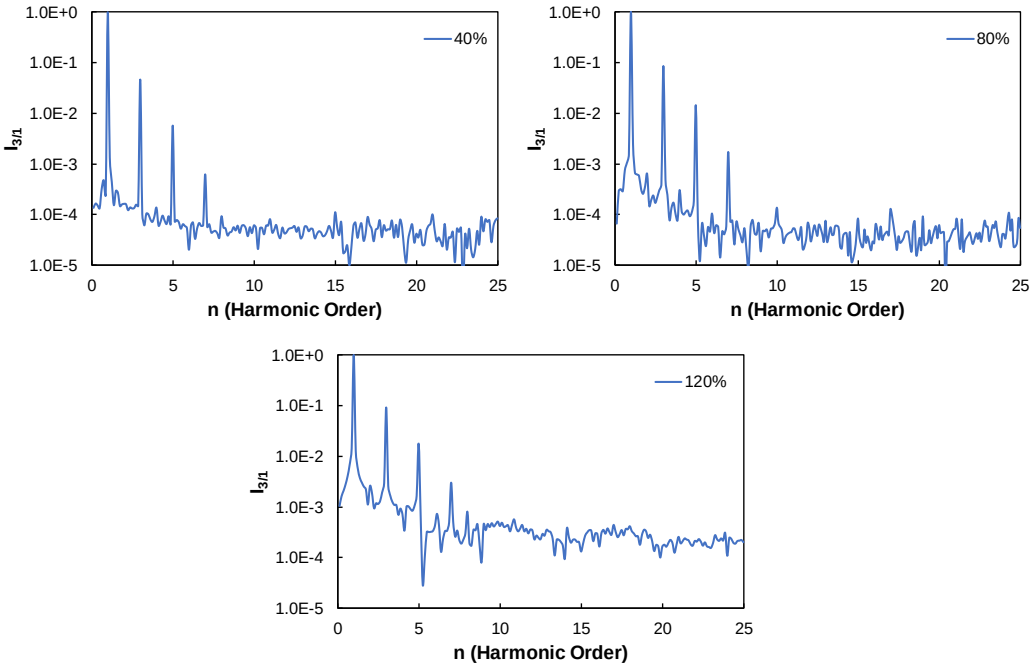

Figure 6-26: Fourier Transform Spectra for PG 70-16(Y) for Time Sweep Tests Conducted at Multiple Strain Levels at 40°C and 1 Hz.

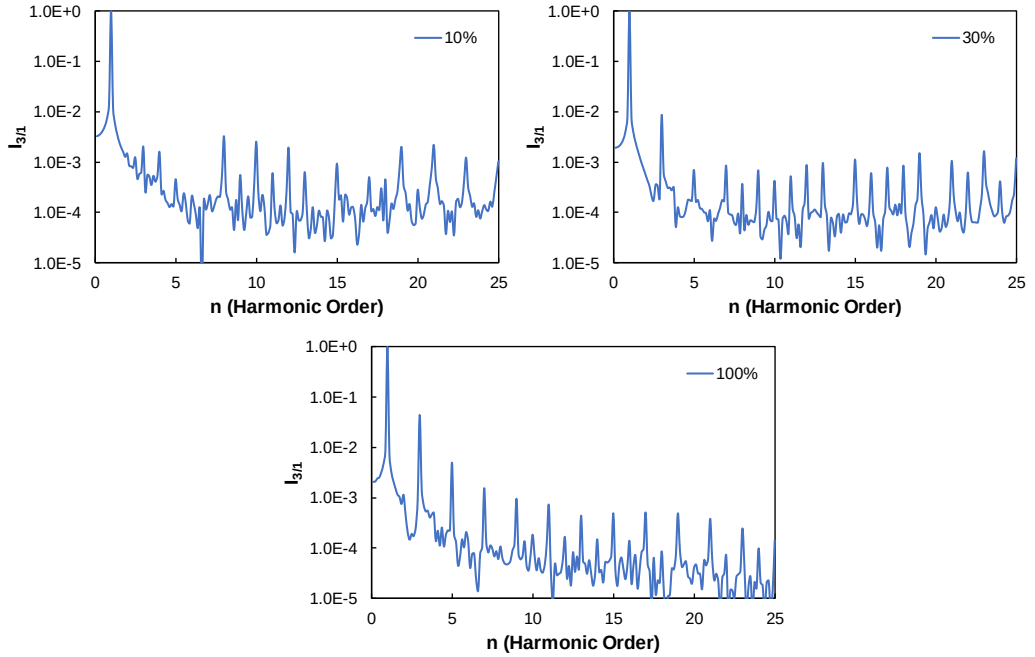

Figure 6-27: Fourier Transform Spectra for PG 70-16(Y) for Time Sweep Tests Conducted at Multiple Strain Levels at 64°C and 10 Hz.

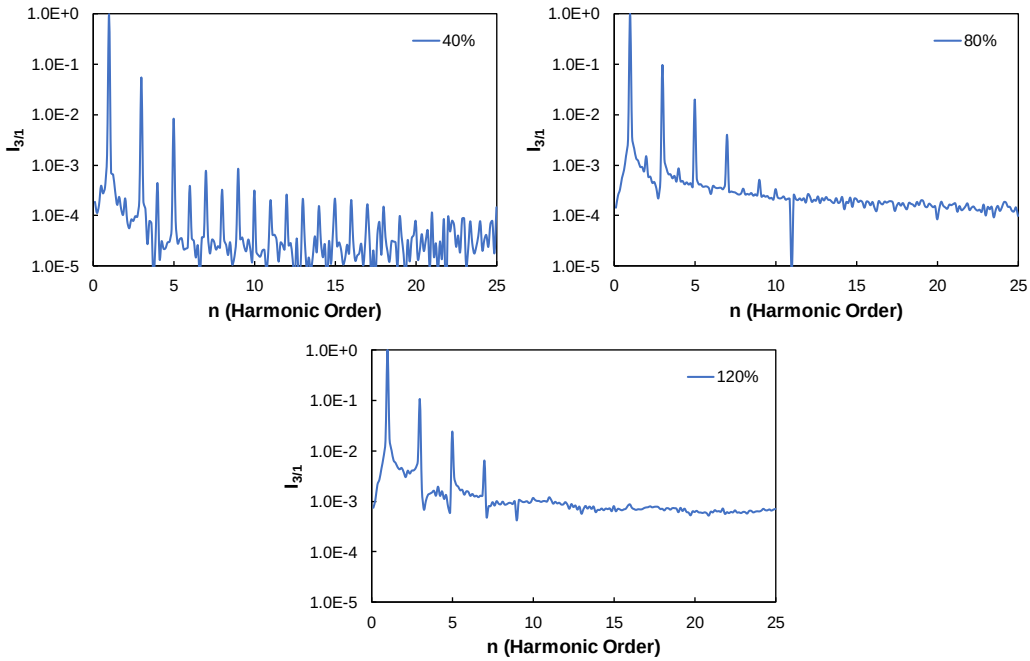

Figure 6-28: Fourier Transform Spectra for PG 76-16(Y) for Time Sweep Tests Conducted at Multiple Strain Levels at 40°C and 1 Hz.

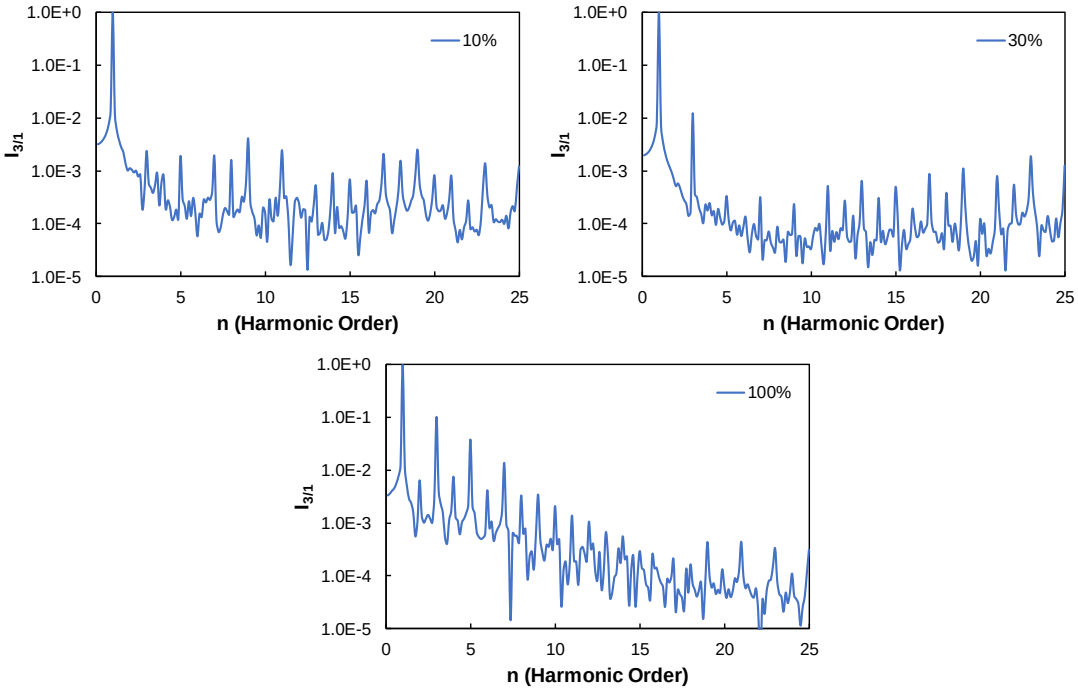

Figure 6-29: Fourier Transform Spectra for PG 76-16(Y) for Time Sweep Tests Conducted at Multiple Strain Levels at 64°C and 10 Hz.

The next analysis conducted was for the RSS test. As mentioned earlier, the analysis for the RSS test was carried out at the highest strain increment of G2-B1 and G2-B5. The Fourier transform spectra resulting from these strain increments at 40°C, 1 Hz and 64°C, 10 Hz are presented in Figure 6-30 through Figure 6-33. For the RSS tests conducted at 40°C and 1 Hz, the higher order harmonics that can be clearly identified are at n=3, and n=5. Whereas, for the RSS test conducted at 64°C and 10 Hz only the third harmonic can clearly be distinguished for PG 70-16(Y), but both third and fifth harmonics can be identified without hindrance of noise for PG 76-16(Y).

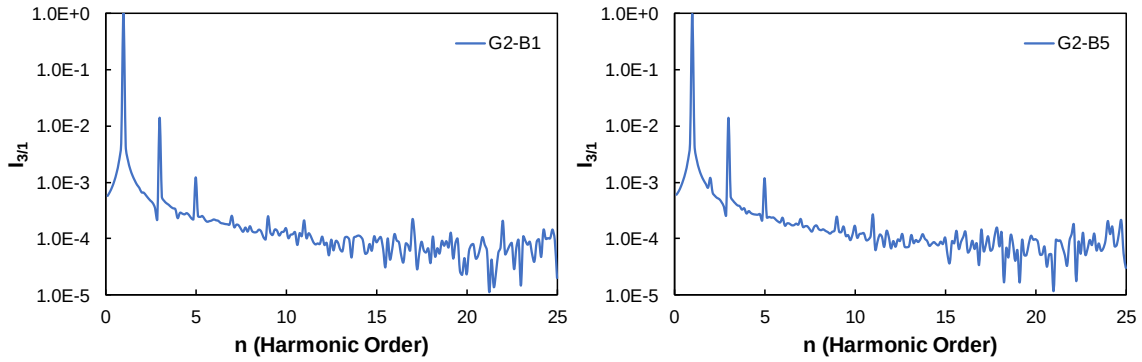

Figure 6-30: Fourier Transform Spectra for PG 70-16(Y) for Highest Strain Increment of Step G2-B1 and G2-B5 of the Repeated Strain Sweep Test Conducted at 40°C and 1 Hz.

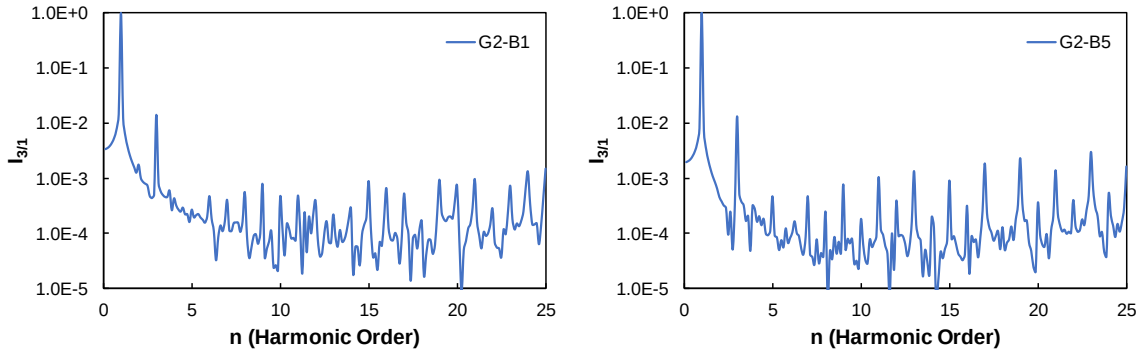

Figure 6-31: Fourier Transform Spectra for PG 70-16(Y) for Highest Strain Increment of Step G2-B1 and G2-B5 of the Repeated Strain Sweep Test Conducted at 64°C and 10 Hz.

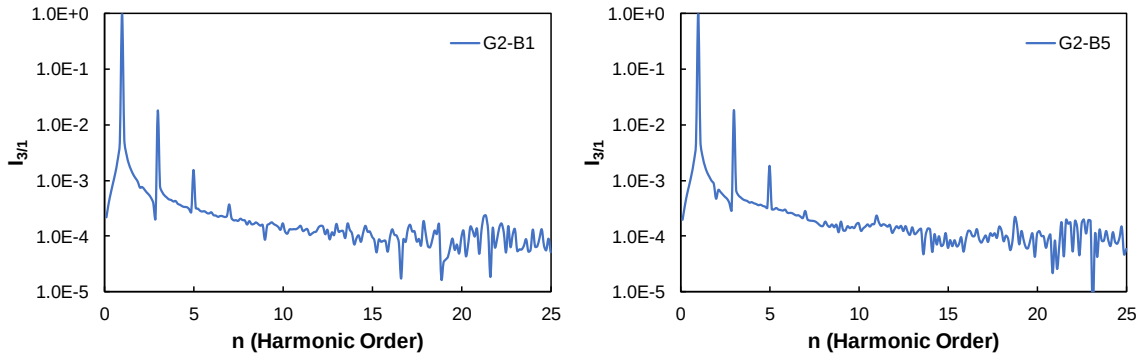

Figure 6-32: Fourier Transform Spectra for PG 76-16(Y) for Highest Strain Increment of Step G2-B1 and G2-B5 of the Repeated Strain Sweep Test Conducted at 40°C and 1 Hz.

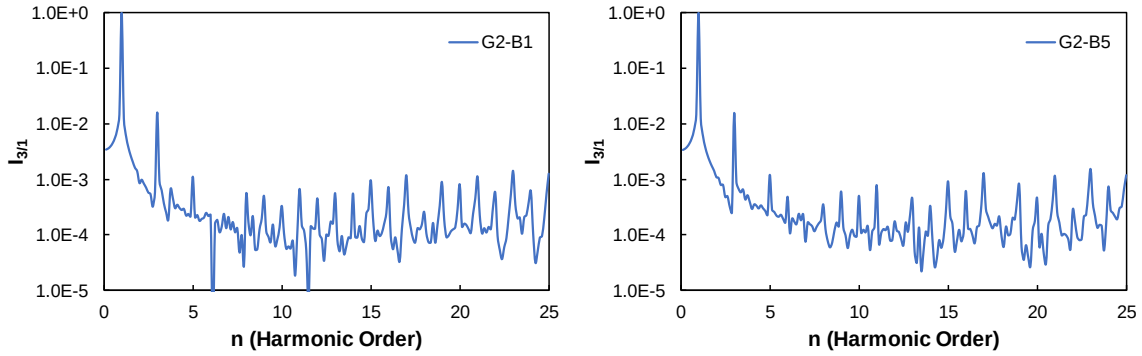

Figure 6-33: Fourier Transform Spectra for PG 76-16(Y) for Highest Strain Increment of Step G2-B1 and G2-B5 of the Repeated Strain Sweep Test Conducted at 64°C and 10 Hz.

After the detection of the higher order harmonics, the next step in the analysis process is calculation of the quantification parameter, Q. The parameter is dependent on the normalized intensity of the third harmonic and the strain amplitude. The value of the normalized intensity, $I_{3/1}$, can be found from the output files generated post the analysis on MITlaos. The value, γ_o, is the absolute value of zero to peak strain level at which the analysis is conducted. Though this value is known, the precise value can be obtained from the output files also. Meaning, the machine may be asked to apply 60% strain, but actually the strain applied may be 60.4%. These differences are detected by MITlaos and reflected

in the γ_o value in the output files. As per Hyun et al., the coefficient Q provides insight into how a material transitions from linear to non-linear domain. Thereby the analysis based on the non-linear coefficient is particularly useful in context of RSS test. However, Q values from both time sweep test and RSS test are presented here. For the time sweep test, the Q values at the three analysis locations, before failure, at failure and after failure are estimated. These values are tabulated in Table 12. $I_{3/1}$ is a strain dependent quantity whose value for a given condition changes only with change in strain level. Thereby in a time sweep test where the strain level is constant throughout the test, the value of $I_{3/1}$ is not expected to change by. This holds true for four of the six cases presented in Table 12. The exceptions being, time sweep tests at 80% and 120%. It can be seen that the $I_{3/1}$ value goes down as the test progresses. The significance of this difference is not known, as fundamentally the value should not change. However, the effect of this difference can be assessed. Ultimately, the $I_{3/1}$ value is used to calculate the Q parameter. Though there exists differences in the Q parameter these differences are in line with that observed in cases where $I_{3/1}$ remains stable. Also, the parameter $I_{3/1}$ and Q in Hyun et al.'s work are assessed in the logarithmic domain. Thereby, such small differences might not be important.

Table 12: The Values of $I_{3/1}$, γ_o, and Q for PG 70-16(Y) and PG 76-16(Y) from the Time Sweep Tests Analyzed at Three Different Locations.

Test Conditions	Asphalt Binder	Before Drop in δ			At Peak δ			After Drop in δ		
		$I_{3/1}$	γ_o	Q	$I_{3/1}$	γ_o	Q	$I_{3/1}$	γ_o	Q
40°C, 1Hz 40%	PG 70-16(Y)	0.056	0.200	1.397	0.061	0.201	1.523	0.064	0.201	1.598
	PG 76-16(Y)	0.056	0.200	1.393	0.055	0.201	1.375	0.053	0.201	1.323
40°C, 1Hz 80%	PG 70-16(Y)	0.102	0.416	0.588	0.085	0.404	0.521	0.077	0.404	0.469
	PG 76-16(Y)	0.105	0.404	0.642	0.097	0.407	0.586	0.086	0.408	0.521
40°C, 1Hz 120%	PG 70-16(Y)	0.124	0.613	0.329	0.091	0.640	0.223	0.086	0.633	0.213
	PG 76-16(Y)	0.121	0.620	0.314	0.106	0.650	0.252	0.106	0.632	0.266

64°C, 10Hz 10%	PG 70-16(Y)	0.002	0.050	0.667	0.002	0.049	0.824	0.002	0.049	0.849
	PG 76-16(Y)	0.001	0.049	0.558	0.002	0.049	0.996	0.001	0.049	0.318
64°C, 10Hz 30%	PG 70-16(Y)	0.009	0.149	0.414	0.009	0.150	0.386	0.008	0.150	0.341
	PG 76-16(Y)	0.013	0.149	0.597	0.012	0.149	0.551	0.012	0.151	0.509
64°C, 10Hz 100%	PG 70-16(Y)	0.046	0.501	0.185	0.044	0.505	0.173	0.046	0.501	0.183
	PG 76-16(Y)	0.105	0.523	0.383	0.103	0.515	0.390	0.103	0.525	0.375

Hyun et al. in their work used the Giesekus model, Pom-Pom model to study the evolution of $I_{3/1}$ and Q as a function of strain amplitude. The authors, then verified the model using their own experiments on monodisperse linear polystyrene. The relationships are shown in Figure 6-34.

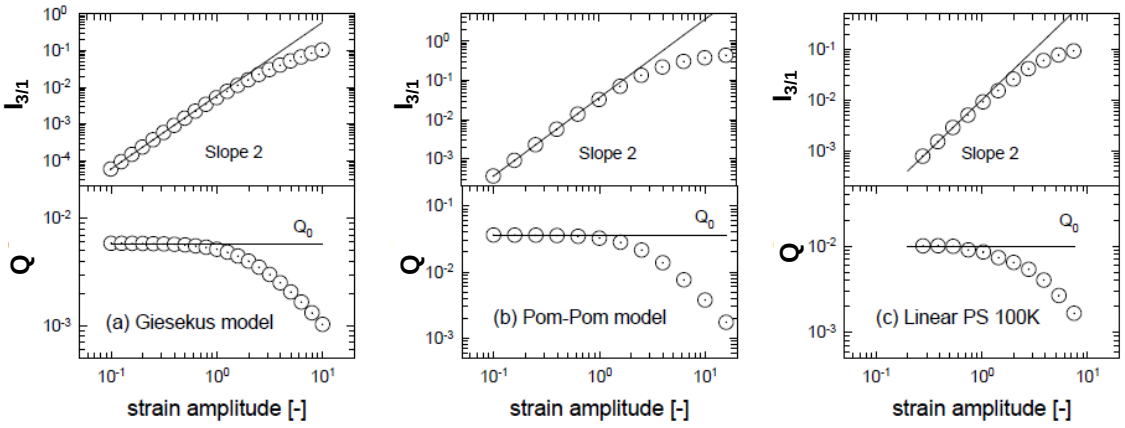

Figure 6-34: $I_{3/1}$ and Q as a Function of Strain Amplitude as Presented in Hyun et al. (2011).

There are two striking observations from the relationships. First, the $I_{3/1}$ and strain amplitude relationship obeys a power law relationship, with a slope of 2 in the medium amplitude sweep domain. It can be seen that the relationship deviates from the designated power law function at high strain amplitudes. The second observation, is regarding the relationship between Q and the strain amplitude. The relationship can be best described using a linear function in the logarithmic domain. It can be seen that the Q values attains a

near constant values at lower strain amplitudes. This region is in the medium amplitude oscillatory sweep (MAOS) range as described by the author. The range beyond the MAOS range is the SAOS range, small amplitude oscillatory sweep region, which is nothing but the LVE region. The authors named this constant value of Q as zero-strain non-linearity, Q_0, which like zero shear viscosity is a constant at relatively low strain amplitude, and depends on the loading frequency. The author's idea with defining Q_0 was to quantify the inherent non-linearity based on frequency and independent of strain amplitude.

Analysis, similar to that performed by Hyun et al. is performed here, and the $I_{3/1}$ and Q plots as a function of strain amplitude for the time sweep experiments are shown in Figure 6-35 and Figure 6-36.

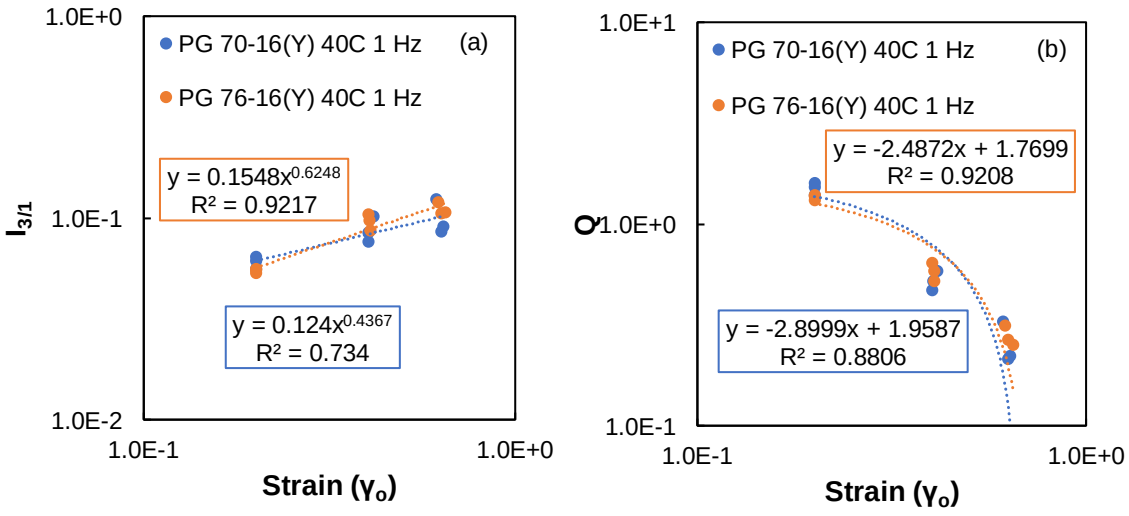

Figure 6-35: Variation of $I_{3/1}$ and Q as a Function of Strain Amplitude for the Time Sweep Tests Performed at 40°C and 1 Hz.

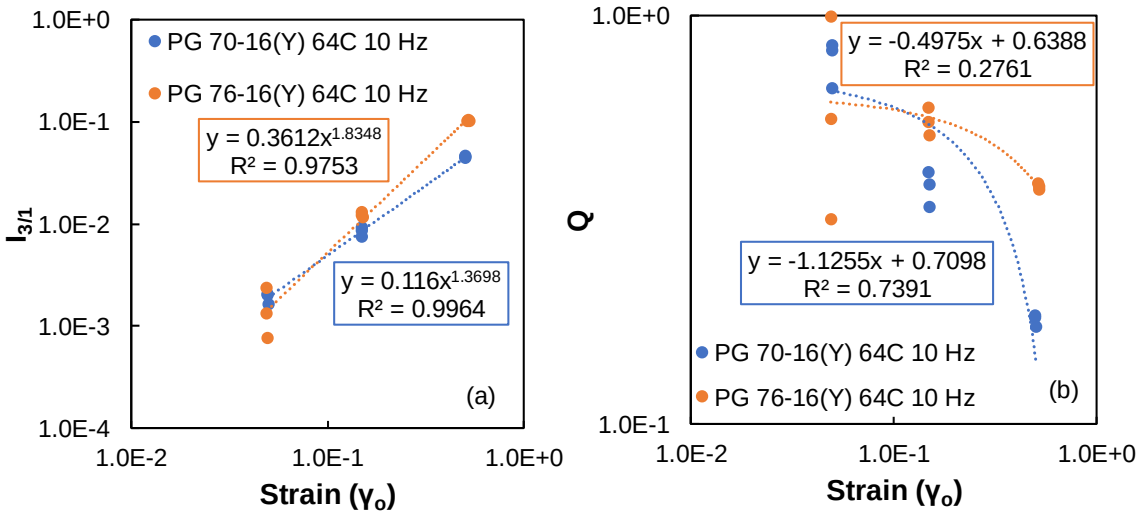

Figure 6-36: Variation of $I_{3/1}$ and Q as a Function of Strain Amplitude for the Time Sweep Tests Performed at 64°C and 10 Hz.

It can be seen from Figure 6-35(a) that the slope of the power law function is not equal to 2, in fact it is less than 2. Indicating that, possibly the strain levels used at 40°C and 1 Hz were higher than the MAOS range for the material. The trends seen in Figure 6-35(b) is similar to that seen in Figure 6-34, with absence of the constant Q region. It should be noted that the points plotted in Figure 6-35 and Figure 6-36 include the data from all the three analysis regions, i.e. before failure, at failure and after failure. The slope in Figure 6-36(a) is now closer to 2, indicating that the strain levels used in the test were closer to the MAOS range at 64°C and 10 Hz for the given study materials. However, in part (b) of the same figure, a clear breakdown in the relationship can be seen, especially in the case of PG 76-16(Y) at lower strain levels. This is because of the variability of $I_{3/1}$ at10% strain level. This strain just exceeds the LVE limit of the PG 76-16(Y) binder at 64°C and 10 Hz, and thereby the intensity of the third harmonic is very small and subject to variability along the test. The relationship in the case of PG 70-16(Y) is satisfactory in spite of the variability.

Next, for the RSS test, the Q values are estimated at each and every strain increment of the G2-B1 post the linear viscoelastic limit. This is the first step in the RSS test which has both linear and non-linear components. Fundamentally, since $I_{3/1}$ is zero in the LVE region, the values of Q are only tabulated in the NLVE region. These values are presented in Table 13. If the same analysis steps that were followed for the strain sweep test are repeated, interesting results are obtained and these are presented in Figure 6-37 and Figure 6-38.

Table 13: The Values of $I_{3/1}$, γ_o, and Q for PG 70-16(Y) and PG 76-16(Y) from the Repeated Strain Sweep Tests from Post LVE Range of Step G2-B1.

70-16(Y) 40°C 1 Hz			70-16(Y) 64°C 10 Hz			76-16(Y) 40°C 1 Hz			76-16(Y) 64°C 10 Hz		
$I_{3/1}$	γ_o	Q	$I_{3/1}$	γ_o	Q	$I_{3/1}$	γ_o	Q	$I_{3/1}$	γ_o	Q
0.001	0.040	0.835	0.003	0.060	0.837	0.003	0.041	1.723	0.002	0.059	0.640
0.003	0.051	1.064	0.003	0.076	0.562	0.004	0.052	1.560	0.004	0.075	0.621
0.005	0.065	1.139	0.005	0.095	0.607	0.006	0.066	1.470	0.006	0.096	0.625
0.008	0.083	1.234	0.009	0.121	0.592	0.007	0.066	1.607	0.010	0.122	0.661
0.014	0.105	1.277	0.014	0.156	0.560	0.011	0.084	1.569	0.016	0.155	0.669
-	-	-	-	-	-	0.018	0.106	1.569	-	-	-

It can be seen in part (a) of both Figure 6-37 and Figure 6-38 that the slope of the power law function in both cases is closer to the value of two. This indicates two things. First, that the strain levels employed in the RSS test are in the MAOS region and second that the validity of the quantification parameter "Q" can now be proven for asphalt as well. In part (b) of both the figures, the relationship seems to show a flat slope, leading to a constant Q value, similar to that seen in Figure 6-34.

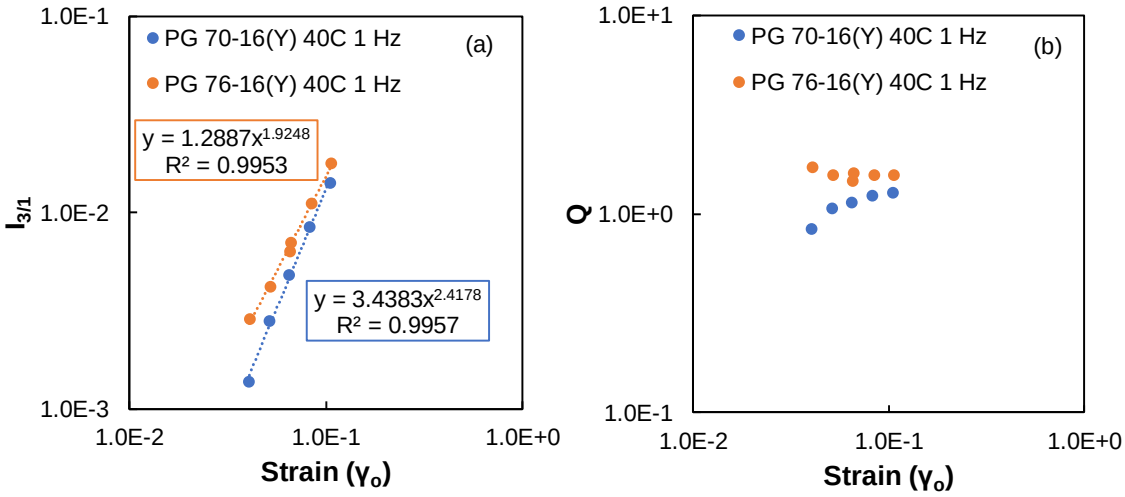

Figure 6-37: Variation of $I_{3/1}$ and Q as a Function of Strain Amplitude for the Post LVE Range for Step G2-B1of the Repeated Strain Sweep Tests at 40°C and 1 Hz.

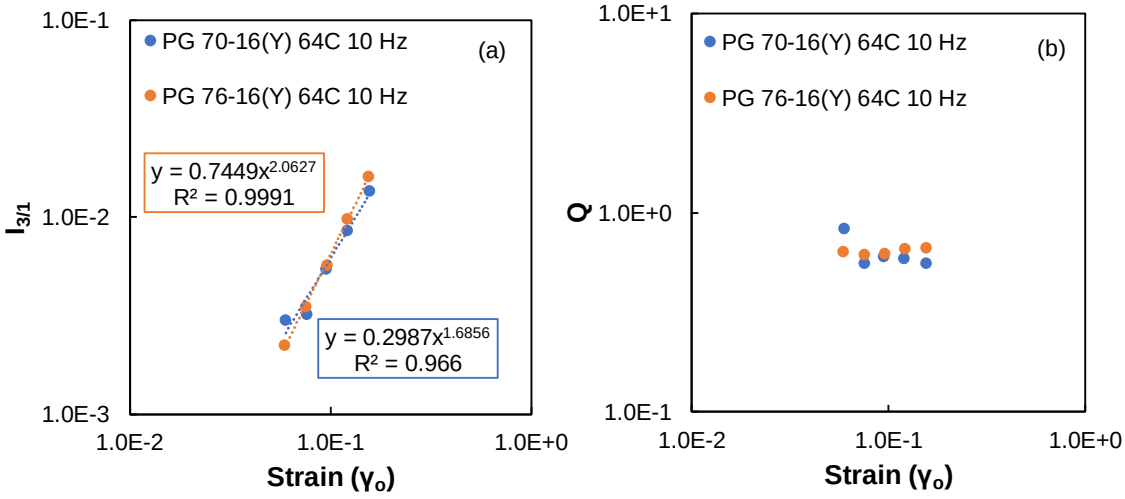

Figure 6-38: Variation of $I_{3/1}$ and Q as a Function of Strain Amplitude for the Post LVE Range for Step G2-B1of the Repeated Strain Sweep Tests at 64°C and 10 Hz.

What is required is a strain sweep that encompasses the MAOS range seen in RSS test and LAOS range seen in time sweep. While, there were no RSS experiments that encompassed the whole MAOS and LAOS range, approximate adjustments were made so that the complete picture of relationship between strain magnitude and Q can be observed. These adjustments involved taking the $I_{3/1}$ and γ_0 values at failure from the time sweep test and

including them in the data set generated for the RSS test. This was done for the 40°C and 1 Hz cases, and the results are shown in Figure 6-39. The relationship has been fit to a linear function in logarithmic space. The relationship produced here is similar to that shown in Figure 6-34 for linear polystrene. This assumes significance because like for polymers Q_0 can be calculated for asphalts also.

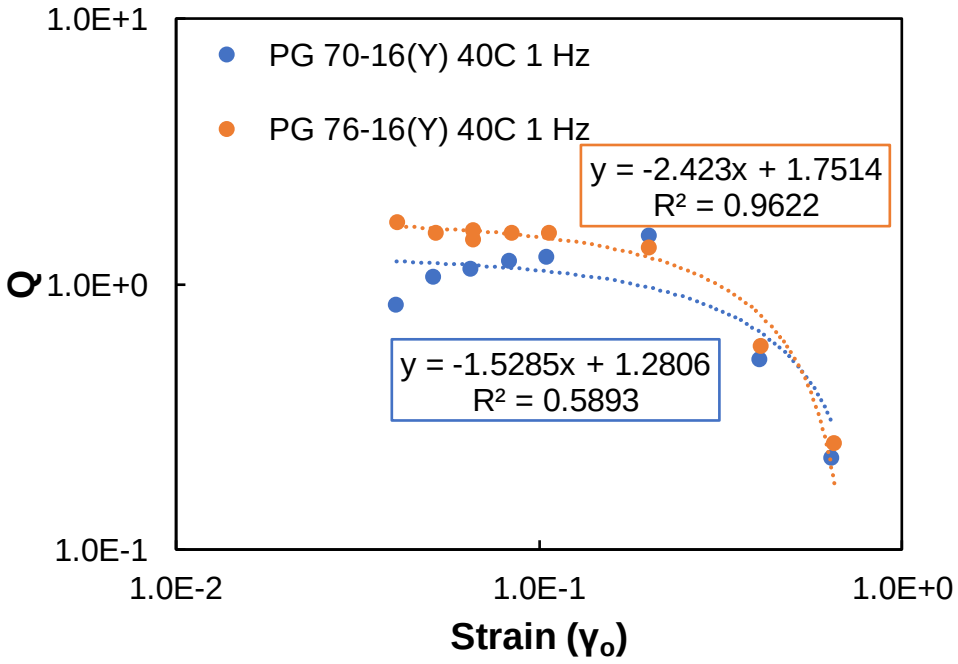

Figure 6-39: Q as a Function of Strain Amplitude Encompassing MAOS and LAOS Ranges for PG 70-16(Y) at 40°C and 1 Hz.

The discussion around Q_0 is of importance because the authors Hyun et al. have used the parameter to quantify inherent mechanical non-linearity between polymers of different topology such as linear polymers and branched chain polymers. The authors found that Q_0 reflects the relaxation process of disentanglement of polymer chain including reputation, contour length fluctuation and constraint release. In broad terms, the authors were able to relate non-linear properties to molecular structure properties by determining

a relationship between relaxation process of polymer chains and the non-linear coefficient. These findings provide essential cues, and set the stage for extending the study into asphalt domain to relate NLVE and molecular structure properties.

6.4.6 Relating NLVE Properties to Molecular Structure

As mentioned in the section above the findings from polymer literature can be extended into asphalt domain to relate NLVE and molecular structure of asphalt binders. In this study, the high temperature time sweeps and RSS tests were conducted on only two test binders, thereby limiting the possibility of developing any relationship using Q_0. However, another NLVE characterization test was performed in this study, the MSCR test, which will be discussed in detail in the next chapter. The parameter from this test, the non-recoverable creep compliance at 3.2 kPa, $J_{nr3.2}$, can be used to gain initial insights on the relationship between NLVE and molecular structure. To this end, a relationship between $J_{nr3.2}$ at 64°C and number average molecular weight, M_n, was developed for all original and RTFO aged PG 70-XX and PG 76-XX asphalts for which molecular weight distribution was presented in Chapter 4. This relationship is presented in Figure 6-40.Though the maximum R^2 seen is only 0.62, it can be interpreted that binders with higher molecular weight may lead to high compliance or low stiffness asphalt binders.

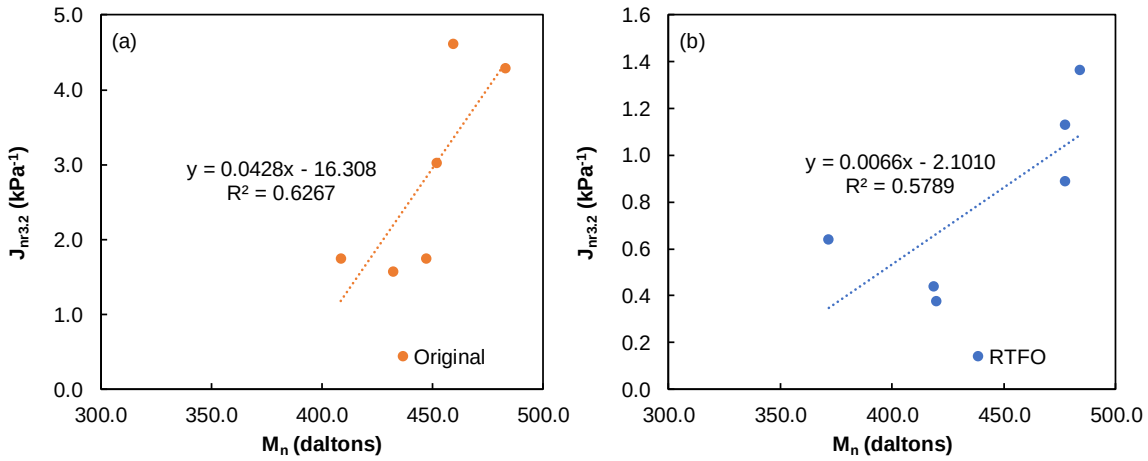

Figure 6-40: Relationship between $J_{nr3.2}$ and M_n for (a) Original and (b) RTFO Aged Asphalt Binders.

The relationship presented above is the first step in relating NLVE properties to molecular structure of asphalt binder. The study should be further expanded especially involving more asphalts to perform high temperature time sweep and RSS test, so that the Q_0 value can be calculated and be related to molecular structure parameters.

In summary, in this chapter first the technical details associated with performing the LAOS tests, such as the oxidation level at which the binder is to be used, the test temperature required for a successful test, etc. are discussed. Next, the use of analytical tool of MITlaos for the analysis of the data generated from the LAOS tests is discussed in an elaborate and step by step manner. Subsequently, the results from the binders chosen for the LAOS analysis are discussed. The first step of which involved investigation of distortion in stress-strain relationships after which the detection of non-linearity taken up and finally, the detected non-linear behavior was quantified with the aid of the outputs obtained from the MITlaos program.

Chapter 7 NLVE Studies III – Jnr Difference Study Using High Temperature Creep and Recovery Experiments

In this chapter, the focus is on another test that evaluates the non-linear viscoelastic behavior of asphalt binders. The main distinction between this chapter and the preceding chapter lies in the magnitude of the strain levels generated during test. While the maximum strain level evaluated in the preceding chapter was around 120%, in this chapter the strain magnitude for many asphalts is in excess 1000%. This indicates that the material might transition into plastic phase, and the behavior might actually be non-linear elasto-viscoplastic.

The Multiple Stress Creep and Recovery (MSCR) test was conceptualized to overcome the limitations of the current standard method for grading asphalt, AASHTO M 320, particularly with respect to characterizing polymer modified binders (Bahia 2001). The test since has gained acceptance at both federal and state level and is currently standardized as AASHTO T 350 and ASTM D 7405. The MSCR test measures the non-recoverable creep compliance, J_{nr}, which is characterized at strain levels exceeding the linear viscoelastic limit of the material and produces enough deformation to capture asphalt binder modification benefits. Three parameters from the test, non-recovered creep compliance at 3.2 kPa ($J_{nr3.2}$), Recovery at 3.2 kPa ($R_{3.2}$) and the difference in non-recoverable creep compliance (J_{nrdiff}) are part of the new asphalt binder grading protocol presented under AASHTO M332.

The parts of this chapter are published as: Stempihar, J., A. Gundla, and B.S. Underwood, (2018). Interpreting Stress Sensitivity in the Multiple Stress Creep and Recovery Test. *Journal of Materials in Civil Engineering*, 30(2).

While the specifics of the MSCR test and the parameters have been described in Chapter 3, in this chapter the analysis and discussion is focused on the J_{nrdiff} parameter, more specifically its physical relevance. The parameter in its current use in the specification is intended to restrict the stress sensitivity of the binder and the threshold for the parameter is set at 75% in the AASHTO M332 specification. A detailed discussion of the origin of the parameter, its intended use, limitations, and alternatives is presented in the following paragraphs and form the remainder of this chapter.

7.1 Origin of the J_{nrdiff} Parameter

One major motivation for developing AASHTO T 350 was inadequacies with applying the AASHTO M 320 Superpave rutting parameter, $|G^*|/\sin\delta$, to modified asphalt binders (D'Angelo and Dongre 2002, Dongre and D'Angelo 2003), specifically, poor correlation to asphalt mixture rutting (Minnesota Department of Transportation 2015). In comparison, studies show J_{nr} has a much better correlation to asphalt mixture rutting for unmodified and modified asphalt binder mixtures and performance relationships between J_{nr} and rut depth have been developed (D'Angelo et al. 2007, D'Angelo 2009). While there is general agreement that the J_{nr} parameter demonstrates better correlation to pavement performance than its predecessor, $|G^*|/\sin\delta$, there are concerns with respect to the impact of uncertainties when translating controlled laboratory testing protocols to in-service conditions. These concerns are generally framed under the assumptions of how the material will react to load levels above those tested in the laboratory or how they will react to temperatures slightly above or below what was considered in the laboratory. From years of experience with AASHTO M 320, engineers have developed a sense of comfort and

certainty with respect to these changes and the $|G^*|/\sin\delta$ parameter, but are understandably less confident with J_{nr}. To provide a level of certainty with the J_{nr} specification, developers included a parameter, J_{nrdiff}, that is intended to provide certainty that even if stress levels are exceeded or temperatures are higher than what was originally considered that the asphalt binder would adequately perform. During MSCR test development (D'Angelo et al. 2007), the stress levels tested ranged from 0.1 kPa to 25.6 kPa. A plot of J_{nr} versus stress provided an indication of the trend of change in non-recoverable creep compliance (J_{nr}) across the range of applied stress. As a means to quantify the trend of change in J_{nr} across the range of applied stress, a J_{nrdiff} parameter (percent difference J_{nr} between 0.1 and 3.2 kPa) was defined. While not explicitly stated or well defined in literature, the original intent of placing an upper specification limit of 75% on the J_{nrdiff} parameter was to set a limit on the change in non-recoverable creep compliance (J_{nr}) of an asphalt binder as a safety factor in the event that a pavement experiences higher loading stress or higher than expected temperatures (D'Angelo 2009, D'Angelo 2010, Anderson 2011).

7.2 Limitations of the J_{nrdiff} Parameter and Potential Alternatives

While rutting performance correlations to J_{nr} have been documented for both unmodified and modified asphalt binders, relationships between laboratory measured changes in J_{nr} across the range of applied stress (currently assessed using J_{nrdiff}) and changes in field performance are nonexistent in the literature. Thus, the ability of J_{nrdiff} to provide meaningful insight into the relationship between laboratory measured changes in J_{nr} across the range of applied stress to changes in field performance of the asphalt mixture (due to increased stresses and higher temperatures) remains unknown. As a result, a problem exists

with the current AASHTO M 332 specification, specifically related to the inclusion of the J_{nrdiff} parameter. States and suppliers working with AASHTO T 350 and the AASHTO M 332 specification have reported challenges with meeting the J_{nrdiff} specification especially for modified asphalt binders with low J_{nr}. This problem becomes more pronounced for asphalt binders with $J_{nr3.2}$ values less than 0.5 kPa^{-1}. Reported J_{nrdiff} values can be more than 400% difference (Dongre 2016) for modified asphalt binders that anecdotally perform well in pavements. It has also become apparent that J_{nrdiff} is extremely variable. Proficiency sampling across the hundreds of laboratories that participate in the AASHTO accreditation process shows that many labs receive very low scores on J_{nrdiff} despite having very good scores on the other AASHTO T 350 parameters (Dongre 2016).

As a potential solution to addressing the aforementioned specification problem, Dongre (2016) presented a modification to the MSCR method to stabilize the observed variation in the J_{nrdiff} parameter. This modification included testing at 0.32 kPa rather than 0.1 kPa and increasing the loading time from one to three seconds. While the decreased variability results obtained were promising, the fact remains that asphalt binders with small $J_{nr3.2}$ can still have very large J_{nrdiff} values. Essentially, this method attempts to overcome the issue by modifying the test procedure to yield higher J_{nr} values at the lower stress level by increasing the load time and thus reducing the recoverable strain. While this approach deserves consideration, it does not address the larger challenge of relating laboratory measured changes in J_{nr} across the range of applied stress to changes in field performance.

In this dissertation, the study taken up to investigate the J_{nrdiff} parameter and to propose alternative is segmented into two phases, phase 1 and phase 2. Presented in phase

1 is an alternative parameter to J_{nrdiff} based on the argument that J_{nrdiff} is not able to accurately describe the trend in non-recoverable creep compliance (J_{nr}) across the range of applied stress of asphalt binders, nor relate laboratory data to expected changes in field performance. An alternate analysis to describe the J_{nr} – applied stress response of asphalt binders in AASHTO T 350 is proposed which is based both on literature and numerous personal communications with industry experts on the subject matter. Using a performance-based approach, a conceptual specification limit using the new parameter is developed and compared to a database of asphalt binder test results. Next, multi-temperature test data are used to evaluate the new parameter as an indicator of change in J_{nr} for an incremental increase in test temperature. The phase 1 analysis and its corresponding discussions have been documented and published by Stempihar et al. (2017).

The performance relationships developed as part of phase 1 were based on a linear, arithmetic relationship between $J_{nr3.2}$ and observed rut depths on the Mississippi I-55 test sections. No actual rutting tests were conducted. In phase 2 of the study, MSCR test data from the study binders and the rutting data from the Hamburg wheel tracking test are used to verify and validate the relationships developed in phase 1 of the study. Detailed discussions on the new alternative parameter and the ensuing relationships are presented in the following sections.

7.3 Phase 1: Scrutiny of the J_{nrdiff} Parameter, Development of Alternative Measure, and Performance Relationships

7.3.1 Visual Assessment of Stress Sensitivity

AASHTO T 350 defines the J_{nrdiff} simply as the percent difference between J_{nr} at 3.2 kPa and 0.1 kPa stress levels for a given asphalt binder as shown in Equation (50).

$$J_{nrdiff} = \frac{[J_{nr3.2} - J_{nr0.1}]}{J_{nr0.1}} \times 100 \quad (50)$$

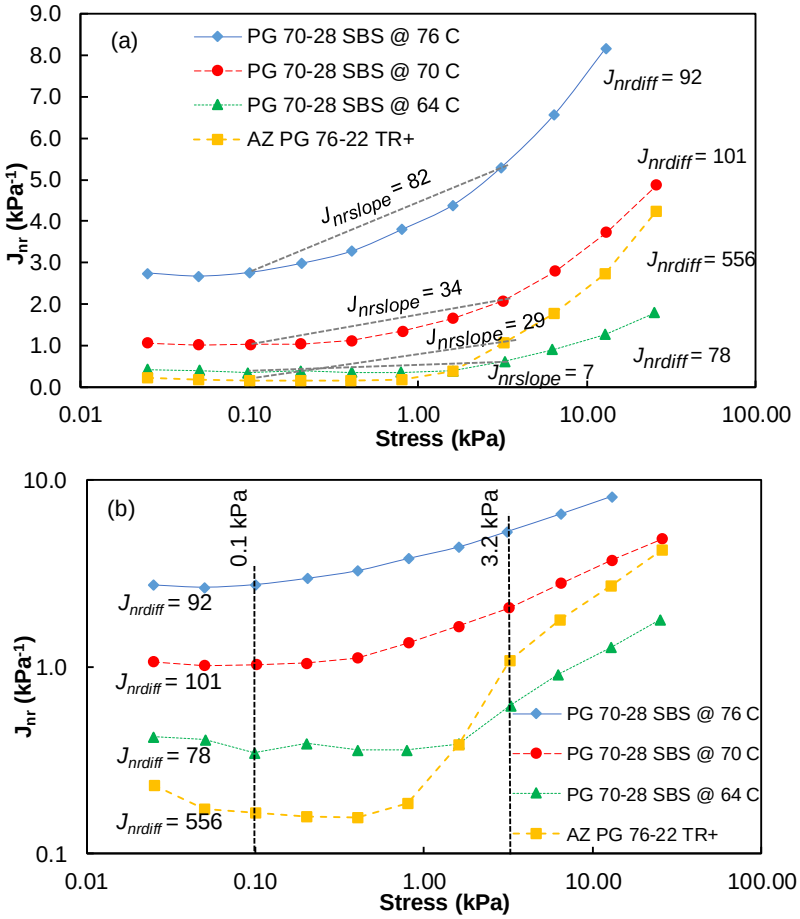

Figure 7-1: Change in J_{nr} versus applied stress trends for modified asphalt binders a) semi-logarithmic scale, b) logarithmic scale, PG 70-28 SBS data from (Anderson, 2011).

Figure 7-1 provides semi-logarithmic and logarithmic plots of the effect of stress on J_{nr} for the PG 70-28 SBS asphalt binder originally presented by D'Angelo (D'Angelo 2009) during development of the test method. An Arizona PG 76-22 TR+ asphalt binder (X5), modified with digested crumb rubber and SBS polymer, is also included in the plot for demonstration purposes, and J_{nrdiff} values are included in Figure 7-1 for comparison purposes. From these data, it is apparent that none of the asphalt binders pass the J_{nrdiff} limit of 75% maximum specified in AASHTO M 332.

In semi-logarithmic space, the PG 70-28 SBS asphalt binder tested at 76°C visually appears to have a slightly higher incremental change in J_{nr} with increasing stress level compared to the same asphalt binder tested at the high-grade temperature of 70°C. However, the J_{nrdiff} values of 92% and 101%, respectively tell a different story and imply that the asphalt binder is more sensitive to change in applied stress at 70°C than 76°C. Next, consider the AZ PG 76-22 TR+ and PG 70-28 SBS tested at 64°C. These asphalts show a similar change in J_{nr} value with increases in stress levels up to around a stress level of 3.2 kPa and thus the parameter used to quantify change in J_{nr} in this range of applied stress would be expected to yield similar values for these asphalt binders. After 3.2 kPa, the J_{nr} for AZ PG 76-22 TR+ shows a greater change with stress level increases but J_{nrdiff} is limited to between 0.1 and 3.2 kPa and thus does not make any pretense to predict behaviors in this portion of the relationship. Although the visual change in J_{nr} with stress levels is similar for the AZ PG 76-22 TR+ and the PG 70-28 SBS, J_{nrdiff} values are 556% and 78%, respectively. Based on the visual comparison it can be concluded that a J_{nrdiff} value of 556% is not an accurate representation of the stress sensitivity of the AZ PG 76-

22 TR+ asphalt binder, which most resembles the behavior of the PG 70-28 SBS tested at 64°C, with a J_{nrdiff} of 78%.

However, correlating visual examinations in semi-logarithmic space with the J_{nrdiff} is likely not appropriate given the mathematical definition of J_{nrdiff}. In logarithmic space, it is found that visual indications of the sensitivity of J_{nr} to stress increases agrees with the J_{nrdiff} values. The AZ PG 76-22 TR+ is most sensitive to applied stress followed by PG 70-28 SBS tested at 70°C, PG 70-28 SBS tested at 76°C, and PG 70-28 SBS tested at 64°C. The J_{nrdiff} values are 556, 101, 92 and 78%, respectively. The PG 70-28 SBS tested at 76°C and 70°C appear to have similar responses to increased stress which is reflected in the similar J_{nrdiff} values of 92 and 101%, respectively. While the 556% difference for the AZ PG 76-22 TR+ is a questionable value, Figure 7-1 shows a very large change in J_{nr} between 0.1 and 3.2 kPa compared to the other asphalt binder test results. Thus, in logarithmic space, J_{nrdiff} appears to provide a reasonable ranking of the trend of J_{nr} as applied stress increases. The specific structural or compositional reasons for these differences and behaviors are not explored here; however, similar rapid stress dependency has been associated with bifurcation of the asphalt fractions upon shearing (Coussot et al. 2002, Mendes et al. 2015). Here it can be postulated that this stress dependency is mitigated somewhat by the presence of the polymeric additive, which serves to both reduce the overall compliance of the binder and also restrict unabated flow. In this case, the binder may perform perfectly adequately (and anecdotal evidence suggests this is the case) since the high stress levels needed to instigate the bifurcation may not exist in real pavements. This connection to microstructure and composition is merely a hypothesis, which is not explored in greater detail here.

The question remains as to whether the fully logarithmic domain or the semi-logarithmic domain is the more accurate space for assessment of stress sensitivity. It is the believed that the semi-logarithmic interpretation is the more accurate space as further demonstrated in the following sections.

7.3.2 Proposed Measure of Stress Sensitivity

Based on the above arguments regarding semi-logarithmic space, the definition of stress sensitivity presented herein, and unfair biasing of low compliance asphalts, a new parameter to describe the change in non-recoverable creep compliance of an asphalt binder to an incremental change in applied stress is defined. This parameter, $J_{nrslope,}$ is defined as the slope (in percent) of the J_{nr} – stress relationship between 0.1 kPa and 3.2 kPa stress levels as shown in Equation (51), where $J_{nrslope}$ = percent slope of non-recoverable creep compliance between 0.1 and 3.2 kPa. $J_{nrslope}$ does not include $J_{nr0.1}$ in the denominator, and thus it yields a constant value for the same J_{nr} – stress relationship regardless of the $J_{nr3.2}$ magnitude. Given this fact, $J_{nrslope}$ provides equivalent assessment of stress sensitivity for a range $J_{nr3.2}$ values and does not unfairly penalize modified asphalt binders with low $J_{nr3.2}$.

$$J_{nrslope} = \frac{dJ_{nr}}{d\tau} = \frac{\left[J_{nr3.2} - J_{nr0.1}\right]}{3.1} \times 100 \tag{51}$$

Figure 7-1 provides a comparison of the $J_{nrslope}$ and J_{nrdiff} parameters to rank the visual change in J_{nr} over a range of applied stress levels for different asphalt binders. According to $J_{nrslope}$, the asphalt binder with the largest change in J_{nr} is PG 70-28 SBS tested at 76°C, followed by the PG 70-28 SBS tested at 70°C, AZ PG 76-22 TR+ and finally, PG 70-28 SBS tested at 64°C. Visual examination of Figure 7-1 confirms these

rankings. In comparison, J_{nrdiff} inaccurately ranks the change in J_{nr} from highest to lowest as AZ PG 76-22 TR+, PG 70-28 SBS tested at 70°C, PG 70-28 SBS tested at 76°C, and PG 70-28 SBS tested at 64°C. Further examination shows that the change in J_{nr} (up to 3.2 kPa) is similar between AZ PG 76-22 TR+ and PG 70-28 SBS tested at 70°C and $J_{nrslope}$ accurately captures this observation with values of 34% and 29%, respectively. In comparison, J_{nrdiff} implies the change in J_{nr} for AZ PG 76-22 TR+ is 5.5 times greater than PG 70-28 SBS tested at 70°C which is not accurate by the observed data. In comparison, J_{nrdiff} for the PG 70-28 SBS tested at 76°C and 70°C are similar at 92% and 101% respectively, yet the $J_{nrslope}$ is nearly 2.5 times greater for the PG 70-28 SBS tested at 76°C which is visually evident. Again, interpreting stress sensitivity in this semi-logarithmic domain, the $J_{nrslope}$ parameter is in better agreement with a visual assessment of the change in J_{nr} – stress trends of these two asphalt binders.

7.3.3 Relationship to Performance

7.3.3.1 Incremental Rutting

As indicated earlier, the Initial development of allowable $J_{nr3.2}$ limits for different traffic levels in M 332 were based on a linear, arithmetic relationship between $J_{nr3.2}$ and observed rut depths on the Mississippi I-55 test sections. MSCR test data indicated that a 50% reduction in $J_{nr3.2}$ resulted in an approximate observed field rut depth reduction of 50% (D'Angelo 2009 and D'Angelo 2010). To support the authors' belief that stress sensitivity of asphalt binders should be assessed in the semi-logarithmic domain, a comparison between an incremental change in rutting (50% in this case) and the resultant J_{nrdiff} and $J_{nrslope}$ values is presented in Figure 7-2 for the Arizona asphalt binders described in a

previous section. For this comparison, rut depth was first predicted for $J_{nr3.2}$ using the I-55 relationship and then this resultant rut depth was increased by 50%. Next, resultant $J_{nr3.2}$ was back-calculated using the I-55 relationship and the resultant rut depth. Finally, resultant J_{nrdiff} and $J_{nrslope}$ were calculated using the original $J_{nr0.1}$ and resultant $J_{nr3.2}$ value associated with increased rut depth.

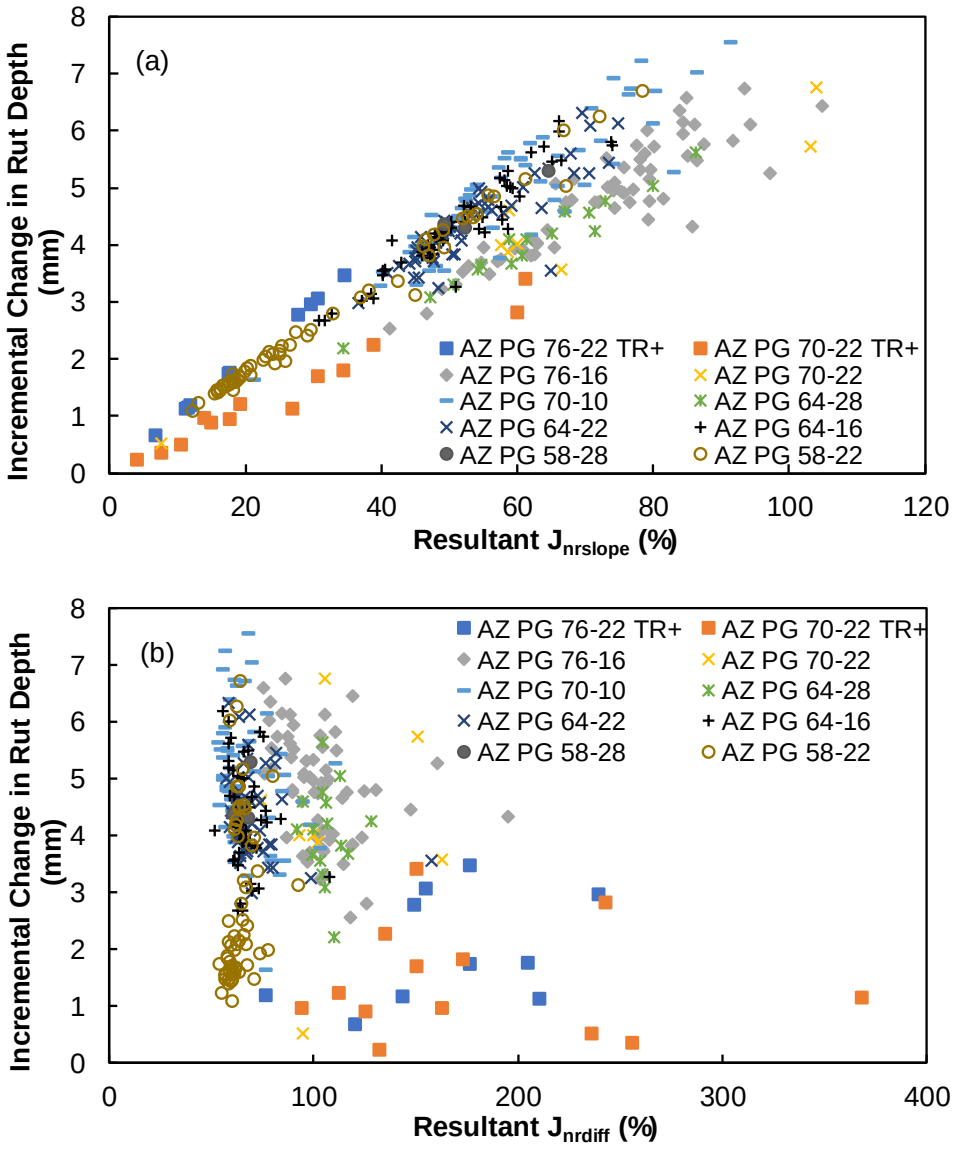

Figure 7-2: Relationship to an incremental increase in rutting for a) $J_{nrslope}$ and b) J_{nrdiff}.

Figure 7-2 shows that stress sensitivity, quantified using $J_{nrslope}$ in semi-logarithmic domain has a much better relationship to an incremental change in rutting than the J_{nrdiff} parameter. Thus, $J_{nrslope}$ can provide a much better characterization of the change in non-recoverable creep compliance (between 0.1 to 3.2 kPa, semi-logarithmic domain) and associated incremental changes in rut depth. This correlation between $J_{nrslope}$ and an incremental change in rutting further supports the belief that stress sensitivity of an asphalt binder should be assessed in the semi-logarithmic domain.

7.3.3.2 Temperature Surrogacy

As discussed earlier, one original intent of J_{nrdiff} limit was to ensure that the change in non-recoverable creep compliance of asphalt binders was such that, if tested at a temperature of 6°C higher, the new $J_{nr0.1}$ value was at or below the $J_{nr3.2}$ at the lower temperature. In this context, limiting the change in J_{nr} between 0.1 kPa and 3.2 kPa, J_{nrdiff} essentially serves as a surrogate parameter to limit the non-recoverable creep compliance of the asphalt binder if in practice it were exposed to a temperature 6°C higher than the specified performance grade temperature. However, literature does not present validation of this concept through a comparison between J_{nrdiff} and a change in $J_{nr3.2}$ when the same asphalt binder is tested at a 6°C incremental temperature increase. To explore a potential correlation between $J_{nrslope}$, derived from $J_{nr3.2}$ – stress data, to the change in $J_{nr3.2}$ for a 6°C incremental temperature increase in AASHTO T 350, multi-temperature asphalt binder test data (same asphalt binders, different test temperatures) were extracted from the Arizona, Arizona Western Cooperative Test Group (AZ WCTG), Montana, (Table 14) and D'Angelo (2009) datasets. This unique dataset provided the opportunity to evaluate the

$J_{nrslope}$ parameter as a surrogate measure of the change in non-recoverable creep across test temperatures. The dataset was examined using two different calculation methods: 1) $J_{nrslope}$ was compared to the change in $J_{nr3.2}$ as defined in Equation (52) and 2) J_{nrdiff} was compared to the percent difference $J_{nr3.2}$ as defined in Equation (53).

$$\frac{dJ_{nr3.2}}{dT} = \frac{\left[J_{nr3.2(T+6)} - J_{nr3.2(T)}\right]}{6} \tag{52}$$

$$J_{nr3.2diff} = \frac{\left[J_{nr3.2(T+6)} - J_{nr3.2(T)}\right]}{J_{nr3.2(T)}} \times 100 \tag{53}$$

where $dJ_{nr3.2}/dT$ = change in $J_{nr3.2}$ for a 6°C increase in test temperature; $J_{nr3.2diff}$ = percent difference $J_{nr3.2}$ for a 6°C increase in test temperature, $J_{nr3.2(T)}$ = average non-recoverable creep compliance at 3.2 kPa (test temperature, T(°C), and $J_{nr3.2(T+6)}$ = average non-recoverable creep compliance at 3.2 kPa (T+6 (°C)).

Table 14: Summary of MSCR Binder Database Used for Phase 1 Analysis

Grade	No. Tests (Arizona)	No. Tests (Montana)	No. Tests (AZ WCTG)
PG 76-22TR+	10	-	-
PG 76-22NV	-	-	2
PG 70-22TR+	13	-	-
PG 70-22ER	-	-	4
PG 76-28	-	-	8
PG 76-16	63	-	-
PG 70-22	8	-	-
PG 70-28	-	731	2
PG 70-10	61	-	-
PG 64-28	16	1,222	2
PG 64-22NV	-	-	2
PG 64-22	54	74	-
PG 64-16	52	-	-
PG 58-28	3	212	-
PG 58-22	59	-	-

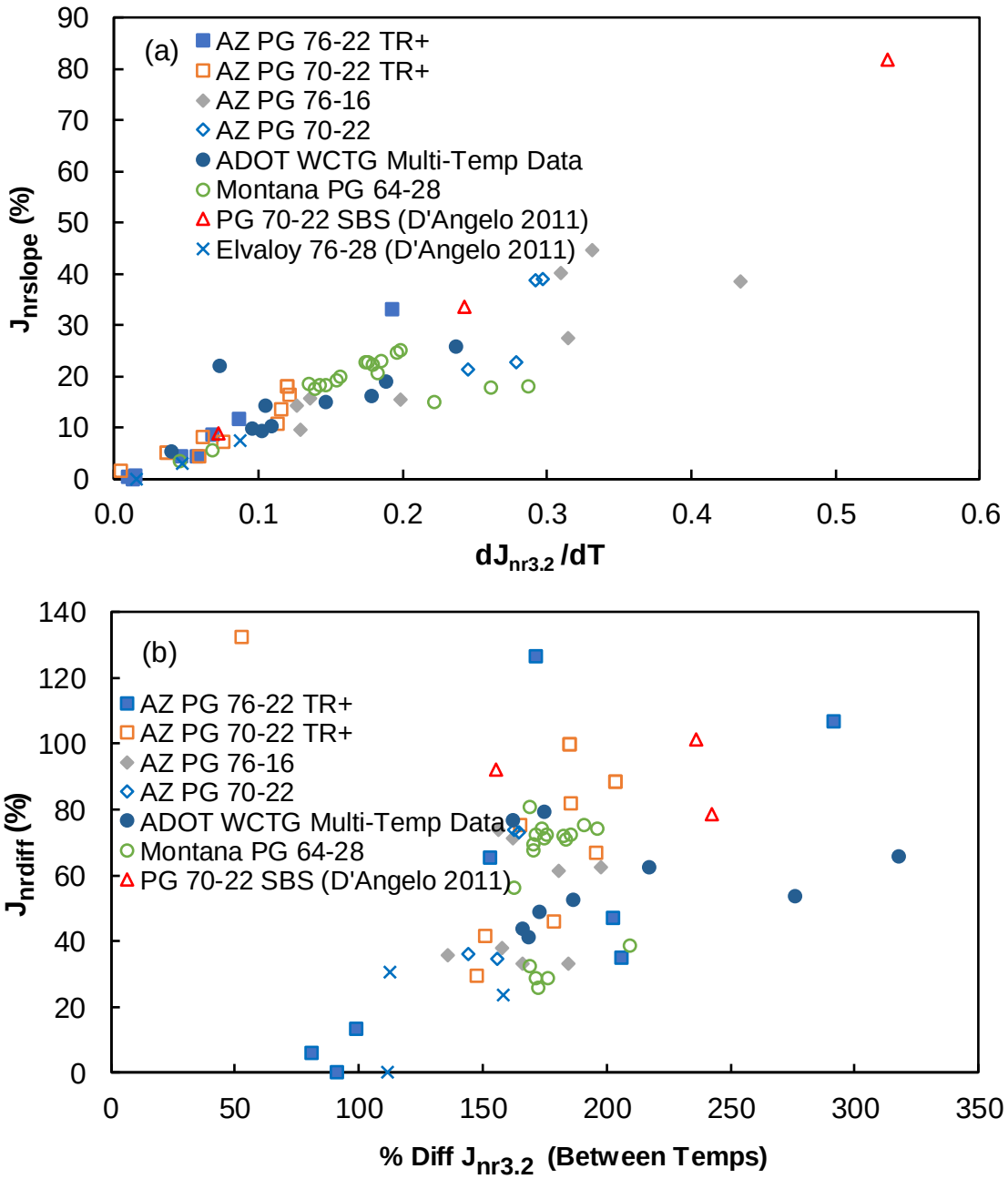

Figure 7-3: Plot of a) $J_{nrslope}$ and b) J_{nrdiff} compared to change in $J_{nr3.2}$ between temperatures.

Figure 7-3 presents a graphical summary of the correlation between $J_{nrslope}$ and change in $J_{nr3.2}$ for a 6°C incremental temperature increase in AASHTO T 350. The plot also includes a comparison to J_{nrdiff} as an indicator of temperature sensitivity. $J_{nrslope}$ shows

a much better correlation to the change in $J_{nr3.2}$ for a 6°C incremental temperature increase in test temperature. In comparison, J_{nrdiff} does not demonstrate a correlation with the percent difference in $J_{nr3.2}$ for a 6°C increase in test temperature. Based on these findings, the $J_{nrslope}$ parameter demonstrates potential to serve as a good indicator of temperature and stress sensitivity of an asphalt binder in AASHTO T 350.

As discussed earlier, J_{nrdiff} currently serves to address the uncertainty between the stresses levels applied in the MSCR test and actual stress levels exerted on asphalt pavements. Equally important is addressing the uncertainty between increased temperature in the MSCR test and the impacts of increased temperature on asphalt pavements. $J_{nrslope}$ provides a promising means to address this uncertainly.

7.3.4 Proposed $J_{nrslope}$ Specification Limit

Based on the observed correlation of $J_{nrslope}$ to an incremental change in rutting and $J_{nrslope}$ as a potential surrogate indicator of temperature sensitivity, the authors propose that a $J_{nrslope}$ specification limit be developed. To begin constructing this specification limit, $J_{nr0.1}$ and $J_{nr3.2}$ values were extracted from a database (Table 1) containing AASHTO T 350 test results for common asphalt binder grades used in Arizona and Montana. J_{nrdiff} was calculated for all data and the Arizona data were plotted against $J_{nr3.2}$ and the J_{nrdiff} specification limit of 75% in Figure 7-4. Approximately one half of the premium Arizona PG 76-22 TR+ and PG 70-22 TR+ asphalt binders do not meet the current 75% J_{nrdiff} specification despite anecdotal evidence of acceptable field performance. Also, Figure 7-4 demonstrates the impact of magnitude dependency of J_{nrdiff}, further supporting the authors' belief that stress sensitivity should be assessed in the arithmetic domain.

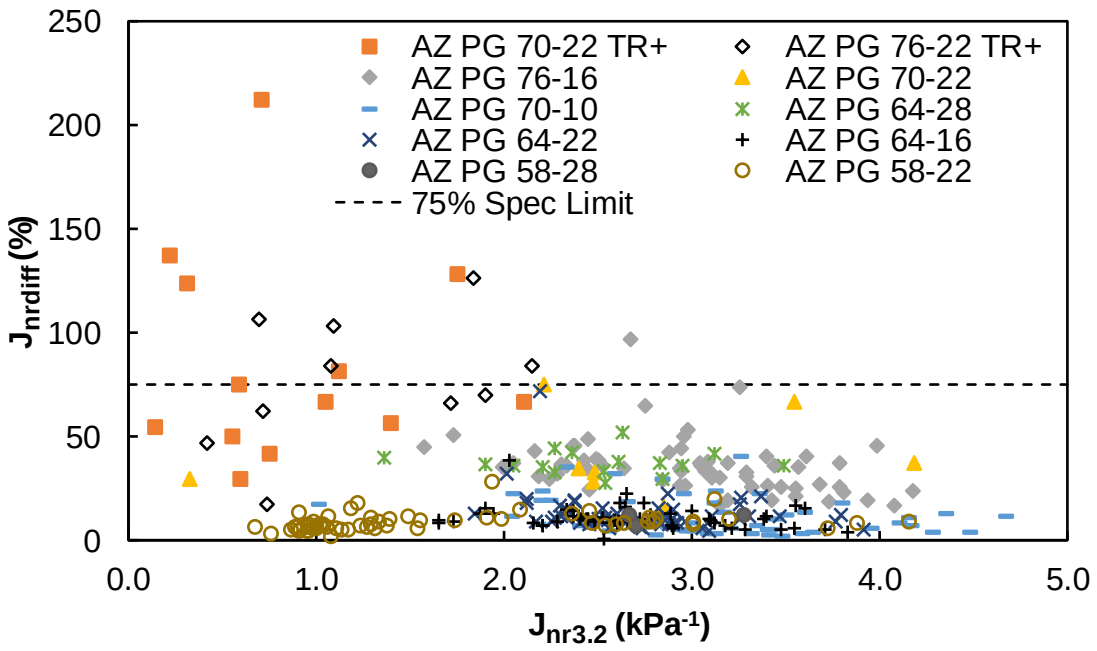

Figure 7-4: Comparison of J_{nrdiff} to $J_{nr3.2}$ and the 75% J_{nrdiff} specification limit for Arizona asphalt binders.

Motivated by the original stated intent of the J_{nrdiff} parameter, it is proposed to base the allowable range on limiting the change in J_{nr} for an incremental change in applied stress. This proposed method follows the interpreted logic behind the original intent of J_{nrdiff} such that if an asphalt binder is tested at a temperature of 6°C higher, the new $J_{nr0.1}$ value is less than or equal to $J_{nr3.2}$ at the lower temperature. The $J_{nrslope}$ values for the conceptual specification limit were determined by setting $J_{nr0.1}$ for the next higher traffic grade to $J_{nr3.2}$ of the previous traffic grade and then calculating the maximum $J_{nrslope}$ using $J_{nr0.1}$ and the maximum allowable $J_{nr3.2}$ value in that traffic grade. Figure 7-5 presents a plot of the potential specification limit comparing the Arizona asphalt binder data and an additional set of asphalt binder data obtained from Montana.

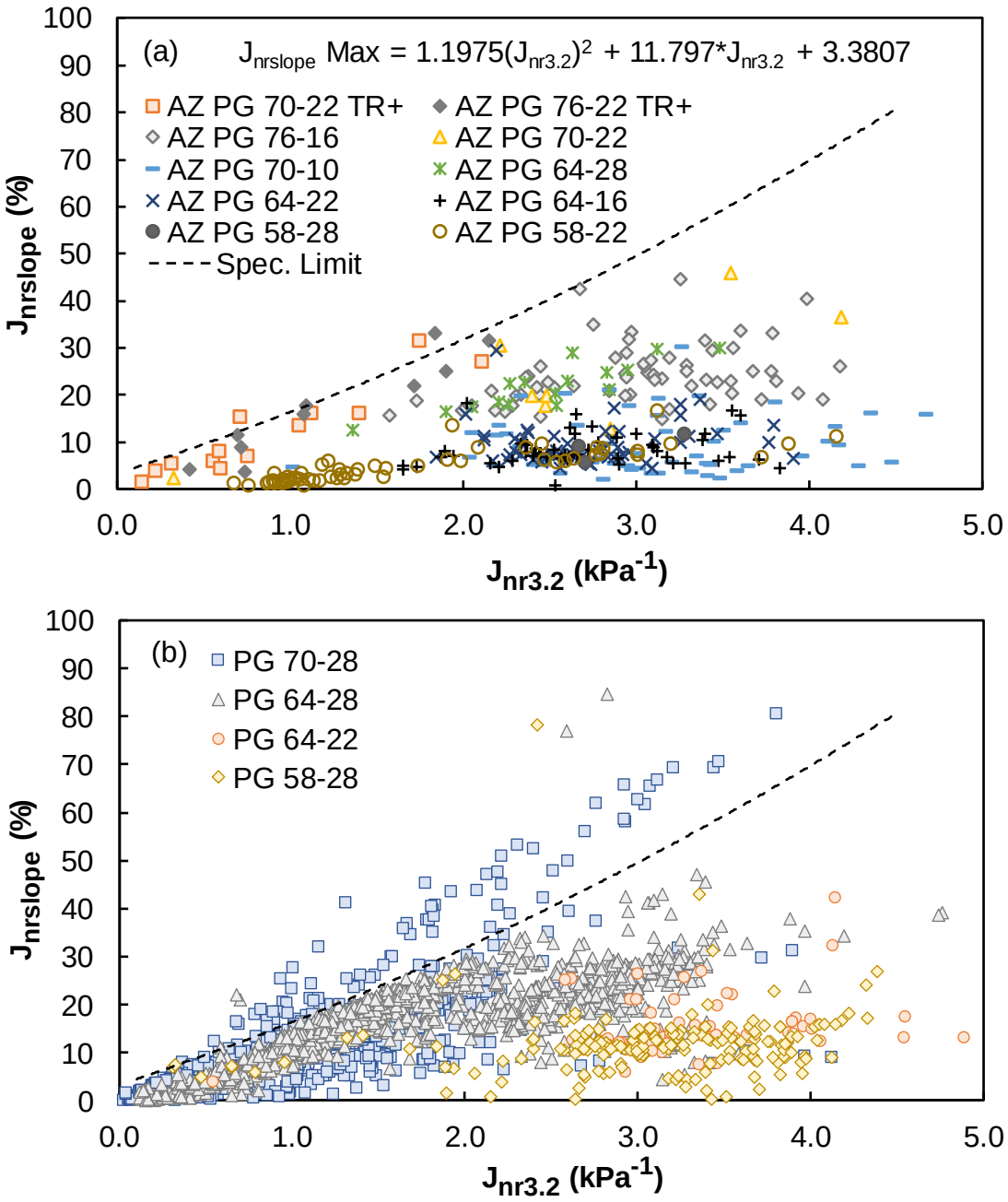

Figure 7-5: Potential specification limit for $J_{nrslope}$ with a) Arizona and b) Montana asphalt binder data.

Of all the ~340 asphalt binder specimens in the Arizona database, only four specimens fail the potential specification limit for $J_{nrslope}$. These four specimens are samples of premium asphalt binders (denoted TR+) with terminally digested crumb rubber plus SBS polymer

and anecdotally perform well in Arizona pavements. Figure 7-5 also compares the Montana data to the potential specification limit. Approximately 11% of Montana PG 70-28 asphalt binder specimens exceed the limit. Again, PG 70-28 is considered a high quality asphalt binder and anecdotally performs well in asphalt pavements on Montana highways. While the $J_{nrslope}$ based specification limit anecdotally corresponds to changes in field performance, further vetting of an actual $J_{nrslope}$ specification limit is necessary.

7.4 Phase 2: Validation of the Developed Relationships Using Study Asphalts and Laboratory Rutting Data

As mentioned earlier, the incremental rutting data calculated in the relationships shown in Figure 7-2, are based on the Jnr – rutting relationship from the Mississippi I-55 study. However, in phase 2 of this study the same relationships are explored but now the data from the MSCR test performed on the study binders and laboratory rutting data from the Hamburg wheel tracking test is used. Also, the obtained MSCR data for the study binders are included in the relationships presented in Figure 7-3, primarily to see if the study asphalts follow the developed trends and as a means to confirm that $J_{nrslope}$ is a better indicator of temperature surrogacy than J_{nrdiff}. Finally, the J_{nrdiff} and the $J_{nrslope}$ values from the study asphalts are included in Figure 7-4 and Figure 7-5 to visually observe the binders that pass the J_{nrdiff} and the $J_{nrslope}$ criteria's.

7.4.1 Incremental Rutting

In Figure 7-2 it was seen that the stress sensitivity, quantified using $J_{nrslope}$ in semi-logarithmic domain has a much better relationship to an incremental change in rutting than the J_{nrdiff} parameter. However, the rutting data used in that relationship is calculated using

the Mississippi I-55 relationship for a given $J_{nr3.2}$ and then increasing the rut depth by 50% and back calculating the resultant $J_{nr3.2}$. Subsequently, the J_{nrdiff} and $J_{nrslope}$ parameters were calculated based on the resultant $J_{nr3.2}$ and the old $J_{nr0.1}$. In phase 2 of the study, actual rutting data from laboratory rutting tests is used.

Of the 15 study asphalts mentioned in Chapter 3, 12 were selected for asphalt mixture performance testing. One of the tests performed on the mixtures was Hamburg wheel tracking test, to test the rutting potential of the Arizona asphalt mixtures. The test on each mixture was performed at least two temperatures, based on its PG "S" grade of the asphalt binder used. The test temperatures used are summarized in Table 15. These temperatures are related to the effective temperatures proposed as part of the NCHRP 9-22 study by El-Basyouny and Jeong (2009). It was found that locations in Arizona currently using PG 64S-XX, PG 70S-XX, and PG 76S-XX have an effective temperature of 50°C, 56°C and 62°C respectively. Thus for comparisons where mixture rutting is related to binder test data, rutting at 50°C, 56°C and 62°C is related to binder properties at 64°C, 70°C, and 76°C respectively. The incremental rut depth for each mixture was calculated by taking the difference of the rut depths at two temperatures. The rutting data for the mixtures and the incremental rut depths are presented in Table 16. The prefix "T", "G", and "S" to the binder notation in the mixture rutting results below indicates the source of the aggregate, which is Tucson, Globe and Snowflake respectively.

Table 15: HWT Test Temperatures by Asphalt Binder Grade

Asphalt Binder Grade	Test Temperatures (°C)
PG 76S-XX	62 and 56
PG 70S-XX	56 and 50
PG 64S-XX	50 and 44

Table 16: Rut Depths and Incremental Rut Depths of Study Asphalt Mixtures

Group	Mixture Notation	Rut Depth (mm)				$D_{rutting\ 44\text{-}50}$	$D_{rutting\ 50\text{-}56}$	$D_{rutting\ 56\text{-}62}$	$D_{rutting\ 50\text{-}62}$
		44°C	50°C	56°C	62°C				
1	TX1	–	3.77	13.39	19.71	–	9.63	6.32	15.95
	SY1	2.75	8.88	–	–	6.13	–	–	–
	GY3	–	3.45	3.71	–	–	0.26	–	–
	GY4	–	2.61	–	6.52	–	–	–	3.92
	SZ1	3.11	12.37	–	–	9.27	–	–	–
	GZ2	–	3.21	4.87	–	–	1.66	–	–
	TZ4	–	3.16	2.43	3.34	–	0.74	0.91	0.18
2	SX3	3.49	5.67	–	–	2.18	–	–	–
	GX4	–	4.60	6.93	–	–	2.33	–	–
	GX5	–	2.54	–	8.80	–	–	–	6.27
	TY5	–	3.27	3.92	11.90	–	0.65	7.98	8.63
	GY6	–	2.10	–	5.17	–	–	–	3.07

The parameters, $J_{nr3.2}$, J_{nrdiff}, and $J_{nrslope}$ for the study binders is presented in Table 17 and Table 18.

Table 17: $J_{nr3.2}$, J_{nrdiff}, and $J_{nrslope}$ for Study Binders at 58°C and 64°C

Group	Binder Notation	58°C			64°C		
		$J_{nr3.2}$	J_{nrdiff}	$J_{nrslope}$	$J_{nr3.2}$	J_{nrdiff}	$J_{nrslope}$
1	X1	–	–	–	1.59	5.09	2.48
	Y1	1.29	10.14	3.82	3.24	11.35	10.66
	Y3	–	–	–	1.36	34.72	11.32
	Y4	–	–	–	0.64	11.75	2.18
	Z1	0.90	7.83	2.11	2.40	10.54	7.37
	Z2	–	–	–	1.13	31.20	8.66
	Z4	–	–	–	0.38	20.67	2.06
2	X3	0.47	198.16	10.02	1.02	408.81	26.42
	X4	0.40	146.75	7.65	0.98	249.48	22.60
	X5	–	–	–	0.11	197.43	2.29
	Y5	–	–	–	0.06	54.01	0.71
	Y6	–	–	–	0.02	130.93	0.43

Table 18: $J_{nr3.2}$, J_{nrdiff}, and $J_{nrslope}$ for Study Binders at 70°C and 76°C

Group	Binder Notation	64°C			70°C		
		$J_{nr3.2}$	J_{nrdiff}	$J_{nrslope}$	$J_{nr3.2}$	J_{nrdiff}	$J_{nrslope}$
1	X1	4.03	5.87	7.08	8.60	5.77	15.11
	Y1	7.51	11.69	25.35	–	–	–
	Y3	3.53	39.57	32.27	7.97	40.84	74.50
	Y4	1.73	16.03	7.69	2.46	17.96	20.45
	Z1	5.85	11.77	19.85	–	–	–
	Z2	2.89	34.92	24.18	6.82	34.47	56.42
	Z4	1.03	30.98	7.84	2.54	36.35	21.87
2	X3	2.84	690.13	78.00	–	–	–
	X4	2.31	384.55	58.97	–	–	–
	X5	0.28	343.70	7.05	1.10	830.04	31.66
	Y5	0.12	45.19	1.18	0.39	122.38	6.84
	Y6	0.04	97.14	0.56	0.07	57.92	0.81

The study binder data provided in Table 16, Table 17, and Table 18 are now translated on to incremental rut depth vs J_{nrdiff}, and $J_{nrslope}$ presented in Figure 7-2. The combined data set is presented in Figure 7-6. In part (a) of the figure, it can be seen that seven of the 12 study mixtures for which incremental rut depth was calculated, align well with the simulated incremental rut depth data when plotted against $J_{nrslope}$. However, there are five other mixtures which lie away from the trend and are identified in the figure. The reason for the delineation is the high incremental rutting of the mixtures which is in turn due to the stripping in these mixtures. In part (b) of the figure, apart from the mixtures that have stripping, the remaining mixtures are seen to have the same scatter that was observed from the simulated incremental rut depths. Two notable data points in far right of the figure are that of polymer modified mixtures, which have J_{nrdiff} values in excess of 350%. Overall, the data from the study binders and mixtures follows the trend presented using the

simulated incremental rut depth data. And, it re-iterates $J_{nrslope}$'s capability of providing a much better characterization of the change in J_{nr} (between 0.1 to 3.2 kPa, semi-logarithmic domain) and associated incremental changes in rut depth.

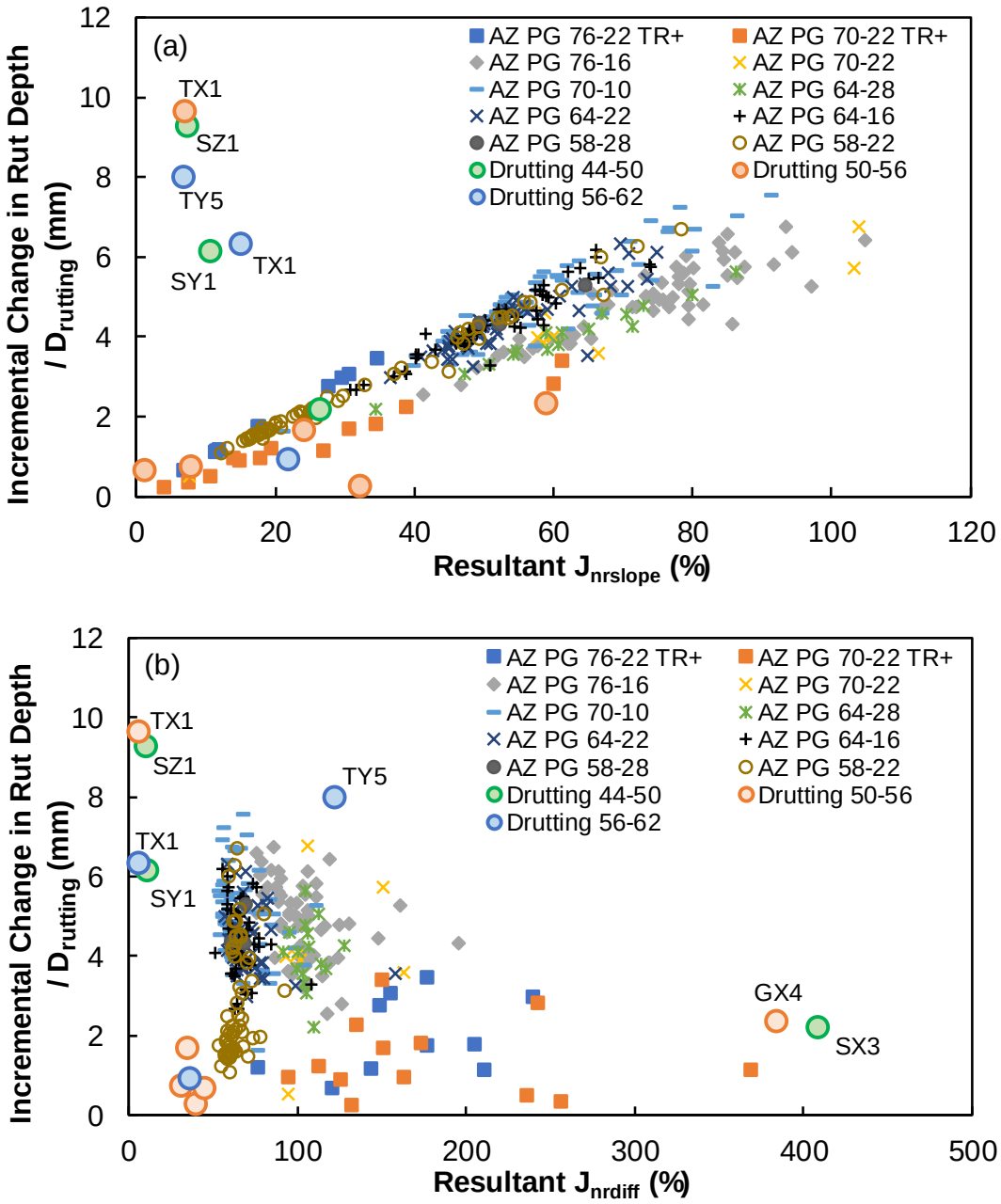

Figure 7-6: Relationship to an incremental increase in rutting for a) $J_{nrslope}$ and b) J_{nrdiff} Including Laboratory Calculated Rut Depths.

7.4.2 Temperature Surrogacy

In this section, the $J_{nrslope}$ and J_{nrdiff} parameters of the study binders are evaluated as a surrogate measure of the change in non-recoverable creep compliance across test temperatures. The examination performed is similar to that described in section 7.3.3.2 wherein $J_{nrslope}$ was compared to the change in $J_{nr3.2}$ as defined in Equation (52) and J_{nrdiff} was compared to the percent difference $J_{nr3.2}$ as defined in Equation (53). The resulting relationship is superimposed on the relationship predicted using other binder databases and as shown in section 7.3.3.2. This is shown in Figure 7-7. With regard to the first relationship presented in part (a) of the figure, most of the data from the study binders seems to align well with that from other binder databases. However, there do exist some exceptions and they are identified in the figure. The delineation from the established relationship basically means that there exists a greater difference between the $J_{nr3.2}$ at the lower temperature and the $J_{nr0.1}$ at 6°C higher for these binders than other binders which correlate linearly. While for the non-polymer modified asphalts X1, Y1, and Z1, $J_{nr0.1}$ at 6°C is much greater than $J_{nr3.2}$ at lower temperature, for X4, which is a polymer modified asphalt, the $J_{nr0.1}$ at 6°C is much lower than $J_{nr3.2}$ at lower temperature. For part (b) of the figure, the scatter in the J_{nrdiff} relationship for the study binders is similar to that observed using other binder databases, wherein the correlation is weaker in comparison to that observed in the $J_{nrslope}$ relationship. It should be noted that five data points in part (b) of the figure as not shown as their J_{nrdiff} values were in excess of 500% and presenting them would obscure all other data. Based on the relationships presented in Figure 7-7, it can be concluded that even for

the study binders, $J_{nrslope}$ is a better indicator of change in non-recoverable creep compliance as a function of temperature than J_{nrdiff}.

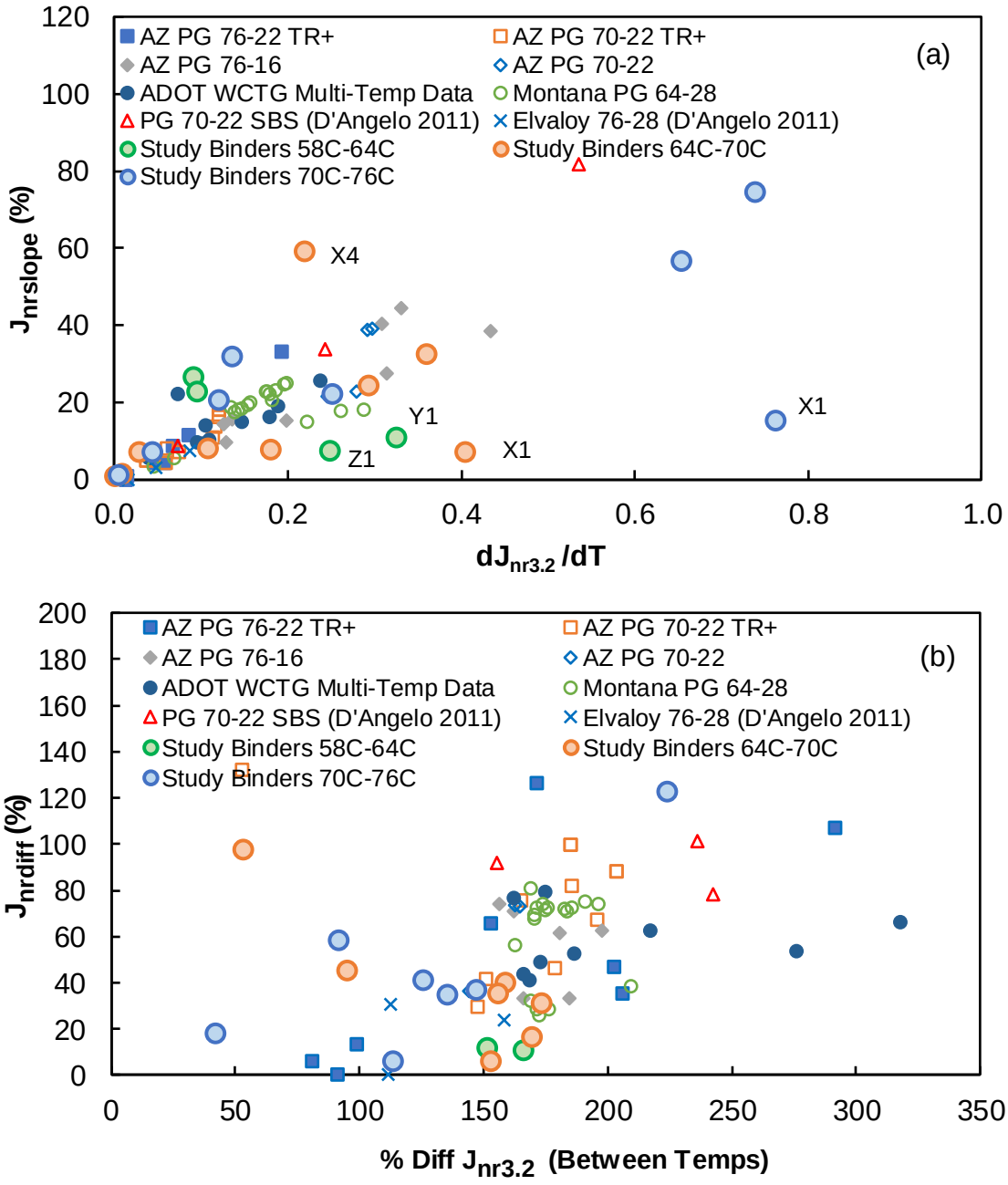

Figure 7-7: Plot of a) $J_{nrslope}$ and b) J_{nrdiff} from Study Binders and Other Binder Databases compared to change in $J_{nr3.2}$ between temperatures.

7.4.3 Checking Study Binders for Fulfillment of $J_{nrslope}$ Specification Criteria

While the methodology for arriving at the $J_{nrslope}$ specification criteria was explained in section 7.3.4, in this section it is intended to compare the study binders against the developed $J_{nrslope}$ specification criteria. Firstly, the fulfillment of J_{nrdiff} criteria is evaluated. It is to be noted that in this section the $J_{nrslope}$ and J_{nrdiff} are assessed only at the respective binder's PG high temperature. It can be seen from Figure 7-8(a) that all the non-polymer modified binders used in the study are within the J_{nrdiff} 75% specification limit. Whereas the four of the five polymer modified binders used in the study fail the specification criteria. As mentioned earlier, this is primarily because polymer modified binders have very low $J_{nr0.1}$ value and as a result J_{nrdiff} parameter is higher. However, the J_{nrdiff} parameter unfairly penalizes these asphalts, as these asphalts especially X5, PG 76-22 TR+, is known to be premium binder for Arizona DOT and has traditionally performed well in the field.

It can be seen from Figure 7-9, except three binders, all remaining binders fulfill the developed $J_{nrslope}$ specification criteria. All the three binders are polymer modified binders, including the PG 76-22TR+ binder, which is the only polymer modified asphalt currently part of the Arizona binder specifications. It should be noted here that Y6, which earlier failed the J_{nrdiff} specification, now passes under the $J_{nrslope}$ criteria. Also, the three polymer modified binders that fail the specification, are not far from the specification line, which is an improvement over where the binders were located in the J_{nrdiff} space, which might lead to false interpretation of stress sensitivity.

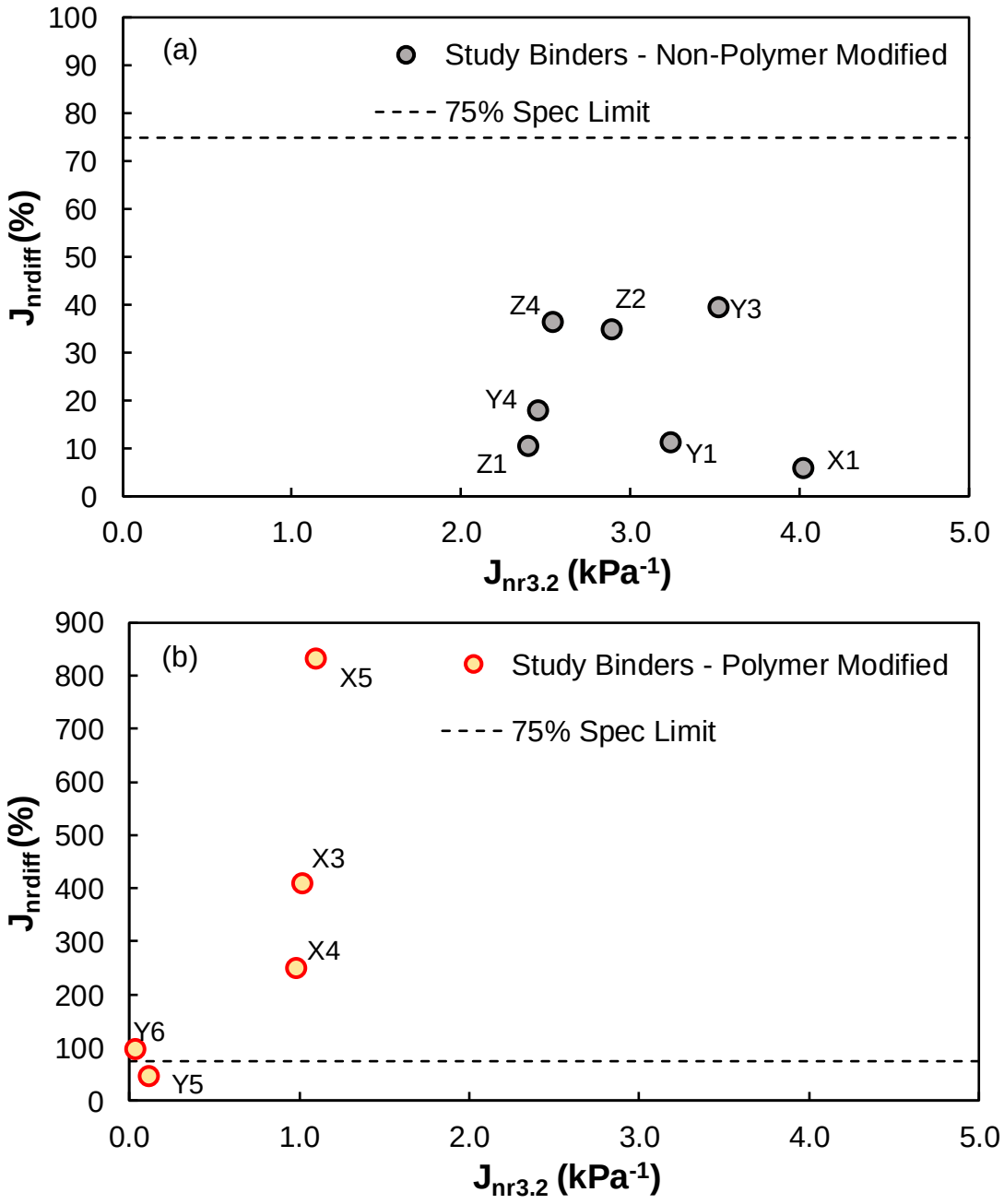

Figure 7-8: Comparison of J_{nrdiff} to $J_{nr3.2}$ and the 75% J_{nrdiff} Specification Limit for Study Asphalt Binders.

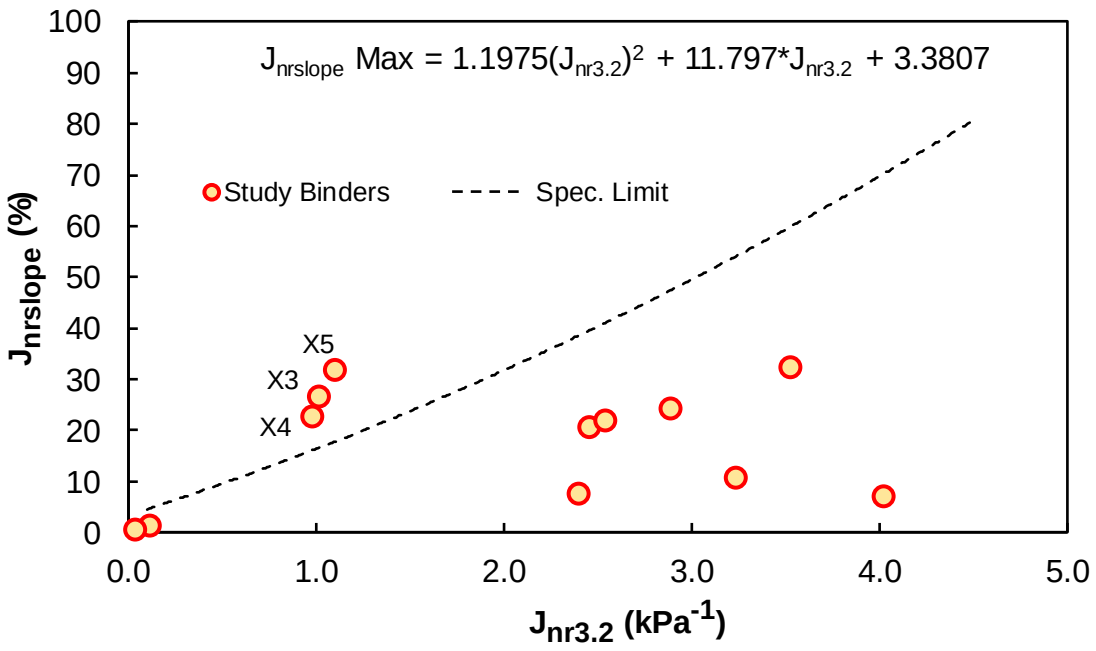

Figure 7-9: Comparison of $J_{nrslope}$ to $J_{nr3.2}$ and the Developed $J_{nrslope}$ Specification Limit for Study Asphalt Binders.

7.5 Recent Developments in MSCR Specifications

In order to overcome the issue of high J_{nrdiff} the reasons for which were explained earlier in this chapter, a modification to stress levels used in the MSCR test is being proposed. This modification deals with the first stress level after the conditioning cycles. As per AASHTO T 350, this stress level is currently 0.1 kPa. Suggestions are to increase this stress level to 0.8 kPa. The idea being that by doing so, really low values of J_{nr} can be avoided in the denominator. The other stress levels, i.e. conditioning at 0.1 kPa and second stress level at 3.2 kPa still remain the same. A small evaluation was carried out using two polymer modified study binder to check the effect on J_{nrdiff}. The two binders were selected such that one of the binder failed the J_{nrdiff} criteria by a marginal amount and the other binder failed the criteria by a large amount. These two binders were PG 70V-16(Y) and PG 76-22TR(X) respectively. The results from MSCR test using 0.8 kPa as first stress level are presented

in Table 19 and Table 20. Also presented in the tables are the values obtained using the current specification i.e. first stress level at 0.1 kPa.

Table 19: Comparison of Results from MSCR Tests with First Stress Level at 0.1 kPa and 0.8 kPa for PG 70V-16(Y) at 70°C.

Parameter	Value		Parameter	Value
$R_{0.1}$ (%)	98.26		$R_{0.8}$ (%)	96.28
$R_{3.2}$ (%)	96.25		$R_{3.2}$ (%)	96.50
R_{Diff} (%)	2.05		R_{Diff} (%)	-0.23
$J_{nr0.1}$ (kPa^{-1})	0.019		$J_{nr0.8}$ (kPa^{-1})	0.030
$J_{nr3.2}$ (kPa^{-1})	0.036		$J_{nr3.2}$ (kPa^{-1})	0.026
Jnr_{Diff} (%)	97.14		Jnr_{Diff} (%)	-13.79

Table 20: Comparison of Results from MSCR Tests with First Stress Level at 0.1 kPa and 0.8 kPa for PG 76-22TR(X) at 70°C.

Parameter	Value		Parameter	Value
$R_{0.1}$ (%)	95.65		$R_{0.8}$ (%)	88.40
$R_{3.2}$ (%)	80.49		$R_{3.2}$ (%)	84.15
R_{Diff} (%)	15.85		R_{Diff} (%)	4.81
$J_{nr0.1}$ (kPa^{-1})	0.064		$J_{nr0.8}$ (kPa^{-1})	0.134
$J_{nr3.2}$ (kPa^{-1})	0.283		$J_{nr3.2}$ (kPa^{-1})	0.179
Jnr_{Diff} (%)	343.70		Jnr_{Diff} (%)	33.11

It can be seen from the tables, J_{nrdiff} decreases drastically in both binders and in case of PG 70V-16 goes to negative when 0.8 kPa is used. However, more critical observations are in the value of $J_{nr3.2}$. It can be seen from both the binders that they become less compliant when at 3.2 kPa when 0.8 kPa is used as the first stress level. The main conclusion that can be drawn from these results is that order of testing does induce different mechanisms which are leading to different values of the same test parameters.

7.6 Conclusions from J_{nrdiff} Study

In this chapter, the non-linear viscoelastic data pertaining to the multiple stress creep and recovery test is gathered for analysis. The main focus of the analysis is the in-depth scrutiny of the current parameter in the AASHTO M 332 specification, J_{nrdiff}, which represents stress sensitivity. Based on the binder datasets analyzed and presented in this chapter, following conclusions can be made:

- J_{nrdiff} is an inaccurate representation of change in J_{nr} of asphalt binders between 0.1 and 3.2 kPa and unfairly penalizes asphalt binders with low $J_{nr3.2}$ especially polymer modified asphalts.
- An alternate parameter was proposed ($J_{nrslope}$) that is a more appropriate representation of stress sensitivity and does not penalize asphalt binders with low $J_{nr3.2}$ values. $J_{nrslope}$ was able to accurately rank four modified asphalt binders based on visual observation of J_{nr} – stress trends whereas J_{nrdiff} provided incorrect rankings.
- $J_{nrslope}$ showed a much better relationship to an incremental change in rut depth using the Mississippi I-55 performance relationship and also using the laboratory rut depth and MSCR data obtained for the study materials. This further supports $J_{nrslope}$ as a more appropriate measure of stress sensitivity in the semi-logarithmic domain and a likely indicator of changes in performance due to higher loading stresses or temperatures in asphalt pavements.

- $J_{nrslope}$ also demonstrates the ability to capture changes in $J_{nr3.2}$ with respect to increases in test temperature and has the potential to serve as an indicator of temperature sensitivity in AASHTO T 350.
- A conceptual, performance-based specification limit for $J_{nrslope}$ was presented and evaluated using a dataset containing AASHTO T 350 test results from the study binders, Arizona MSCR database, AZ WCTG, and Montana asphalt binders.
- Since all study binders were sourced from Arizona and the analysis database also included many AZ binders, it can be argued that if a future binder specification for the state is developed along the lines of AASHTO M 332, $J_{nrslope}$ should be considered in lieu of J_{nrdiff}.

Chapter 8 Summary and Future Work

8.1 Summary and Conclusions

Asphalt binder is a complex hydrocarbon whose performance is an interplay between its mechanical and chemical properties. Thereby, historically, both the chemical properties and the viscoelastic properties of asphalt binders were studied in parallel to have a complete understanding of the behavior of asphalt binder. This led to the development of physico-chemical relationships, that relate the viscoelastic properties of asphalt binders to its chemical structure. However, the stresses and strains experienced by the pavement, far exceed the LVE region and are in the NLVE region. Thereby, the objectives of this study were two-fold. The first objective of this study was to gain insight into the molecular structure of asphalt by studying their molecular weight distributions, obtained from the mass spectroscopy technique of Laser Desorption Mass Spectroscopy (LDMS) and then relate these molecular structure attributes to asphalt's linear viscoelastic (LVE) properties. Another parallel objective of the study was to have a clear understanding of the NLVE behavior of asphalt using various characterization techniques and analysis methodologies at different temperature conditions. Summary and conclusions drawn from this research effort are summarized below.

8.1.1 Relating Linear Viscoelastic Properties and Molecular Structure

- All the polymer modified and non-polymer modified binders were first conditioned in pressurized aging vessel at 110°C so that both unaged and aged properties can be evaluated.

- These binders were then used to perform temperature-frequency sweep experiments at multiple temperatures and frequencies.
- The data from these tests were fit to a Christensen-Anderson-Marasteanu (CAM) model to develop the mastercurves for each asphalt binder.
- LVE parameters such as $|G^*_c|$, $|G^*_g|$, and R value were calculated for these binders using optimization.
- Using the storage modulus data from the temperature-frequency tests, discrete relaxation spectra was modeled and developed using the Maxwell model.
- To overcome the inaccuracies in prediction of relaxation spectra using loss modulus, and to characterize a singular relaxation spectrum for both storage and loss modulus, a continuous relaxation spectrum was developed.
- The unique characteristic of the continuous relaxation spectrum is that it can characterize the spectrum with few number of coefficients and in a way, that allows to minimize the errors with respect to both loss and storage modulus.
- For the chemical characterization, Laser Desorption Mass Spectroscopy (LDMS) tests were performed on asphalt binders to calculate the MWD and subsequently calculate the number average molecular weights (M_n).
- For non-polymer modified asphalts, these M_n values were then related to the R value from the LVE experiments, which indicates the width of the relaxation spectrum. It was observed that there exists a very good linear fit among the two parameters. This indicates that, as the number average molecular weight of the binders increase, they require more time to relax the developed stresses.

8.1.2 Non-Linear Viscoelastic Studies

- The non-linear viscoelastic behavior of asphalt binder was characterized using three different tests, namely, the time sweep test, the repeated stress/strain sweep (RSS) test and the Multiple Stress Creep and Recovery (MSCR) test. The main distinguishing feature among the tests is the temperature and the strain level at which the tests were carried out.
- The time sweep fatigue tests were conducted at intermediate temperature at strain levels ranging from 5% to 15%. The purpose of the test was to demonstrate the use of time sweep fatigue tests at intermediate temperature for NLVE characterization. The results from the tests were used to characterize the continuum damage model and develop the damage characteristic curves.
- It was found from the tests that fatigue resistance of majority of the binders increased with aging. Which follows the theory proposed by the researchers that aging reduces the modulus mismatch among the phases in the asphalt microstructure and thereby delays the occurrence of cracking thus leading to a longer fatigue life.
- In the second NLVE study, Large Amplitude Oscillatory Shear (LAOS) tests were carried out at high temperatures using time sweep fatigue tests and RSS tests. The tests were conducted to observe and estimate non-linearity using a analytical tool called MITlaos. The tool uses on Fourier transform analysis and is used to deconvolve stress-strain history into their harmonic constituents and identify nonlinearity.

- Non-linearity, if present was characterized by the presence of higher order harmonics in the Fourier transform spectra.
- Detailed description of how the data analysis needs to be performed using MITlaos has been provided.
- Distortion in the stress-strain relationship which was absent at intermediate temperatures was seen at higher temperatures. The distortion was also coupled with observation of higher order harmonics in the Fourier transform spectra.
- In order to quantify the observed non-linearity, a parameter "*Q*" was used, which is a function of the intensity of the third harmonic and the strain level.
- Based on the results obtained for the values of *Q*, it was seen that the *Q* value was more or less constant in the Medium Amplitude Oscillatory Shear (MAOS) region and started declining in the LAOS region. The relationship was best described using a linear fit in the logarithmic domain.
- The third NLVE study performed involved utilizing the MSCR test for NLVE characterization.
- The focus of the study was surrounded around the scrutiny of the J_{nrdiff} parameter of the MSCR test, which was included in the AASHTO M332 specification to control stress sensitivity of asphalt binders.
- J_{nrdiff} is an inaccurate representation of change in J_{nr} of asphalt binders between 0.1 and 3.2 kPa and unfairly penalizes asphalt binders with low $J_{nr3.2}$ especially polymer modified asphalts.

- An alternate parameter was proposed ($J_{nrslope}$) that is a more appropriate representation of stress sensitivity and does not penalize asphalt binders with low $J_{nr3.2}$ values. $J_{nrslope}$ was able to accurately rank four modified asphalt binders based on visual observation of J_{nr} – stress trends whereas J_{nrdiff} provided incorrect rankings.
- $J_{nrslope}$ showed a much better relationship to an incremental change in rut depth using the Mississippi I-55 performance relationship and also using the laboratory rut depth and MSCR data obtained for the study materials. This further supports $J_{nrslope}$ as a more appropriate measure of stress sensitivity in the semi-logarithmic domain and a likely indicator of changes in performance due to higher loading stresses or temperatures in asphalt pavements.
- $J_{nrslope}$ also demonstrates the ability to capture changes in $J_{nr3.2}$ with respect to increases in test temperature and has the potential to serve as an indicator of temperature sensitivity in AASHTO T 350.

In summary, this research effort contributes to the existing literature in physico-chemical relationships in asphalt binder by developing relationships between viscoelastic property of asphalt, R, and the number average molecular weight, M_n. Further, the study also, investigated non-linear viscoelasticity behavior at different conditions and utilized analytical tools such as MITlaos to quantify non-linearity. The parameters developed from these NLVE tests can be utilized in future to develop physico-chemical relationships in the NLVE domain.

8.1.3 Practical Significance of the Study

The practical significance of the study is as follows:

- The relationship between M_n and R can be utilized to engineer the asphalt binders to achieve desirable LVE characteristics.
- The data generated from LDMS test can be used as a consistency measure.
- The LDMS test can also be used to assess blend properties of two or more asphalt binders.

8.2 Future Work

The findings from this research effort recommend the continuation of the work in the following areas.

- One of the limitations of the current study involves constraining the molecular weight distribution between 200-1500 daltons. The polymer modified asphalts contain polymers such as SBS, whose molecular weight is excess of 100,000 daltons. The mass spectroscopic measurements at these high molecular weights have not been conducted in the current study. Including the contribution of polymer in the MWD of polymer modified asphalts will increase their molecular weight. Subsequently, using these molecular weights, the R vs M_n relationship needs to re-analyzed. Development of physico-chemical relationships in the Non-linear viscoelastic domain.
- Another potential use for LDMS, is in its use in identification of specific compounds. Compounds such as Polyphosphoric acid (PPA) are used as stiffening agents in asphalt. If not used in specified quantities, PPA can have detrimental

effect as it will embrittle the pavement, thereby leading to failure. The use of LDMS for this purpose, can be explored by doping neat binder with high levels of PPA as well as those typically used and subsequently testing it using LDMS for detection of PPA.

- In the current study, the physico-chemical relationships were developed only in the linear viscoelastic domain. However, this research demonstrated the characterization of NLVE properties as well of quantification of non-linearity using the parameter "*Q*". The parameter which when plotted against strain showed a distinct relationship from which, the value Q_0 can be calculated. Polymer researchers have developed a relationship between Q_0 and the relaxation process of polymer chains. This add promise to the fact that the relationship can be explored for applicability to asphalt also.
- For MSCR based stress sensitivity work presented in this study, a conceptual, performance-based specification limit for $J_{nrslope}$ was presented and evaluated using a dataset containing AASHTO T 350 test results from the study binders, Arizona MSCR database, AZ WCTG, and Montana asphalt binders. Since all study binders were sourced from Arizona and the analysis database also included many AZ binders, a future binder specification for the state can be developed along the lines of AASHTO M 332, wherein $J_{nrslope}$ is considered in lieu of J_{nrdiff}.

REFERENCES

1. M. Freemantle. “What’s That Stuff-Asphalt?” Chemical and Engineering News, *American Chemical Society*, Volume 77, No. 47, 1999.

2. J. C. Petersen. "Chemical Composition of Asphalt as Related to Asphalt Durability: State of the Art." *Transportation Research Record* 999: 13.

3. Corbett, Luke W. "Refinery processing of asphalt cement." *Transportation Research Record* 999 (1984): 1-6.

4. Boussingault, J. B. "Extrait d'un mémoire sur la composition des bitumes." *CR Acad Sci* 3 (1836): 375-8.

5. Richardson, Clifford. *The modern asphalt pavement*. J. Wiley & sons, 1905.

6. Lesueur, D. The Colloidal Structure of Bitumen: Consequences on the Rheology and on the Mechanisms of Bitumen Modification. *Advances in Colloid and Interface Science*, Vol. 145, pp. 42–82, 2009.

7. Rostler FS. Fractional composition: Analytical and functional significance. In: Hoiberg AJ, editor. *Bituminous Materials: Asphalts, Tars and Pitches*. New York: Interscience Publishers; 1965. pp. 151–222. Vol. 2, Part 1.

8. Corbett, Luke W. "Composition of asphalt based on generic fractionation, using solvent deasphaltening, elution-adsorption chromatography, and densimetric characterization." *Analytical Chemistry* 41, no. 4 (1969): 576-579.

9. Nellensteyn, F. J. "The constitution of asphalt." *J. Inst. Pet* 10 (1924): 311-325.

10. Pfeiffer, J. Ph, and R. N. J. Saal. "Asphaltic bitumen as colloid system." *The Journal of Physical Chemistry* 44, no. 2 (1940): 139-149.

11. Saal, R. N. J., and J. W. A. Labout. "Rheological Properties of Asphaltic Bitumen." *The Journal of Physical Chemistry* 44, no. 2 (1940): 149-165.

12. Read, J. and Whiteoak D., 2003. *The Shell Bitumen Handbook*. 5th Ed. London: Thomas Telford Publishing;

13. Sandler Mass Spectrometry User’s Group. “Introduction to MALDI-TOF MS.” University of California, San Francisco, 2003.

14. Petersen, J. C., R. E. Robertson, J. F. Branthaver, P. M. Harnsberger, J. J. Duvall, S. S. Kim, D. A. Anderson, D. W. Christiansen, and H. U. Bahia. "Binder

characterization and evaluation: Volume 1." *Rep. No. SHRP-A-367, Strategic Highway Research Program, National Research Council, Washington, DC* (1994).

15. Lesueur, Didier, Jean-François Gerard, Pierre Claudy, Jean-Marie Letoffe, Jean-Pascal Planche, and Didier Martin. "A structure-related model to describe asphalt linear viscoelasticity." *Journal of Rheology* 40, no. 5 (1996): 813-836.

16. Loeber, L., O. Sutton, J. V. J. M. Morel, J-M. Valleton, and G. Muller. "New direct observations of asphalts and asphalt binders by scanning electron microscopy and atomic force microscopy." *Journal of microscopy* 182, no. 1 (1996): 32-39.

17. Clerc, R. J., and M. J. O'Neal. "The mass spectrometric analysis of asphalt. A preliminary investigation." *Analytical Chemistry* 33, no. 3 (1961): 380-382.

18. Karas, Michael, Doris Bachmann, and Franz Hillenkamp. "Influence of the wavelength in high-irradiance ultraviolet laser desorption mass spectrometry of organic molecules." *Analytical chemistry* 57, no. 14 (1985): 2935-2939.

19. Lázaro, Maria-Jesus, Alan A. Herod, Mike Cocksedge, Mark Domin, and Rafael Kandiyoti. "Molecular mass determinations in coal-derived liquids by MALDI mass spectrometry and size-exclusion chromatography." *Fuel* 76, no. 13 (1997): 1225-1233.

20. Fonnesbeck, Jacqueline Eileen. "Structural elucidation of asphalt using NMR spectroscopy and GPC fractionation with laser desorption mass spectrometry." PhD diss., Montana State University-Bozeman, College of Letters & Science, 1997.

21. Domin, M., Alan Herod, Rafael Kandiyoti, John W. Larsen, M. J. Lazaro, Shang Li, and Parviz Rahimi. "A comparative study of bitumen molecular-weight distributions." *Energy & Fuels* 13, no. 3 (1999): 552-557.

22. Jongepier, R., and Kuilman, B. 1969. "Characteristics of the Rheology of Bitumens," *Proceedings of the Association of Asphalt Paving Technologists*, vol. 38, pp. 98-122.

23. Dickinson, E.J., and Witt, H.P. 1974. "The Dynamic Shear Modulus of Paving Asphalts as a Function of Frequency," *Transactions of the Society of Rheology*, vol. 18, no. 4, pp. 591-606.

24. Christensen, D. W., and D. A. Anderson. 1992. "Interpretation of dynamic mechanical test data for paving grade asphalt cements (with discussion)." *Journal of the Association of Asphalt Paving Technologists* 61.

25. Stastna, J., L. Zanzotto, and J. Berti. "How Good Are Some Rheological Models of Dynamic Material Functions of Asphalt? (With Discussion)." *Journal of the Association of Asphalt Paving Technologists* 66 (1997).

26. Trouton, Fred T. "On the coefficient of viscous traction and its relation to that of viscosity." *Proceedings of the Royal Society of London. Series A 77,* no. 519 (1906): 426-440.

27. Saal, R. N. J., and G. Koens. "Investigation into the plastic properties of asphaltic bitumen." J. *Inst. Pet* 19 (1933): 176-212.

28. Komatsu, Hideo, Takeo Mitsui, and Shigeharu Onogi. "Nonlinear viscoelastic properties of semisolid emulsions." *Transactions of the Society of Rheology* 17, no. 2 (1973): 351-364.

29. Dodge, James S., and Irvin M. Krieger. "Oscillatory shear of nonlinear fluids I. Preliminary investigation." *Transactions of the Society of Rheology* 15, no. 4 (1971): 589-601.

30. Tee, T-T., and J. M. Dealy. "Nonlinear viscoelasticity of polymer melts." *Transactions of the Society of Rheology* 19, no. 4 (1975): 595-615.

31. Underwood, B. Shane, and Y. Richard Kim. "Nonlinear viscoelastic analysis of asphalt cement and asphalt mastics." *International Journal of Pavement Engineering* 16, no. 6 (2015): 510-529.

32. Kyu, H., M. Wilhelm, C.O. Klein, K.S. Cho, J.G. Nam, K.H. Ahn, S.J. Lee, R.H. Ewoldt, and G.H. McKinley. “A review of nonlinear oscillatory shear tests: Analysis and application of large amplitude oscillatory shear (LAOS).” *Progress in Polymer Science*, 36 (12), pp. 1697-1753. 2011.

33. Masad, E., C.W. Huang, G. Airey, A. Muliana. “Nonlinear viscoelastic analysis of unaged and aged asphalt binders.” *Construction and Building Materials*, 22(11), pp. 2170-2179. 2008.

34. Motamed, A., A. Bhasin, and K.M. Liechti. “Interaction nonlinearity in asphalt binders.” *Mechanics of Time-Dependent Materials*, 16(2), pp. 145-167. 2012

35. Schapery, R.A. “Nonlinear viscoelastic and viscoplastic constitutive equations with growing damage.” *International Journal of Fracture*, 97(1), pp. 33-66. 1999.

36. AASHTO. 2014. Standard Method of Test for Multiple Stress Creep Recovery (MSCR) Test of Asphalt Binder Using a Dynamic Shear Rheometer (DSR).

AASHTO T 350. Washington D.C.: American Association of State Highway Transportation Officials: 2014.

37. D'Angelo, J., R. Kluttz, R. Dongre, K. Stephens, and L. Zanzotto. 2007. "Revision of the Superpave High Temperature Binder Specification: The Multiple Stress Creep Recovery Test." *Journal of Association of Asphalt Paving Technologists* 76: 123-162.

38. C. Hintz and H. Bahia. "Simplification of linear amplitude sweep test and specification parameter." *Transportation Research Record: Journal of the Transportation Research Board* 2370 (2013): 10-16.

39. Kim, Y. Richard, Cassie Castorena, Michael Elwardany, Farhad Yousefi Rad, Shane Underwood, Akshay Gundla, Padmini Gudipudi, Mike J. Farrar, and Ronald R. Glaser. "Long-term aging of asphalt mixtures for performance testing and prediction." *National Cooperative Highway Research Program, Research Report 871*, 2018.

40. Gundla, A., Gudipudi, P., & Underwood, B. S. (2017). Evaluation of the sensitivity of asphalt concrete modulus to binder oxidation with a multiple length scale study. *Construction and Building Materials*, 152, 954-963.

41. Christensen DW, Anderson DA. Chemical-Physical Property Relationships for Asphalt Cements and the Dispersed Polar Fluid Model. InProc., *204th American Chemical Society National Meeting* 1992 Aug 23 (pp. 3-4).

42. Jemison, H. B., B. L. Burr, R. R. Davison, J. A. Bullin, and C. J. Glover. 1992. "Application and use of the ATR, FT-IR method to asphalt aging studies." *Fuel Science &Technology International* 10(4-6): 795-808.

43. Petersen, J. Claine, and Ronald Glaser. 2011. "Asphalt oxidation mechanisms and the role of oxidation products on age hardening revisited." *Road Materials and Pavement Design* 12(4): 795-819.

44. Cooper, A.R. 1989. "Determination of molecular weight." Wiley-Interscience, 605 Third Avenue, New York, New York 10158-0012, USA.

45. Malkin, A. Ya. "Continuous relaxation spectrum-its advantages and methods of calculation." *Applied Mechanics and Engineering* 11, no. 2 (2006): 235.

46. Kontogiorgos, Vassilis. *Calculation of relaxation spectra from stress relaxation measurements*. InTech, 2010.

47. Ferry, J.D. 1980. *Viscoelastic Properties of Polymers*. 3rd edition, Wiley, New York.

48. Schapery, R. A., and S. W. Park. 1999. "Methods of interconversion between linear viscoelastic material functions. Part II—an approximate analytical method." *International Journal of Solids and Structures* 36, no. 11, 1677-1699.

49. Liu, Hanqi, Rong Luo, and Huijie Lv. "Establishing continuous relaxation spectrum based on complex modulus tests to construct relaxation modulus master curves in compliance with linear viscoelastic theory." Construction and Building Materials 165 (2018): 372-384.

50. Jemison, H. B., B. L. Burr, R. R. Davison, J. A. Bullin, and C. J. Glover. "Application and use of the ATR, FT-IR method to asphalt aging studies." Fuel science & technology international 10, no. 4-6 (1992): 795-808.

51. Nadgorny, M., Gentekos, D. T., Xiao, Z., Singleton, S. P., Fors, B. P., & Connal, L. A. (2017). Manipulation of Molecular Weight Distribution Shape as a New Strategy to Control Processing Parameters. Macromolecular rapid communications, 38(19), 1700352.

52. Petersen, J. Claine, and Ronald Glaser. "Asphalt oxidation mechanisms and the role of oxidation products on age hardening revisited." Road Materials and Pavement Design 12, no. 4 (2011): 795-819.

53. Jahangir, R., D.N. Little, and A. Bhasin (2015). A Study of the Evolution of Microstructure due to Aging and Tensile Loading, Paper Submitted for Presentation at 95th Annual Meeting of the Transportation Research Board, Washington, D.C.

54. Underwood, B.S. *Multiscale Constitutive Modeling of Asphalt Concrete*. Ph.D. Dissertation, North Carolina State University, Raleigh, NC, 2011.

55. Kose, S, M. Guler, H.U. Bahia, and E. Masad (2000). ―Distribution of Strains within Hot-Mix Asphalt Binders,‖ *Transportation Research Record*, 1728, National Research Council, Washington, D.C., 21-27.

56. MITlaos, Version 2.1 Beta for MATLAB, Ewoldt, R.H., P. Winter, and G.H. McKinley, Hatsopoulos Microfluids Laboratory, Department of Mechanical Engineering, Massachusetts Institute of Technology.

57. Hyun, Kyu, and Manfred Wilhelm. "Establishing a new mechanical nonlinear coefficient Q from FT-rheology: First investigation of entangled linear and comb polymer model systems." *Macromolecules* 42, no. 1 (2008): 411-422.

58. Farrar, M.J., J.P. Planche, A.O. Cookman, and S. Salmans. Ablaos: Asphalt Binder Large Amplitude Oscillatory Shear, presented at Petersens Asphalt Research Conference, Laramie, Wyoming, 2014.

59. Gundla, A. and B.S. Underwood (2016). "Using Repeated Stress Sweep to Investigate Non-linearity in Asphalt Binders and Mastics by Fourier Transform Analysis," Proceedings *International Society for Asphalt Pavements Symposium and 53rd Petersen Asphalt Research Conference*, Jackson, Wyoming.

60. Diab, Aboelkasim, and Zhanping You. "Small and large strain rheological characterizations of polymer-and crumb rubber-modified asphalt binders." *Construction and Building Materials* 144 (2017): 168-177.

61. Bahia, Hussain U., D. I. Hanson, M. Zeng, H. Zhai, M. A. Khatri, and R. M. Anderson. *Characterization of modified asphalt binders in superpave mix design*. No. Project 9-10 FY'96. 2001.

62. D'Angelo, J., and R. Dongre. (2002). Superpave Binder Specifications and their Performance Relationship to Modified Binders. *Proceedings, Canadian Technical Asphalt Association*, 2002.

63. D'Angelo, J., R. Kluttz, R. Dongre, K. Stephens, and L. Zanzotto. (2007). "Revision of the Superpave high temperature binder specification: The multiple stress creep recovery test." *J. Assoc. Asphalt Paving Technol*., 76, 123-162.

64. D'Angelo, J. (2009). "Development of a Performance Based Binder Specification for Rutting Using Creep and Recovery Testing*." Ph.D. Dissertation*, University of Calgary, Alberta, Canada.

65. D'Angelo, J. (2010). "New high- temperature binder specification using multistress creep and recovery." *Transportation Research Circular E-C147: Development in Asphalt Binder Specifications.* Transportation Research Board, Washington, D.C., 1-13.

66. Anderson, R.M. (2011). "Understanding the MSCR test and its use in the PG asphalt binder specification." *Asphalt Institute Webinar*.

67. Dongre, R. (2016). "Variability in J_{nr} difference value obtained in AASHTO M332 MSCR test – cause and implications." Presented at *53rd Petersen Asphalt Research Conference*, Jackson, Wyoming.

68. Stempihar, Jeffrey, Akshay Gundla, and B. Shane Underwood. "Interpreting Stress Sensitivity in the Multiple Stress Creep and Recovery Test." *Journal of Materials in Civil Engineering* 30, no. 2 (2017): 04017283.

69. Minnesota Department of Transportation. (2015). “Asphalt binder multiple stress creep recovery overview.” Minnesota Department of Transportation.

APPENDIX A

PILOT STUDY TO DETERMINE THE SAMPLE PREPARATION METHODOLOGY FOR LDMS TEST

Sample Preparation:

For preparing the samples for LDMS testing, different trials were performed to identify the most suitable method to prepare the samples. These trials included testing at different dilution ratios and using different matrices to evaluate the method that provided the best spectra among all. The attributes that were evaluated among different methods were the general shape of the spectra, the signal quality and noise. Most of the trials were performed using only one asphalt binder, which is B2 binder, PG 64-22. In some cases, binder B1, PG 58-28, was also used. The different matrices evaluated and the dilution ratios evaluated are presented in Table A- 1 and Table A- 2.

Table A- 1: Matrices Used for Preliminary Evaluation.

Matrix	**Preparation Method**
Dihydroxybenzoic Acid (DHB)	10 mg/ml of 90:10 ethanol - water mix
Sinapic Acid - 1 (SA-1)	15 mg/ml of Toluene
Silver Fluoroacetate (AGF)	14.7 mg/ml of Acetone
Sinapic Acid - 2 (SA-2)	15 mg/ml of Acetone
Anthracenecarbonitrile (ACN)	13.6 mg/ml of Toluene
α-Cyano-4-hydroxycinnamic Acid (CHCA)	Diluted in 50% Acetonitrile + 1% Trifluoroacetic Acid

Table A- 2: Dilution Ratios and the Binders Used for Preliminary Evaluation.

Binder	**Dilution Ratio**	**Diluting Solvent**
PG 58-28	6 mg/ml	Toluene
	125 mg/ml	
PG 64-22	1.25 mg/ml	
	6 mg/ml	
	125 mg/ml	

As an example, the preparation of a sample for LDMS using 125 mg/ml dilution ratio is explained here. Samples for other dilution ratios were prepared in a similar manner. First,

0.625 g of asphalt was weighed out in a small beaker. To this, 5 ml of toluene was added. The beaker containing the solute and the solvent was manually agitated to speed up the dilution. The samples were agitated for about 10 minutes or until complete dissolution was seen. Note, that polymer modified asphalts took slightly longer time to dissolve. Once the solution was prepared it was transferred in a small glass vial. Care was taken so that the solution doesn't come into contact with plastic cap on top of the glass vials. Subsequently, from the vial, using a micro pipette, 0.5µl of this solution was placed on the LDMS sample target.

The above described procedure is for when a matrix is not used. If matrix is used, then asphalt solution is mixed in 1:1 ratio by volume with the matrix solution and 0.5 µl of this solution was placed on the LDMS sample target. While the above conditions are for the preliminary conditions, detailed description of the experiment methodology and analysis technique employed for the main study binders is provided in the following paragraphs. The results from the preliminary tests are shown in Figure A- 1 through Figure A- 5.

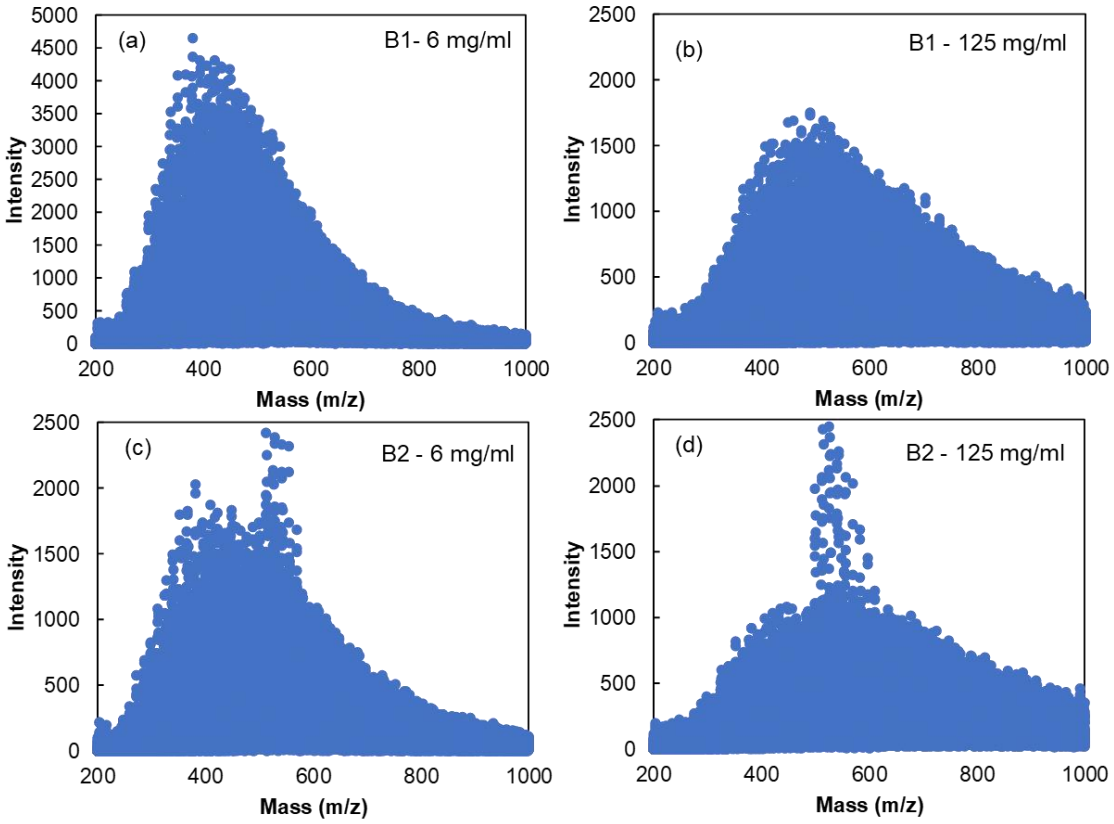

Figure A- 1: Molecular Weight Distribution of B1 and B2 Asphalts at 6 mg/ml and 125 mg/ml Dilution Levels.

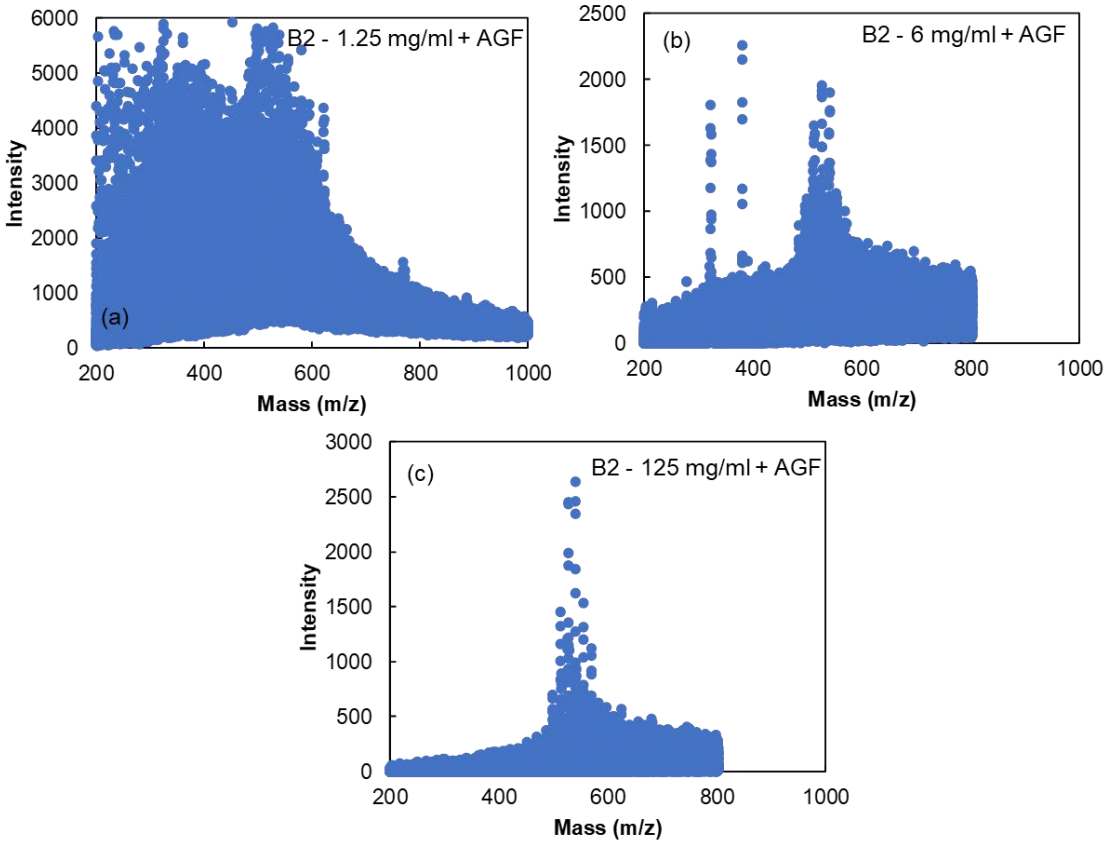

Figure A- 2: Molecular Weight Distribution of B2 Asphalt at 6 mg/ml and 125 mg/ml Dilution Levels Using Silver Fluoroacetate (AGF) Matrix.

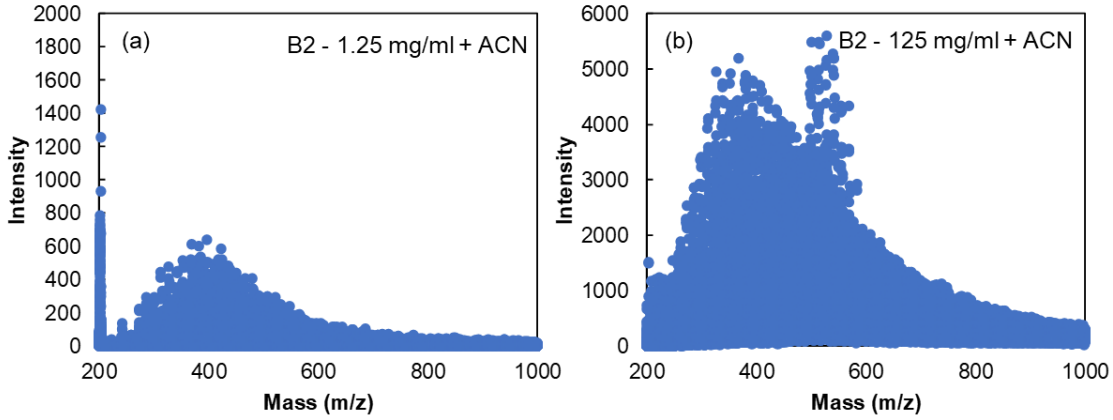

Figure A- 3: Molecular Weight Distribution of B2 Asphalt at 1.25 mg/ml and 125 mg/ml Dilution Levels Using Anthracenecarbonitrile (ACN) Matrix.

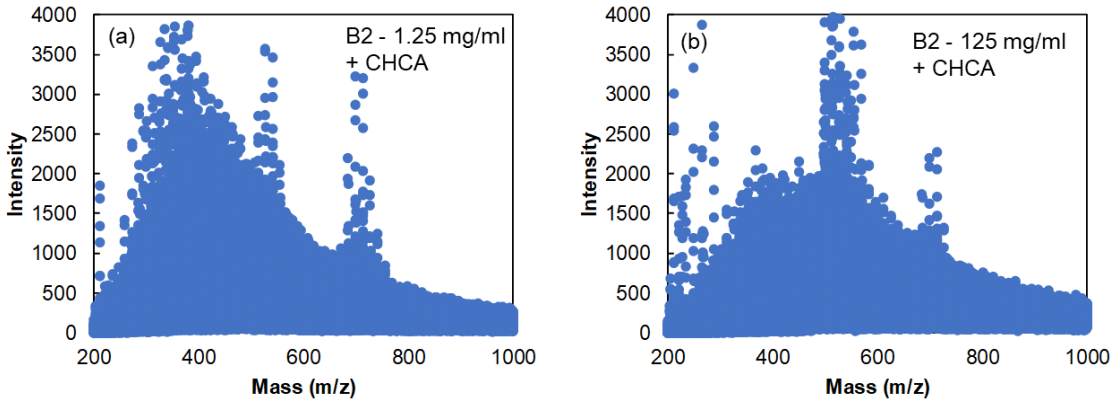

Figure A- 4: Molecular Weight Distribution of B2 Asphalt at 1.25 mg/ml and 125 mg/ml Dilution Levels Using α-Cyano-4-hydroxycinnamic Acid (CHCA) Matrix.

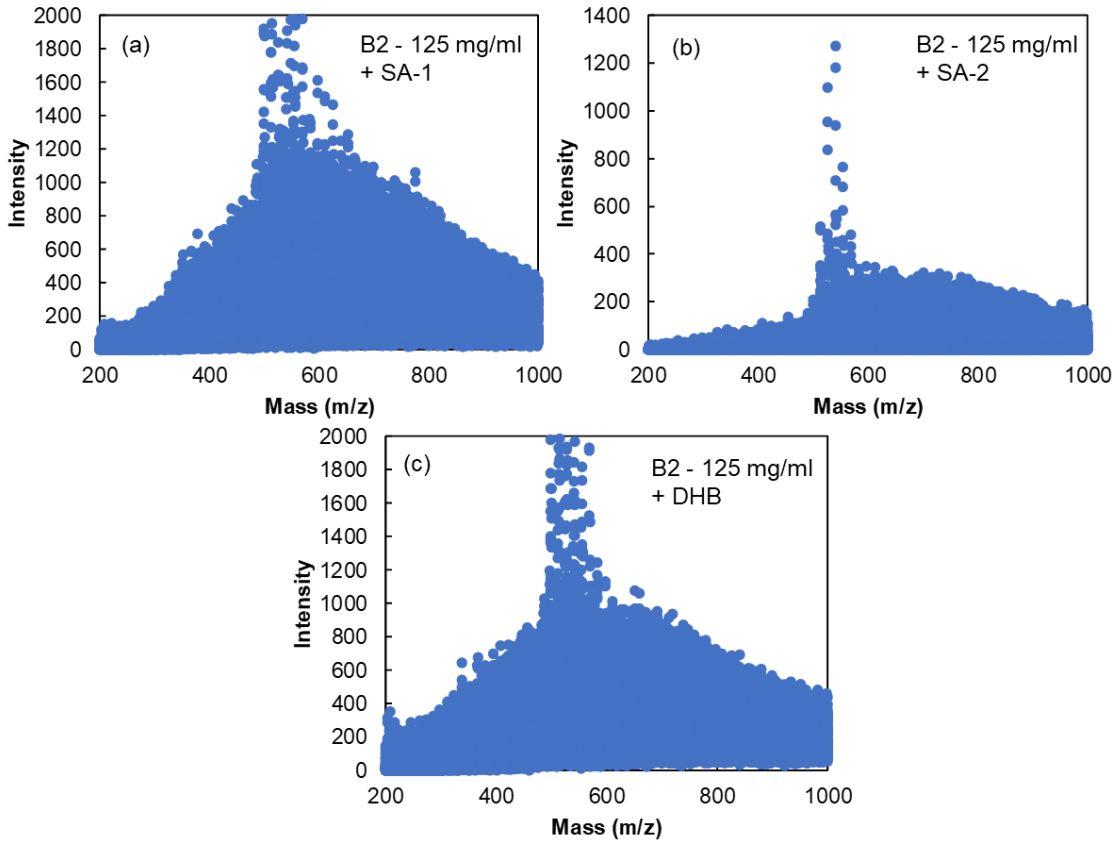

Figure A- 5: Molecular Weight Distribution of B2 Asphalt at 125 mg/ml Using Matrices: (a) Sinapic Acid in Toluene; (b) Sinapic Acid in Acetone; and (c) Dihydroxybenzoic Acid.

Firstly, in Figure A- 1 through Figure A- 5 it can be seen that the Y axis limits for some of the part figures are different. For ease of comparison, it is often desired to make the Y axis and X Axis limits the same. In this assessment, the Y axis limits had to be changed from one part figure to the other, in order to make a good assessment of the quality of spectra and also to check for noise in the data.

In Figure A- 1, the spectra obtained from the LDMS test without the use of any matrix is shown for binders B1 and B2 at two dilution levels, i.e. 6 mg/ml and 125 mg/ml. The obtained spectra follow the general trend expected for asphalt binders. The quality of the spectra, gauged by the spectral intensity is good for both 6 mg/ml and 125 mg/ml samples.

In Figure A- 2, molecular weight distribution spectra of B2 asphalt at 6 mg/ml and 125 mg/ml dilution levels using silver fluoroacetate (AGF) matrix is presented. The quality of the spectra obtained is poor compared to the spectra obtained when no matrix was used. For two cases, data was obtained only until 800 daltons, because of which no data is seen between 800-1000 daltons. But this has no bearing on the obtained spectra being inferior.

In Figure A- 3, molecular weight distribution spectra of B2 asphalt at 1.25 and 125 mg/ml dilution level using anthracenecarbonitrile (ACN) matrix is presented. While the shape of the spectra is similar to that obtained using the control samples, the signal intensity obtained using 1.25 mg/ml is inferior. The quality of spectra obtained using 125 mg/ml is comparable to the control samples.

In Figure A- 4, molecular weight distribution spectra of B2 asphalt at 1.25 and 125 mg/ml dilution levels using α-Cyano-4-hydroxycinnamic acid (CHCA) matrix is presented. The spectra look comparable to that obtained using the control samples. The only concern is the noise in the spectra between 200-400 daltons, which is more prominent in the 125 mg/ml case.

The last set of trials were performed using B2 asphalt at 125 mg/ml dilution level using sinapic acid and dihydroxybenzoic acid matrices. The sinapic acid matrix was prepared in two different solvents, toluene (SA-1) and acetone (SA-2). It can be seen from Figure A- 5 that the type of solvent does have an impact, as the spectra produced using SA-1 is seen to have better signal quality than SA-2 and also the shape of the spectra is similar to that obtained using the control samples. While the signal intensity of the spectra using DHB is slightly inferior to SA-1, the overall shape of the spectra is comparable to that obtained using control or no-matrix samples.

Based on the results from the preliminary study, the spectra obtained using matrices silver fluoroacetate and sinapic acid with acetone produce inferior spectra in comparison to control or no-matrix spectra. While the other matrices, particularly CAN and CHCA also provide good spectra, there is no significant benefit in terms of spectral intensity or noise hindrance in comparison to the control samples. On the other hand, the spectra obtained using the control samples was very clean with minimal to no noise and also similar in shape to that reported in literature by Fonnesbeck et al. (1997). Since both 6 mg/ml and 125 mg/ml provided good spectra, the decision was based on ease and time consumed for preparation of the samples. Preparing a 125 mg/ml sample took less time than preparing a

6 mg/ml sample. Also, it is easier to better control, precision and repeatability when weighing a larger batch of asphalt. And preparing a larger batch using using 6 mg/ml would not be economical as toluene is expensive. Based on the above findings, it was decided that samples for LDMS test on study binders in set 1 will be conducted without the use of any matrix at a dilution level of 125 mg/ml.

APPENDIX B

STEP BY STEP PROCEDURE OF CALCULATION OF CARBONYL AND SULFOXIDE AREAS

The program was developed for the NCHRP 9-54 study and the calculation steps were established based on discussions and input from researchers at the Western Research Institute, which has more than 30 years of experience in analyzing FTIR data.

i. The data are sorted by wavenumber and the absorbance values corresponding to the Carbonyl region (1650 to 1820 cm^{-1}), the Sulfoxide region (1000 to 1050 cm^{-1}), and the wavenumber used to calculation the absorbance adjustment factor (1375 cm^{-1}) are extracted.

ii. The user then enters in the normalization factor if known. If this value is not known then the default of 0.1 is used. The normalization factor is the value that the absorbance should have at the wavenumber used for normalization. The spectrograph adjustment factor is determined by dividing the normalization factor by the measured absorbance at the normalization wavelength. This adjustment process is a common technique used to correct spectrographs for known variations in FTIR scans (detector inconsistencies, pathway differences, etc.) and essentially involves forcing the spectrograph for a number of replicates to have a certain fixed value at a pre-defined wavenumber.

iii. This adjustment factor is then multiplied to the absorbance values at all other wavenumbers.

iv. The normalized peak values of Carbonyl and Sulfoxide are extracted from the spectrograph. Depending on the data collection details, this process may require linear interpolation of the raw data at precisely 1702 cm-1 (Carbonyl) and 1032

cm-1 (Sulfoxide). The total Carbonyl+Sulfoxide peak value is calculated by summing the individual Carbonyl and Sulfoxide peak values.

v. The Carbonyl area (CA) is determined by numerical integration (Trapezoidal rule) of the normalized spectrograph between wavenumbers of 1650 and 1820 cm-1.

vi. The Sulfoxide area (SA) is determined by numerical integration (Trapezoidal rule) of the normalized spectrograph between wavenumbers of 1000 and 1050 cm-1).

vii. The Carbonyl+Sulfoxide Area (C+SA) is determined by adding the CA and SA.

APPENDIX C

DYNAMIC MODULUS MASTERCURVES OF ALL STUDY ASPHALT BINDERS DEVELOPED USING CAM MODEL

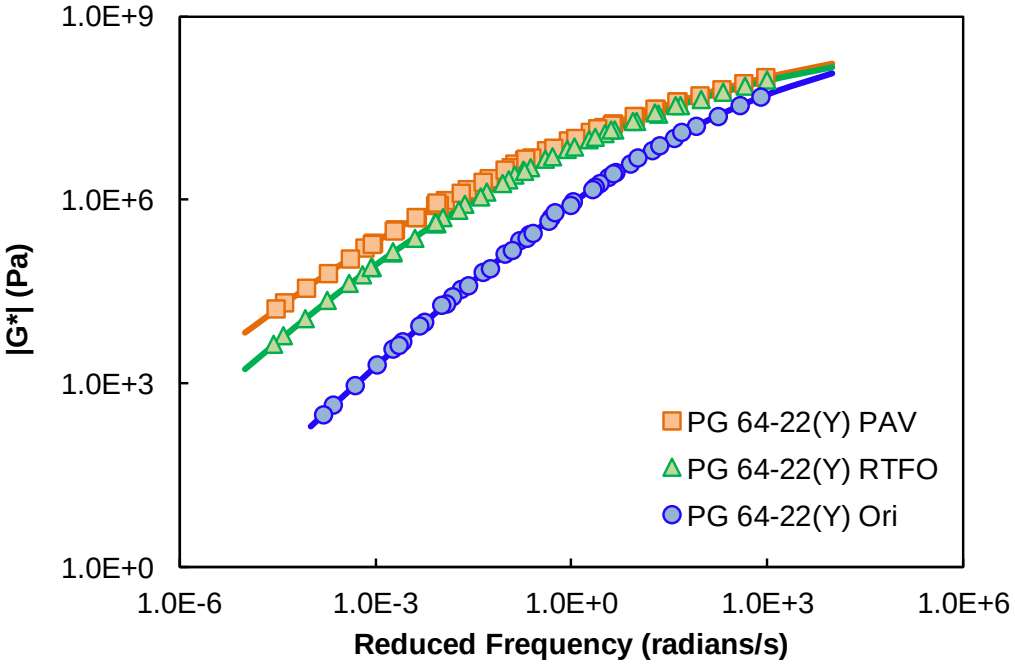

Figure C-6: Dynamic Modulus Mastercurves for Asphalt PG 64-22(Y) at All Three Aging Conditions.

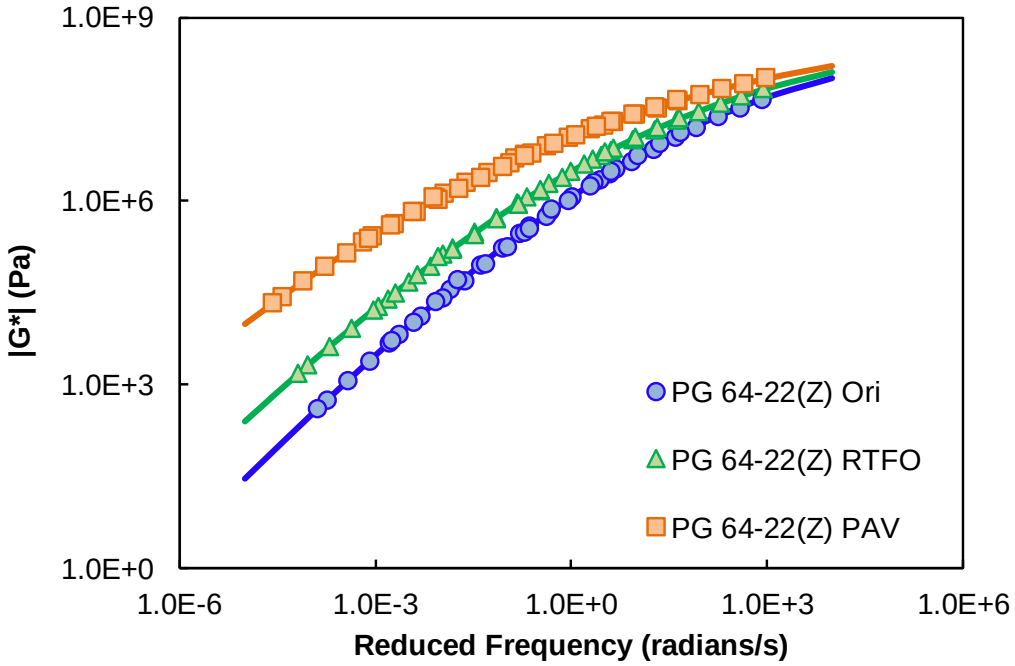

Figure C-7: Dynamic Modulus Mastercurves for Asphalt PG 64-22(Z) at All Three Aging Conditions.

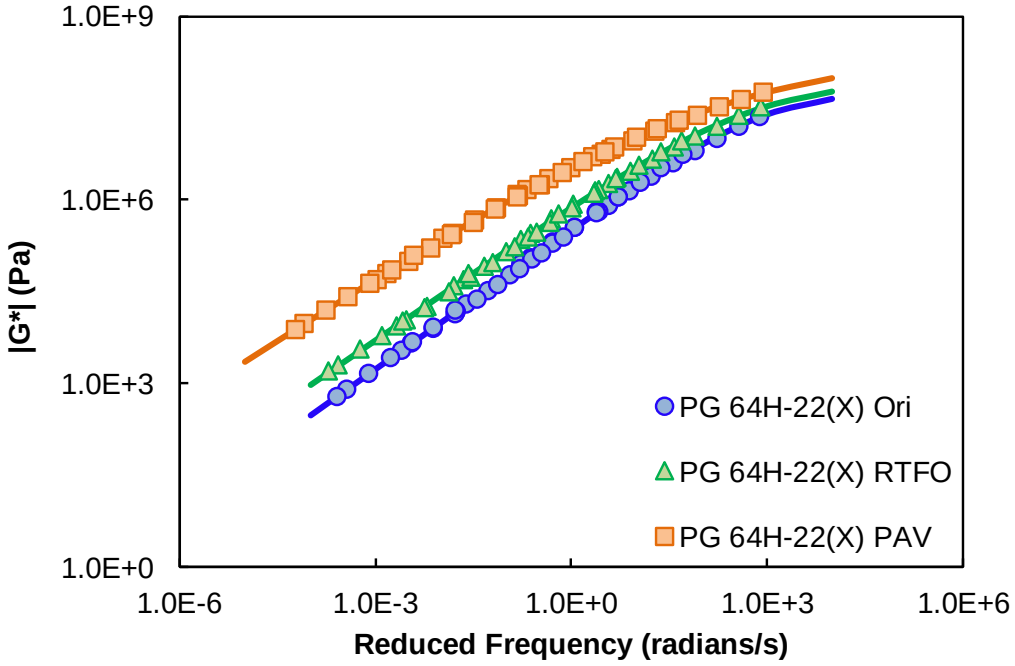

Figure C- 8: Dynamic Modulus Mastercurves for Asphalt PG 64H-22(X) at All Three Aging Conditions

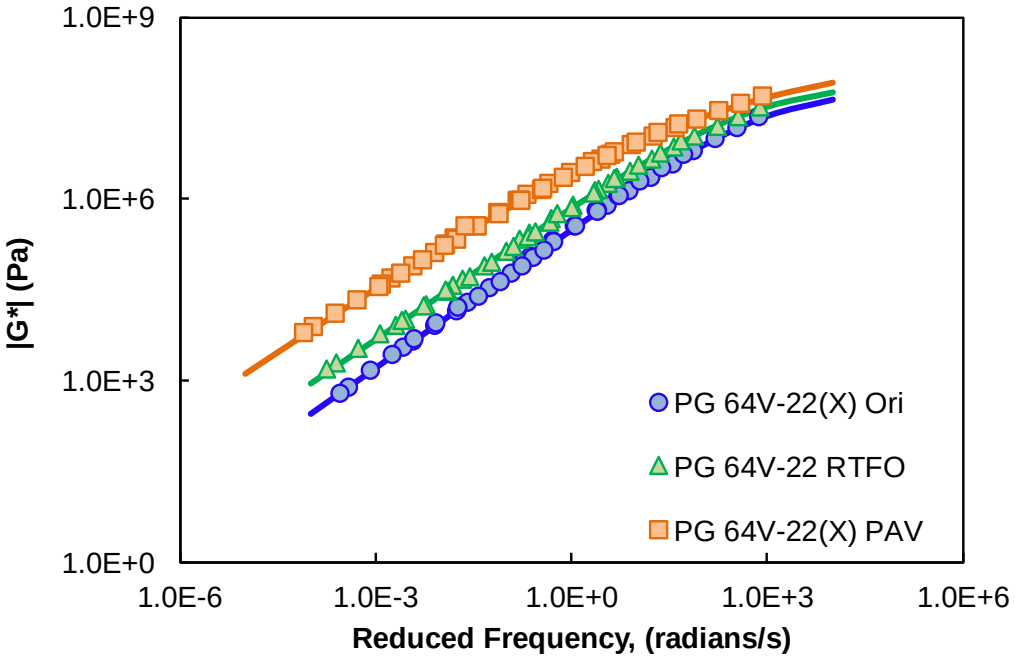

Figure C- 9: Dynamic Modulus Mastercurves for Asphalt PG 64V-22(X) at All Three Aging Conditions

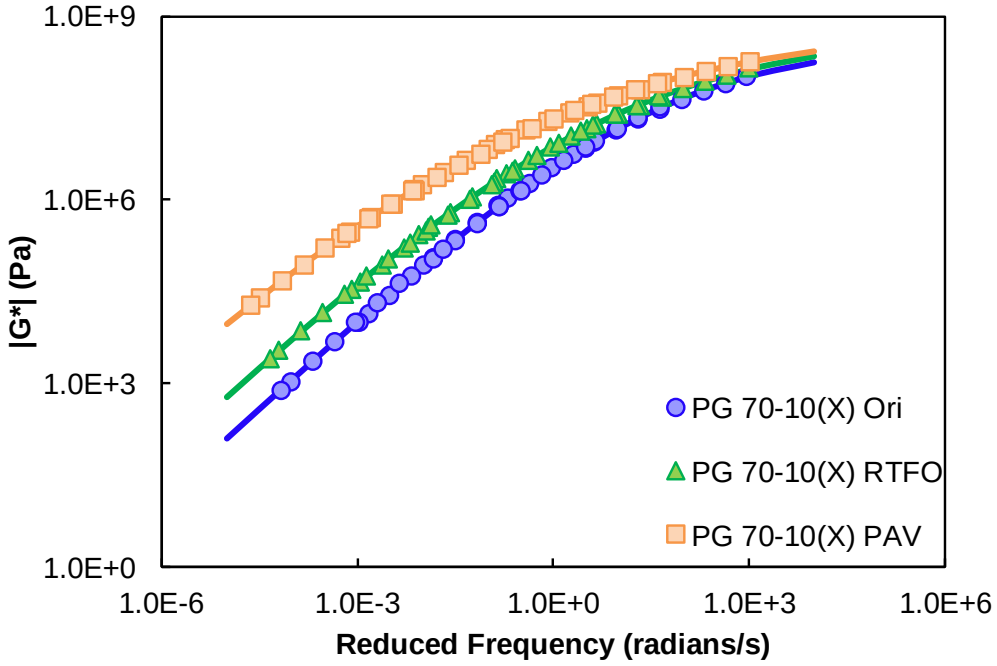

Figure C- 10: Dynamic Modulus Mastercurves for Asphalt PG 70-10(X) at All Three Aging Conditions

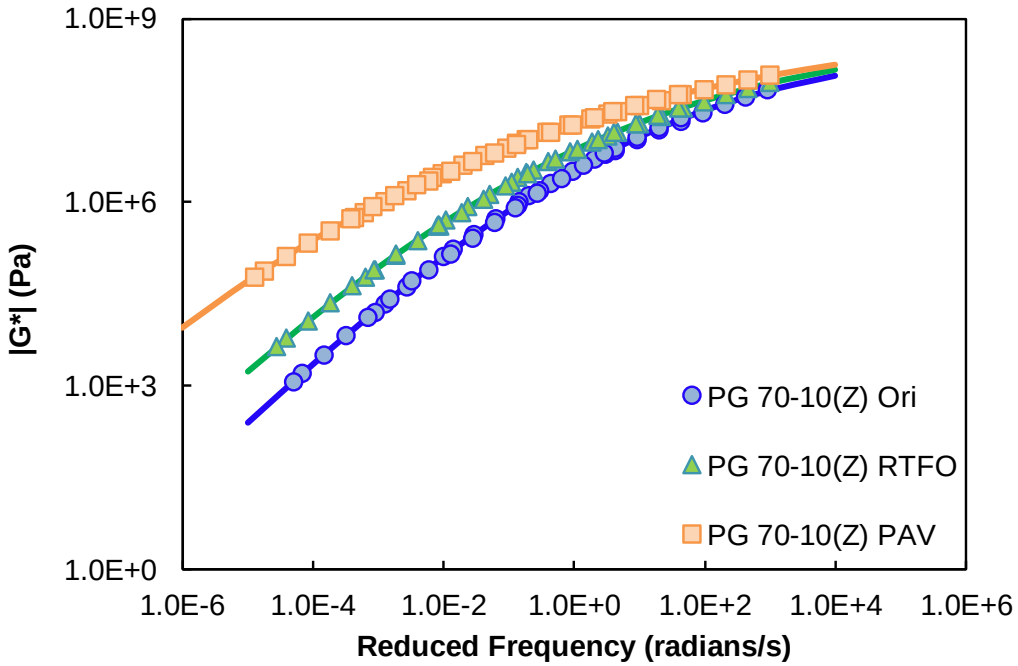

Figure C- 11: Dynamic Modulus Mastercurves for Asphalt PG 70-10(Z) at All Three Aging Conditions

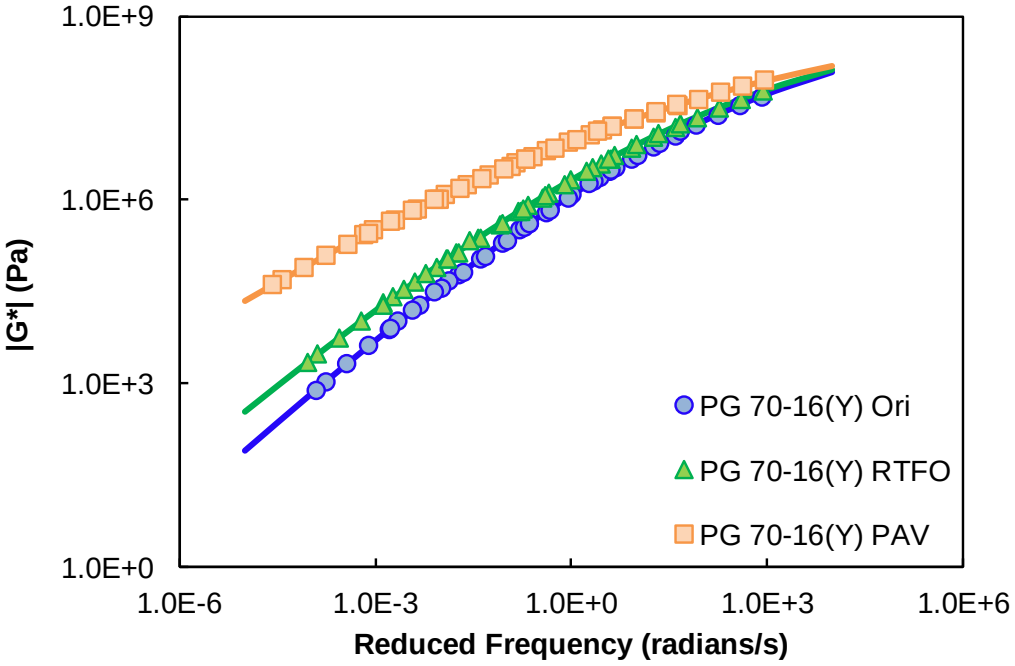

Figure C- 12: Dynamic Modulus Mastercurves for Asphalt PG 70-16(Y) at All Three Aging Conditions

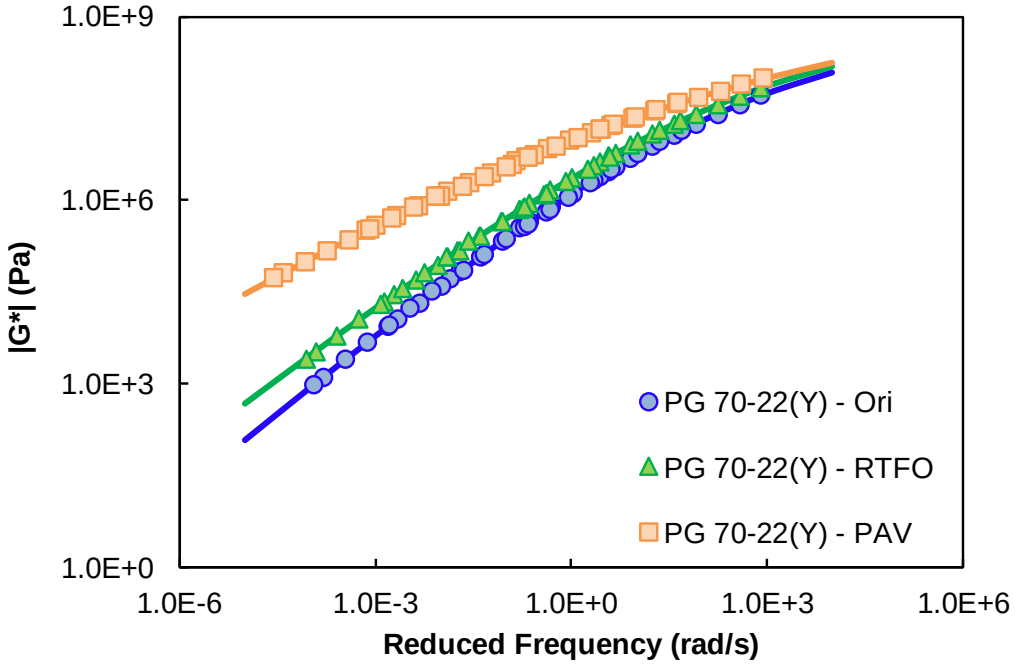

Figure C- 13: Dynamic Modulus Mastercurves for Asphalt PG 70-22(Y) at All Three Aging Conditions

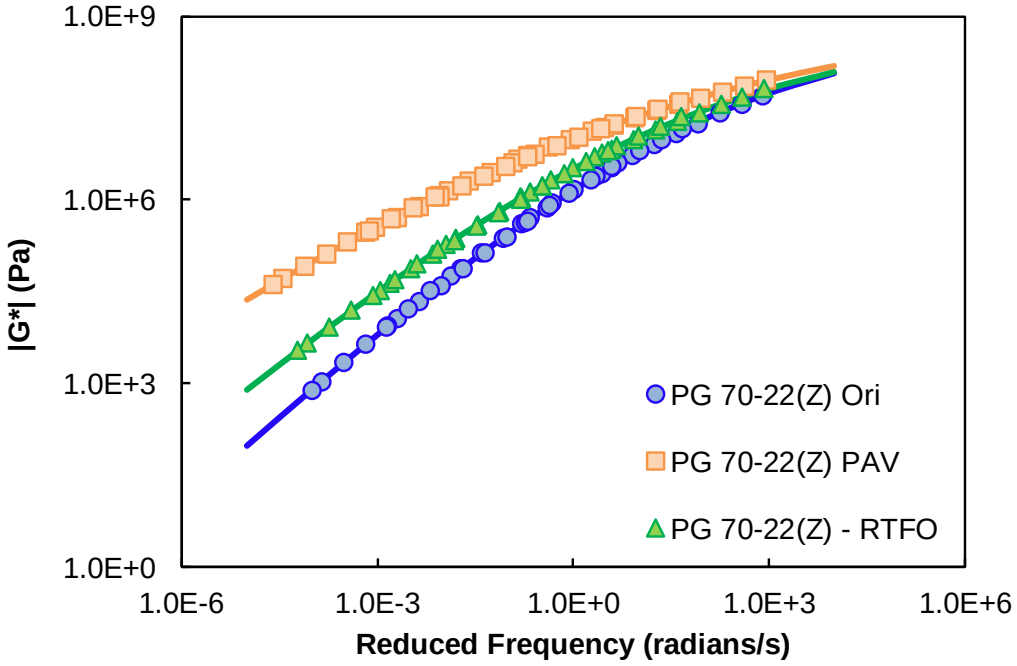

Figure C- 14: Dynamic Modulus Mastercurves for Asphalt PG 70-22(Z) at All Three Aging Conditions

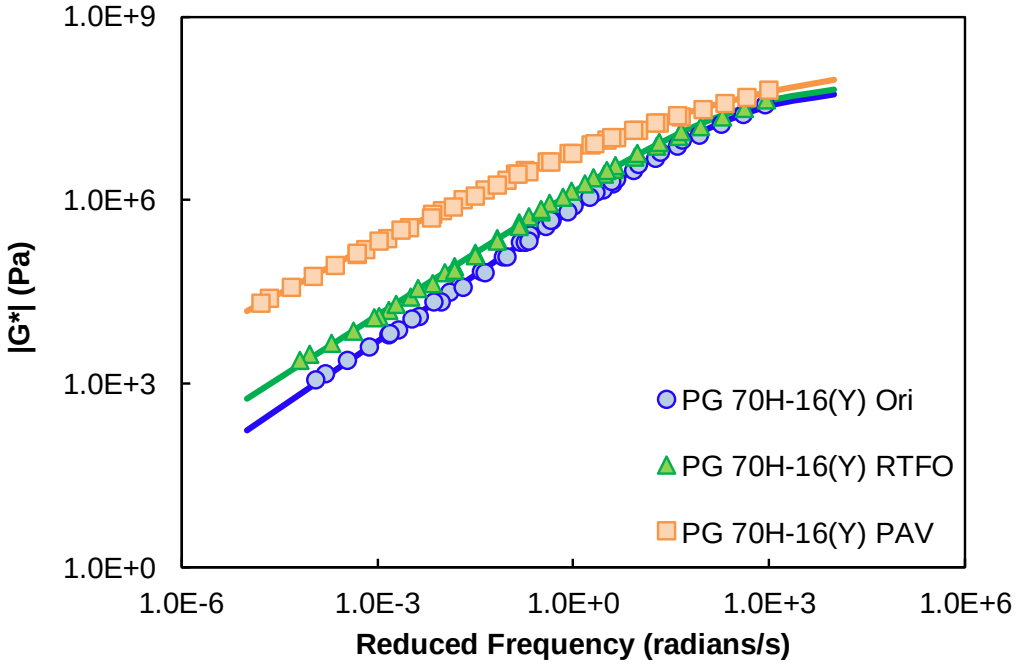

Figure C- 15: Dynamic Modulus Mastercurves for Asphalt PG 70H-16(Y) at All Three Aging Conditions

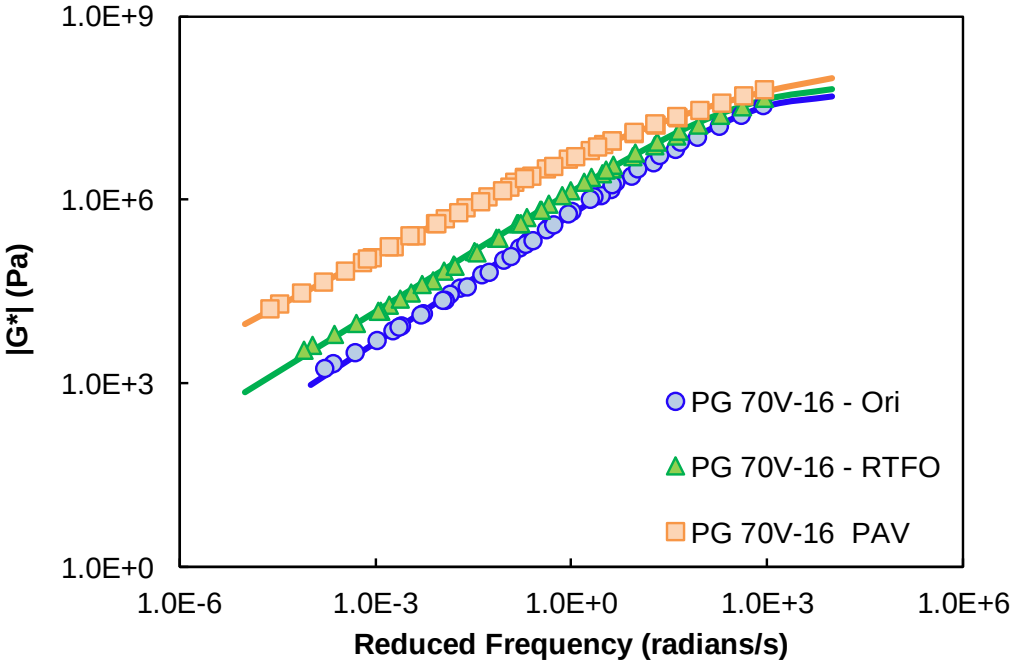

Figure C- 16: Dynamic Modulus Mastercurves for Asphalt PG 70V-16(Y) at All Three Aging Conditions

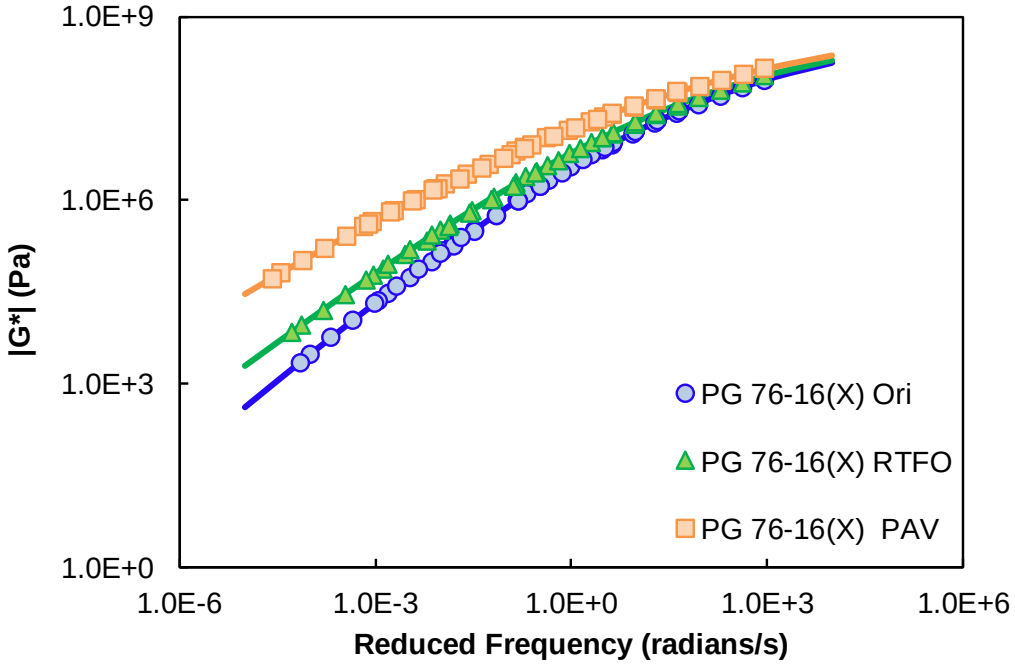

Figure C- 17: Dynamic Modulus Mastercurves for Asphalt PG 76-16(X) at All Three Aging Conditions

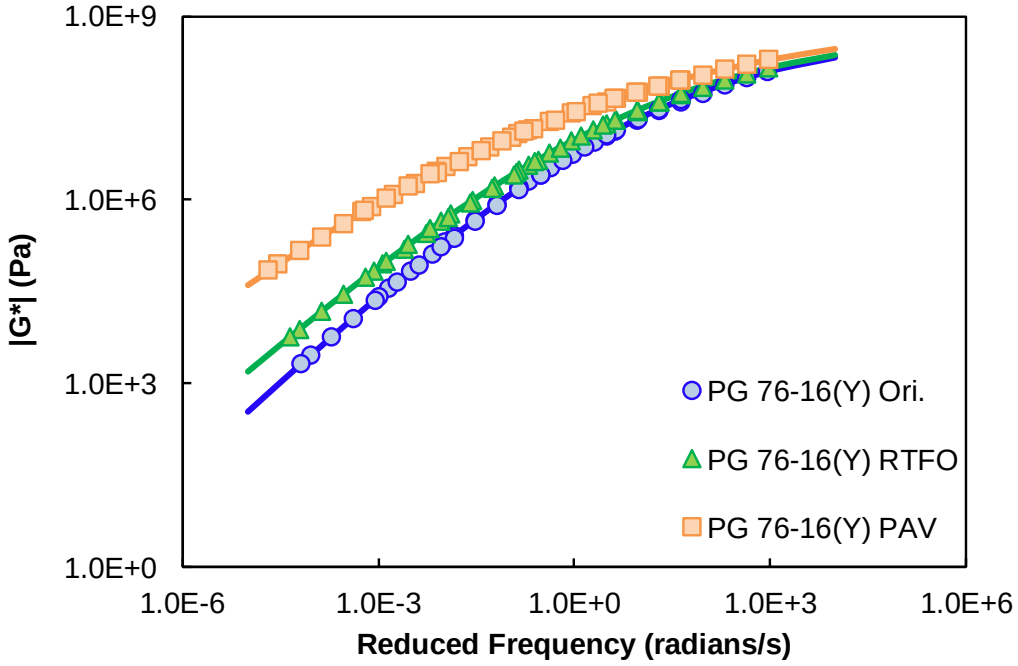

Figure C- 18: Dynamic Modulus Mastercurves for Asphalt PG 76-16(Y) at All Three Aging Conditions

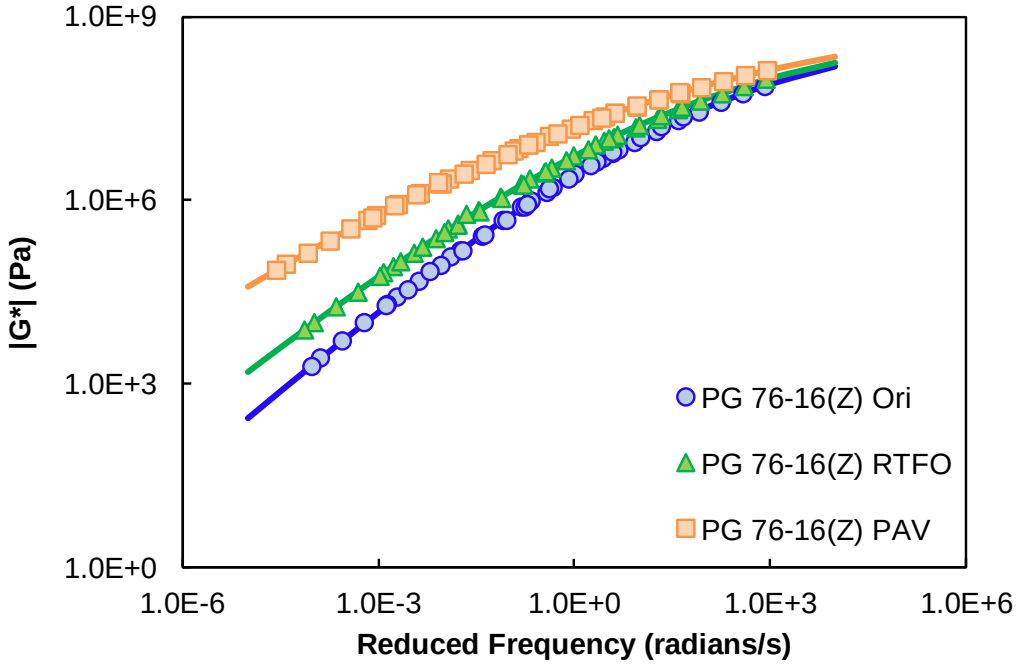

Figure C- 19: Dynamic Modulus Mastercurves for Asphalt PG 76-16(Z) at All Three Aging Conditions

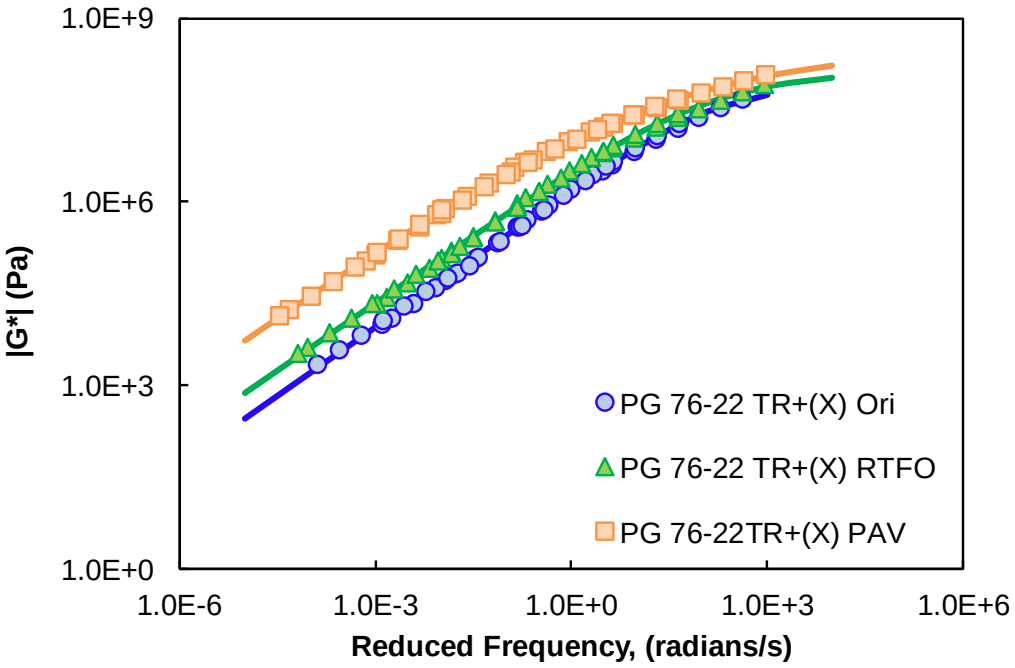

Figure C- 20: Dynamic Modulus Mastercurves for Asphalt PG 76-22TR+(X) at All Three Aging Conditions

APPENDIX D

RHEOLOGY BASED AGING RATIOS FOR STUDY BINDERS AT INTERMEDIATE AND HIGH TEMPERATURES

Table D-1: Rheology Based Aging Ratios of the Study Binders at Intermediate and High Temperatures.

Temperature (°C)	Aging Condition	PG Grade														
		PG 64-22	PG 64-22	PG 70-22	PG 70-22	PG 70-10	PG 70-10	PG 76-16	PG 76-16	PG 76-16	PG 70-16	PG 76-22 TR	PG 64V-22	PG 64H-22	PG 70H-16	PG 70V-16
		Y1	Z1	Y2	Z2	X1	Z3	Y4	Z4	X2	Y3	X5	X4	X3	Y5	Y6
22	Original	1.00	1.00	-	-	-	-	-	1.00	1.00	1.00	1.00	1.00	1.00	1.00	1.00
	RTFO	2.14	2.64	-	-	-	-	-	-	-	-	-	2.07	2.04	-	-
	PAV	6.36	6.83	-	-	-	-	-	-	-	-	-	6.01	6.21	-	-
25	Original	1.00	1.00	1.00	1.00	-	-	-	1.00	1.00	1.00	1.00	1.00	1.00	1.00	1.00
	RTFO	2.25	2.77	1.54	2.30	-	-	-	-	-	-	-	2.03	2.04	-	-
	PAV	7.06	7.80	5.82	8.44	-	-	-	-	-	-	-	6.14	6.60	-	-
28	Original	1.00	1.00	1.00	1.00	-	-	-	1.00	1.00	1.00	1.00	1.00	1.00	1.00	1.00
	RTFO	2.32	2.90	1.57	2.37	-	-	-	-	-	1.82	1.66	2.02	2.07	1.95	1.92
	PAV	7.81	8.72	6.51	9.63	-	-	-	-	-	8.48	5.74	6.28	6.94	9.51	10.82
31	Original	-	-	1.00	1.00	1.00	1.00	1.00	1.00	1.00	1.00	1.00	1.00	1.00	1.00	1.00
	RTFO	-	-	1.62	2.46	2.24	2.30	1.82	2.26	1.73	1.88	1.65	-	-	1.94	1.91
	PAV	-	-	7.24	10.91	8.30	9.32	5.76	8.00	6.26	9.64	6.08	-	-	10.45	11.50
34	Original	-	-	-	-	1.00	1.00	1.00	1.00	1.00	1.00	1.00	1.00	1.00	1.00	1.00
	RTFO	-	-	-	-	2.31	2.41	1.89	2.33	1.77	2.16	1.62	-	-	1.92	1.88
	PAV	-	-	-	-	9.32	10.85	6.61	9.00	6.93	10.79	6.25	-	-	11.15	11.90
37	Original	-	-	-	-	-	-	1.00	1.00	1.00	1.00	1.00	1.00	1.00	1.00	1.00
	RTFO	-	-	-	-	-	-	1.95	2.41	1.83	-	-	-	-	-	-
	PAV	-	-	-	-	-	-	7.51	10.07	7.62	-	-	-	-	-	-
58	Original	1.00	1.00	-	-	-	-	1.00	1.00	1.00	1.00	1.00	1.00	1.00	1.00	1.00
	RTFO	2.76	3.10	-	-	-	-	-	-	-	-	-	1.87	1.86	-	-
	PAV	-	-	-	-	-	-	-	-	-	-	-	-	-	-	-
64	Original	1.00	1.00	1.00	1.00	1.00	1.00	1.00	1.00	1.00	1.00	1.00	1.00	1.00	1.00	1.00
	RTFO	2.64	2.99	1.90	3.12	2.15	2.95	2.18	3.11	2.27	2.33	1.28	1.85	1.87	1.85	1.63
	PAV	10.13	12.08	-	-	-	-	-	-	-	-	-	4.82	5.00	-	-
70	Original	1.00	1.00	1.00	1.00	1.00	1.00	1.00	1.00	1.00	1.00	1.00	1.00	1.00	1.00	1.00
	RTFO	2.50	2.78	1.93	3.09	2.06	2.83	2.20	3.07	2.31	2.36	1.43	1.81	1.88	1.83	1.61
	PAV	-	-	15.36	25.77	10.75	25.75	-	-	-	21.43	-	-	-	10.65	6.31
76	Original	-	-	1.00	1.00	1.00	1.00	1.00	1.00	1.00	1.00	1.00	1.00	1.00	1.00	1.00
	RTFO	-	-	1.92	3.01	1.96	2.66	2.16	3.11	2.38	2.37	1.33	-	-	1.83	1.58
	PAV	-	-	-	-	-	-	15.83	21.87	15.27	-	3.56	-	-	-	-
82	Original	-	-	-	-	-	-	1.00	1.00	1.00	1.00	1.00	1.00	1.00	1.00	1.00
	RTFO	-	-	-	-	-	-	2.10	3.04	2.38	-	1.22	-	-	-	-
	PAV	-	-	-	-	-	-	-	-	-	-	-	-	-	-	-

APPENDIX E

MOLECULAR WEIGHT DISTRIBUTIONS OF ASPHALT BINDERS FIT TO GAMMA DISTRIBUTION FUNCTION

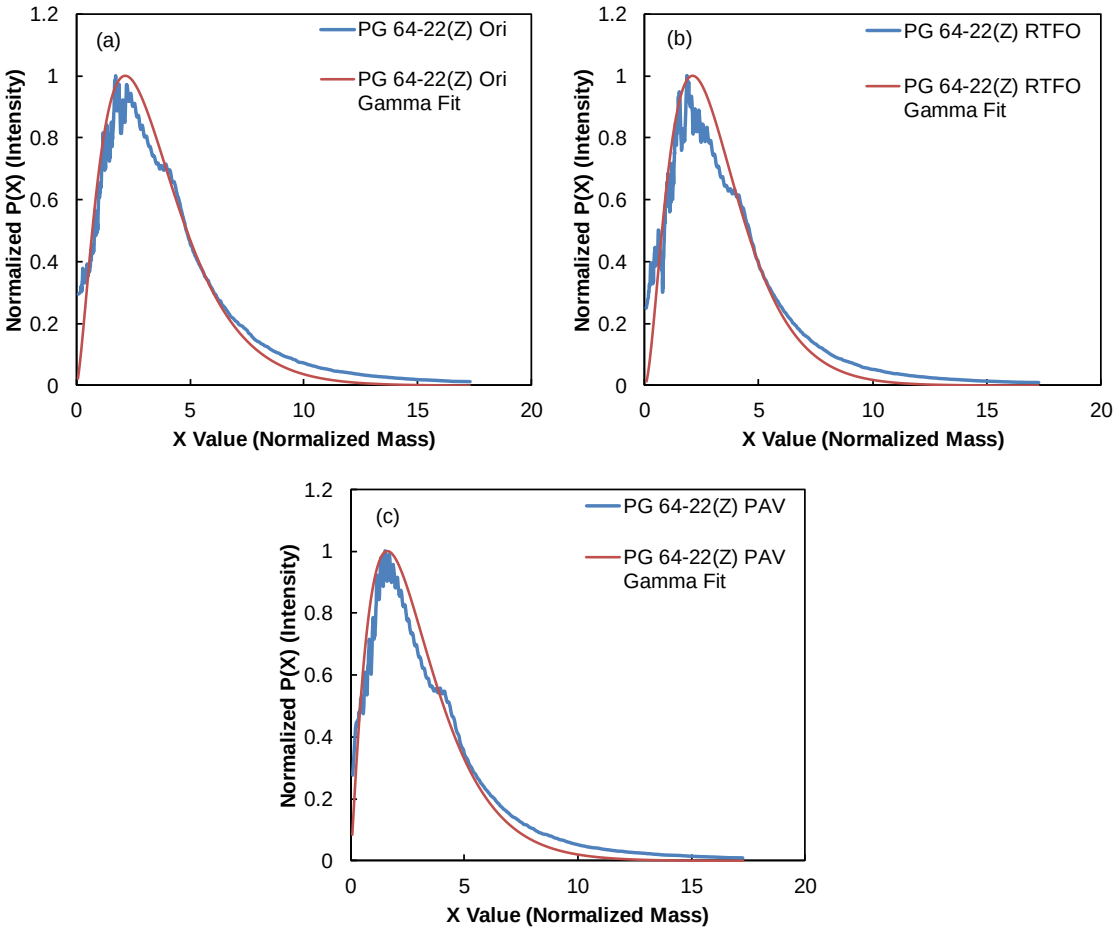

Figure E-1: Molecular Weight Distribution of Asphalt Binder PG 64-22(Z) at (a) Original; (b) RTFO; and (c) PAV Conditions Fit to Gamma Distribution.

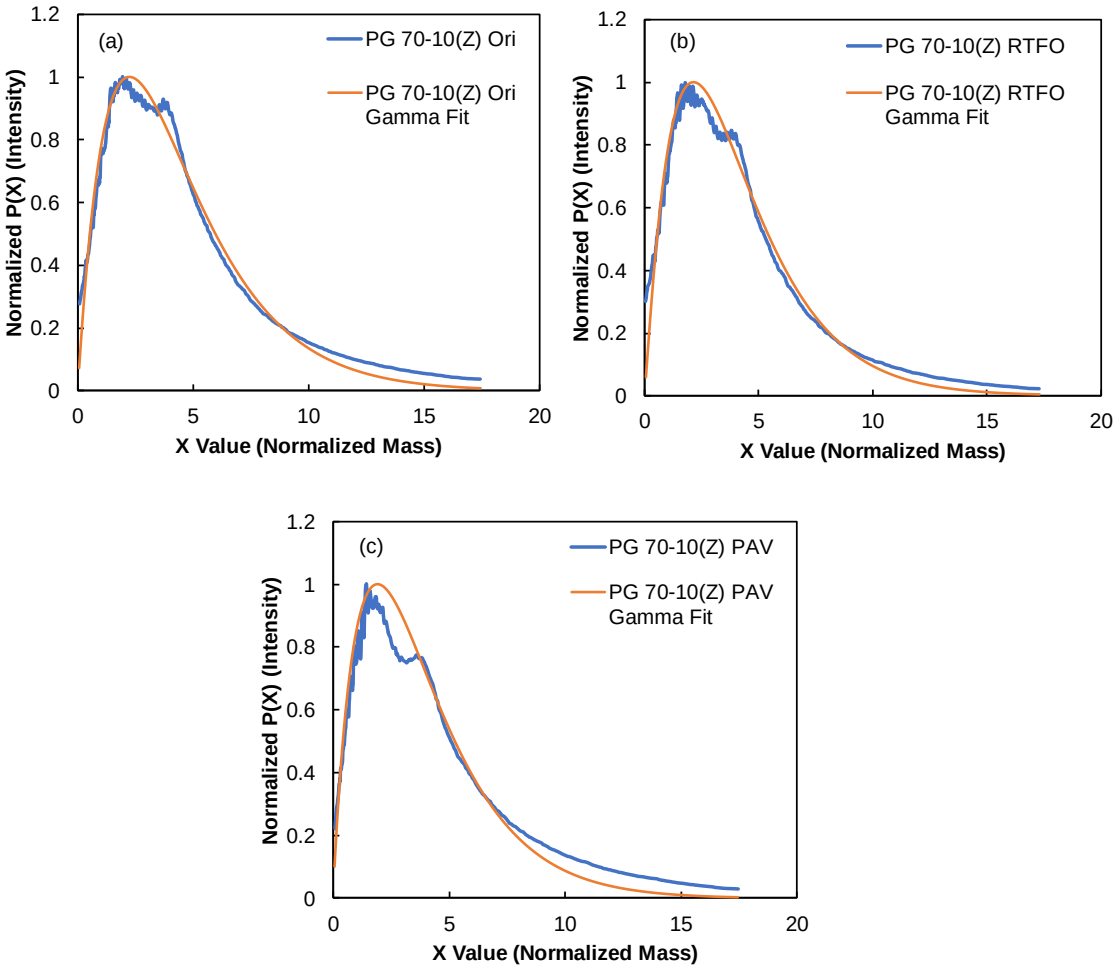

Figure E-2: Molecular Weight Distribution of Asphalt Binder PG 70-10(Z) at (a) Original; (b) RTFO; and (c) PAV Conditions Fit to Gamma Distribution.

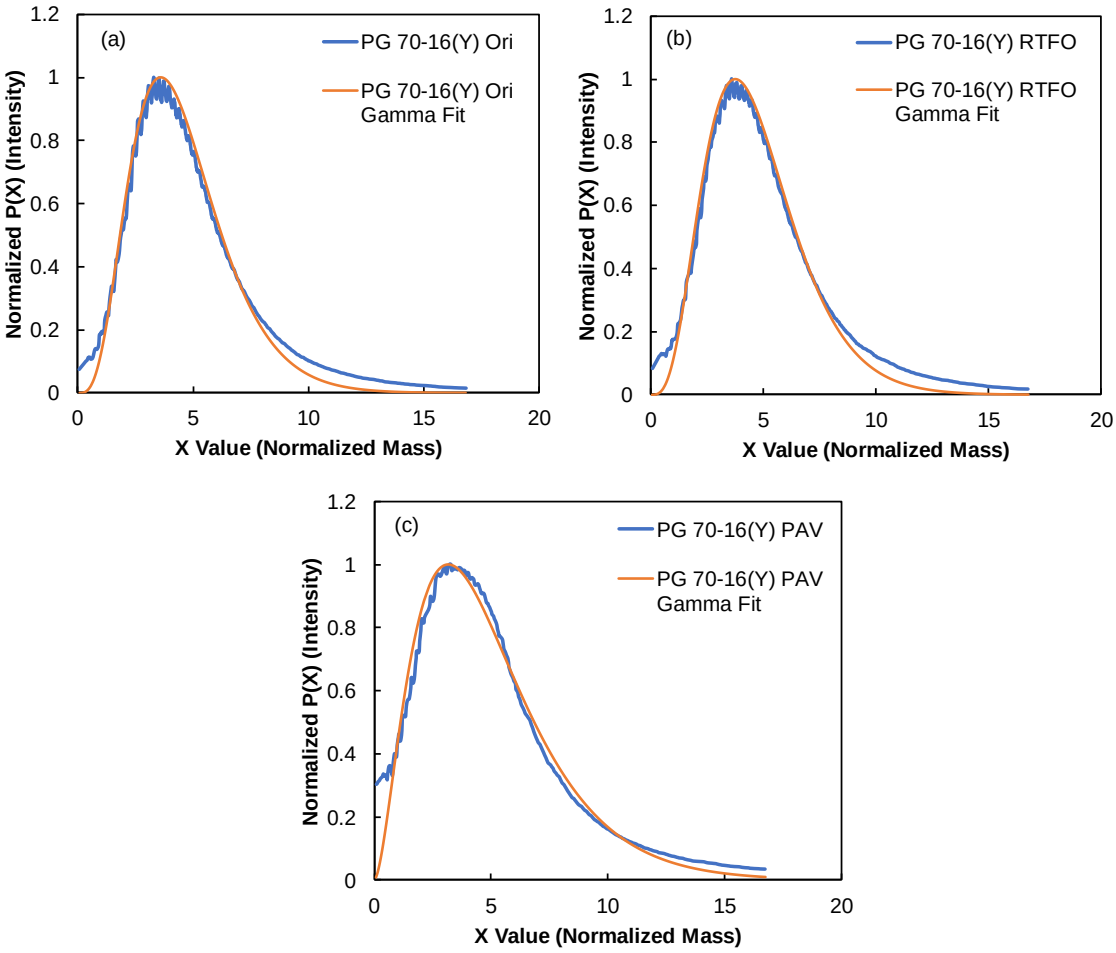

Figure E-3: Molecular Weight Distribution of Asphalt Binder PG 70-16(Y) at (a) Original; (b) RTFO; and (c) PAV Conditions Fit to Gamma Distribution.

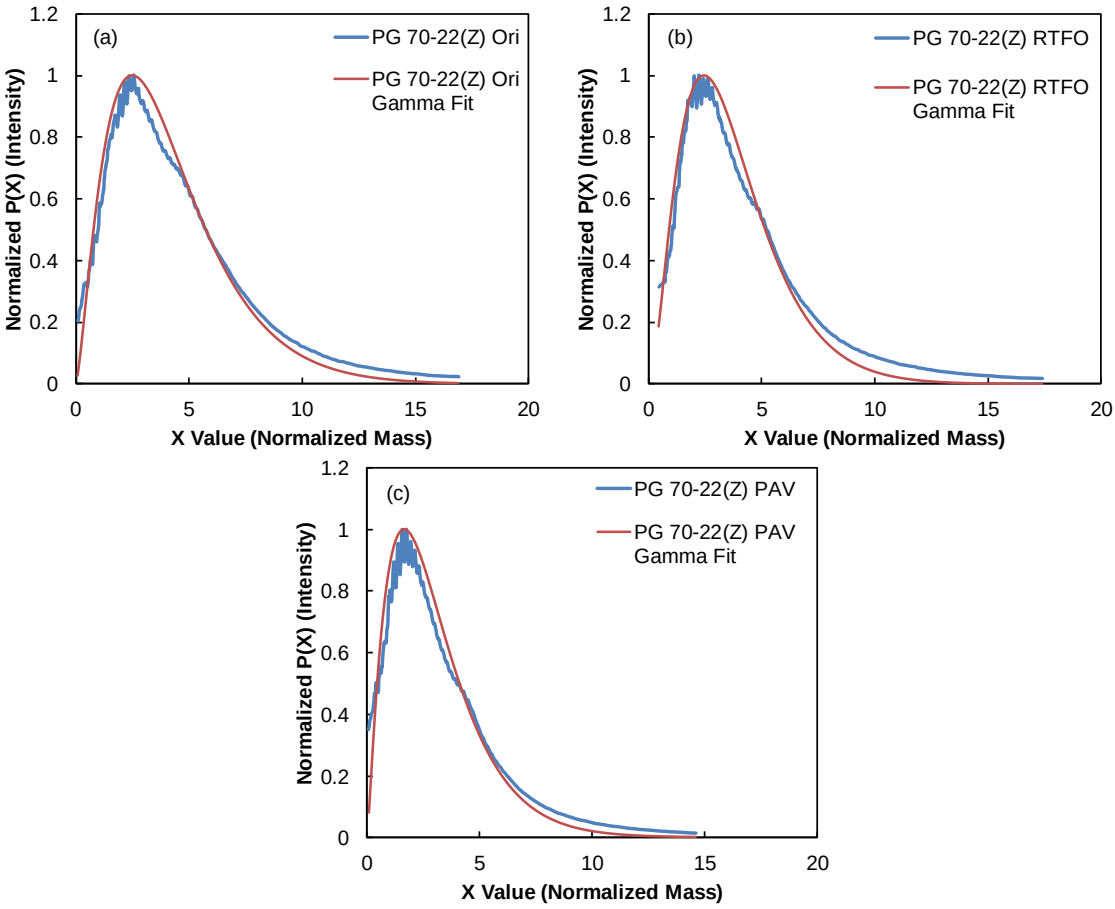

Figure E-4: Molecular Weight Distribution of Asphalt Binder PG 70-22(Z) at (a) Original; (b) RTFO; and (c) PAV Conditions Fit to Gamma Distribution.

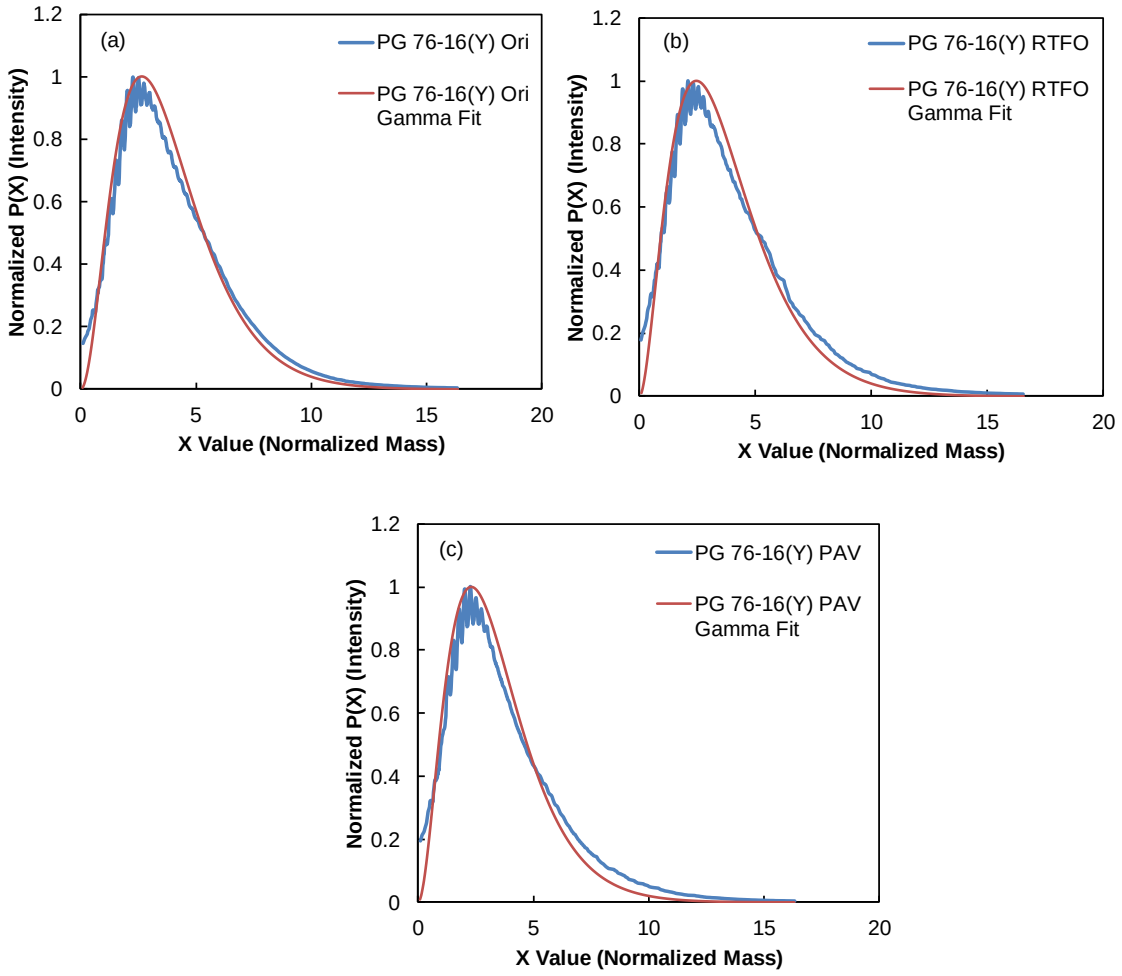

Figure E-5: Molecular Weight Distribution of Asphalt Binder PG 76-16(Y) at (a) Original; (b) RTFO; and (c) PAV Conditions Fit to Gamma Distribution.

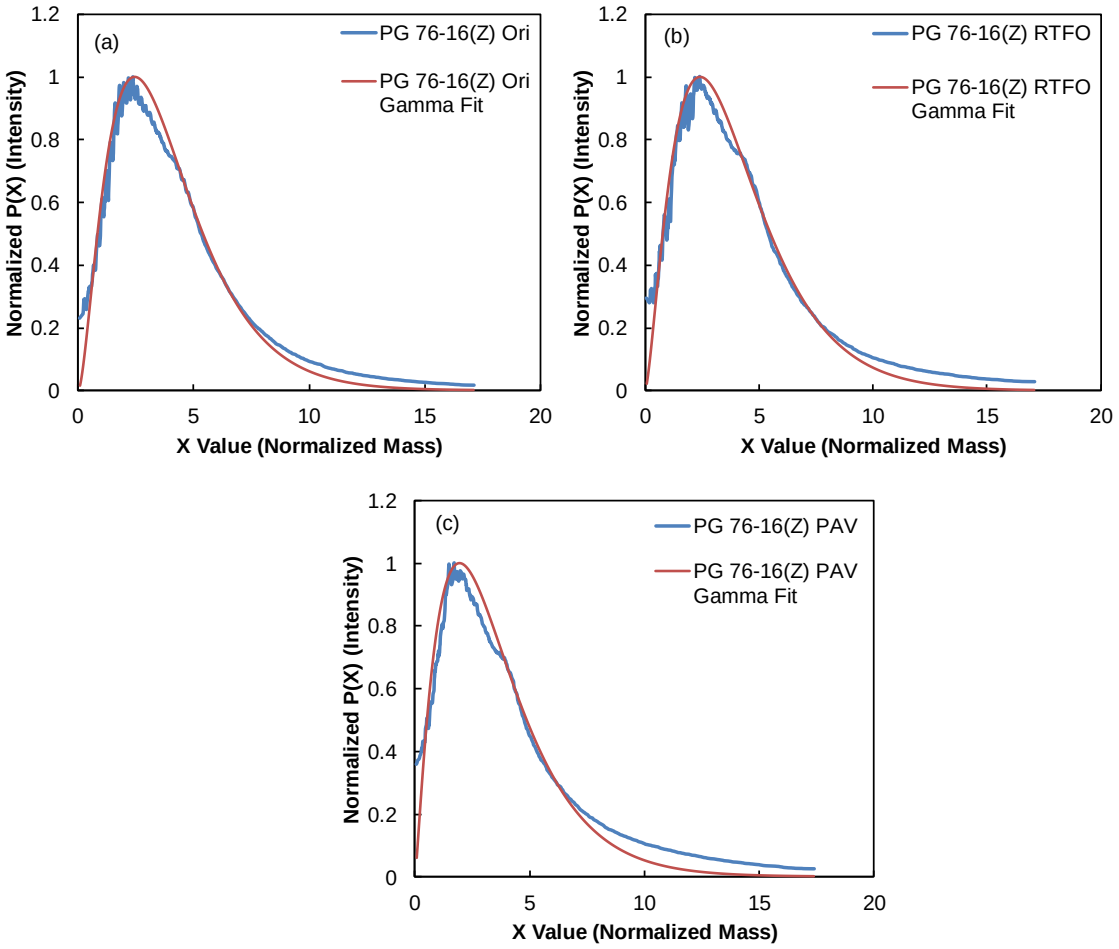

Figure E-6: Molecular Weight Distribution of Asphalt Binder PG 76-16(Z) at (a) Original; (b) RTFO; and (c) PAV Conditions Fit to Gamma Distribution.

Table E-1: Gamma Distribution Parameters and the Corresponding Skewness and Kurtosis Values for the Study Binders.

Binder	Condition	α	β	Skewness	Kurtosis
PG 70-16(Y)	Ori	4.75	0.96	0.92	1.26
	RTFO	3.24	1.19	1.11	1.85
	PAV	3.10	1.32	1.14	1.94
PG 76-16(Y)	Ori	2.57	1.37	1.25	2.34
	RTFO	2.02	2.20	1.41	2.98
	PAV	2.48	1.69	1.27	2.42
PG 76-16(X)	Ori	2.65	1.47	1.23	2.26
	RTFO	4.79	0.99	0.91	1.25
	PAV	2.92	1.28	1.17	2.05
PG 64-22(Z)	Ori	3.06	1.28	1.14	1.96
	RTFO	2.81	1.16	1.19	2.13
	PAV	2.11	1.93	1.38	2.84
PG 70-10(Z)	Ori	2.94	1.27	1.17	2.04
	RTFO	2.52	1.59	1.26	2.39
	PAV	2.78	1.78	1.20	2.16
PG 70-22(Z)	Ori	3.09	1.11	1.14	1.94
	RTFO	2.68	1.30	1.22	2.24
	PAV	2.16	1.40	1.36	2.78
PG 76-16(Z)	Ori	1.95	2.03	1.43	3.08
	RTFO	2.19	1.38	1.35	2.74
	PAV	2.17	1.65	1.36	2.77